AES/GE/10-43 **Conditional simulation for characterising the spatial variability of sand state**

16th Dec 2010 **Bram van den Eijnden**

MSc Thesis Engineering Geology

TU Delft

Department of Geotechnology

Delft University of Technology

Title	:	Conditional simulation for characterising the spatial variability of sand state
Author	:	Bram van den Eijnden
Date	:	16 Dec 2010
Professor	:	M.A. Hicks
Supervisor	:	M.A. Hicks
Committee members	:	D.J.M. Ngan-Tillard R.R. de Jager T. Schweckendiek
TA Report number	:	AES/GE/10-43
Postal Address	:	Section for Geo-Engineering Department of Applied Earth Sciences Delft University of Technology P.O. Box 5028 The Netherlands
Telephone	:	(31) 15 2781328 (secretary)
Telefax	:	(31) 15 2781189

Conditional simulation for characterising the spatial variability of sand state

Bram van den Eijnden
Delft University of Technology

December 2010

Abstract

Properties of soils are spatially variable and to describe the behaviour of soils as a response to loading, this variability appears crucial in giving the correct range of possible solutions for structure response. Because site investigation techniques only provide exact information at a limited part of the site, random field simulations are used to assess this variability over the full test site domain. The random fields use the spatial statistical characteristics that are derived from the site investigation, which in geotechnical application mainly consists of cone penetration tests (CPT's). To reduce the range of possible solutions to be found for structure response analysis, the random fields can be conditioned by the actual CPT measurements.

This report describes the conditioning of the random field in order to generate conditioned simulations of sand state fields. In order to derive the state parameter from the CPT tip resistance, the NorSand constitutive model is calibrated against the results of 55 triaxial tests of a test site in the harbour of Rotterdam. Different methods of calibration using triaxial test data are described and the results are discussed. 140 CPT's of the test site are then transformed into state parameter profiles. The statistical characteristics of the profiles are determined to be used for the simulation of the spatially variable fields of sand state. The statistical characteristics of the profiles are used in the conditional simulation of the fields.

A conditional simulation algorithm to generate realisations of spatially variable sand state fields is derived and demonstrated. Using unconditioned random fields, generated with the Local Average Subdivision (LAS) method, conditioned simulations of the field around the CPT profiles are generated in a post-processing algorithm. The algorithm uses the geometry-dependent property of the kriging estimation error for the exchange of noise terms between estimation fields. The specific properties of the kriging estimator are demonstrated to be suitable to be used for the conditioning. The decrease in uncertainty by the conditioning with respect to the unconditioned random fields is presented. This decrease in uncertainty is used to demonstrate that the effectiveness of the conditioning is a function of the number and location of conditioning points relative to the scales of fluctuation of the field. It is demonstrated that conditioning reduces the range of possible solutions for the simulation of sand state fields with respect to unconditioned fields. This reduction will lead to a smaller range of solutions to be found when the conditional simulations are used in structure response analysis, leading to less uncertainty in design.

The conditional simulation is shown to produce fields that honour the initial distribution function, the correlation structure and the actual CPT profiles in the simulated fields. To demonstrate that conditional simulation can be applied on the test site, a stochastic characterisation of the test site is performed and conditional simulations of the state parameter fields are generated for a small part of the test site.

KEY WORDS: NorSand calibration, CPT interpretation, statistics, stochastic characterisation, conditional simulation, random fields, LAS, kriging.

Acknowledgment

As the author I like to express my thanks to my supervisor Michael Hicks for his guidance, support and his confidence in the results; Boskalis for their contribution in the project by providing me with the extensive amount of data; the members of my committee Michael Hicks, Dominique Ngan-Tillard, Richard de Jager and Timo Schweckendiek for their comments and input in the realisation of this report; Hans Bruining for the idea for the conditional simulation technique; my friends and family for their support and appreciated distraction from my work in times of need.

This project has been carried out as part of TU Delft's involvement in the EU Program IRIS (Integrated European Industrial Risk Reduction System).

Bram van den Eijnden
December 2010

List of symbols

Symbol	[Unit]	description
stress		
u	[FL^{-2}]	pore pressure
η	[-]	ratio of stress invariants
ϕ	[deg]	friction angle
$\sigma_{1,2,3}$	[FL^{-2}]	principal stresses
σ_m, p	[FL^{-2}]	mean total stress
σ'_m, p'	[FL^{-2}]	mean effective stress
σ_q, q	[FL^{-2}]	deviatoric stress invariant
τ	[FL^{-2}]	shear stress
Φ	[Rad]	Lode angle ($\frac{1}{3}\pi$ Rad for triaxial conditions)
strain		
e	[-]	void ratio
n	[-]	porosity
D	[-]	dilatancy
$\dot{D}$	[-]	dilatancy rate
$\epsilon_{1,3}$	[-]	principal strains
ϵ_v	[-]	volumetric strain
ϵ_q	[-]	shear strain
soil model, measurements		
q_c	[FL^{-2}]	CPT tip resistance
q_t	[FL^{-2}]	corrected CPT tip resistance
G	[FL^{-2}]	shear modulus
H	[-]	hardening modulus
K_0	[-]	geostatic/initial stress ratio
M	[-]	critical stress ratio
N	[-]	volumetric coupling parameter
Q_c	[-]	dimensionless CPT tip resistance
ν	[-]	Poisson's ratio
χ	[-]	dilatancy constant
Γ	[-]	reference void ratio on CSL
λ_{cs}	[-]	slope of critical state line
ψ	[-]	state parameter
(geo-)statistics		
n		number of conditioning points
$C(h)$		covariance function
LN		Lognormal distribution
N		number of field points
N		Normal distribution
β		Beta distribution
$\gamma(h)$		variogram

Symbol	**[Unit]**	**description**
μ		mean
$\rho(h)$		correlation function
σ		standard deviation
σ^2		variance
θ		scale of fluctuation
$\chi^2_{\alpha,\nu}$		chi-square corresponding to ν degrees of freedom and α level of significance
$\Gamma(\alpha,\beta)$		gamma function
$\Gamma(D)$		variance function
Γ		Gamma distribution
subscripts		
0		generic, original
10		on ^{10} log base
cs		critical state
cv		constant volume
e		on ln base
i		image condition
ss		steady state
tc		triaxial compression ($\Phi = \pi/6$)
te		triaxial extension ($-\Phi = \pi/6$)
tr		trend-removed
C		conditioned
K		kriged
L		limit value
OK		Ordinary kriging
S		simulated
SK		Simple kriging
superscripts		
$*$		kriging estimation
e		elastic
p		plastic

Contents

Chapter 1

Introduction

Properties of most soils are heterogeneous. In soil modelling this heterogeneity is often avoided by dividing the evaluated soil domain into geotechnical units with homogeneous properties. In this way the properties of a soil are often described with a single characteristic value for each property and the heterogeneity is eliminated. This method of parameter presentation is known as the deterministic approach. To account for the removed heterogeneity, the representative parameter values usually are factored down to achieve a required factor of safety. In cases like these the deterministic approach works fine for soil properties like unit weight, but when the deterministic properties are used for more complex processes, especially when spatial relation between the variation of property values influences the behaviour, a deterministic approach may not be sufficient and the spatial distribution of the variability needs to be taken into account.

Failures of geotechnical structures involving sand in an apparently stable state, like the Fort Peck Dam and the Nerlerk Berm [Jefferies and Been, 2006], have shown that an apparently stable sand can behave in a much more unstable way than expected from a deterministic approach. The deterministic approach of stability calculations might not be sufficient to describe every situation accurately. Hicks and Onisiphorou [2005] showed that a stochastic approach (which includes spatial variability of material properties) can describe mechanisms that dominate the behaviour of the soil as a response to loading. This behaviour can be leading in the determination of the stability in certain cases of variability. For example, this variability can lead to the failure of structures with a predominantly stable state of sand.

1.1 Stochastic approach

When analysing the structure response of a soil that is described in a deterministic way, the analysis will result in a single factor of safety. Opposite to the deterministic approach is the stochastic approach, which involves randomness in an attempt to reproduce the influence of natural variability in the soil. The statistical distributions of the geotechnical properties that can be derived from the available measurements are used to generate random fields of data that satisfy the measured statistics. In this way heterogeneity of the soil is modelled without the need to measure the exact soil state at every location in the soil domain.

The use of random fields to describe soil properties comes with an extreme increase in computational work to be done. In addition to this, analytical solutions can not be used in combination with random fields. Therefore, structural analysis of stochastic fields asks for a finite element approach, which again increases the amount of computational work. Because of the variability that will be present in the random fields (all random fields will give different results) finite element programs need to analyse multiple realisations to give a reliable expectation of the correct result. The better the stochastic reproduction of the soil, the better the estimate of the correct result within a certain number of times that the program is run.

To simulate the soil as accurate as possible, all available information on the soil needs to be accounted for in the simulation. Unconditioned simulation, as it has been used in preceding research (e.g. [Hicks and Onisiphorou, 2005], [Hicks and Spencer, 2010]), uses the (spatial) statistics that are derived from the available information to simulate soil state fields. These unconditioned random fields honour the statistics of the measurements, but not the measurements themselves. Because the information that the in-situ measurements give are not incorporated in the random fields, the range

of possible realisations is larger than strictly necessary. A possible improvement to reduce the range of possible realisations, is to include the information of the actual measurements in the random field simulations by conditioning the random field at the locations of the measurements. In this way the range of possible random field simulations to be generated, is reduced and the uncertainty in the result of the application of the fields in finite element calculations will decrease.

1.2 Research questions

The current status of research is that the statistical characterisation of cone penetration test (CPT) profiles is used to generate unconditioned random fields. These random fields simulate the variability of sand deposits that are uniform in the sense of material properties and are variable in state. The actual measurements on which the statistics are based are not incorporated in the realisations. Main research objective of this project is to include the actual profiles in the random fields to realise a conditioned simulation of the sand state of the deposit. Therefore the research questions are formulated as follows;

- How can random fields be conditioned by CPT profiles?
- How does the conditioning of the random fields decrease the range of possible simulations?
- What are the requirements for site investigation for the conditioning to be useful?
- Can the conditioning be applied to a test site?

By answering these questions, it is the objective to develop an algorithm for conditional simulation of sand state fields, with CPT profiles as conditioning data. Although the ultimate objective is to condition 3D random fields for the use of finite element analyses, only 1D and 2D cases are discussed in this report.

1.3 Outline of the report

This report describes the necessary work in order to generate random fields constrained by the available CPT-profiles. To illustrate the conditioning and to demonstrate that the conditioning can be applied an actual site, a test site is used. The data of this test site are used as characterisation and simulation examples of the conditioning method that is discussed. To be able to use the test data, the data need to be calibrated to enable interpretation. The calibration and interpretation of the test data are part of this report. The work for this report can be split into three parts:

1. calibration of the soil model (to be able to interpret the CPT data with respect to state parameter);
2. determination of statistical properties of the test site (to be used in the simulation);
3. generation of conditioned random fields and evaluation of the conditional simulation algorithm.

The first two parts have been the subject of a preceding MSc thesis by Bakhtiari [2006] and a code for statistical evaluation is already available. This code has been developed by Gitman [2006] as a continuation of the work by Wong [2004]. The MSc thesis and the code have been the leading references for the work that has been done on the first two parts. The third part of this work is the application of the results from the first two parts in the construction of conditioned random fields. It presents a technique to condition a random field by the post-processing of unconditioned random fields. The conditioning performance is evaluated with respect to uncertainty and computational expense.

The report starts with the description of some fundamental definitions and mechanisms that are used throughout the report, followed by a theoretical background of the main aspects involved in this report in chapter 2. After this, the work on the three different parts is described and discussed. Chapter 3 describes the NorSand constitutive model and its calibration. Chapter 4 describes the statistical interpretation of the CPT profiles after which the data that are needed for the conditioning are derived. The random field generation and conditioning algorithm are discussed, applied and evaluated in chapter 5, after which the results of this report are summarised in the conclusions in chapter 6. The recommendations in chapter 7 describe the possible points of improvement on the work for this report.

Not all findings have been added in the main part of the report. Some alternative methods, considerations and ideas that were expected to be promising, but which are not evaluated enough to become part of the main report, are gathered in several appendices. In the light of possible improvements in methods and algorithms, the considerations in the appendices might be worth looking at.

1.4 Test site

The test site that is used for this report is a site in the harbour of Rotterdam. Triaxial compression tests and cone penetration tests (CPT's) from a sand fill for a future quay wall are available for the calibration of a constitutive model and for the interpretation of the in-situ state of the material. The location where the tests come from is a future quay wall that is part of a container terminal. Land for the entire project is reclaimed from the North Sea.

The building material for the land is sand. The sand that is needed for the project is dredged from a site in the North Sea and will be referred to as North Sea sand or NZ-sand. The sand is dredged and transported by suction hopper dredgers. The placement technique that is used depends on the water depth; dumping in deep water, rainbowing when the water is not deep enough for dumping and pipeline transport when the site is no longer accessible for rainbowing. The sand has been placed at a level of 11m below chart datum to 5m above chart datum (NAP). Before the in-situ tests that are used in this report were carried out no ground improvement has taken place. As far as known by the author, no further ground improvement has been carried out afterwards as well.

The reclaimed land is part of a new harbour area and will be used as a quay. At the locations of the in-situ measurements that are used in this report, a quay wall with a gantry crane will be constructed. The sand considered in this report was placed in a strip of approximately 2 km in length with a width of 140m. The initial level of the reclaimed land was constructed at 5.40m +NAP. CPT's were taken in two rows (one at the location of the quay wall and one at the axis of the crane rail). Afterwards the level was changed.

Chapter 2

Conventions, basic equations and mechanisms

Before the project-specific part of this report starts, some basic definitions need to be clarified. This section gives a short overview of the definitions that form the basic elements of this report. The definitions of the terms, as well as an explanation of the basic mechanisms and physical equations are given in this section.

2.1 General

2.1.1 Sets and series; spatial correlation

Data sets: Data points in a set are independent realisations of a certain distribution. This means that the different points are spatially independent and therefore the order in the set is not important. An example of this is the subsequent result of throwing a dice; the order of the results is not important and the value of a point has no influence on the subsequent value. Data sets are independent realisations of a certain distribution.

Data series: A data series is a series of data points forms a sequence in time or space. The cone penetration profiles that are evaluated in this report for example are data series. This means that the points are depth-related and order-dependent, implying a certain trend or spatial relation between the points in the series. For the description of data series, a the relation between the data points as a function of their location is important and needs to be incorporated in the description.

2.1.2 Deterministic against stochastic approach

Heterogeneity is a subject that is often avoided by the assumption of limited influence of the variations in the values considered. Spatially variable (heterogeneous) materials are then described by a characteristic value, representing the properties over a domain in which the properties described are considered to be close enough to the characteristic value to discard the small local differences.

The method in which such a generalisation is made is referred to as deterministic method and implies that the properties are described by a determined value. The big advantage of a deterministic approach is that it can be used in analytical solutions of engineering problems and is easy to work with. The deterministic value can be the expected value in the domain (the mean) or a certain lower or upper bound value to include a certain probability. Including this probability leads to the possibility of probabilistic approach with probabilities on different expected behaviour. The influence of spatial variability however is not included in such an approach and influences of this variability can often not be analyzed with a deterministic description of the domain.

In case the variability is desired to be part of the characterisation, measurements of this variability are required. Because accurate measurements are only available for a limited part of the site (CPT measurements are 1D profiles in a 3D domain of interest), not all variations in the domain can be measured. Therefore, variability has to be synthesised with the use of a random process. This synthesised variability needs to satisfy the statistics of the domain to describe the variability in the correct way.

Therefore, the statistical properties (statistical distribution and spatial correlation) need to be determined from data that is available in the analysed domain. This approach of generating realisations of the domain (random fields) with equal statistical properties is a stochastic approach. The generation of random fields is not obvious and different methods are available, usually differing in accuracy of reproducing the statistical properties and in computational expense. Section 5.1 elaborates on the methods to generate random fields.

2.2 Soil mechanics

This section describes some of the soil mechanics *mechanisms* that will be used later in the report. Because these mechanisms are of importance in the understanding of the specific constitutive model that will be used, a definition is given before continuing with the description of the application. Often different definitions of a single mechanism exists, of which only the relevant definitions are discussed here. This section gives a short description and definition of the mechanisms as used in this report.

2.2.1 Stress and strains

A compression-positive sign convention is used throughout this report. This means that compressive stresses are positive and a decrease in volume gives positive volumetric strains. All laboratory tests are done under triaxial loading where $\sigma_2 = \sigma_3$. This significantly simplifies the equations of the NorSand soil model (described later in 3.1). Based on principle stress and strain and the triaxial loading conditions in both laboratory tests and in-situ conditions, the different stress and strain definitions are as follows:

σ_1, σ_3	principle total stresses	
σ'_1, σ'_3	principle effective stresses	
ϵ_1, ϵ_3	principle strains	
u	water pressure	
p	mean total stress	$\frac{1}{3}(\sigma_1 + 2\sigma_3)$
p'	mean effective stress	$\frac{1}{3}(\sigma'_1 + 2\sigma'_3) = p - u$
q	deviatoric stress	$\sigma_1 - \sigma_3 = \sigma'_1 - \sigma'_3$
τ	shear stress	$\frac{1}{2}q = \frac{1}{2}(\sigma_1 - \sigma_3)$
η	stress ratio	$\frac{q}{p'} = \frac{3(\sigma'_1 - \sigma'_3)}{\sigma'_1 + 2\sigma'_3}$
ϕ	friction angle	$\sin^{-1}\left(\frac{\sigma_1 - \sigma_3}{\sigma_1 + \sigma_3}\right)$
ϵ_v	volumetric strain	$\epsilon_1 + 2\epsilon_3$
ϵ_q	deviatoric strain	$\frac{2}{3}(\epsilon_1 - \epsilon_3)$
n	porosity	pore volume over bulk volume V_{pore}/V_{bulk}
e	void ratio	pore volume over grain volume $V_{pore}/V_{grain} = \frac{n}{1-n}$

The stress ratio η is the slope of the failure line in the $q-p'$ plane and therefore represents a friction angle ϕ in the $\tau - \sigma'_1$ space. Reworking the equations for the friction angle in the τ-σ the (Mohr-Coulomb) and the stress ratio η in the q-p' plane gives equation 2.1:

$$\phi = \sin^{-1}\left(\frac{3\eta}{6+\eta}\right), \quad \eta = \frac{6\sin\phi}{3-\sin\phi} \tag{2.1}$$

2.2.2 Mechanisms

Throughout the report a number of mechanisms are used of which multiple definitions exist. This section describes the general mechanisms used, together with their definition and conventions as used in this report.

Dilatancy D: Dilatancy is the effect of volume change that occurs when a particular material is sheared. Dilatancy is the general term for both the increase and decrease of volume and is used for both the absolute amount of volume change from the initial stage and the rate of this change. In this report the dilatancy is defined as the rate of the volume change relative to the deviatoric strain rate. Because of the compression-positive convention, positive dilatancy D corresponds to a decrease in volume. Equation 2.2 gives the formal definition. Next to the term dilatancy, the adjectives 'dilatant' and 'contractant' are used to denote negative and positive dilatancy D. In other words, dilatant behaviour indicates volume increase and contractant behaviour volume decrease at shearing.

$$D = \frac{\dot{\epsilon_v}}{\dot{\epsilon_q}} \tag{2.2}$$

Because the dilatancy is the ratio of volumetric and deviatoric strain, and total strain can be divided into elastic strain (ϵ^e) and plastic strain (ϵ^p), a plastic component for dilatancy can be defined . This plastic dilatancy D^p is defined by equation 2.3.

$$D^p = \frac{\dot{\epsilon}_v^p}{\dot{\epsilon}_q^p} \tag{2.3}$$

To be able to deal with the plastic component of the dilatancy, it has to be possible to distinguish between the plastic and elastic components of both volumetric and deviatoric strain. For this the stiffness moduli need to be incorporated in equation 2.2. In this report this has not been done; the plastic dilatancy is considered to be equal to the total dilatancy. This can be justified arguing that the plastic dilatancy is considered to be the leading part of the total dilatancy. The consideration of the stiffness parameters would imply the introduction of two more parameters G and ν in the interpretation itself.

Critical state: Critical state is the state in which the soil is at constant stress and volumetric strain for continuing shear strain. This condition was generalised by Jefferies [1993] in the two following axioms:

1. *Axiom 1. A unique locus exists in q,p',e-space such that soil can be deformed without limit at constant stress and constant void ratio; this locus is called the critical state locus (CSL)*

$$\exists C(e, q, p') \,|_{\dot{p}=0}| \ni \dot{\epsilon}_p \equiv 0 \wedge \ddot{\epsilon}_p \equiv 0 \forall \epsilon_q \tag{2.4}$$

2. *Axiom 2. The CSL forms the ultimate condition of all distortional processes in soil, so that all monotonic distortional stress state paths tend to this locus;*

$$\psi \to 0 \text{ as } \epsilon_q \to \infty \tag{2.5}$$

As mentioned in Axiom 1, the critical state is a unique locus in q,p',e-space. The exact location of the critical state locus depends on the constitutive model used to describe the soil behaviour. This report uses the NorSand model as constitutive model (see section 3.1). This model uses equation 2.6 to define the void ratio at the critical state as a function of p'. Γ and $\lambda_{cs,e}$ are material properties in this function. Γ is the critical void ratio at reference stress $p' = 1$kPa, λ_{cs} is the slope of the critical state line in either $e - ln(p')$ or $e - log(p')$ space.

$$e_{cs} = \Gamma - \lambda_{cs,e} ln(p') \tag{2.6}$$

This equation is valid only over a confined range of $\ln(p')$, because the behaviour of the soil is influenced by particle crushing at higher stress conditions and other mechanisms that become dominant at low stress ranges.

State parameter ψ The concept of the state parameter was introduced to combine stress state and void ratio into a single parameter [Been and Jefferies, 1985]. The state parameter is by definition the difference between the void ration e and critical state void ratio e_{cs}:

$$\psi = e - e_{cs} \tag{2.7}$$

This definition results in a negative state parameter for dense material and a positive state parameter for loose material. The advantage of the state parameter is that the state of the soil with respect to the critical state is defined by a single parameter. An illustration of the state parameter and its relation with the void-ratio and the critical state line is given in figure 2.1. At higher stresses, the slope of the critical state line increases as an effect of grain crushing.

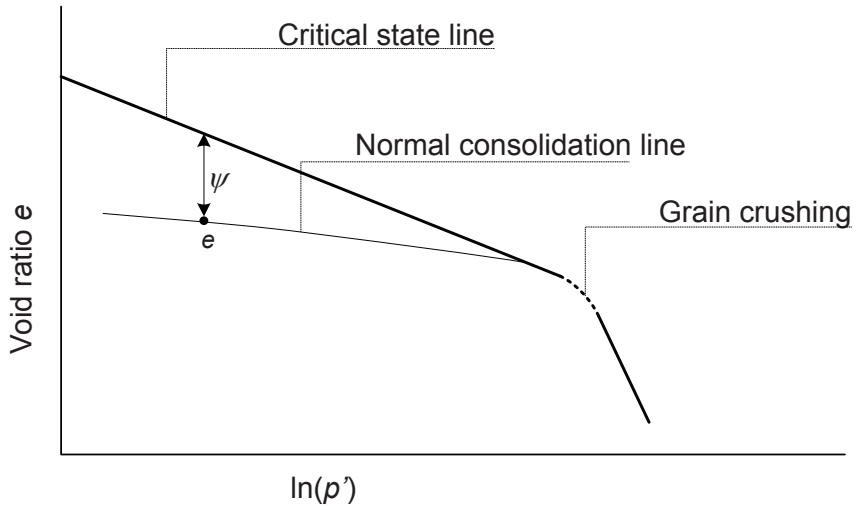

Figure 2.1: Example of the critical state line and the definition of the state parameter with respect to uniform stress p' and void ration e.

2.3 Statistics theory

As briefly mentioned above, a data series involves a distribution of points over a certain range and a correlation between the points based on their location. The distribution of the points over the domain is described by the distribution function (point statistics), whereas the spatial correlation is described by a correlation structure which generalises the dependency of a point on its neighbouring points.

Vanmarcke [1977] stated that a soil property can be stochastically described by three parameters:

- mean μ
- standard deviation σ
- scale of fluctuation θ

The mean and standard deviation are both statistical properties that are independent of the location of the data points. The scale of fluctuation is a property that describes the spatial variability of a soil; it represents the range over which the properties depend on their neighbouring points as a function of their mutual distance. Throughout this section all functions will be clarified using a single cone penetration test profile (tip resistance q_c) as an example. All examples are therefore referring to the example profile as it is given in figure 2.2.

2.3.1 Mean and trend lines

The mean of a set of data is defined as the sum of all data points divided by the number of data points. This gives a single-value representation of the average value of the data. It can be seen as a trend line

of the zeroth degree that actually does not represent a trend at all. It is therefore suitable for a dataset without any spatial relation between the data points. When the data forms a data series instead of a set of points, a trend in the data can be present. The mean value of these data neglects the presence of this trend and therefore a polynomial can be fitted to the data series. A possible way to find the polynomial is by a least-square fit of the data. This N-degree polynomial describes the trend of the data in N+1 degrees. The mean value of the data series is equal to the zeroth-degree polynomial fit. The first degree polynomial is the linear regression line. The polynomial trend line can be used to remove the trend of the data series that is needed to determine the scale of fluctuation. An example of the zeroth order regression line (the profile mean) and the first order regression line (the linear trend line) is given in figure 2.2.

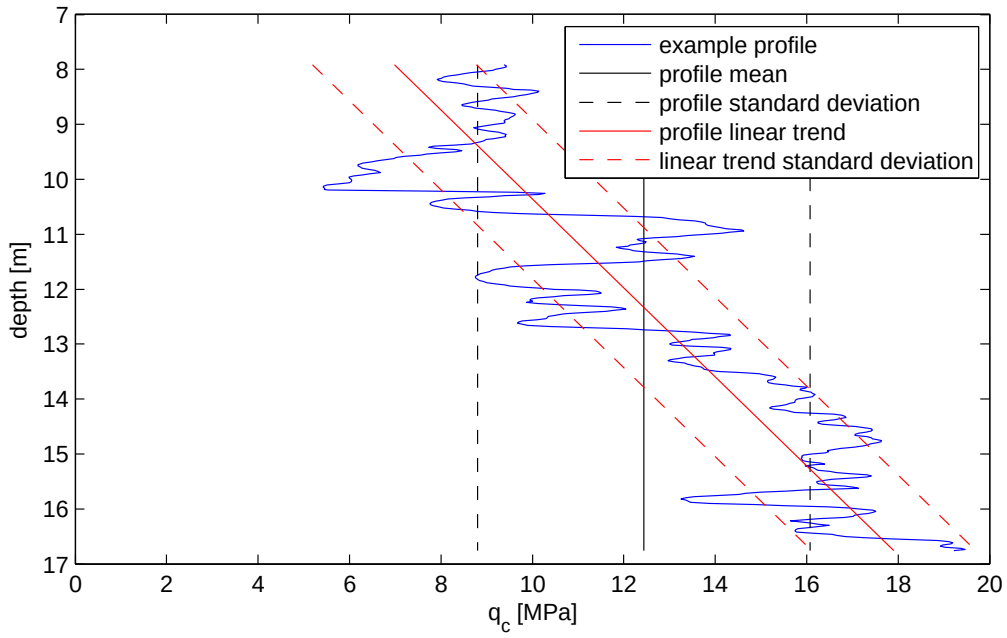

Figure 2.2: Profile that will be used as an example for all the statistical processes, together with it's mean, first-order trend line and standard deviation with respect to both.

2.3.2 Local average

The local average (or moving average) $Z_D(x)$ over a (continuous) profile $Z(x)$ is found when the average over an averaging domain D is taken over the initial profile. The averaging domain D is the range over which the average is taken and usually forms the range $x - D/2$ to $x + D/2$, see equation 2.8.

$$Z_D(x) = \frac{1}{D} \int_{u=x-D/2}^{u=x+D/2} X(u)\, du \tag{2.8}$$

In figure 2.3 the moving average over the example profiles is used to determine the local average profile for different domains. The CPT profiles are discrete profiles with a data-spacing d. The number of readings over which the average is taken is denoted by n. This gives an averaging range D of $D_n = (n-1)d$.

Another way of looking at the local average, is by considering the moving average as the result of a convolution of a uniform distribution $U(-D/2, D/2)$ over the profile $Z(x)$. This is a somewhat inconvenient way of expression, but gives the possibility to change the uniform distribution that is used for the average by another shape function ($f(D)$) to give a weighted averaging with a weighting factor as a function of the domain D around location x as given in equation 2.9. For example, a normal distribution function could be used instead of the uniform distribution to determine the moving average. In this way, the data points close to x have more influence on the average than the points further away.

$$Z_D(x) = (Z(x) \star f(D,x)) = \int_{\zeta=-\infty}^{\zeta=\infty} Z(\zeta) f(D, x-\zeta)\ d\zeta \tag{2.9}$$

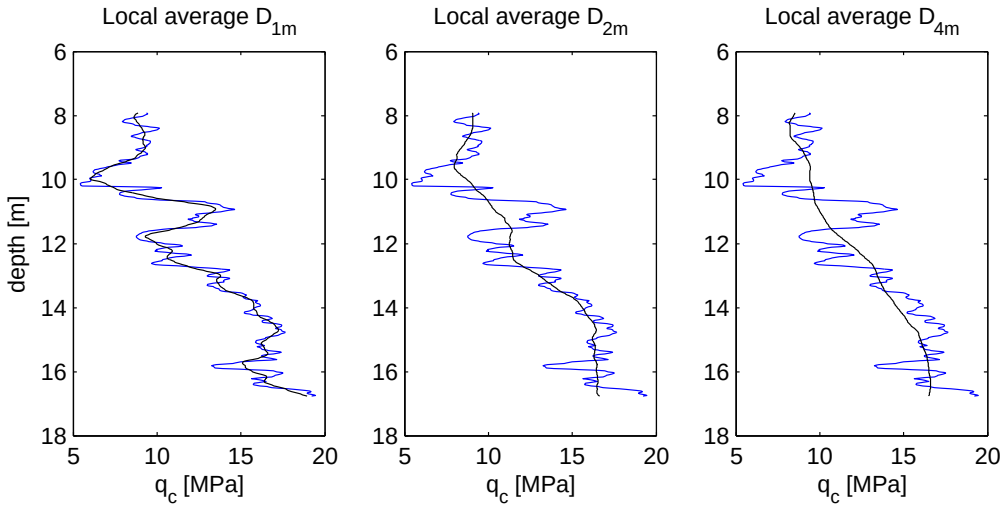

Figure 2.3: Local average over the profile with averaging domain of 1m, 2m and 4m. The averaging uses equal weights over the full averaging domain. This means that the averaging distribution ($f(D)$ from equation 2.9) is uniform $U(-D/2, D/2)$ over the range $[-1/2D; +1/2D]$.

The moving average is related to the variance function. The standard deviation of the averaged profile as a function of the averaging domain gives the variance function. The variance function is used to determine the scale of fluctuation later in this report.

2.3.3 Statistical distributions

A set of data consists of a number of different values. These values are usually not all the same and are distributed over a certain range. The range over which the data are distributed and the way the data are distributed over this range is described by the statistical distribution. The statistical distribution is a function of usually two parameters and a variable. The function can be expressed in two different ways; the cumulative distribution function $CDF(z)$ gives the expectation of a data point to be smaller than the variable z on a scale from 0 to 1; the probability density function $PDF(z)$ gives the probability that the data point is located at variable z. The area under the probability density function is equal to 1. Integration of $PDF(x)$ over the range $-\infty : z]$ gives $CDF(z)$;

$$CDF(z) = \int_{-\infty}^{z} PDF(\tau) d\tau \tag{2.10}$$

Both $PDF(z)$ and $CDF(z)$ will be used in this report to indicate the distributions. The probability density function is a very indicative function to visualise the distributions, but is more difficult to work with. The cumulative distribution function is easy to produce for a given set of data by plotting the observed points against their relative ranking.

2.3.4 Theoretical distribution functions

The experimental distribution of soil properties show resemblance with a number of theoretical distribution functions. Because the number of data points that form the observed distribution is always finite, the perfectly smooth true distribution will never be realised. However, the observed distribution can be approximated with a theoretical distribution for which an analytical function is available. Not all theoretical distributions come close to the possible true distributions of soils. Four of them that are sometimes suitable for the description of soils are Normal, Lognormal, Beta and Gamma-distributions. Their mathematical characteristics are described in appendix A.

2.3.5 Generic distribution function

The distribution that best describes the data is of importance in order to be able to generate representable data for the random fields. This is usually done based on the distribution equation that comes closest to the observed distribution. An alternative is to use the distribution that is actually observed in the field, the generic distribution.

To visualise the generic distribution from a profile consisting of N data points, the data points are sorted in ascending way and plotted against the expected CDF, given by the series

$$\frac{1}{2N}, \quad \frac{3}{2N}, \quad \frac{5}{2N}, \quad \ldots, \quad \frac{2N-3}{2N}, \quad \frac{2N-1}{2N}. \tag{2.11}$$

In this way a distribution graph $CDF(Z)$ is constructed that describes the distribution of the dataset without generalisation. To generate random numbers that correspond to this generic distribution graph, random numbers with a standard-uniform distribution are generated. These numbers are transformed into probabilities and from the probabilities the initial data points are read from the generic CDF graph (see figure 2.4).

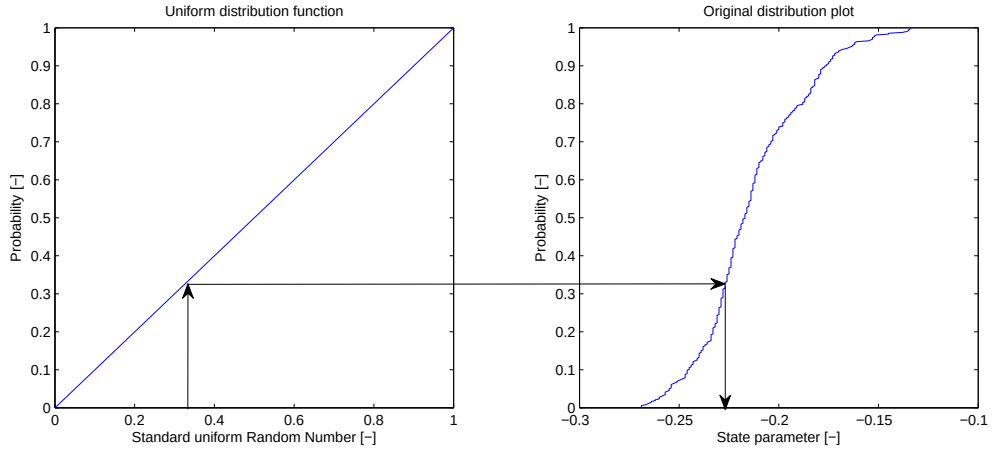

Figure 2.4: Method for the simulation of random numbers from an experimental distribution function.

This principle can not only be used to generate random numbers from an arbitrary distribution function, but also to transform any generic distribution function into its uniform transform [Journel, 1994]. In the same way, the data with a generic distribution can be transformed in for example a standard-normal distribution and back. This has big advantages with respect to the conditional simulation that requires a normal distribution of the data (see section 5).

2.4 Spatial variability

In addition to the point statistics (mean and standard deviation, type of distribution function) that describe the not-spatially dependent properties of sets and series, the spatial statistics (relation between the points in a series dependent on the (relative) location) are important for the correct description of a field. The variability of a field can be described by a function. In this report the term correlation structure is used for all functions describing the spatial variability of a field. Correlation function $\rho(h)$, covariance function $C(h)$, variance function $\Gamma(D_n)$ and variogram $\gamma(h)$ are different correlation structures and all contain the same information. The correlation structure contains the information about the scale and shape of the correlation between spatially distributed points and is a function of point distance or domain size. These different functions are derived and discussed in this section. At the end of the section the methods to determine the correlation structure parameters are discussed.

Covariance function: The variance is the 'second moment' of a data set, which means that it is the expected value of the squared difference from the mean of a data point:

$$var(X) = E[(X_i - E(X))^2] \tag{2.12}$$

To compare two different data series (X and Y), the variance can be applied on both series in the following way, creating the covariance:

$$cov(X,Y) = E[(X_i - E(X))(Y_i - E(Y))] \tag{2.13}$$

The covariance is used to indicate the resemblance between two data sets. Instead of two different data sets, the covariance of a data set with itself can be determined as the auto-covariance or cross-covariance;

$$cross - cov(X,X) = E[(X_i - E(X))(X_j - E(X))] \tag{2.14}$$

In the case of cross-covariance, no spatial properties in the data are considered and the average of all different combinations of data points is looked at. When the data form a series with spatial coordinates, the covariance between two points in the series can be expected to be dependent on the spacing between the two points. Therefore, instead of determining the covariance as a single characteristic value to characterise the relation between all data points, the covariance is determined as a function of the distance between the points. In this way the covariance function $C(h)$ is created with lag distance h as the distance between two points.

$$C(h) = E[X(z) \cdot X(z+h)] - E[X(z)]^2 \text{ for all } z, z+h \in D \tag{2.15}$$

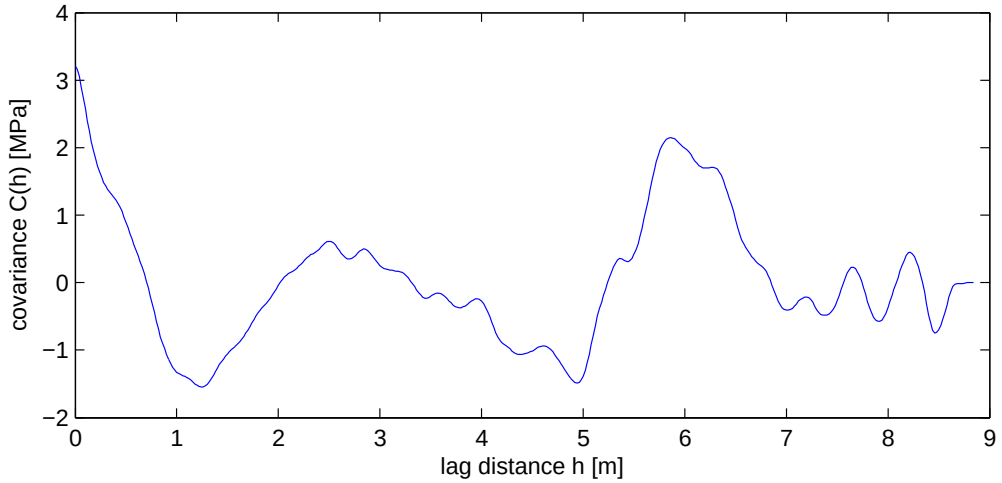

Figure 2.5: Covariance function $C(h)$ over the example profile. The trend has been removed by subtraction of the least-square fit of a first order polynomial to the profile.

The covariance function is defined on the assumption of a stationary data series, which means that the expected value E[$X(z)$] is independent of z. In practice, this means that the depth-dependent trend that might be present in the profiles has to be removed. To remove the trend in the profile, the trend first has to be determined. To be able to determine the trend, the shape of the trend line needs to be known. In theory, a trend of every shape can be fitted to the data. In this report, a linear depth-dependent trend is fitted to the data. To determine the depth trend $T(y)$ a first-order polynomial ($T(y) = ay + b$) is fitted to the data by least-square estimate. This trend is then subtracted from the profile to obtain the zero-mean stationary profile.

2.4.1 (Semi-)variogram

The variogram $\gamma(h)$ is a method to present the spatial variability in a similar way as the covariance function. The definition of the variogram is

$$\gamma(h) = \frac{1}{2} E\left[\left(X\left(z+h\right) - X(z)\right)^2\right]. \tag{2.16}$$

This definition can be rewritten with the definition of the covariance function $C(h)$ (equation 2.15) into:

$$\gamma(h) = C(0) - C(h) \tag{2.17}$$

Although the definition of the variogram is very simple, it can be quite difficult to find a decent variogram based on real data. This is the effect of large fluctuations in the differences between two points that are to be compared. To find an experimental variogram, the square of the difference between each possible pair of points has to be plotted against the distance between these pairs. The expectation of all these squared differences at the same distance from one to another gives the experimental experimental variogram $\gamma(h) = C^*(0) - C^*(z)$. The experimental variogram for the example profile (figure 2.2) is given in figure 2.6. Usually, the variogram is fitted by a theoretical variogram that can be described by a function $f(z)$ for the ease of application.

The variogram is used as the input for the correlation structure in the kriging estimation later in this report. It contains the exact same information as the covariance function.

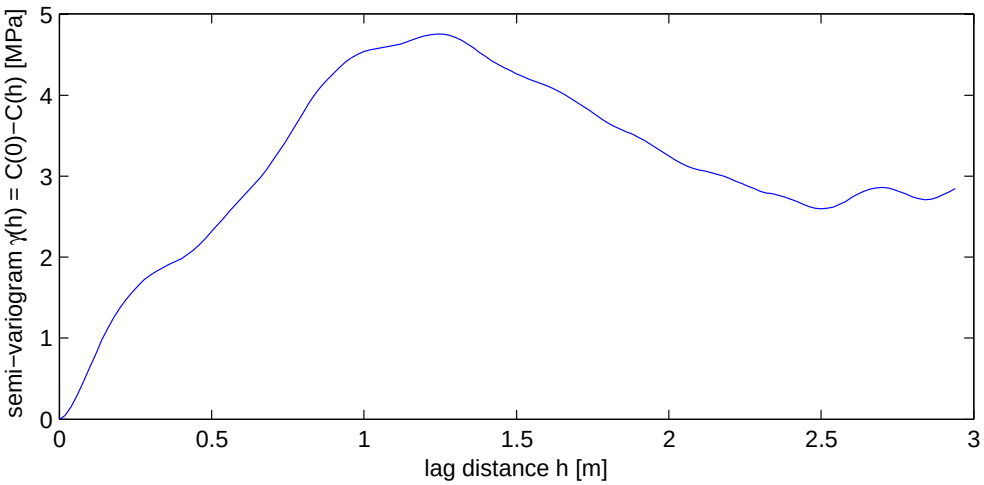

Figure 2.6: Semi-variogram $\gamma(h)$ of the example profile.

2.4.2 Variance function

The variance function is based on the difference in variance between the original data and a moving average smoothed version of this original data. The area over which the averaging takes place is the variable in the variance function. The ratio between the original variance and the moving average variance is a measure of the scale of variation of the data. By averaging the data over an averaging domain D_n, the variations on the small scale (within D_n) are removed. The variance function expresses in general the ratio of the variance that has a larger scale of fluctuation then the averaging domain.

To find the variance function, a moving average series for the CPT-profile is obtained where the averaging domain D_n (the domain over the lag distance h) is the domain D between n data points. When d is the spacing distance between the data points in the CPT-profile, the size of the averaging domain D_n equals $(n-1)d$. The variance σ_n^2 over the averaged series is divided by the initial variance σ^2 of the original profile to obtain the variance function Γ;

$$\Gamma\left(D_n\right) = \frac{\sigma_n^2}{\sigma^2} \tag{2.18}$$

When the variance function is determined for the full range of possible lag distances D_n, a graph of the variance function against the averaging domain D_n can be constructed (figure 2.7). For an averaging domain D_n=0 the variance function Γ is 1 because $\sigma_n^2 = \sigma^2$. The variance function decreases towards zero with increasing averaging domain because a larger averaging domain decreases the fluctuations in the profile.

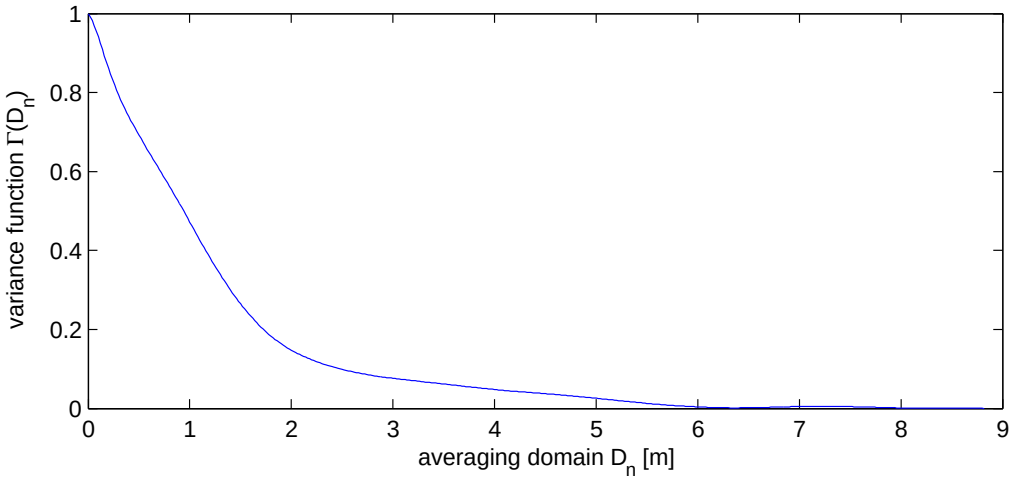

Figure 2.7: Variance function $\Gamma^2(D_n)$ over the example profile.

The variance function is related to the covariance function as described by equation 2.19. Because the variance function intergrates the covariance function over the domain $[0; h] = D_n$, the variance function $\Gamma(D_n)$ is much smoother than the covariance function $C(h)$. Despite the difference in shape, both functions contain the exact same information about the correlation structure.

$$\Gamma(D_n) = \frac{2}{D_n\sigma^2}\int_0^{D_n} C(h)dh - \frac{2}{D_n^2\sigma^2}\int_0^{D_n} hC(h)dh \tag{2.19}$$

Scale of fluctuation: The scale of fluctuation θ was described by Wickremesinghe and Campanella [1993] as the distance over which the data show a strong correlation. This scale of fluctuation can be used as a characteristic value in the description of soil variability. For large averaging ranges D_n the multiplication of the variance function with the averaging range gives the scale of fluctuation θ.

$$\theta = \Gamma^2(D_n)D_n \qquad \text{for larger } D_n \tag{2.20}$$

The size of the domain D_n at which the scale of fluctuation can be determined accurately is somewhat vague and depends on the scale of fluctuation itself, the shape of the correlation function and the length of the profile over which the scale of fluctuation is determined. The length of the profile that is evaluated is of importance because the variance function will equal zero when the average distance equals the profile length. As an effect of this, the graph of $\Gamma(D_n)D_n$ does not converge to the scale of fluctuation, but to zero for larger averaging domain D_n (see figure 2.8). Wickremesinghe and Campanella [1993] do not quantify the size of D_n at which $\Gamma(D_n)D_n$ is accurate enough to give the scale of fluctuation.

Vanmarcke [1984] gives a more distinctive definition of the scale of fluctuation θ. This θ is the same scale of fluctuation as discussed by Wickremesinghe and Campanella [1993], but is defined as follows;

$$\theta = \lim_{D_n\to\infty} D_n\Gamma(D_n) \tag{2.21}$$

This, however, can be a somewhat impractical definition in case of small domains to be analysed. The scale of fluctuation can be determined in different ways as will be discussed in the following section.

Scale of fluctuation θ from the variance function: To be able to determine a characteristic value from the variance function graph, it is multiplied by averaging domain D_n. The result is a graph starting at 0 and increasing with increasing averaging domain to a maximum. For larger values of D_n the graph gives the scale of fluctuation θ [Wickremesinghe and Campanella, 1993].

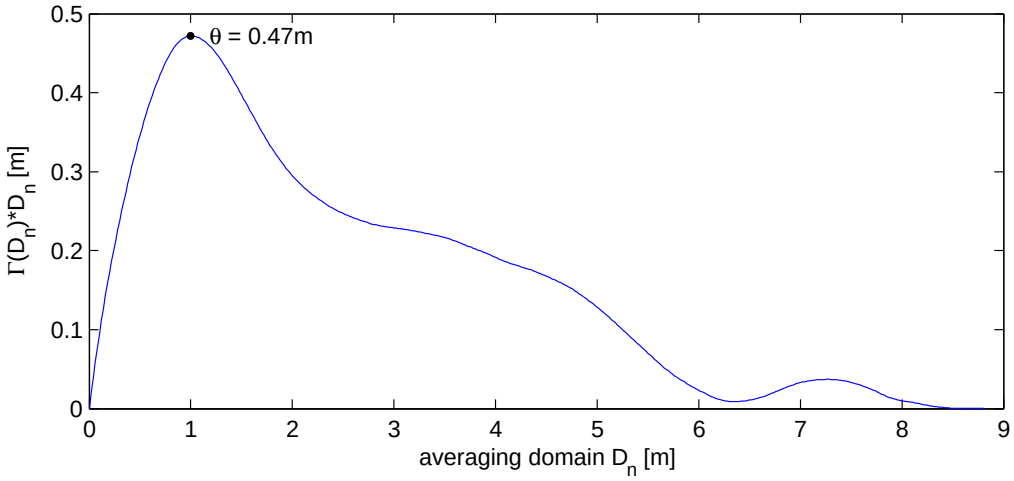

Figure 2.8: Scale of fluctuation $\theta = \Gamma(D_n) \cdot D_n$ of the example profile. The scale of fluctuation for the example profile is 0.47m.

An alternative is to derive the experimental correlation function or experimental covariance function and fit a theoretical function to this experimental result. The best fit will give the scale of fluctuation as part of the theoretical function.

Theoretical correlation structures: All definitions of the different correlation structures given above can be used to produce the experimental (based on the available sample data), or generic correlation structures. These experimental correlation structures are the most likely correlation structures of the sample data. To be able to apply the correlation structures in random field generation or kriging (see chapter 5), a theoretical function $f(\theta, h)$ as a function of the scale of fluctuation θ and lag distance h is used. This function is an approximation of the experimental correlation structure and is given by an equation that can be applied in the simulation algorithms.

Different theoretical correlation structures can be used, with a variety of shapes. In this report, two types of correlation structures are used; the exponential correlation structure and an approximation of this exponential correlation function. The choice between these correlation functions is mainly based on the restrictions by the already existing codes for unconditioned simulation that are used further down in this report (section 5.2.2). Later in this report it is shown that the (approximate) exponential correlation structure is an adequate method to approximate the experimental correlation structure close enough. The correlation function of the exponential correlation function $C(h)$ is given by

$$C(h) = \sigma^2 exp\left(-\frac{2|h|}{\theta}\right). \tag{2.22}$$

The exponential variance function that corresponds to this function can be determined when equation 2.19 and 2.22 are combined. The exponential variance function is given by

$$\Gamma(D) = \frac{\sigma^2\theta^2}{2D^2}\left[\frac{2|D|}{\theta} + exp\left(\frac{-2|D|}{\theta}\right) - 1\right]. \tag{2.23}$$

This function can be approximated by a correlation function that is given as an approximation of many common wide-band processes by Vanmarcke [1984]. This approximation has an advantage over the exponential correlation function when it is used to determine the conditional variance and conditional scale of fluctuation in the LAS method to generate 2-D random fields (see section 5.2.2). The approximate variance function is given by

$$\Gamma(D) = \left(1 + \left(\frac{D}{\theta}\right)^m\right)^{-1/m} \qquad \text{with } m = 3/2. \tag{2.24}$$

In combination with 2.19, the corresponding approximate covariance function can be derived to be

$$\rho(h) = \left[1 - \frac{m-1}{2}\left(\frac{h}{\theta}\right)^m\right]\left[1 + \left(\frac{h}{\theta}\right)^m\right]^{-(1/m)-2}. \tag{2.25}$$

The quality of the approximation is shown in figure 2.9, in which the exponential correlation function and variance function are plotted together with the approximations given by equations 2.24 and 2.25. In this example, the scale of fluctuation is 1m.

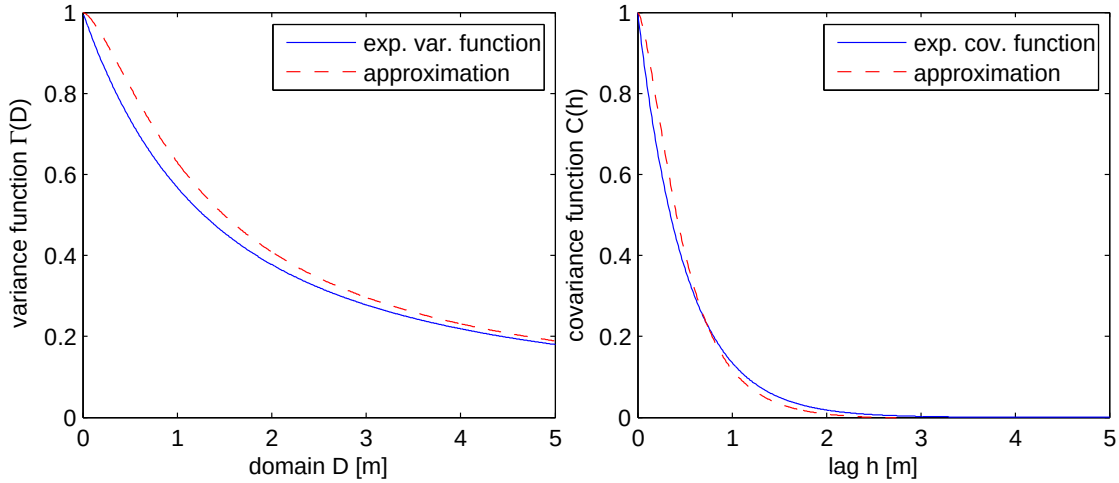

Figure 2.9: Difference between the exponential correlation structure and the approximations of the exponential correlation structure given by equations 2.24 and 2.25

2.5 Parameter estimation

In case a theoretical distribution function is desired to describe an experimental distribution, the theoretical distribution function needs to be calibrated against the test data. This means that for different theoretical distribution functions the parameters need to be estimated in order to fit the experimental data. In addition to this the distribution function that can be fitted best to the data needs to be determined. The procedure that is used to estimate the parameters is discussed in this section.

2.5.1 Maximum Likelihood Estimator

The true distribution of the data is estimated by a best fit of an expected distribution through the sample data. The expected distribution is given by the probability function that includes function parameters. The function parameters need to be determined to fit the sample data as well as possible. A best fit is made with the use of Maximum Likelihood Estimation (MLE).
The procedure of the MLE is to define the function parameters Θ_i that form the distribution function with the highest probability of generating the sample data. The concept is very straight-forward, but the implementation can be computationally complex. The mathematical background is described below.

Given is the theoretical probability density function

$$f(x|\Theta_1, \Theta_2, \ldots, \Theta_n) \tag{2.26}$$

in which $\Theta_1, \Theta_2, \ldots, \Theta_n$ are the n function variables of the distribution function $f(x)$. To determine the most likely values for the function parameters, the likelihood of generating the sample data $\hat{x}$ is maximised. The likelihood L, defined as the product of the probability density of each single sample point $\hat{x}_i$, is calculated as follows;

$$L = L(\hat{x}_1, \hat{x}_2, \ldots, \hat{x}_N | \Theta_1, \Theta_2, \ldots, \Theta_n) = \prod_{i=1}^{N} f(x_i | \Theta_1, \Theta_2, \ldots, \Theta_n) \tag{2.27}$$

The maximum likelihood estimators of all function variables are found by maximising L. To find the maximum value for L, it is easier to look at $\Lambda = ln(L)$;

$$\Lambda = ln(L) = \sum_{i=1}^{N} ln\left(f(\hat{x}_i | \Theta_1, \Theta_2, \ldots, \Theta_n)\right) \tag{2.28}$$

The maximum of Λ is found by the simultaneous solution to n equations such that;

$$\frac{\partial(\Lambda)}{\partial \Theta_j} = 0 \quad , j = 1, 2, \ldots, n \tag{2.29}$$

When the theoretical distribution function is used for $f(x)$ in equation 2.28 and equation 2.29 is satisfied, an analytical solution can be found for some of the used distribution functions. The results of the analytical solutons are the familiar definitions of the mean and standard deviation given in table 2.1. Beta and Gamma-distributions have no closed-form solution for the maximum likelihood estimation.

For the MLE of the Beta and Gamma distribution function, numerical approximations have to be used, which are not discussed in this report. To use the maximum likelihood estimation for the Beta and Gamma distributions the default commands in Matlab are used.

	MLE $\hat{\mu}$	MLE $\hat{\sigma}$
Normal	$\hat{\mu} = \frac{1}{N}\sum_{i=1}^{N} \hat{x}_i$	$\hat{\sigma} = \sqrt{\frac{1}{N}\sum_{i=1}^{N}(\hat{x}_i - \hat{\mu})^2}$
Lognormal	$\hat{\mu} = \frac{1}{N}\sum_{i=1}^{N} ln(\hat{x}_i)$	$\hat{\sigma} = \sqrt{\frac{1}{N}\sum_{i=1}^{N}\left(ln(\hat{x}_i) - \hat{\mu}\right)^2}$

Table 2.1: Maximum likelihood estimators for the Normal and the Lognormal distributions. Note that the analytical solution for the standard deviation is a biased estimator instead of the unbiased estimator that is used in the rest of this report.

2.5.2 Chi-square goodness of fit

The distribution function with its function parameters as determined by the maximum likelihood estimation can be tested for its accuracy. The Chi-square (χ^2) goodness-of-fit is a method that is used to give an estimate of how well a set of data points is described by a given distribution function. The observed probability O is compared with the expected probability E. E is the expected PDF of the data points given by the distribution that is tested for. To be able to compare the finite number of results of a test data set, the results are divided into n bins. The bins are equally distributed over the full range of data points. The number of points in bin i is used as the variable O_i. Based on the distribution function that is tested for, the expected number of points E_i is calculated. The square difference of E_i and O_i is taken and for scaling the result is divided by E_i. The sum of all these values is taken to end up with the χ^2-score as given in 2.30. The lower the χ^2-score, the better the fit.

$$\chi^2 = \sum_{i=1}^{n} \frac{(O_i - E_i)^2}{E_i} \tag{2.30}$$

The chi-square goodness of fit is meant to test the likelihood that a dataset is generated according to a certain distribution function. The hypothesis h_0 that the data set does indeed come from the

distribution is tested based on the chi-square distribution. If h_0 is true, the experimental distribution (O) will converge to the theoretical distribution (E) for an increasing number of points that is tested. This is the effect of the Law of Large Numbers. A similar effect is that the chi-square score is independent of the total number of points in the data set; the expected value for the difference between the observed bin count and the expected bin count $\mathrm{E}[|E_i - O_i|]$ increases with $\sqrt{(N)}$. Because $E_i \sim N$, the expected result for the chi-square score $E[\chi^2]$ is independent from N.

This independency is only valid when the experimental data come from the distribution that is tested for. If the true distribution is different from the theoretical distribution that is tested for, the observed distribution converges to this true distribution and gives a larger chi-square score for larger N. The problem with experimental data compared to synthetic data arises at the moment that the generic distribution, from which the data points come from, is not exactly similar to the theoretical distribution that is tested for. This will almost certainly be the case. Because the experimental data converge to its true distribution, the expected value for the chi-square score increases more and more. In other words, the more data points that are available from the generic distribution, the clearer it is that this set of datapoints does not exactly match the theoretical distribution.

Probability of the chi-square score: The chi-square score corresponds to a probability of the hypothesis of the distribution function being true. The cumulative distribution function described the probability that the theoretical distribution will give the observed distribution or a better one. This probability depends on the number of degrees of freedom ν. This is the number of bins minus the number of constraints. Constraints in this case are the estimated values for the distribution (2 parameters to describe the expected distribution) and the constraint of total probability ($\mathrm{P} \leq 1$). This means that the number of degrees of freedom ν is given by $\nu = n - 3$. The chi-square probability density function and chi-square distribution function are given by the following equations;
Probability density function

$$f(x,\nu) = \frac{1}{2^{\nu/2}\Gamma(\nu/2)} x^{\nu/2-1} e^{-x/2} \qquad \Gamma(\nu/2) = \int_0^\infty t^{\nu/2-t} e^{-t} dt \tag{2.31}$$

Cumulative distribution function

$$F(x,\nu) = \frac{1}{\Gamma(\nu/2)} \gamma(\nu/2, x/2) \qquad \gamma(\nu/2, x/2) = \int_0^{x/2} t^{\nu/2-1} e^{-x/2} dt \tag{2.32}$$

Although the chi square goodness of fit does not perform very well in case of testing experimental distributions, the method is used to determine the best distribution from the distyribution functions that were calibrated using MLE. The lowes chi square score has the highest probability of being the generic distribution and therefore is used as the distribution.

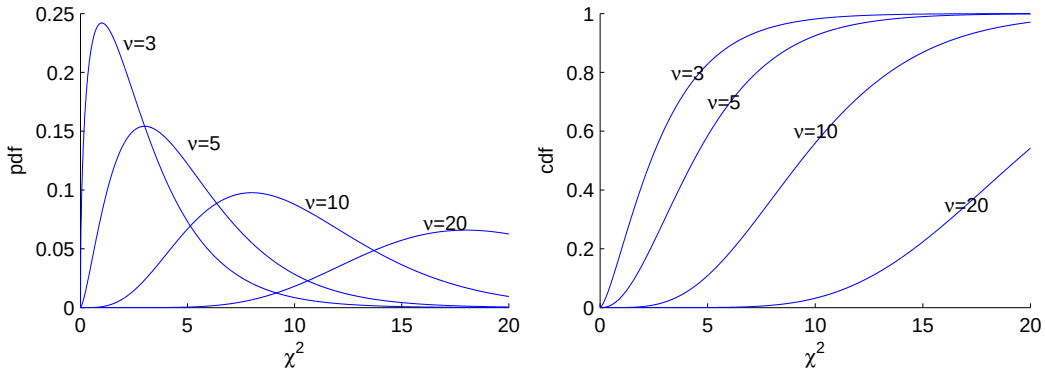

Figure 2.10: Chi-square distribution for different numbers of degrees of freedom. On the left the probability density function (pdf), on the right the cumulative distribution function (cdf) for different numbers of degrees of freedom ν.

Discussion of the chi-square method: Both strength and weakness of the method comes with the derivation of each squared difference by the expected count in the bin. An advantage of this is

that all differences in the bins are weighted equally in the result with respect to the expected result. This however gives problems when bins are expected to have a number of expected data points close to zero ($\ll 1$) and the observer number is 1 or more. In this case the ratio between the difference $(E-O)$ and the expected value E is very large, which results in a very large χ^2. Because of this effect, a single outlier can turn an almost perfect fit (χ^2) into a very bad fit with a very high (χ^2). In the default chi-square command in Matlab, this problem is partly solved by pooling each bin with less than 5 expected counts with the adjacent bin. In this way wider bins exit at the edges when a very small expected value is present. In the code by Gitman [2006] the problem is solved by not taking the bin in the summation for the chi-square score when the chance of a single point being located in that bin is smaller than 10^{-4}.

Chapter 3

Constitutive model calibration

The behaviour of a soil as a response to loading can be described by a constitutive model. This soil model is a generalisation of the sometimes complex and unpredictable behaviour of a soil. It therefore simplifies the material behaviour into a practical set of equations linking the state variables (e.g. stress, void ratio) together to derive the material behaviour with the use of the material properties (e.g. friction angle, elastic modulus).

In this report, the NorSand constitutive model is used to describe the behaviour of sand as a response to loading. This chapter gives an introduction to the NorSand model and describes the calibration of this model based on triaxial compression tests performed on the sand. An overview of the NorSand model is given in the first section of this chapter, after which the theoretical procedure of the calibration is presented. An output of the full calculation of the calibration procedure is given in the appendices. The specific appendices will be referred to in the text.

3.1 Introduction to the NorSand model

3.1.1 Why the NorSand model?

To be able to use sand state as a single variable to model the sand behaviour, a state dependent material model is needed that can be used to describe the behaviour of loose and dense sand. The original critical state soil models (original Cam Clay-like models) are not suitable to describe the behaviour of loose sands in general and liquefaction-related problems in particular. The NorSand model, a Cam Clay-like critical state constitutive model, can deal with loose sand states and liquefaction. Because relationships between the CPT tip resistance and the NorSand state parameter were determined and because the NorSand model can be calibrated against triaxial tests, NorSand is used as the constitutive model.

The NorSand model was first published by Jefferies [1993]. Since then several additions were made and the model can now be used with different definitions for critical state and hardening laws. In this report the version as published by Jefferies and Shuttle [2005] is used, together with Nova's rule that was present in the earliest versions of NorSand. The NorSand soil model is a critical state constitutive soil model similar to Cam-type soil models and contains the state parameter as a model variable. The advantage of the state parameter as a model variable is that the full state of the soil is described by this single variable. Because all other parameters are constant, this makes it possible to generate univariate random fields to describe the full behaviour of a soil with spatially variable state. This is a great advantage over models that need multiple parameters to describe the sand state.

3.1.2 Basics and equations of the NorSand model

As said above, the NorSand model is a critical state constitutive soil model. The model makes use of several material parameters that determine the specific properties of a sand. In NorSand all material properties are unitless. The material parameters are summarised in table 3.1, with a range in which the parameters can be expected given by Jefferies and Shuttle [2005].

λ_e	0.01 - 0.07	soil compressibility slope of critical state line in $\ln(p')$ space
Γ	0.8 - 1.4	reference point for CSL, at 1 kPa
M	1.2 - 1.5	critical friction ratio, triaxial compression conditions
N	0 - 0.4	scaling parameter for the stress dilatancy relationship
H	50 - 500	Hardening modulus
χ	2.5 - 4.5	dilatancy-ψ relation
I_r	100 - 800	dimensionless shear rigidity, G/p', $f(p')$
ν	0.1 - 0.3	Poisson's ratio

Table 3.1: Material parameters in NorSand with the range that can be expected for each parameter [Jefferies and Shuttle, 2005].

The NorSand model is an elasto-plasticity model and therefore contains a yield surface, a flow rule and a hardening law. The NorSand model uses an internal model variable, the image condition, denoted by subscript i. The image condition is the condition at which one of the two requirements ($\dot{\epsilon_p} = 0$) for critical state is reached. For this point, which lies at the top of the yield surface, the parameters ψ_i, p'_i and M_i can be determined. The image condition changes with changing stress and void ratio. In case the image condition is situated at the critical state line, the critical state is reached. All equations describing the NorSand model are given in table 3.2. This is based on the summary that is given by Jefferies and Shuttle [2005], from which all equations that are not used are left out, $\bar{\sigma}_m$ is changed for p' and for the Lode angle $\frac{1}{6}\pi$ is chosen (triaxial compression). This has been done because in this report all stress conditions are triaxial compression and stress rotation is not of interest in this project.

Yield surface and image condition The yield surface of the NorSand model is described by equation 3.2. Because of normality (yielding in the normal direction to the yield surface) and convexity, only one point on the yield surface satisfies the first condition for the critical state ($\dot{\epsilon_p} = 0$). This point is an image of the critical state and is located at the top of the yield surface. The second condition for the critical state ($\ddot{\epsilon_p} = 0$) is satisfied at the critical state line only. Therefore, the critical state is reached at the moment the image condition is located at the critical state line.

NorSand contains a fully associated flow rule (flow direction normal to the yield surface). To simulate the correct behaviour of the sand in unloading, the yield surface is extended with an internal cap that keeps the dilatancy to a minimum level. The internal cap is the vertical line in the yield cap in figure 3.1. The minimum dilatancy (note; negative dilatancy for contraction) is contained in the equation

$$\left(\frac{p_i}{p}\right)_{max} = exp(-\chi\psi_i/M). \tag{3.1}$$

This equation contains parameters defined at the image condition (subscript i indicates the image condition). The point of the image condition is an image of the critical state locus and is located at the top of the yield surface (see figure 3.1).

$$\frac{\eta}{M_i} = 1 - \ln\left(\frac{p}{p_i}\right) \qquad \text{with } \left(\tfrac{p_i}{p}\right) = exp(-\chi\psi_i/M_i) \tag{3.2}$$

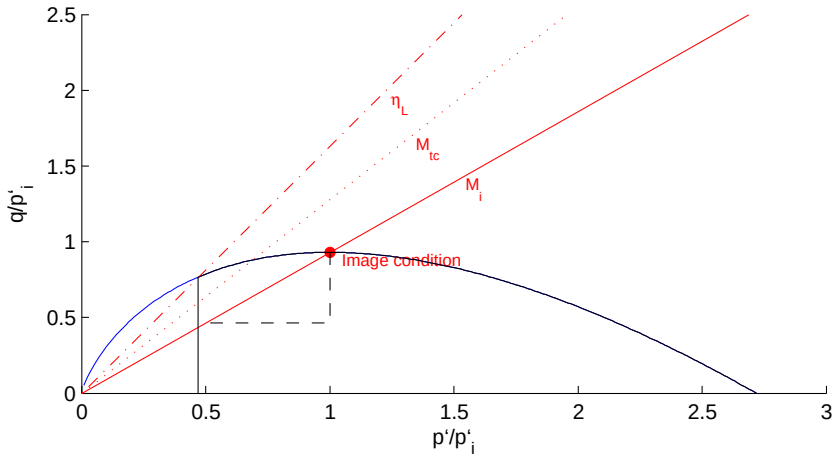

Figure 3.1: Yield surface for NorSand, represented in a dimensionless axis system (p and q are divided by p_i).

Elasticity The NorSand model uses isotropic elasticity. To keep the elasticity dimensionless and include elasticity in shear, the elasticity is included in the model as a dimensionless shear rigidity I_r and a constant Poisson's ratio ν. Shear rigidity is included for the implementation in finite element programs. Anisotropic elasticity is not included because anisotropy remains highly academic and theoretical and it is already difficult enough to determine parameters for an isotropic model [Jefferies and Been, 2006].

Internal model variables	$\psi_i = \psi + \lambda \ln(p_i/p)$ where $\psi = e - e_{cs}$ $M_i = M - \lvert\psi_i\rvert$
Critical state	$e_{cs} = \Gamma - \lambda \ln(p)$
Yield surface & Internal cap	$\frac{\eta}{M_i} = 1 - \ln\left(\frac{p}{p_i}\right)$ with $\left(\frac{p_i}{p}\right) = exp(-\chi\psi_i/M_i)$
Hardening rule	**On outer yield surface:** $\frac{\dot{p}_i}{p_i} = H\left(\frac{p}{p_i}\right)^2 \left[\left(\frac{p_i}{p}\right)_{max} - \frac{p_i}{p}\right]\dot{\epsilon}_q^p$ **On internal cap:** $\frac{\dot{p}_i}{p_i} = -\frac{H}{2}\lvert\dot{\epsilon}_q^p\rvert$
Stress dilatancy	$D^p = \dot{\epsilon}_q^p / \lvert\dot{\epsilon}_q^p\rvert M_i - \eta$
Elasticity	$I_r = \frac{G}{p}$ with $K = \frac{2(1+\nu)}{3(1-2\nu)}G$

Table 3.2: Summary of NorSand at triaxial compression conditions after Jefferies and Shuttle [2005]

To be able to use CPT profiles (cone resistance q_c and sleeve friction) to give a state parameter profile, the NorSand model needs to be calibrated for the material. In other words, the material properties need to be determined to be able to use the sand state (stress and void ratio) to determine the state parameter ψ. The state parameters are given by the CPT-profiles and a calibration of cone penetration tests for sand is given by Shuttle and Jefferies [1998].

3.1.3 Method of interpretation; from CPT-profile to state parameter

Next to material properties, soil models use material states to describe the behaviour of the soil. To combine all state characteristics in one parameter, the state parameter is used. The state parameter is a combination of different types of state (void state and stress state). Because the void ratio e is not easily measured in-situ, a direct relationship between cone resistance q_c and state parameter ψ is used. The $q_c - \psi$ relationship that is used in this report is the method described by Shuttle and Jefferies [1998]. This method is based on the methodology by Been and Jefferies [1986] and Been et al. [1986] which basically is a relation between the dimensionless cone resistance Q_c and state parameter ψ depending only on the material property λ. Different authors came up with additional parameters that are of influence on the relationship. The final method by Shuttle and Jefferies [1998] gives a relation between Q_c and ψ including the NorSand material properties G, M, N, H, λ and ν. The relationship has been

derived by numerical simulation to calibrate the model against calibration chamber test results. This relation is given by equations 3.3, 3.4 and 3.5. A summary of the discussion on the improvements of the initial relationship and the final relationship that is used in this report can be found in the MSc thesis by Bakhtiari [2006].

The method of relating the state parameter to the CPT profiles that is used in this report is the method described by Jefferies and Shuttle [2005]

$$Q_c = \frac{q_c - p}{p'} = k \cdot exp(-m\psi) \tag{3.3}$$

$$k = \big(f_1(I_r) f_2(M) f_3(N) f_4(H) f_5(\lambda_{ss}) f_6(\nu)\big)^{1.45} \tag{3.4}$$

$$m = 1.45 f_7(I_r) f_8(M) f_9(N) f_{10}(H) f_{11}(\lambda_{ss}) f_{12}(\nu) \tag{3.5}$$

with:

$$\begin{array}{lll} f_1(I_r) & = 3.76 + 1.12ln(I_r), & I_r = G/p' \\ f_2(M) & = 1 + 1.06(M - 1.25) & \\ f_3(N) & = 1 - 0.30(N - 0.2) & \\ f_4(H) & = (H/100)^{0.326} & \\ f_5(\lambda) & = 1 - 1.55(\lambda - 0.01) & \\ f_6(\nu) & = 1 & \\ f_7(I_r) & = 1.04 + 0.46ln(I_r) & \\ f_8(M) & = 1 - 0.40(M - 1.25) & \\ f_9(N) & = 1 - 0.30(N - 0.2) & \\ f_{10}(H) & = (H/100)^{0.15} & \\ f_{11}(\lambda) & = 1 - 2.21(\lambda - 0.01) & \\ f_{12}(\nu) & = 1 & \end{array} \tag{3.6}$$

To be able to transform the CPT-profiles into ψ-profiles, the following NorSand material properties are needed:

- G, shear modulus
- M, critical state stress ratio
- N, stress-dilatancy scaling parameter
- H, hardening modulus
- λ, slope critical state line

These material properties are determined from triaxial tests as described in section 3.2. The material parameters that are used for the conversion from cone resistance Q_c to state parameter ψ are calibrated using triaxial test data. Every parameter is fitted to the data in the best possible way, and is therefore an estimate of the true property. Deviations from the parameters used for the conversion can lead to differences in state parameter profile. How large the influence of differences in the material parameters is will be discussed in the next section.

3.2 Calibration procedure of the NorSand parameters

The calibration of the NorSand model is described extensively by Bakhtiari [2006]. For this project, the same procedure is intended to follow. The calibration of the NorSand model is based on triaxial test data. From these tests the parameters that are needed in the statistical interpretation of the CPT data are determined. A description of the methods of calibation of the NorSand constitutive model is given below.

3.2.1 Critical stress ratio M and stress dilatancy parameter N

The stress ratio η is the ratio between the deviatoric stress q and the mean effective stress p'. The stress ratio η at the critical state is denoted with the symbol M. Four methods to determine M are presented in this chapter, for which the subscripts indicate the method of interpretation. All four methods of interpretation are meant to determine the same physical property, but show some differences caused by the specific method applied. All methods use triaxial tests, which gives the critical stress ratio for triaxial conditions M_{tc}. In this report the subscript $_{tc}$ will not be used and M_{tc} and M in general are considered to be the same for all conditions. The four methods to determine the critical state stress ratio M ($M_{ET}, M_{MC}, M_{SD}, M_{BM}$) are given below. A graphical presentation of the different methods to determine M can be found in figure 3.3.

End of test $\mathbf{M}_{ET}$: Triaxial compression tests can be expected to reach the critical state eventually. Reading the stress ratio at the end of the test therefore gives an indication of the location of the critical state stress ratio. The best estimates for M are given by the tests that actually reach the critical state. Figure 3.3 shows M_{ET} for a dilatant test that reaches critical state. Taking the average over the results for M_{ET} gives the final value for M_{ET}. The quality of the result depends largely on whether or not the critical state has been reached at the end of the test. Therefore it should be checked if the triaxial tests are not far from critical state at the end of testing.

Maximum contraction $\mathbf{M}_{MC}$: At maximum contraction the dilation D is zero and therefore $\dot{\epsilon_v} = 0$. When elastic strain rates are neglected, one of the two conditions of the critical state is reached. The mobilised friction angle at maximum contraction M_{MC} therefore gives an indication of the critical state friction angle M. In figure 3.3 the point at which maximum contraction occurs is shown.
Negussey et al. [1987] discussed the effect of sample state in triaxial testing on the resemblance between M (determined in ring shear test) and M_{MC} (determined in triaxial test). They showed that for loose samples M and M_{MC} are equal. For medium and dense sands, M_{MC} was showed to depend on both relative density (void ratio) and confining pressure (p_0). M_{MC} increases with confining pressure and initial void ratio, which means that M_{MC} increases with initial state parameter ψ_0 for dilatant sands, towards M at ψ_0=0. The modelling of a triaxial test (discussed later in this report) with the NorSand model for different initial state parameters, as shown in figure 3.2, supports the results of the tests performed by Negussey et al. [1987]. The figure shows the influence of the initial state parameter (both e_0 and p_0 have been changed) and the independency of M_{MS} from initial state for loose initial state parameter. For medium and dense states ($\psi_0 \leq 0$) M_{MC} depends on the initial state parameter ψ_0.

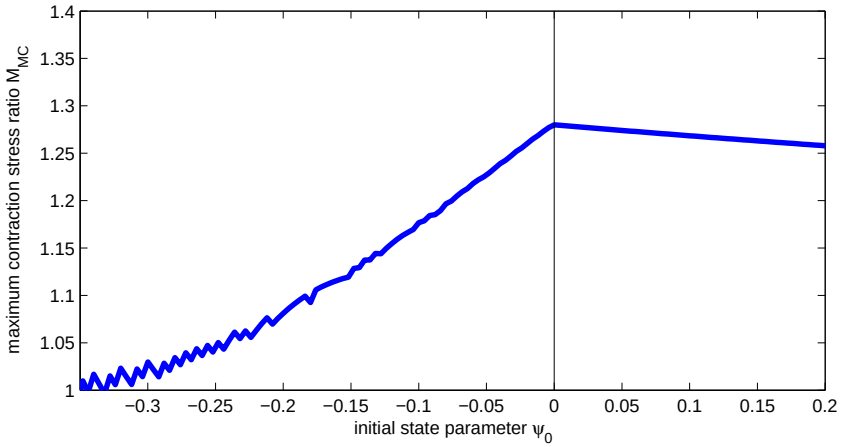

Figure 3.2: Maximum contraction stress ratio M_{MC} as a function of initial state parameter, resulting from numerical modelling of triaxial compression tests with the NorSand model

Stress dilatancy $\mathbf{M}_{SD}$ and N: To deal with the fact that critical state is reached at large strains, extrapolation is applied on the $\eta - D$ plot to define η at zero dilatancy. This can be done in a $\eta - D$ plot by extrapolation to the $D = 0$ line. The dilatancy rate is determined with a central difference method as given in equation 3.7.

$$D_i = \frac{\epsilon_{v,i+1} - \epsilon_{v,i-1}}{\epsilon_{q,i+1} - \epsilon_{q,i-1}} \tag{3.7}$$

The relation between D (D is assumed to be equal to D^p) and η is controlled by the coupling parameter N. The flow rule in the NorSand model can be rewritten into equation 3.8 from which it can be seen that the slope of the line in $\eta - D$ space is given by $N - 1$ when D^p is considered to be equal to D. Therefore the elastic part of the dilation has to be zero which is not the case because η is not constant. This can be corrected for when the elastic strain rates ϵ_v^e and ϵ_q^e are included in the calculation for D^p. In this report the influence of the elastic dilation is neglected and D^p is expected to be equal to D.

Localisation can not be accounted for in a way of quantifying the effect. Results with high N and low M need to be checked to see is localisation has affected the test results. The quantitative effect can not be determined exactly, because it is unknown how large the localisation region is.

$$\eta = (N - 1)\, D^p + M \tag{3.8}$$

Because of the possible formation of shear bands during dilation, the results of the stress-dilatancy method should be evaluated carefully. Especially the value found for N is highly influenced by an incorrect dilation rate which is the result of localisation. Because localisation will occur only in the post-peak part of the test, the dilation in tests of dense samples are affected. Individual $\eta - D$ plots can be checked looking at the post-peak portion of the curve; a straight line will indicate a reliable M_{SD}, curved and shifted parts of the graph can indicate localisation. Because contractant samples do not have any post-peak portion, the contractant samples are evaluated at the pre-peak portion.
Some graphs contain an unload-reload loop to determine the elastic stiffness parameter G. This loop contains very large steps that influence the dilatancy leading to a distorted η-D graph. Because at unloading and reloading the stress ratio η is changed rapidly, the $\eta - D$ graph is distorted. This gives an extreme negative peak in the $\eta - D$ curve that needs to be filtered out for a proper presentation. The "cleaning" of the graph from the unloading-reloading loop is done by cutting the part of the reloading loop out of the curve, which has no further effect on the interpretation of M and N.

Bishop's method M_{BM}: For Bishop's method the peak friction η_{peak} is plotted against the dilatancy D for all tests. This is done because at peak strength $\ddot{\epsilon_v}$=0, which implies that $\dot{D}$ is zero at peak friction. Therefore one of the two conditions for critical state is satisfied and the test has reached the image condition. The points of all tests are on a theoretical line showing the relation between dilatancy and stress ratio at the image condition M_i. The interpolation/extrapolation of the points to the $D = 0$ line that is given by the intersection of the trend line with the $D = 0$ line gives the critical state location because D=0 and $\dot{D}$=0.

By modelling different triaxial tests and determining the peak friction ratio and dilation at peak friction ratio, it is found that the relation between minimum dilation and maximum peak strength is not exactly linear. Figure 3.4 shows that N can best be derived from the slope of the regression line close to $D = 0$ in case the regression line is not linear.

N is determined by the slope of the trend line. Like the slope in the post-peak part of the curve in the plot for the stress-dilatancy method, the slope of the trend line through the points of maximum dilation is equal to N-1.

3.2.2 Peak friction ratio η_{peak}

The peak friction ratio is determined because it is used in the code by Gitman [2006] to be used as a variable next to tip resistance and state parameter. In the code it is used as a first-order function of the state parameter.

The peak friction is easily determined by taking the maximum value from the $\eta - D$ plot. This is done for both the Lab A and Lab B data. An overview together with mean effective stress p' and state parameter ψ is given below. The peak friction is not a model parameter in the NorSand model. The peak stress ratio can be transformed to the Mohr-Coulomb peak friction angle ϕ_{peak} using equation 2.1.

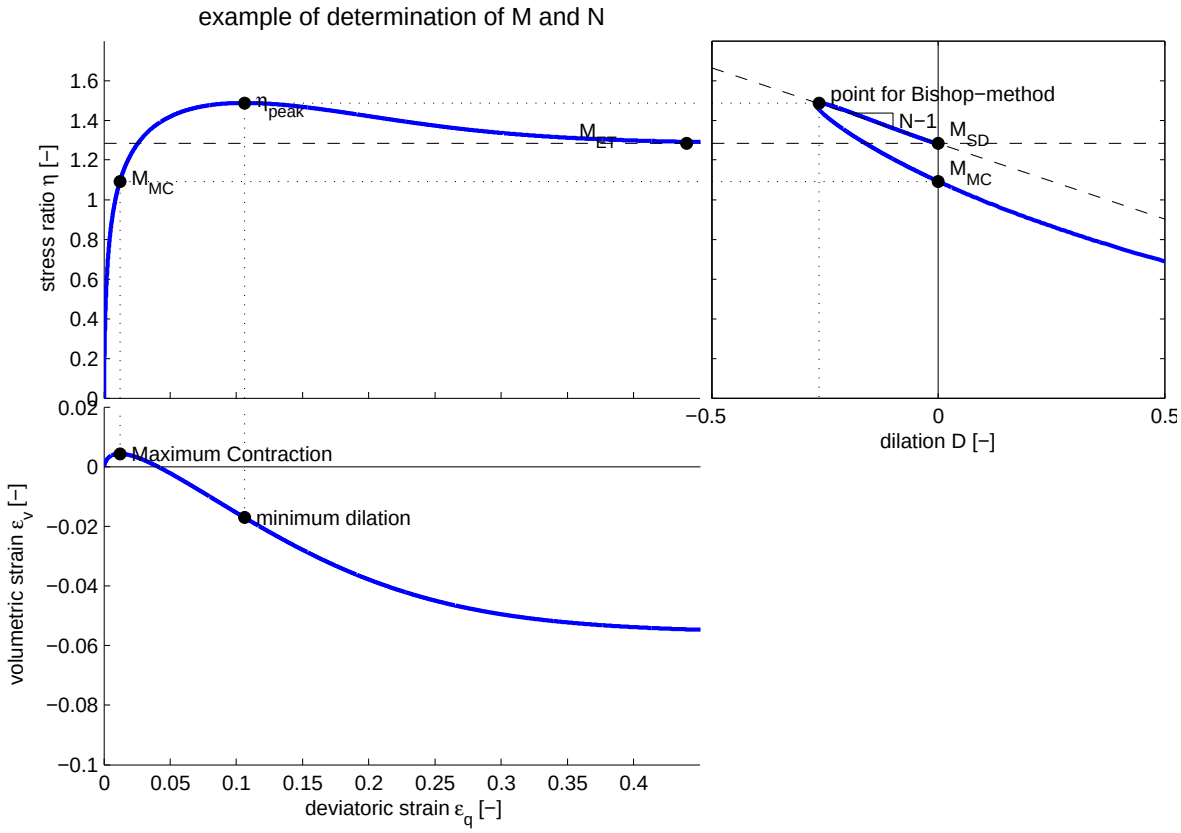

Figure 3.3: Example of the calibration of M_{ET}, M_{MC}, M_{SD} and N_{SD}, generated by modelling the triaxial behaviour of sand.

3.2.3 Shear modulus G and dimensionless shear rigidity I_r

Different methods for the determination of the elastic shear modulus G are described by Bakhtiari [2006]. Only one is based on triaxial tests and this is the method described here. The shear modulus G at test conditions is equal to one-third of the slope of the unload-reload loop in $q-\epsilon_q$ space, as given in equation 3.9.

$$G = \frac{1}{3}\frac{dq'}{d\epsilon_q} \tag{3.9}$$

The shear modulus G is a material property that depends on the mean effective stress. In other words; $G = f(p')$. The relation between p' and G is given by equation 3.10,

$$G = G_{ref}\left(\frac{p'}{p'_{ref}}\right)^b \tag{3.10}$$

where G_{ref} is the shear modulus at reference stress p'_{ref} =1kPa. To find the equation for G as a function of p', the constants G_{ref} and b need to be determined. This is done by the linear trend line in $\ln G$-$\ln p'$ space through all values found for G at a certain level of p'. The level for p' is found by taking the average over the natural logarithm of p' of each reading in the loop.

The dimensionless shear rigidity I_r can be found as G/p'. This means that when G=$G(p')$, I_r=$I_r(p')$.

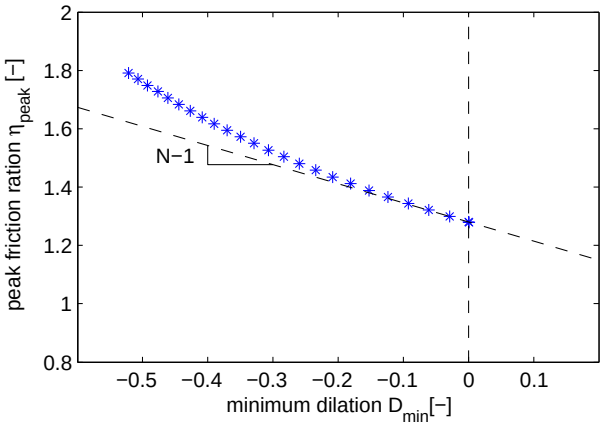

Figure 3.4: Example of the Bishop's method with slope N-1 at zero dilation. The difference in slope as a function of minimum dilation D_{min} is the influence of elastic dilation D_e. In the graph total dilation is plotted although, ideally, only plastic dilatancy D_p should be plotted.

3.2.4 Critical state line λ_{cs} and Γ

The critical state void ratio e_{cs} is a function of the stress regime; in other words $e_{cs} = f(p')$. An idealised function for the relation between e_{cs} and p' is;

$$e_{cs} = \Gamma - \lambda_{cs,e} \ln(p') \tag{3.11}$$

where Γ is the critical state void ratio at the reference pressure p'_{ref}=1kPa. The slope of the critical state line ($-\lambda_{cs}$) can be determined based on either ^{10}log or natural logarithm ln which gives $\lambda_{cs,10}$ or $\lambda_{cs,e}$. The difference between both values is a factor $\ln(10) = 2.3$.

Different methods are described by Bakhtiari [2006] to determine the critical state line. For this project, not for all these methods the appropriate data is available. Three method that are used to determine λ and Γ for which enough data are available are described here.

Triaxial test method: For all tests that reach critical state, the void ratio e can be plotted against $\ln p'$. The best linear fit through the points gives an estimate of the critical state line and gives λ_{cs} and Γ. Because this method uses the void ratio at critical state, the selection of the correct void ratios at the critical points is crucial for a proper fit. Dilatant samples are less suitable, because during dilation shear band can form. This will result in an underestimation of the critical state void ratio for dilatant samples.

Fines content approach: The fines content approach is an empirical method suggested by Bouckovalas et al. [2002]. It gives a rough indication of the critical state line based on the fines content $f(\%)$.

$$\lambda = 0.018 + 0.0027 f(\%) \tag{3.12}$$

$$\Gamma = 0.863 + 0.011 f(\%) \tag{3.13}$$

The equations are the result of a statistical interpretation of 42 types of silty sand. Grain sizes of the sands used for the derivation of the equations were in the range of 100μm to 500μm for D_{50} with percentage of fines $f(\%)$ ranging from 0 to 10% [Bouckovalas et al., 2002]. The fines content approach is not intended to use instead of triaxial tests, but to give an expected trend of the critical state line to be found.

Assumed-χ method (Intersection Method): Combination of several relations used in the NorSand model gives the following equation.

$$e_0 - \frac{D_{min}}{\chi} = \Gamma - \lambda_{cs_e} \ln p', \qquad \Gamma = e_0 - \frac{D_{min}}{\chi} + \lambda_{cs_e} \ln p' \tag{3.14}$$

In this equation χ (chi) has to be assumed and when e_0, D_{min} and $\ln p'$ are used for each test individually, different functions for the relation $\Gamma - \lambda_{cs,e}$ are found. The intersection of the combination of two of these functions gives a possible solution for Γ and $\lambda_{cs,e}$. Taking the average over a carefully made selection of all the intersections gives the correct values for Γ and $\lambda_{cs,e}$.
Because p' is not constant during the test, an average value has to be used for $\ln p'$. The average used is the average of the natural logarithm of all p'-readings in the test.
Because the void ratio is included in this method, dilatant behaviour might give an inaccurate result because of the possible development of a shear band. To avoid the effects of this, only contractant samples are used for this method. The value for χ that has to be assumed lies in the range of 2.5-4.5 [Jefferies and Shuttle, 2005].

3.2.5 Hardening modulus H

The hardening modulus H is the last parameter to be calibrated. The calibration consists of fitting the test data using the values found for the other parameters and modelling the test results as good as possible for a single value of H. Because NorSand can not be expressed in a closed-form equation, an iterative scheme is needed. A scheme that can be used is provided with the book of Jefferies and Been [2006]. The scheme is part of an EXCEL-sheet to simulate triaxial compressions to fit the parameters for the NorSand soil model. The part of the scheme that is used for the simulation of triaxial compression is given below. Using the calibrated results for M,N,λ,ν,I_r and H, the material behaviour under triaxial compression is modelled for an assumed value for H. In this way triaxial test data can be simulated. The modelled response can be fitted to the triaxial test data by variation of H. The best fit with the triaxial test data gives the best estimation for the value of H.

Disadvantage of this method is that the value for H has to correct for the deficiencies in the calibration of the other parameters. In this way small differences in the calibration of the other parameters can lead to large differences in the result for H. This is discussed further in section 3.4.5.
Iteration scheme

Input: M,N, λ, ν, I_r, H

$d\epsilon_q = 0.5/7000$ (small incremental value)

$\dot{p} = 0$(initial value)

$\psi = \psi_0$(initial value)

for j = 2:total

$G = G_1 p^{b_G}$

$K = \dfrac{2G(1-\nu)}{3*(1-2*\nu}$

$M_i = M - \chi N|\psi|$

$D_p = M_i - \eta$

$d\epsilon_v = D_p d\epsilon_q$

$d\epsilon_1 = d\epsilon_q + d\epsilon_v/3$

$D_{min} = \chi\psi$

$p_i/p_{max} = e^{-D_{min}/M_i}$

$\dot{p_i}/p_i = He^{1-\eta/M_i}\left(\dfrac{p_i/p_{max}}{p_i/p} - 1\right)d\epsilon_q = He^{1-\eta/M_i}\big(p/p_{max} - 1\big)d\epsilon_q$

$\eta_{ratio} = 1 + \dfrac{M_i}{3-\eta}$

$\eta = \eta + \dot{\eta}$ (stress update)

$\dot{p} = p\dfrac{\dot{\eta}}{3-\eta}$

$\dot{q} = p\dot{\eta} + \eta\dot{p}$

$p = p + \dot{p}$

$p_i/p = e^{\eta/M_i - 1}$

$d\epsilon_{q,e} = \dfrac{\dot{q}}{3G}$

$d\epsilon_{v,e} = \dot{p}/K$

$\epsilon_1 = \epsilon_1 + d\epsilon_1 + d\epsilon_{q,e} + d\epsilon_{v,e}/3$

$\epsilon_v = \epsilon_v + d\epsilon_v + d\epsilon_{v,e}$

$curve = \epsilon_v + d\epsilon_v + d\epsilon_{v,e}$

updated stresses and strains are stored
next j

3.3 Available data

The data that are used in this project are cone penetration tests (CPT's) (in-situ measurements) and triaxial compression tests (laboratory tests). The triaxial compression tests were performed by two different laboratories, refered to as "Lab A" and "Lab B".

3.3.1 Triaxial compression tests

The parameters of the NorSand soil model needed for the relation between the cone penetration data and the state parameter are derived from triaxial compression tests. Lab B performed 12 triaxial tests on 12 samples. From these 12 tests, 10 can be used to determine the material parameters. All 10 tests were performed on reconstituted samples under drained conditions in a dense state. Lab A performed 45 triaxial compression tests on 15 different reconstituted samples of the sand. Lab A-tests are performed under both dilatant and contractant conditions. All tests were performed under drained conditions.

The numbering of the original triaxial test data is changed to have an easier test-ID to work with. The original test-ID numbers of the Lab A-data can be found in table 3.4. The triaxial test results have already been used for the interpretation of some soil parameters and these parameters were presented together with the raw data. Some of these already available parameters will be used in the calibration of NorSand. An overview of the relevant results is given below.

Project,boring	test-ID in report	state	p'_0 [kPa]	poisson's ratio ν	Dilatancy Ψ [deg]
2009-447,Boring 3, monster 1	1	dense	49	0.28	11.5
2009-447,Boring 3, monster 1	2	dense	99	0.38	15.2
2009-447,Boring 3, monster 1	3	dense	199	0.36	13.8
2009-447,Boring 3, monster 1	4	dense	101	0.37	13.7
2009-447,Boring 3, monster 1	5	dense	199	0.37	14.8
2009-447,Boring 3, monster 1	6	dense	48	0.27	18.1
2009-447,Boring 3, monster 1	7	dense	99	0.27	15.9
2009-447,Boring 3, monster 1	8	dense	199	0.37	15.8
2009-447,Boring 3, monster 1	9	dense	99	0.27	12.8
2009-447,Boring 3, monster 1	10	dense	199	0.29	17.2
average				**0.323**	**14.86**

Table 3.3: Available test results for the Lab B-data. Calculation method is not known

Canister-sample#	test-ID	state	p'_0 [kPa]
1607-1B	1.1	dense	35
	1.2	loose	78
	1.3	loose	108
1609-3B	2.1	dense	75
	2.2	dense	156
	2.3	dense	224
1611-2B	3.1	loose	70
	3.2	dense	145
	3.3	loose	210
4361-2B	4.1	loose	69
	4.2	dense	145
	4.3	loose	220
5559 2B	5.1	dense	69
	5.2	dense	143
	5.3	loose*	210
4351-1	6.1	dense	45
	6.2	dense	91
	6.3	dense	135
4352-2	7.1	dense	75
	7.2	dense	150
	7.3	dense	224
1607-1	8.1	dense	35
	8.2	dense	72
	8.3	dense	108

Canister-sample#	test-ID	state	p'_0 [kPa]
1609-3	9.1	l/d	74
	9.2	dense	155
	9.3	dense	224
1610-1	10.1	dense	35
	10.2	dense	74
	10.3	d/l*	107
1611-2	11.1	dense	71
	11.2	dense	140
	11.3	d/l*	208
4361-2	12.1	dense	69
	12.2	dense	142
	12.3	dense	219
4370-3	13.1	loose	99
	13.2	loose	203
	13.3	loose	299
5559-2	14.1	dense	69.15
	14.2	dense	140
	14.3	dense	209
5560-3	15.1	dense	89
	15.2	dense	181
	15.3	dense	268

Table 3.4: available test results for the Lab A-data. The states with * are not taken into account in the assumed-chi method and the critical state line.

Both Lab A- and Lab B-data come with sieving curves from which the grain size distribution can be derived. In this way, the results of the calibration can be compared with results for similar sands found in literature.

Grain sizes Lab A-samples				
Borehole	Sample	$D_{50}[\mu m]$	uniformity D_{10}/D_{50}	fines [%]($\leq 63\mu m$)
B5.1-001	1	240	1.76	0.7
	2	241	1.78	0.1
	3	244	1.73	1.4
B5.1-002	1	281	1.94	1.4
	2	220	1.67	1.3
B5.1-003	1	294	1.98	2.5
	2	249	1.91	2.0
	3	213	1.59	1.4
B5.1-004	1	286	2.01	1.0
	2	274	2.04	0.8
	3	234	1.77	0.9
B5.1-005	1	331	2.17	0.1
	2	267	1.93	0.9
	3	215	1.80	1.7
B5.2-001	1	221	1.59	0.8
	2	225	1.68	1.2
	3	310	1.93	1.3
B5.2-002	1	314	1.93	1.4
	2	372	2.11	1.1
	3	369	1.96	0.7
Average		**270**	**1.86**	**1.1**

Table 3.5: Grain size distribution for the Lab A-samples

	D_{50} [μm]	fines [%]
Lab B-data	265	1.9

Table 3.6: Grain size distribution for the Lab B-samples

3.4 Description of the calibration

This section describes the actual calibration of the NorSand model. The procedures described in section 3.2 are used and changed where needed. It is described which tests are used for the calibration and which choices are made with regard to the rejection of individual tests (e.g. because of failed tests or outlying results).

3.4.1 M and N

For the determination of M and N, all four methods described in section 3.2.1 are applied. This has resulted in a number of values that were the result of the different methods. The results of these different methods can be compared to determine the final value for M and N.

End-of-test method M_{ET}: The available triaxial tests are all tested up to a maximum axial strain of 15%. Because most samples do not reach the critical state within this 15% of axial strain, the results of the end-of-test method for the critical state friction ration M are biased; contractant samples underestimate and dilatant samples overestimate M. To deal with this, M_{ET} is plotted against the dilatancy at the end of the test D_{ET} to be able to distiguish between the contractant or dilatant behaviour that is still present at 15% of axial strain. In case the tests did reach critical state (or are at the image condition) the results are located at the $D_{ET} = 0$ line.

The intersection of least square fit of the results in the $M_{ET} - D_{ET}$ plot with the $D_{ET} = 0$ line is expected to give a better estimate for the critical state stress ratio M. The scatter plot with the best linear fit for both the Lab A-data and the Lab B-data is given in figure 3.5. All loose samples but one reached critical state deformation before the end of the test. Therefore the points representing loose samples line up at the $D = 0$ line. Next to the linear trend line, the average of the individual results is given for comparison in table 3.7.

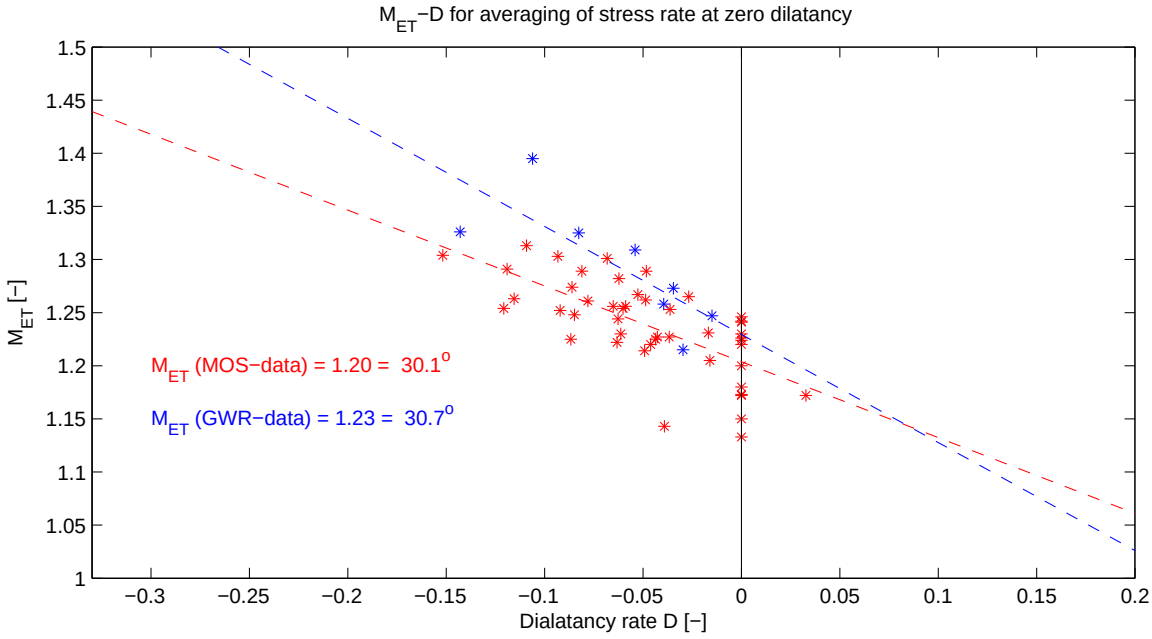

Figure 3.5: M_{ET} against total dilatancy at the end of the test. Critical state friction angle might be interpreted as the intersection of the trend line D=0. Strictly speaking, only the plastic dilatancy D_p has to be considered.

Maximum contraction method $\mathbf{M}_{MC}$: All dilatant samples reached a point of maximum contraction; most of the contractant samples reached the critical state and, for those samples, the final state is the maximum contraction. In section 3.2.1 it is shown that the stress ratio at maximum contraction is influenced by the initial state parameter ψ_0. Using the critical state line (discussed below) and the initial state of the sand, the initial state parameter is determined for all tests and plotted against the results of M_{MC} (see fig 3.6). Because a function for the dependency of M_{MC} on ψ_0 is unknown, a linear regression line is used to approximate the relation between the experimental results for M_{MC} and ψ_0.

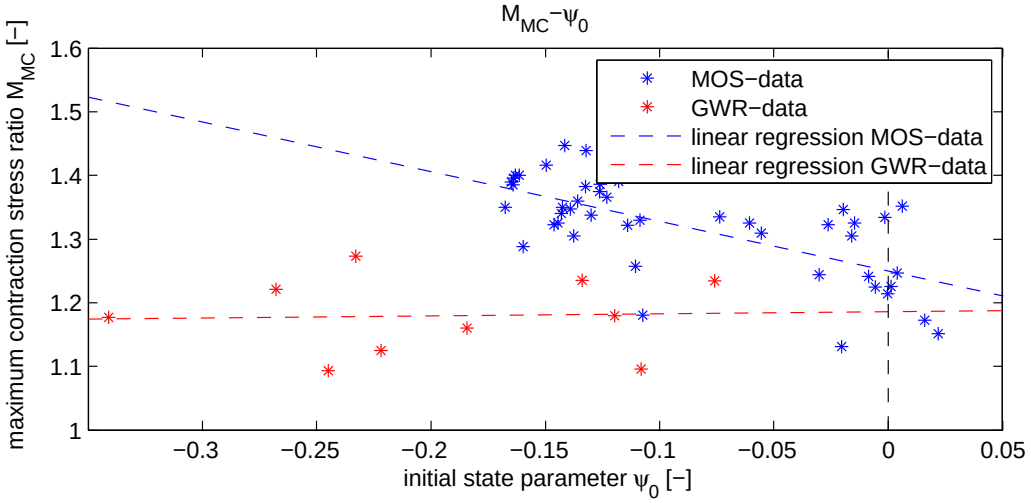

Figure 3.6: M_{MC} against ψ_0. The expected trend in the dilatant part of the graph, as expected according figure 3.2 is not present in the actual test data.

Because the linear regression lines in figure 3.6 do not come close to the modelled graph of figure 3.2, the results of the regression line (the intersection with the $D = 0$ line, being 1.19 for Lab B data and 1.25 for Lab A data) are not necessarily more reliable than the average over the results for M_{MC}. The average and standard deviation of the results for M_{MC} are given in table 3.7.

Stress dilatancy method $\mathbf{M}_{SD}$: Stress-dilatancy plots are produced and η_{peak} and D_{min} are determined for all tests. The post-peak portion of the stress-dilatancy plot is theoretically linear and can be expressed as $\eta = M_{SD} + (N-1)D$, defining both parameters that need to be interpreted. The best linear fit (least square) of the post-peak section of the curve is used to determine M and N; M is the intersection with the $D = 0$ line and N-1 is the slope of the line.

Because of the fine reading spacing of the Lab A-data combined with the limited number of digits in the readings of volume change, the dilation calculated with equation 2.2 consists of zeros and extreme high or low values. This is the result of the volume change that only changes every few readings. To correct for this, the dilation is calculated over an average of multiple readings to average out the volume change readings. Averaging over 6 readings proves to be sufficient to average out the effect of the small reading interval and gives a new form of equation 2.2, given by equation 3.15. The result of this averaging is a smoother curve. A larger range for averaging will give an even smoother curve, but the accuracy is limited for larger range of averaging.

$$D_i = \frac{\sum_{n=1}^{6} (\epsilon_{v,i+n} - \epsilon_{v,i-n})}{\sum_{n=1}^{6} (\epsilon_{q,i+n} - \epsilon_{q,i-n})} \tag{3.15}$$

For the dilatant samples, the post-peak section of the curve is used to determine N by the slope of the curve. From the contractant samples, which have no peak and therefore no post-peak section, the slope is determined at the part just before the peak stress ratio M_{peak}. This gives a similar result as the dilatant samples after the peak strength.

From all individual results, the average values for M and N are determined, together with the standard deviation in the individual results for comparison with the other results. Average and standard deviation are given in table 3.7.

Taking the average of all results proves to be not correct to determine N because, for the Lab A-data, the value found for N is not realistic. When the distribution of the results found for N is looked at (figure 3.7) it becomes clear that the average of all results is not likely to be the correct final result for N. The results show a large part of the values found for N below zero and the range over which the values can be found is large. The reason for such a low values probably is localisation during testing. Because at localisation in the post-peak portion of triaxial compression, the apparent dilation does increase far less then it should do (because it is assumed to take place over the full sample), the slope in the stress-dilatancy plot is lower than it should be and the coupling parameter D gets smaller. The modal value for all results of N seems to be a better choice and in this way N_{SD} is 0.25 as presented in figure 3.7. This modal equals the limit malue of the CDF in the figure.

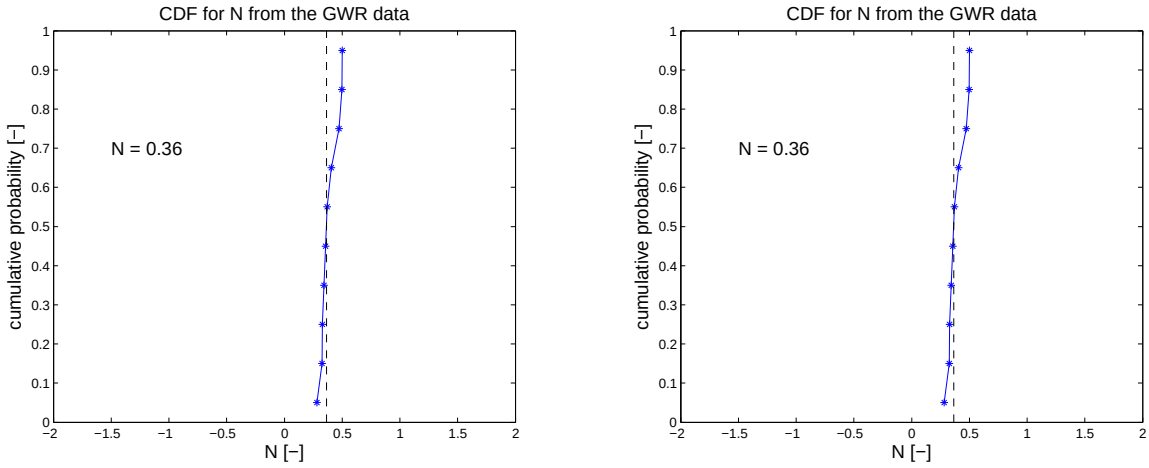

Figure 3.7: Cumulative distribution function of N. The distribution of the individual results for N shows that the average of all results does not give the correct results. The modal value of the results for N seems to give a better final result for N. The outliers at the right part of the Lab A-data results are considered as erroneous, the tail at the left part might be the effect of elastic dilation at lower minimum dilation as discussed in section 3.2.1.

For the Lab B-data, the distribution of the results is presented in the right graph of figure 3.7 to be able to compare with the distribution of the results from the Lab A-data. The variation in the results is very small for the Lab B-data. This small variation suggests that the values for N as they are found from the Lab B tests is more reliable that the values found from the Lab A data.

The effect of the localisation in the Lab A samples on the results for M_{SD} is small compared to the effect on N_{SD}. The values found for M_{SD} will be relatively small due to the localisation effects. The unreliability will be taken into account when the final value for M and N is to be determined.

Bishop's method M_{BM}: All peak friction ratio's with the corresponding dilation rates are plotted in $\eta - D$ space and a linear trend line is constructed through the points. The intersection of the trend line with the $D = 0$ line gives the values for N and M. The results give a very good regression line and Lab B and Lab A data give very similar results. Therefore this method is considered to be a reliable calibration method.

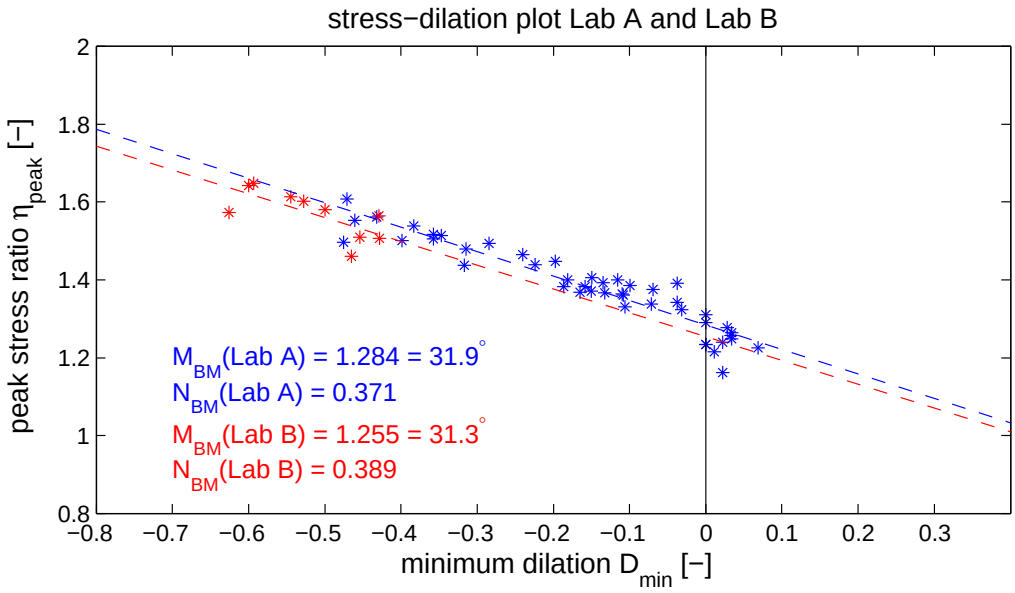

Figure 3.8: Bishop's lines for both data sets.

Final data: All results of the different methods are gathered in tables 3.7 and 3.8. Based on these results the final value for the different parameters are chosen. Because for most of the methods a standard deviation in the results is available, the most likely value for M can be found by combining the probability density functoins of the results for each method. Assuming a normal distribution in the results in each method, a probability function for the most likely value for M can be given by

$$PDF(M) = c \prod N(\mu M_i, \sigma_i), \tag{3.16}$$

where $N(\mu_M, \sigma_M)$ represents the probability density function of the result of the individual methods (mean and standard deviation from table 3.7) and c is a scaling factor to maintain an area of 1 under the probability graph. The resulting probability density function gives a most likely average of all results of $M = 1.282$ with a standard deviation of around 0.025. Compared to the results that were deriver from the linear regression lines (for M_{ET} and M_{BM}), this is a conciderably reasonable result. Taken into account the results of the linear regression line estimates and the good fit of the regression line of the M_{BM} results, the final value for M is kept at 1.28.

method	data	M	ϕ [deg]	σ_M
M_{ET}	Lab A-data, least square fit	1.20	30.1	-
	Lab A-data, mean of results	1.24	30.9	0.10
	Lab B-data, least square fit	1.23	30.7	-
	Lab B-data, mean of results	1.32	32.7	0.044
M_{MC}	Lab A-data, mean of results	1.32	32.8	0.075
	Lab B-data, mean of results	1.26	31.3	0.086
M_{SD}	Lab A-data, mean of results	1.21	30.2	0.056
	Lab B-data, mean of results	1.30	31.3	0.074
M_{BM}	Lab A-data	1.284	31.9	-
	Lab B-data	1.255	31.1	-
Final M		**1.28**	**31.6**	-

Table 3.7: Final results for critical state stress ratio M

To determine the stress-dilatancy coupling parameter N from the two methods that were used, again the reliability in the results is examined. For the stress-dilatancy method the reliability of the results from the Lab A-data is very low. The results for the Lab B data however is very consistent between the tests and is considered as the most reliable estimate. For the Bishop's method, the results

of the linear regression lines through both data sets are very much alike. Because the Lab B data has only samples with high dilatancy, the regression line depends on a small range of dilatancy. Therefore, the result for N_{BM} from the Lab B-data is considered as less reliable and the final value for N is determined as the average of N_{SD} for the Lab B data and N_{BM} for the Lab A data.

method	data	N	σ
N_{SD}	Lab A-data, mean of results	-0.06	0.926
	Lab A-data, modal value	0.25	-
	Lab B-data, mean of results	0.36	0.080
N_{BM}	Lab A-data	0.371	-
	Lab B-data	0.4389	-
Final N		**0.37**	-

Table 3.8: Final results for coupling parameter N as the average of N_{SD} for the Lab B-data and N_{BM} for the Lab A-data

3.4.2 Peak friction ratio η_{peak}

The peak friction ratio that represents the point of minimum void ratio and peak strength during testing is determined from the testing results by taking the maximum of the η-curve. Because peak strength is determined by initial void ratio and confining stress (giving ψ_0 in case the critical state line is known), results are given together with these parameters in table 3.9.

3.4.3 Shear modulus G

One out of every three Lab A triaxial tests (15 in total) are tested with an unloading-reloading loop around peak strength. The slope of the loop in the $\eta - \epsilon_q$ graph is determined by fitting a line between the intersection at the top and the lowest point of the loop. The slope is equal to 3 times the shear modulus G at the average mean effective stress in the loop $\bar{p}'$. All results are plotted in $\ln G - \ln p'$-space and a linear regression line is drawn (figure 3.9). The slope and the intersection of the trend line lead to the following relation between the shear modulus G and the mean effective stress $\bar{p}'$:

$$G = 1923\,(p')^{0.66} \tag{3.17}$$

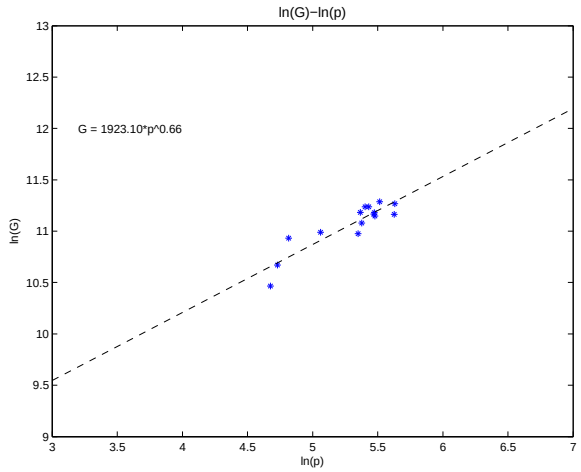

Figure 3.9: $\ln G - \ln p'$ plot to determine $G(p')$

3.4.4 Critical state line Γ and λ

The results of the three applied methods of interpretation are given in the following section.

Triaxial test method for λ and Γ: Because void ratio is used in this method, only contractant samples (see table 3.4) are used to find the critical state line given by $e = \Gamma - \lambda \ln(p')$. Because the Lab B data does not contain loose samples, the critical state line is determined for Lab A data only. Stress paths of all tests are included to show the dilatant behaviour. The dilatant samples do not reach the critical state line, possibly as an effect of localisation with dilatant behaviour. The results of the triaxial test method are given in figure 3.10.

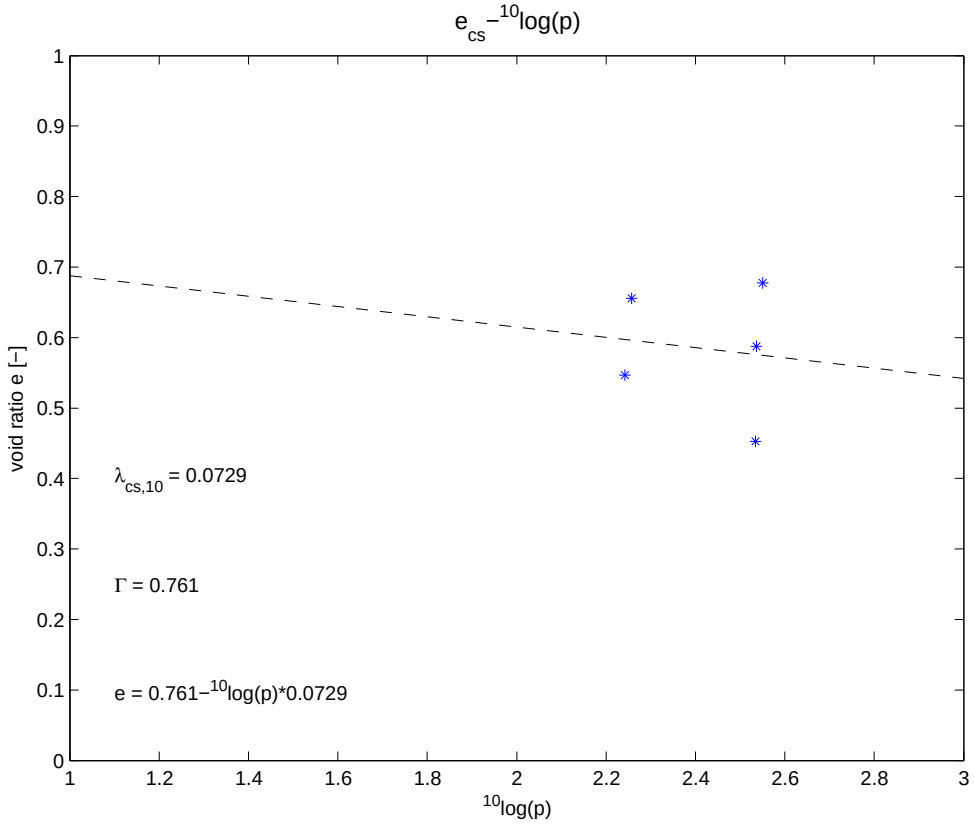

Figure 3.10: Critical state line (based on contractant samples only) and stress paths for all samples tested.

Fines content method for λ and Γ: The result of the fines content method was directly found by applying equations 3.12 and 3.13 on the data given in table 3.5. The method can be used because the grain size and fines content for all samples are in the range of samples that were used to develop the relation of the fines content approach. The results are given in table 3.10. The results however, need to be handles with care and the statement that the fines content is not to be used instead of triaxial testing and only gives an indication of the range of results (3.2.4) has to be kept in mind.

The average of the results from the Lab A-data is given in table 3.11. The result for the Lab B-data, of which only one sieving curve is available and for which $D_{50} = 265\mu$ m and fines content ($\leq 63\mu m = 1.9\%$), is given in table 3.11.

Assumed-χ method for λ and Γ: χ was assumed to be 3.5 and for each test the average effective pressure was determined by equation 3.18. With the results of D_{min}, e_0 and equation 3.14 the Γ-λ lines are constructed and the intersection of each pair if lines is determined (figure 3.12).

$$\ln p'_{average} = \Sigma_{i=1}^{n} \ln p'_i \tag{3.18}$$

Because the intersection points of the different lines are not all located within the range of possible results for Γ and λ, taking the average over all intersection points will give and incorrect result. To find the best point, two different methods are used; one based on the concentration of intersection points

and one on standard deviation of the distance between the lines in vertical and horizontal direction.

Concentration of intersection points. The concentration of intersection points is in fact a probability density function of the distribution along the x- and y-axis of the plot. The maximum value of the plot gives the highest concentration of intersection points and indicates the possible value for Γ or λ. It is constructed by sorting the coordinates of the intersection points and calculating the distance between the points. The distance is then inversed and plotted against the original coordinate to get the concentration of intersection points. The peak of the concentration plot gives the value for either Γ or λ.

To avoid peaks as a result of coinciding intersection points the concentration curve is smoothened by moving average over three point; $c_i = \frac{c_{i-1}-c_i-c_{i+1}}{3}$. This is done several times to reach a reasonable degree of smoothness. The result is shown in figure 3.11. Results are given in table 3.11.

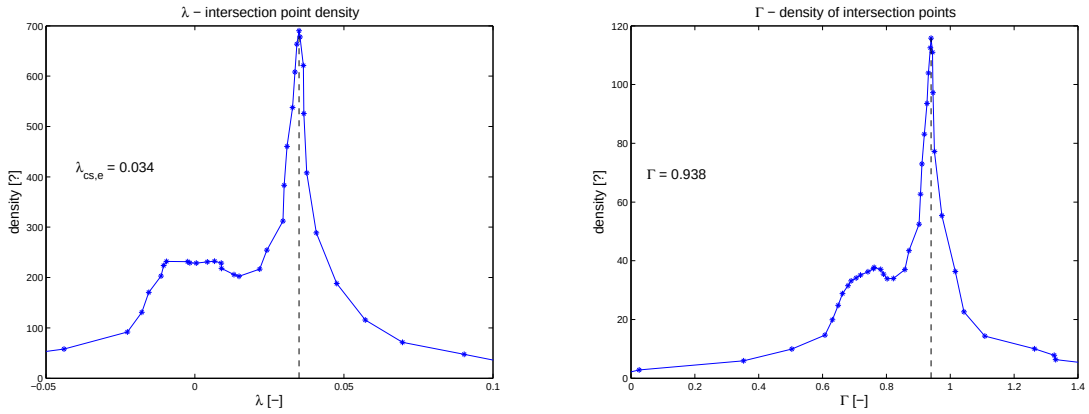

Figure 3.11: results for the method of concentration.

Least standard deviation between lines. To avoid the effect of coinciding interception points on the result, the standard deviation between the Γ-λ-lines is calculated. This is done along a vertical and a horizontal line through the Γ-λ-lines for which all individual values for Γ and λ are calculated. The standard deviation between these values is looked at over the ranges for Γ and λ. The lowest standard deviation indicates the best location for the intersection points and gives the critical state line paameters. The results of the least standard deviation are given by the dotted lines in figure 3.12

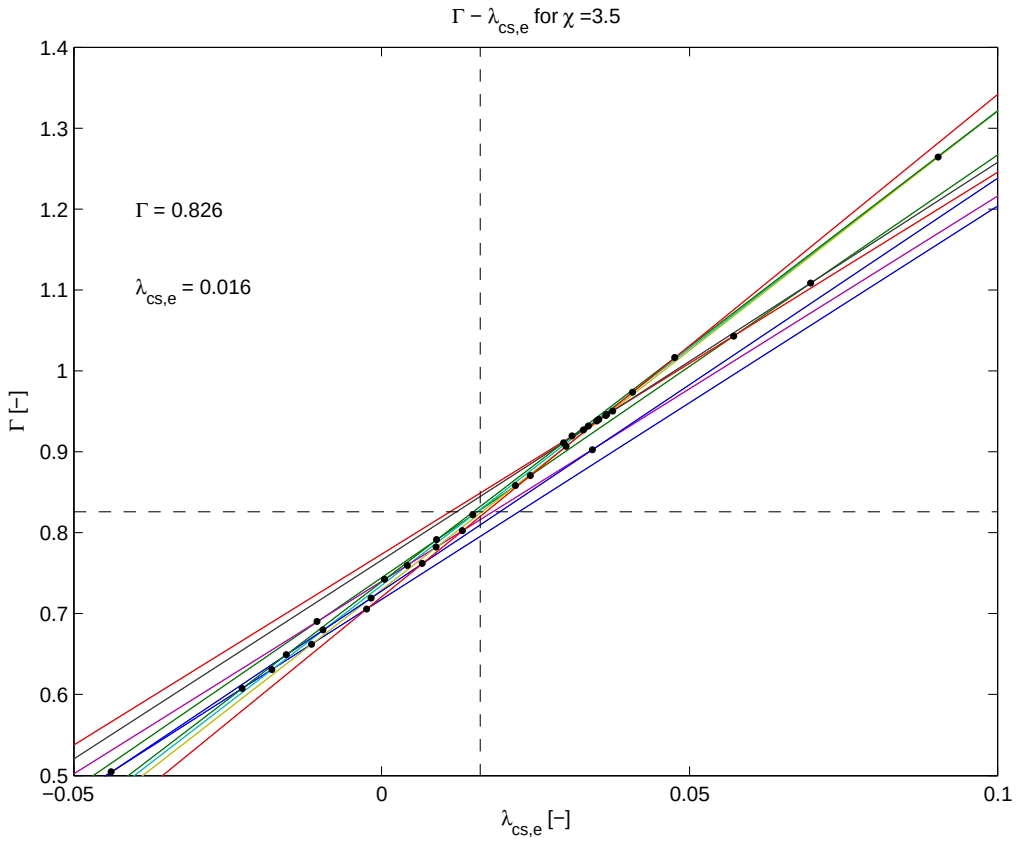

Figure 3.12: Γ-λ-plots for all tests with their points of intersection. The highest concentration of intersection points gives $\lambda_{cs,e} = 0.034$ and $\Gamma = 0.938$. The dashed lines indicate the result for the lowest standard deviation between the lines in horizontal and vertical direction. In this case $\Gamma = 0.826$ and $\lambda_{cs,e} = 0.017$.

Final result for Γ and Λ_{cs}: The different calibration methods for the critical state line parameters that are discussed above do not all give the same result. As discussed above the reliability of some of these methods is low and this should be taken into account when averaging the result. Because the results of the fines content and the assumed chi method with density of cross sections are expected to be unreliable, the average of the other two methods (triaxial method and assumed chi with standard deviation between the lines, both methods that give a similar result) is used. The result of the average between the two methods is rounded towards the results of the two methods that are expected to be unreliable. An overview of the results of the individual methods and the final result are given in table 3.11.

		Lab A-data	Lab B-data
Γ	triaxial approach	0.82	
	fines content approach	0.875	0.884
	assumed-χ std	0.826	-
	assumed-χ concentration	0.938	-
	final Γ	**0.83**	
$\lambda_{cs,e}$	triaxial approach	0.0177	0.0165
	fines content approach	0.0211	0.0231
	assumed-χ std	0.016	-
	assumed-χ concentration	0.034	-
	final $\lambda_{cs,e}$	**0.017**	
$\lambda_{cs,10}$	triaxial approach	0.0407	0.038
	fines content approach	0.0486	0.0532
	assumed-χ std	0.0368	-
	assumed-χ concentration	0.0783	-
	final $\lambda_{cs,10}$	**0.039**	

Table 3.11: Overview of the results of the different methods to determine the critical state line. The final values for the critical state line are the averages of the results of the calibration methods that are assumed to be the most reliable.

3.4.5 Hardening modulus H

By transferring the script of forward iteration of the NorSand model [Jefferies and Been, 2006] from EXCEL into Matlab (in which all the calibration in this report is done), an easy way to change the parameters for all the individual tests is found. Adjusting the code gives the possibility to fit the model in different ways. Only H is taken as an unknown, although a best fit can basically be made by varying all parameters. Because the hardening modulus needs to be presented as a unique value (instead of $H(\psi)$), the best way to fit the model to the test data is looking for a single value for H that fits as good as possible to tests. This has been tried and it proved to be difficult because a simple procedure to find the best fit could not be found. Because of this, each test is modelled for an individual value of H and the final value for H is taken from these results.

The other parameters in the model are taken as the final value as presented in the sections above being:

- M = 1.28
- N = 0.36
- G = 1923*$p^{0.66}$
- Γ = 0.83
- λ_e = 0.017
- χ = 3.5

To find the best fit of the model with the individual tests a least-square fit between the model curve and the test curve is used. The curve that is used to fit the model is the ϵ_v-ϵ_q curve, because this curve is the most representative for the behaviour of the soil. Because the post-peak section of the test results is influenced by strain localisation, only the pre-peak section of the curve is used in the least square fit. To be able to compare both curves, two new curves are constructed interpolating the curves at the same values of ϵ_q. The points for sampling are taken as follows;

$\epsilon_{q,sample}$ [%] = 0.01, 0.11, ... , $\epsilon_{q,peak}$-0.1,$\epsilon_{q,peak}$, ... , $\epsilon_{q,peak}$+2%-0.1, $\epsilon_{q,peak}$+2%

Because most tests are dilatant, fitting the model is done over a range that is slightly larger than the pre-peak section (some tests are at peak strength very soon and fitting the model over only a few points gives large differences from the test data). From each point in the array, the square difference between the test data and the model result is calculated. The minimum of the sum of all differences for H gives the best estimate for H, see equation 3.19. To find the best fit at a certain value of H, a loop is used to change the value for H until the result of equation 3.19 is at a minimum. This is done starting from $H = 10$ (H is expected in the range 50-500 ([Jefferies and Shuttle, 2005]) with an interval

of $\Delta H = 5$. The loop is stopped at the point where the result of equation 3.19 no longer decreases.

$$\sqrt{\Sigma_{i=1}^{n}(\epsilon_{v,test,sample,i} - \epsilon_{v,model,sample,i})^2} \tag{3.19}$$

Not all tests give a good result for the best fit of H. An explanation for this might be the influence of the other parameters used in the simulation. Because all other parameters (M, N, etc.) are the average results of all tests, the shape of the curves depends only on H. The effect that small differences in the other parameters have on the shape of the curve therefore has to be compensated by the hardening modulus H. This might not work out very well in all cases and therefore can lead to large differences from the test data.

When the two curves are fitted by changing H, the value at the best fit for H can become extremely high or low. The average behaviour of the material can therefore not be described by the mean of all values found for H. To see what the effect of the extreme values for H is, the cumulative density can be looked at (figure 3.13). This shows that the largest concentration of results is in the lower range and that the average of all results is not at this location because of the extreme outliers. The median or modal value of all results seems to give a better representation of the value for H.

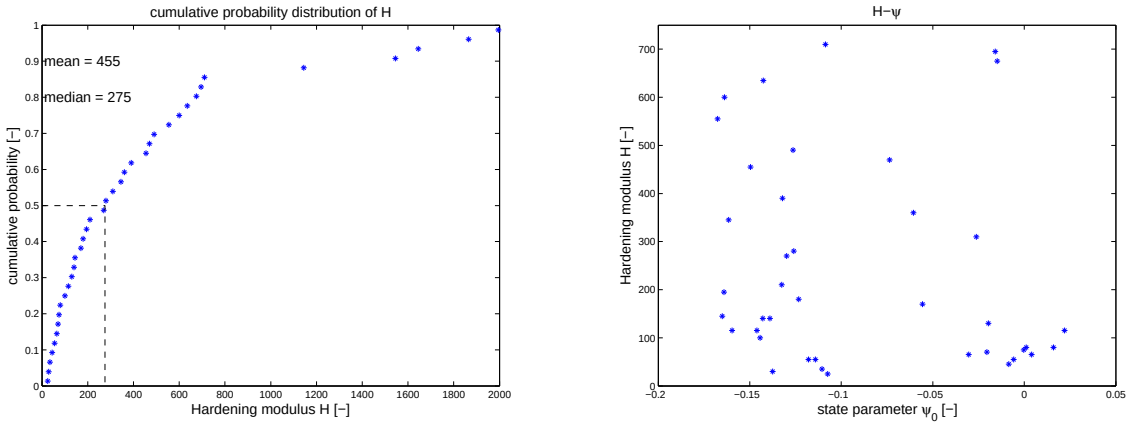

Figure 3.13: Cumulative distribution of all results for H (left) and H against ψ_0 (right).

Jefferies and Been [2006] suggested that the hardening modulus is a function of ψ_0, but plotting H against ψ_0 does not give any relation between the two (see figure 3.13). Because this relationship is not found, an average value is taken for H. An average value can only be taken from an representative set of sample points. A set of points from a lot of dense samples for example might give a systematic error when a relation between the state parameter and the hardening modulus was present. The same goes for the median and modal value. However, since such a relation does not seem to be present, the average value over the reasonable results might be used. Because the distribution of results in the range of 0-700 is reasonably uniform, the average over the results in this range can be taken. In this way, the average result for the value of H comes at 243. This is close to the median of all test results. The final value for H is therefore chosen to be 243.
Because H is determined as the last parameter of the calibration and it has to cover for all deficiencies of the averaging of the other parameters, the value found for H is very uncertain. The curves of all individual results of the calibration of H are given in appendix C.2.

3.5 NorSand soil model parameters

3.5.1 NorSand calibration results

With all parameters of the NorSand model determined above, the soil model is calibrated and the material behaviour is described by the NorSand model with the following parameters:

parameter	value
M	1.28
N	0.36
Γ	0.83
λ_e	0.017
λ_{10}	0.039
G	$1932 * p'^{0.66}$ [kPa]
I_r	$1932 * p'^{-0.34}$
H	243

Table 3.12: Overview of the calibrated NorSand parameters

3.5.2 NorSand soil properties in literature

To compare the results of the calibration with other materials, tables with results for other sands as found in literature are presented below (tables 3.13 and 3.14). From these results, the calibration results for the NZ-sand look similar to comparable sands.

Soil	Γ	$\lambda_{cs,e}$	M	χ	H	I_r	ν
Erksak sand	0.817	0.014	1.26	4.1	70-1400ψ	150-1000	0.2
Ticino sand	0.962	0.0248	1.23	3.5	115-420ψ	300-500	0.2
Hilton Mines sand	1.315	0.0738	1.39	3.5	65	300-500	0.2
Brasted sand	0.902	0.02	1.27	2.8	50-1125ψ	500	0.2
Nevada sand	0.910	0.020	1.20	3.5	100-300ψ	175	0.2
Bennett silty sand	0.450	0.018	1.40	3.5	100 to 150	300-500	0.2
Bonnie sand	1.10	0.07	1.32	3.8	20 to 45	40-80	0.2
Bothkennar clay	2.76	0.181	1.83	3.5	300	36.6	0.2
North Sea sand	0.83	0.017	1.28	3.5	243	-	0.32

Table 3.13: Some examples of Calibrated Soil Property Sets for NorSand after Jefferies and Shuttle [2005].

$(a)LaboratoryStandardSands$	$D_{50}/Fines[-/\%]$	Γ_1	λ_{10}	M_{tc}
Leighton Buzzard	120/5	0.972	0.054	**1.24**
Castro sand B	150/0	**0.791**	**0.041**	1.22
Nevada	150/7.5	0.910	**0.045**	1.20
Toyoura	160/0	1.043	0.085	
Toyoura	210/0	1.000	**0.039**	**1.24**
Reid Bedford	240/0	1.014	0.065	**1.29**
Castro Sand C	280/0	0.988	**0.038**	1.37
Monterey	370/0	**0.878**	0.029	**1.29**
Hokksund	390/0	0.934	0.054	**1.29**
Leighton Buzzard: 30% mica	450/0	1.610	0.385	
Leighton Buzzard: 17% mica	470/0	1.110	0.160	
Leighton Buzzard	500/0	0.690	**0.040**	
Leighton Buzzard: 10% mica	500/0	0.990	0.145	
Ottawa	530/0	0.754	0.028	1.13
Ticino-4	530/0	0.986	0.056	**1.24**
Ticino-8	530/0	0.943	0.031	
Ticino-9	530/0	0.970	0.050	
$(b)NaturalSands$				
San Fernando 7	75/50	**0.815**	0.106	
Amauligak I-65	80/48	1.634	0.358	**1.29**
Amauligak F-24	140/10	0.946	0.083	1.37
Alaskan Beaufort	140/10	0.920	0.053	1.20
Alaskan Beuafort	140/5	0.910	**0.037**	1.22
Amauligak F-24	144/21	0.966	0.124	1.33
Fraser River (Massey)	200/¡5	1.071	**0.038**	
Duncan Dam	200/6.5	1.170	0.085	
Isserk	210/10	0.933	0.123	**1.24**
Isserk	210/2	**0.833**	**0.043**	1.22
Isserk	210/5	**0.879**	0.089	**1.24**
Nerlerk	270/1.9	**0.849**	0.049	**1.29**
Bennett silty sand (a)	270/34	0.457	**0.041**	1.40
Nerlerk	280/12	**0.800**	0.070	**1.24**
Nerlerk	280/2	0.880	**0.040**	1.20
Kogyuk	280/5	0.902	0.062	1.20
San Fernando 3	290/11	**0.869**	0.093	
Amauligak I-65	290/3	1.023	0.095	**1.31**
Amauligak I-65	310/9	1.018	0.153	1.42
Erksak	320/1	**0.875**	**0.043**	**1.27**
Erksak	330/0.7	**0.816**	0.031	**1.27**
Kogyuk	350/10	1.095	0.205	**1.24**
Kogyuk	350/2	**0.844**	0.064	**1.31**
Kogyuk	350/5	0.924	0.104	**1.31**
Erksak	355/3	**0.848**	0.054	1.18
Bennett silty sand (b)	370/26	0.435	0.050	1.43
Bennett silty sand (c)	410/20	0.430	0.034	1.43
West Kowlon Sand	730/0.5	0.710	0.080	
Chek Lap Kok	1000/0.5	0.905	0.130	
North Sea sand	**280/1**	**0.83**	**0.039**	**1.28**

Table 3.14: Critical state properties for some soils, sorted on grain size, after Jefferies and Been [2006]. The bold fonts show the properties similar to the calibration results for the NZ-sand. The corresponding grain sizes are in the range of the grain sizes of this project.

Lab A-data					**Lab B-data**				
Test-ID	η_{peak} [-]	ϕ_{peak}[deg]	e_0 [-]	p_0 [kPa]	Test-ID	η_{peak} [-]	ϕ_{peak}[deg]	e_0 [-]	p_0 [kPa]
1.1	1.40	34.6	0.755	35	1	1.564	38.3	0.688	49
1.2	1.28	31.8	0.726	78	2	1.614	39.5	0.484	99
1.3	1.27	31.5	0.754	108	3	1.51	37.1	0.632	199
2.1	1.37	33.8	0.683	75	4	1.564	38.3	0.632	49
2.2	1.37	33.8	0.684	156	5	1.46	36.0	0.399	101
2.3	1.34	33.2	0.682	224	6	1.573	38.5	0.58	199
3.1	1.16	29.1	0.78	70	7	1.643	40.2	0.53	48
3.2	1.38	34.0	0.726	145	8	1.581	38.7	0.507	99
3.3	1.23	30.6	0.755	210	9	1.602	39.2	0.507	199
4.1	1.26	31.3	0.749	69	10	1.643	40.2	0.606	48
4.2	1.38	34.2	0.719	145	11	1.507	37.0	0.507	99
4.3	1.25	31.1	0.739	220	12	1.648	40.3	0.462	199
5.1	1.29	32.1	0.647	69					
5.2	1.32	32.8	0.632	143					
5.3	1.23	30.8	0.632	210					
6.1	1.46	36.0	0.598	45					
6.2	1.56	38.3	0.589	91					
6.3	1.49	36.7	0.585	135					
7.1	1.61	39.4	0.615	75					
7.2	1.51	37.2	0.619	150					
7.3	1.54	37.8	0.606	224					
8.1	1.50	36.9	0.634	35					
8.2	1.50	36.8	0.631	72					
8.3	1.39	34.4	0.611	108					
9.1	1.34	33.3	0.755	74					
9.2	1.36	33.7	0.728	155					
9.3	1.39	34.3	0.744	224					
10.1	1.40	34.6	0.627	35					
10.2	1.33	33.0	0.597	74					
10.3	1.31	32.5	0.613	107					
11.1	1.44	35.5	0.649	71					
11.2	1.48	36.4	0.614	140					
11.3	1.39	34.4	0.621	208					
12.1	1.44	35.5	0.615	69					
12.2	1.41	34.7	0.623	142					
12.3	1.38	34.2	0.609	219					
13.1	1.21	30.3	0.731	99					
13.2	1.23	30.8	0.739	203					
13.3	1.24	30.9	0.727	299					
14.1	1.55	38.1	0.595	69					
14.2	1.51	37.0	0.582	140					
14.3	1.52	37.3	0.59	209					
15.1	1.45	35.7	0.589	89					
15.2	1.37	33.9	0.596	181					
15.3	1.37	33.8	0.591	269					

Table 3.9: Peak friction ratio of all triaxial tests to compare to the void ratio and initial stress state.

Individual results fines content approach Lab A-data					
Borehole	Sample	$D_{50}[\mu m]$	fines $[\%](\leq 63\mu m)$	$\lambda_{cs,e}$	Γ
B5.1-001	1	240	0.7	0.0199	0.871
	2	241	0.1	0.0183	0.864
	3	244	1.4	0.0218	0.878
B5.1-002	1	281	1.4	0.0218	0.878
	2	220	1.3	0.0215	0.877
B5.1-003	1	294	2.5	0.0248	0.891
	2	249	2.0	0.0234	0.885
	3	213	1.4	0.0218	0.878
B5.1-004	1	286	1.0	0.0207	0.874
	2	274	0.8	0.0202	0.872
	3	234	0.9	0.0204	0.873
B5.1-005	1	331	0.1	0.0183	0.864
	2	267	0.9	0.0204	0.873
	3	215	1.7	0.0226	0.882
B5.2-001	1	221	0.8	0.0202	0.872
	2	225	1.2	0.0212	0.876
	3	310	1.3	0.0215	0.877
B5.2-002	1	314	1.4	0.0218	0.878
	2	372	1.1	0.0210	0.875
	3	369	0.7	0.0199	0.871

Table 3.10: Results for the fines content approach of the individual samples.

Chapter 4

Statistic characterisation

The actual statistical interpretation of the cone penetration tests (CPT's) is described in this section. Interpretation is done with the use of an already existing code, written in Matlab [Gitman, 2006]. This original code is adjusted to fit the needs of this particular project.

A flowchart of the procedure of the statistical characterisation and derivation of the state parameter profile from a single CPT is given in figure 4.1. This procedure is the part of the procedure that is of interest for the conditional simulation later in this report. The analysis of the original profiles (with trend) is not added in this flowchart and is only partly discussed in this report.

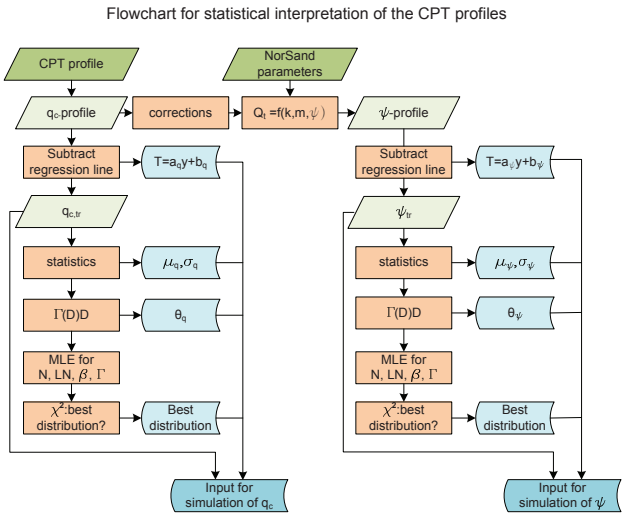

Figure 4.1: Flowchart of the statistical characterisation of the CPT profiles, which is part of the interpretation code.

4.1 Available data: CPT's

The available cone penetration test data consist of 140 data files from individual tests. The tests were performed in two parallel lines at test locations. One line is on the location of the future quay wall, the other is on the location of the future crane axis.

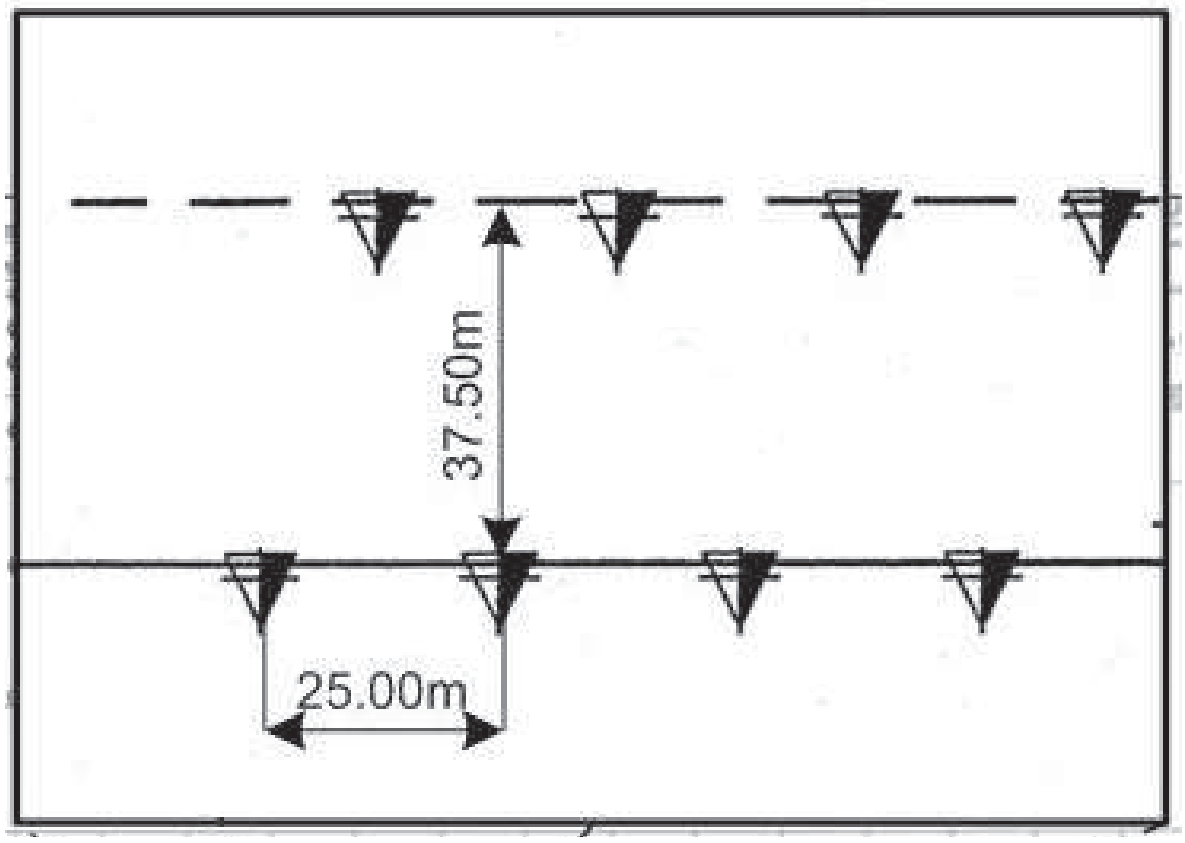

Figure 4.2: Detail of the CPT locations.

The CPT's are taken to a depth of approximately 45m, which is far beyond the depth of the dumped material. The CPT's have readings every 2cm and are stored in .GEF (Geographical Exchange Format) text files.

4.2 CPT interpretation and correction

Before the CPT data can be used to determine the statistical properties, the data need to be interpreted and corrected. This mainly consists of filtering of peak values in the profile and correcting depth and pore water pressure. The corrections that are performed are described in this section.

4.2.1 Pore water pressure

From the 141 CPT's, only 9 contain a pore water pressure reading (see figure 4.3). To avoid a bias between the profiles that contain pore water pressure and the ones that do not, correction for the pore pressure is done based on hydrostatic pressure for all profiles. Because from the pore water pressure reading it is not clear what the (average) water table is, the average water table at the test site is used. The expected water table at the test site is 9cm +NAP [Rijkswaterstaat, 2010]. This level is used as the average water table at the test site to calculate the pore water pressure for the correction of the CPT-profiles. The pore water pressure u is used in the correction for unequal area (to be discussed in section 4.2.2) and to calculate the expected stress state (see section 3.1).

4.2.2 Correction of measurements

The tip resistance that is measured has to be corrected for the water pressure that is active on the different sides of the cone tip. This correction is often referred to as "the unequal area effect" [Lunne et al., 1997]. It is basically a correction for the area within the cone tip on which no water pressure is active. The following equation is used to obtain the corrected total resistance q_t from the measured

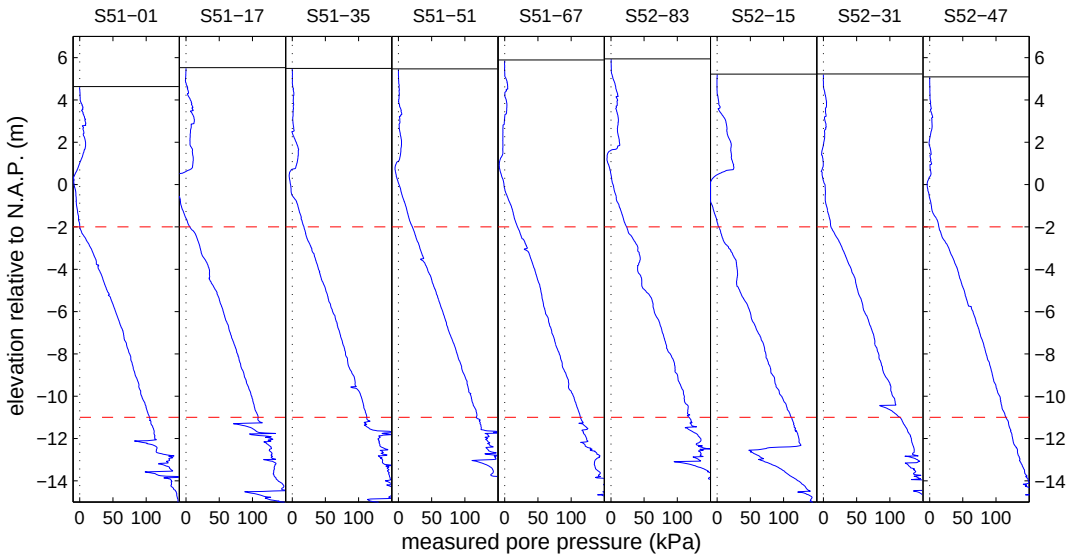

Figure 4.3: The available pore water pressure profiles. Note that the water table varies from place to place, probably due to the tide. The red dashed lines present the boundaries of the homogeneous zone that is used for the interpretation of the statistics. Justification for this zone is further discussed in section 4.3

cone resistance q_c:

$$q_t = q_c + u_2(1 - a) \tag{4.1}$$

Here u_2 is the pore pressure active on the back of the cone tip and $(1 - a)$ is the ratio of area on which no pore pressure is active, based on the cone area ratio a, which usually is around 0.6. Because the pore pressure u has generally not been measured, the expected pore pressure u is calculated based on hydrostatic equilibrium. Excessive pore pressures (during testing) are not expected because of the high hydro-conductivity of sand and the absence of clay in the profile (see figure 4.3).

Although [Lunne et al., 1997] used q_c for the interpretation of the state parameter, in this report q_t is used because the original code already included a correction for the unequal area effect. The tip resistance shown in all profiles is q_t.

Normalisation of the profile is performed to determine the normalised cone tip resistance Q_t according to equation 4.2. The pore pressure profile u that is based on the hydrostatic pressure is used for the difference between the total and effective mean stresses p and p'.

$$Q_t = \frac{q_t - p}{p'} \tag{4.2}$$

4.3 Determination of state parameter

The state parameter is determined as described in sections (3.1.3). All individual state parameter profiles are stored in a text file to be used for further interpretation. The state parameter profile is plotted together with the original CPT-profiles (tip resistance, sleeve friction and friction ratio). In the same profile, the trend, being the linear regression line through all points in the evaluated domain, of the profile is indicated. See appendix D.1

4.4 Results for all the statistical properties

The determination of all statistical properties is programmed in the code by Gitman [2006]. The results of the determination can be found in the appendices; for each CPT-profile a single-page overview is made including the CPT and state parameter profiles (see appendix D.1). A tabular overview of all these results together and an interpretation of all data put together is also given in D.2.

To determine over which domain the profiles need to be interpreted, all tip resistance profiles are depicted together in figure 4.4 with the average tip resistance (red profile). Based on the average tip resistance profile the homegeneous zone is chosen as the domain [-10.6m ; -2.4m] with respect to chart datum (N.A.P.).

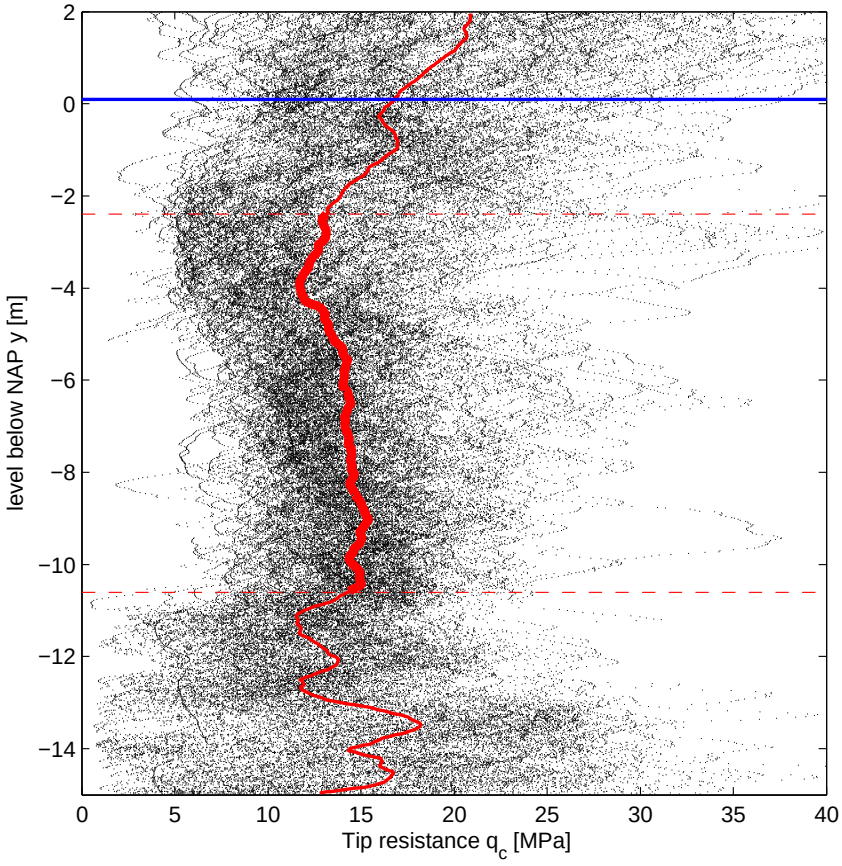

Figure 4.4: All 140 CPT profiles together to determine the homogeneous zone to be evaluated. The red profile is the average over all profiles. The red dashed lines indicate the boundaries of the zone that is assumed to be homogeneous.

The results of the statistical interpretation are nothing more than the application of all the theory discussed above and can be used in the next chapter as input for the simulation. A summary of the results is given in table 4.1. This table represents the mean and standard deviation of the results that are found for the individual profiles. a and b are the parameters of the regression line $ay + b$ in the profile $P(y) = ay + b + Z(y)$. μ is the mean of the profile $P(y)$ and σ is the standard deviation in the trend-removed profile $Z(y)$. The mean of the standard deviations of profiles $Z(y)$ is determined by the square root of the average of the variances in individual profiles $Z(y)$ $\left(\sqrt{\frac{1}{n-1}\sum_{i=1}^{n}\sigma_i^2}\right)$ The scale of fluctuation θ is determined on the trend-removed profile $Z(y)$. Note that $Z(y)$ is first order stationary because the linear regression line is removed from the profile $P(y)$.

Interesting is the small difference between the scales of fluctuation derived from the state parameter and the tip resistance. It suggests that the transformation of the data (from tip resistance to state parameter) has no significant effect on the scale of fluctuation.

The results given in Table 4.1 are the average of the results of all individual profiles. Conclusions based on these averages should be handeled with care, because of the possible correlation between the different parameters. To show that the different parameters are not completely independent from one another, the correlation matrix is given in table 4.2. The table shows that there is a correlation between some of the parameters.

		μ of individual profile results	σ of individual profile results
ψ	μ	-0.124	0.0218
	σ	0.0393	0.010
	θ	0.627 m	0.265 m
	a	-0.00212 /m	0.00938 /m
	b	-0.1378	0.0714
q_c	μ	13.95 MPa	2.05 MPa
	σ	3.46 MPa	1.18 MPa
	θ	0.620 m	0.269 m
	a	-0.353 MPa/m	0.840 MPa/m
	b	11.651 MPa	6.321 MPa

Table 4.1: Mean and standard deviation of the statistics (μ, σ, θ) and trend line parameters (a and b from $P(y) = ay + b + Z(y)$) of the 141 profiles. Results given are the combined results of all individually analised profiles.

		μ	σ	θ	a	b
ψ	b	0.59	0.20	0.02	0.96	1
	a	0.33	-0.19	-0.11	1	
	θ	-0.25	0.44	1		
	σ	-0.12	1			
	μ	1				

		μ	σ	θ	a	b
q_c	b	0.55	0.17	0.05	0.95	1
	a	0.26	-0.03	-0.07	1	
	θ	0.34	0.57	1		
	σ	0.59	1			
	μ	1				

Table 4.2: Matrix with correlation coefficients between the statistic results. Correlated statistical properties should be handled with care when they are used together.

To give a clear overview of all state parameter profiles in a single figure, the state parameter profiles are all presented in one single graph in figure 4.5. It can be mentioned that in general, all profiles are located on the negative side of the $\psi = 0$ line, which suggests medium to dense state.

Instead of removing the trend of each profile individually, the average trend of all profiles can be evaluated. The decision to look at the overall trend is supported by the assumption that the evaluated zone contains the same material with the same properties. The trend therefore can be expected to be the same at all locations in the zone and the difference in linear regression trend lines is merely the effect of variability that is large compared to the domain depth size and trend.

Type of distribution function: For each profile individually the best distribution function describing the data in the profile is determined for both original and trend-removed profiles of ψ and Q. The best distribution is determined by means of the chi square scores. For the conditional simulation, the distribution of the trend removed profiles is of interest, the distributions of the original profiles are shown to compare with the results of the trend removed profiles. The best distribution functions for the trend removed profiles of both ψ and q_c are the normal and β distributions (see figure 4.6). Concluding that both methods are equally favourable to describe the data might not be correect. The individual chi-square scores should be examined for this. Another option is to look at the distribution of all data together.

The distribution of all data together gives a slightly different result from the individual evaluations as can be interpreted from table 4.3. ψ clearly fits best to a normal distribution when all data together are analysed; for q_c the best distribution seems to be the β distribution or the Γ distribution due to the skewed experimental distribution. The reliability of the chi-square goodness of fit in this particular application has been the point of discussion in other parts of this report and no conclusive solution for the indicated problems have been found. The results of the chi-square evaluation are therefore treated with suspicion. For the time being, the results are used and for ψ the most suitable distribution function is expected to be normal, which is favourable with respect to the simulations in the next

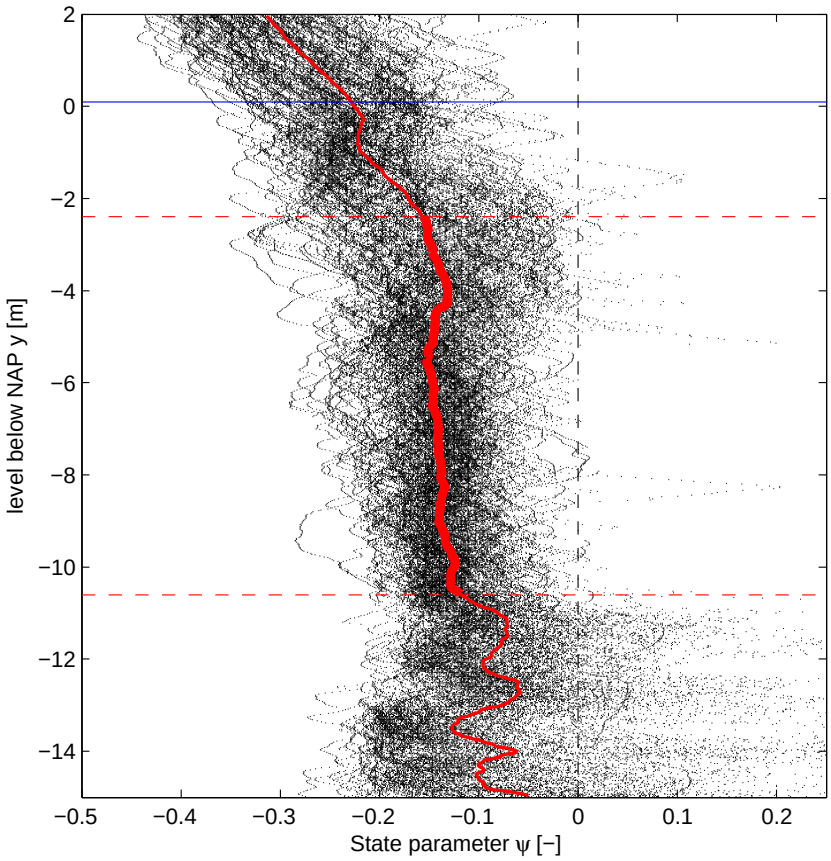

Figure 4.5: All 140 state parameter profiles together. Almost all profiles are below the $\psi = 0$ line and the average profile (red) shows a linear trend with depth. The red dashed lines indicate the boundaries of the zone that is assumed to be homogeneous.

chapter.

distribution	$\psi_{trend-removed}$	$q_{trend-removed}$
Normal	375	1945
LogNormal	4555	2116
Beta	1078	1329
Gamma	2468	1259

Table 4.3: χ^2 scores for all data together for the trend-removed profiles. ψ clearly has a normal distribution, q_c has a Beta or Gamma distribution. χ^2 determined from 20-bin histogram (17 degrees of freedom).

To visualise the fit of all data to the theoretical distribution functions, the most likely fits of the four distributions is compared to the histogram of the data in figure 4.7.

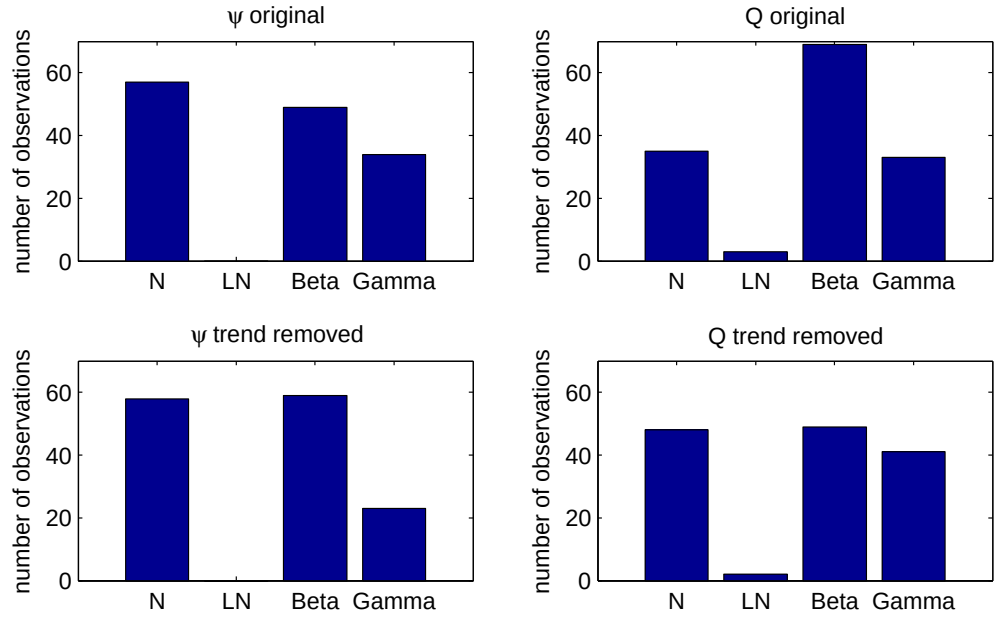

Figure 4.6: Number of profiles for which each distribution is found to be the best distribution based on the chi-square scores. For the trend-removed profiles, Normal and β distributions prove to be the best distributions, followed by the Γ distribution.

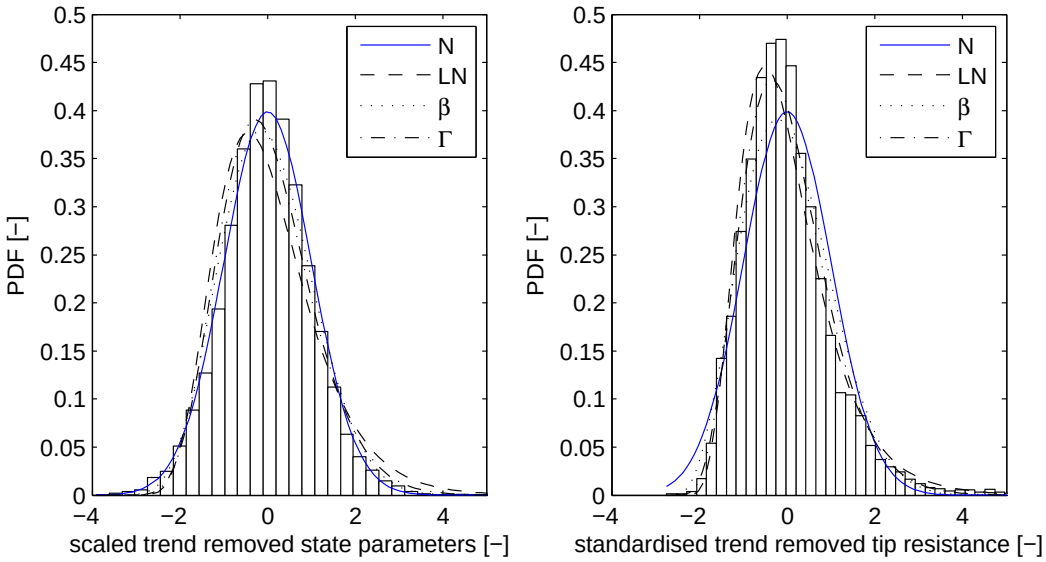

Figure 4.7: Fit of the theoretical distributions to all data. The state parameter fits best to the normal distribution. The tip resistance has a more skewed distribution and therefore better fits the skewed distributions.

Chapter 5

Field simulations

In the previous chapters, the statistics of the soil have been determined to fully characterise the soil properties. Now, based on the statistics, the actual field of the soil is simulated using random fields. The methods to generate these random fields and to condition them to the CPT-profiles are described in this section. First the theoretical background of the methods is given, after which it is shown that the conditioned random fields can be generated to simulate the subsurface. Throughout the chapter, the influences of the applied methods on the reduction of uncertainty are evaluated and quantified. Finally, the performance of the conditioning method with respect to computational expense and reduction of uncertainty is evaluated.

5.1 Random field generators

A number of different methods can be used to produce random fields, all with their specific advantages and disadvantages. Properties that are important for the suitability a specific method are consistency in the correlation structure (the correlation structure that is used as input should be met by the generated random field) and the computational expense of the methods is of importance when applied on larger calculations. Fenton and Griffiths [2007] compare six methods of random field generation algorithms. Three of them (Moving average methods, the Discrete Fourier Transform method and Covariance Matrix Decomposition) are directly rejected because of their computational extensiveness for larger fields. From the other three evaluated methods LAS is proved to be the least computative method. From the other methods the Fast Fourier Transform method does not reproduce te correct correlation structure unless a double-sized domain is evaluated. The LAS method was demonstrated to be the computational least expensive compared to the other five methods and is the only method directly producing local average fields instead of point statistics fields (the values in the LAS method is the average over the cell domain, local average; the values in the other methods are the values at the exact point locations, point statistics).

One method that is not discussed by Fenton and Griffith is the Sequantial Gaussian Simulation (SGS) technique. This method produces the random field in a sequential way by kriging the mean and standard deviation of every subsequent point in the generation of the field. The point value is then obtained by a random normal number. Bruining et al. [1997] found that SGS is the preferred method for generating random fields with an exponential correlation structure. The method however involves solving a system of equations the size of all correlated points in the neighbourhood of the point to be evaluated. A different system of equation has to be solved for every point to be generated. For larger fields with a high resolution compared to the scale of flucuation, this method can be expected to become extremely computational expensive. Next to this, the SGS is not particularly suited for the generation of local average fields. Because the future application of the conditional simulation will be in finite element programming, a direct generation of local average fields is preferred. Therefore the LAS method is used for the realisation of unconditioned random fields.

5.2 Local Average Subdivision

This section describes the LAS procedure and evaluates the possibilities to modify the LAS procedure to condition the random fields that are produced to already known points in the field.

Based on the concept of the variance function, Fenton and Vanmarke [1990] introduced the method of Local Average Subdivision (LAS), a method to generate random fields by subdividing the domain of interest in subsequent steps. Starting with a cell as large as the full domain, in subsequent levels of division, the cell is divided into smaller cells with a cell size that is half the parent cell size. When each new cell is taken as a weighted average of its neighbouring cells plus a white noise term, each level of subdivision can be generated in such a way that the statistical properties (mean, standard deviation and correlation structure) are satisfied. In this way a field is constructed that satisfies the full variance function and the point statistics.
The approach was motivated by the need to represent engineering properties as local averages and to be able to easily condition the realisation to incorporate known data change resolutions within sub-regions [Fenton and Vanmarke, 1990]. Unfortunately, the conditioning was not described by Fenton. Further elaboration on the conditioning can be found further down in this report.

5.2.1 Derivations with 1D example

The LAS method is a method to construct random fields in a top-down recursive method [Fenton and Vanmarke, 1990]. For a 1D field over the domain size D, the process starts at level 0 for which a global average for D is generated (Z_1^0). In level 1, this global average is divided into 2 $1/2D$ sized cells (Z_1^1 and Z_2^1), which need to satisfy the correlation structure and statistics for local averaging. The new cells maintain the global average of the zeroth level. In very subsequent level, the cells in the preceding level (the 'parent' cell Z_j^i) are divided into two cells (Z_{2j}^{i+1} and Z_{2j-1}^{i+1}). The average over the two new cells equals the parent cell and again the correlation structure and the statistics are maintained for the local average at the cell size. Figure 5.1 gives the first 3 levels of subdivision.

Z_1^0							
Z_1^1				Z_2^1			
Z_1^2		Z_2^2		Z_3^2		Z_4^2	
Z_1^3	Z_2^3	Z_3^3	Z_4^3	Z_5^3	Z_6^3	Z_7^3	Z_8^3

Figure 5.1: First 3 levels of subdivision from the expected mean at Z_1^0

To maintain statistics and correlation structure at all levels in accordance with the local average theory, the values Z_{2j}^{i+1} are linear combinations of the parent cell and its $2n$ neighbours plus a white noise term. The linear combination is unbiased (the sum of weights a_m equals zero) and the white noise term is zero-mean, normally distributed. All values Z_{2j-1}^{i+1} are chosen in such a way that the average of Z_{2j-1}^{i+1} and Z_{2j}^{i+1} equals the parent cell to maintain the global average.
Every new cell is a linear combination of the parent cell and $2n$ cells next to this parent cell. If $m{=}-n,\ldots,n$ then the weights a_m^i and the variance of the white noise terms c^i are a function of the correlation structure and the cell domain $D_i = 1/2^i D$. In equations, this method is given by:

$$Z_{2j}^{i+1} = \sum_{k=j-n}^{j+n} a_{k-j}^i Z_k^i + c^{i+1} U_j^{i+1}, \qquad \text{with: } a_m^i = f(D^i, C(h)), c^i = f(D^i, C(h)) \tag{5.1}$$

$$Z_{2j-1}^{i+1} = 2Z_j^i - Z_{2j}^{i+1} \tag{5.2}$$

The only parameters that need to be derived now are the functions for a_m^i and c^i.

The correlation structure for the subsequent level is different than the correlation structure of the final field. This is the effect of the local average in the earlier levels. A formulation for the local average correlation structure is given by Vanmarcke [1984] and makes use of the variance function $\Gamma(h)$. It gives the covariance between two cells at level i at a distance mD^i (equation 5.3):

$$E[Z_k^i Z_{k+m}^i] = \frac{1}{2}\left[(m-1)^2\Gamma((m-1)D^i) - 2m^2\Gamma(mD^i) + (m+1)^2\Gamma((m+1)D^i)\right] \tag{5.3}$$

The variance between the subsequent levels can easily be derived into equation 5.4 when it is noticed that the average of every new pair of cells equals the parent cell;

$$E[Z_{2j}^{i+1} Z_{j+m}^{1}] = \frac{1}{2} E[Z_{2j}^{i+1} Z_{2j+m-1}^{i+1}] + \frac{1}{2} E[Z_{2j}^{i+1} Z_{2j+m}^{i+1}. \tag{5.4}$$

When equation 5.1 is multiplied by Z_m^i and the expectation of the left and right sides of the equation are considered, the white noise term falls out of the equation and equation 5.5 is used as a method to determine the weights a_m^i. The variances can be found with the help of equations 5.4-5.3.

$$E[Z_{2j}^{i+1} Z_{j+m}^{i}] = \sum_{k=j-n}^{j+n} a_{k-j}^{i} E[Z_k^i Z_{j+m}^i] \tag{5.5}$$

The white noise variance between the subsequent levels c^{i+1} can be found by equation 5.6. The expression makes use of the fact that $var(A+B)$=$var(A) + var(B)$.

$$(c^{i+1})^2 = E[(Z_{2j}^{i+1})^2] - \sum_{k=j-n}^{j+n} a_{k-j}^{i} E[Z_{2j}^{i+1} Z_k^i] \tag{5.6}$$

With the last two equations, the parameters a_m^i and c^{i^2} can be determined. These parameters can be used in equation 5.1 to generate realisations of Z_{2j}^{i+1}. In this way, the entire field can be generated. In the general case, n is chosen to be 1, so that m is [-1 0 1]. This means that each cell Z_{2j}^{i+1} has 3 parent cells of which it is a linear combination. At the boundaries of the domain, the parent cell Z_{j-1}^i or Z_{j-1}^i might not exist. In this case equations 5.4-5.3 are solved using only the available parent cells. This influences the weights a. LAS works only for Gaussian fields, because of the summation of random processes at each level. Possibly the best method to generate non-Gaussian fields is to converge Gaussian fields to non-Gaussian fields by means of the cumulative density functions of the fields in a distribution transformation.

To test the LAS-method in combination with the conditioning, a LAS-code is written in Matlab to simulate unconditioned random 1-D fields. This method uses an exponential variance function in the form of equation 2.23. All evaluations of 1-D random fields use this LAS code.

5.2.2 Application of LAS in 2-D

To generate random fields in 2-D an existing code is used. This is initially written in Fortran and now runs as an executable outside Matlab. In this report it will be referred to as Sim2D.
Sim2D uses the approximate exponential variance function (equation 2.24) as the correlation structure. It works out an anisotropic random field by simulation of an isotropic random field that is deformed into an anisotropic field by squashing and stretching. Squashing is the process in which the average of a row or column of adjacent cells forms the value for a single cell of the new field. In this way, multiple square cells of an isotropic field merge into a single square cell of an anisotropic field. Stretching is the interpolation between two adjacent cells to generate a row or column of cells of a field with higher anisotropy. This method is less accurate than squashing, because the interpolation affects the statistics of the field in a different way than the LAS method. Squashing is a process that is in line with the LAS method, because the LAS method guarantees consistent statistics for larger cell domains. The averaging of cells therefore changes the statistics in the same way as the LAS method and the variance function that was used to generate the field is still honoured. Furthermore, squashing uses a more detailed field to start with and therefore incorporates a higher precision of statistics.
As input the code uses:

- k: number of realisations
- n_x: number of columns
- n_y: number of rows
- i: number of subdivision levels used (8-13)
- D_{cell}: cell dimension (square cells)
- θ_v: vertical scale of fluctuation
- μ: field mean
- σ: field standard deviation
- ξ: anisotropy; ratio between horizontal and vertical scale of fluctuation
- $seed$: seed to start the random number generator (large negative number)
- $.false.$: for normal distribution (.true. for lognormal distribution)

The effect of the application of the approximate exponential variance on the correlation structure of the generated fields is discussed in section 5.4.6.

5.2.3 On the conditioning of the LAS method

It is attempted by the author to condition the random field generated with LAS by changing the internal algorithm. It is found that changing the procedure in such a way that assigned cells will have a predefined value after generation of the field with LAS is not preferable. This is discussed in the following section. As an example, the conditioning of a 1D LAS field of 8 cells is tried to be conditioned to $Z(x_0)$ at cell Z_8^3.

For the conditioning of the LAS-procedure, some properties of the weighting functions are used:

- a_0^i=1 and a_{-n}^i=$-a_n^i$, which implies that E[Z_{2j}^{i+1}]=E[Z_j^i]
- $\sum c_i^2$=σ^2
- a_m^i and c_i are independent from Z_j^i

When it is considered that the expected value of every cell in the LAS-generated fields is 0 and the influence of cells Z_{j-1}^i and Z_{j+1}^i on Z_{2j}^{i+1} is expected to be zero, the value Z_j^i is the sum of the white noise terms times the level standard deviation c_i of all individual levels i:

$$Z_j^i = \sum_{k=0}^{i} N_i(0, c_i). \tag{5.7}$$

In this equation $N(0,1)$ is the standard white noise term; a realisation from a standard normal distribution. All white noise terms are independent and therefore the expectation of Z_j^i is zero and the variance at level i is given by

$$E[(Z_j^i)^2] = \sum_{i=0}^{I} c_i^2. \tag{5.8}$$

When Z_j^i is known to be the conditioning point $Z(x_0)$, this constrains the result of the outcome of every white noise term. The white noise terms are now no longer independent from one other; the outcome of $N_0(0, c_0)$ influences all other noise terms to end up at $Z(x_0)$. The sum of $I+1$ dependent variables can be written as a sum of I independent variables $N_i(\hat{b}_i, \hat{c}_i)$;

$$Z(x_0) = \sum_{i=0}^{I-1} N_i(\hat{b}_i, \hat{c}_i) \tag{5.9}$$

with conditioned noise parameters

$$b_i = f(c_0, \ldots, c_I, Z(x_0)) \tag{5.10}$$

$$\hat{c}_i = f(c_0, \ldots, c_I, Z(x_0)). \tag{5.11}$$

The formulation of an equation for b_i and $\hat{c}_i$ has not been found by the author and considered to be of importance only at the moment the further implementation of this method has been proved to work. Considering the values for b and $\hat{c}$ being possible to be found, the application in the LAS method needs to be possible.

Assuming the conditioned noise parameters given in equations 5.10 and 5.11 can be solved before the first level of subdivision is applied, the introduction of the first noise terms will influence the expectation for the cells next to the direct parent cells of the conditioned cell Z_{x_0}. Because these cells only cancel out at the moment the expectation of Z^i_{j-1} and Z^i_{j+1} are the same (which is no longer valid at the moment the noise is introduced) all parent cells of the conditioned cell $Z(x_0)$ at all levels need to be conditioned to ensure conversion towards the value of the conditioned cell. The introduction of all parent cells into the (probably) system of equations that solves the noise parameters for all parent cells is expected to increase to problem to a level at which it is no longer possible to solve in an easy and straightforward way. Considering that this is only for one conditioning point and the introduction of multiple conditioning points in a field of more than one dimensions, it is expected to be unlikely that this approach leads to a conditioning algorithm that can be implemented in an engineering environment.

In an attempt to visualise the internal conditioning of the LAS procedure, figure 5.2 was produced.

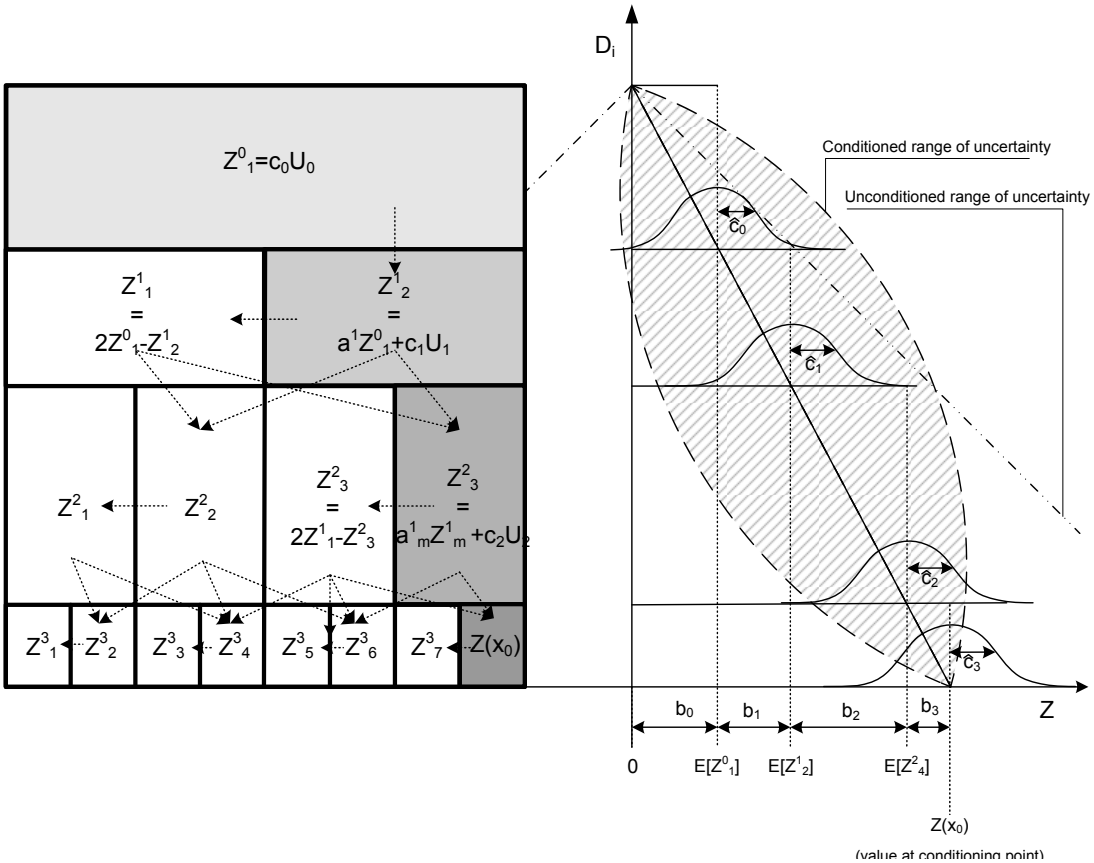

Figure 5.2: Schematic presentation of LAS process with conditioned cell Z^3_8.

5.3 Kriging

Kriging is an interpolation method first described by Matheron, inspired by the work by D.G. Krige on the prediction of gold grades at the Witwaterrand reef system in South-Africa [Cressie, 1990]. Kriging is a "BLUE" method; a *Best Linear Unbiased Estimator*. Given a set of spatially distributed values, it interpolates the field between these values so that the expected error of the generated points in the field is minimised. To predict the error in the result, the kriging method uses the variogram or the

expected mean and covariance structure.
Kriging on itself might not be interesting in the field of the project because estimation is not the purpose. The principles of kriging however are used to condition the random field in a post-prosessing algorithm that will be discussed later. The characteristics of kriging therefore are discussed thorougly to be able to apply kriging in the conditioning of the reandom field.

5.3.1 Simple Kriging

Simple kriging (SK) is the most basic method of kriging. It requires second-order stationary data (expectation of mean and standard deviation are constant on the domain) with a known mean μ. The simple kriging predictor gives the best estimation $Z^*(x_0)$ of the value $Z(x_0)$ as a linear combination of all known values $Z(x_\alpha)$ and the known mean value μ.

$$Z^*(x_0) = \sum_{\alpha=1}^{n} \lambda_\alpha Z(x_\alpha) + \mu \tag{5.12}$$

Z^* is the best estimation in the sense of $var(Z - Z^*)$; the error of the kriged field Z^* with respect to the original field Z is quantified by the variance of the difference between the two. The weights λ_α^{SK} that give this best estimation are given as the solution of the *Simple Kriging System*, given as equation 5.13. The derivation of this system of equations is given in appendix E.1.

$$\begin{pmatrix} C(x_1 - x_1) & \cdots & C(x_1 - x_n) \\ \vdots & \ddots & \vdots \\ C(x_n - x_1) & \cdots & C(x_n - x_n) \end{pmatrix} \begin{pmatrix} \lambda_1^{SK} \\ \vdots \\ \lambda_n^{SK} \end{pmatrix} = \begin{pmatrix} C(x_1 - x_0) \\ \vdots \\ C(x_n - x_0) \end{pmatrix} \tag{5.13}$$

The kriged result Z^*_{SK} that is found by simple kriging is an estimation of the true value $Z(x_0)$. This error is of a normal distribution with mean zero (because of the unbiasedness) and a variation σ^2_{OK}. This variation is given by

$$\sigma^2_{SK} = C(0) - \begin{pmatrix} \lambda_1 \\ \vdots \\ \lambda_n \end{pmatrix}' \begin{pmatrix} C(x_1 - x_0) \\ \vdots \\ C(x_n - x_0) \end{pmatrix}. \tag{5.14}$$

At locations $x_0 = x_i$ for $x_i \in x_\alpha$ the variance equals zero, increasing with larger distance from these points. The maximum variance is given by the variance of the dataset itself as C(0).

5.3.2 Ordinary Kriging

Ordinary kriging is a kriging method that is slightly more general than simple kriging. It requires second-order stationary data (expectation of mean and standard deviation are constant on the domain) and the mean might be unknown. Like simple kriging, ordinary kriging gives the best estimation of $Z(x_0)$ based on the minimum of the variation of the estimation error $Z^* - Z$. Because the mean is considered to be unknown and unbiasedness needs to be guaranteed, the sum of the weights λ_α needs to be 1, to give Z^* as a direct linear combination of $Z(x_\alpha)$:

$$Z^*(x_0) = \sum_{\alpha=1}^{n} \lambda_\alpha Z(x_\alpha), \qquad \text{with} \qquad \sum_{\alpha=1}^{n} \lambda_\alpha = 1 \tag{5.15}$$

When the best estimator is found based on the minimum of $var(Z^* - Z)$, the weights λ are the solution of the *Ordinary Kriging System*, given as equation 5.16. The derivation of this system of equations and the expressions for the estimator and the variation are given in the appendix E.1.

$$\begin{pmatrix} \gamma(x_1 - x_1) & \cdots & \gamma(x_1 - x_n) & 1 \\ \vdots & \ddots & \vdots & \vdots \\ \gamma(x_n - x_1) & \cdots & \gamma(x_n - x_n) & 1 \\ 1 & \cdots & 1 & 0 \end{pmatrix} \begin{pmatrix} \lambda_1^{OK} \\ \vdots \\ \lambda_n^{OK} \\ \mu^{OK} \end{pmatrix} = \begin{pmatrix} \gamma(x_1 - x_0) \\ \vdots \\ \gamma(x_n - x_0) \\ 1 \end{pmatrix} \tag{5.16}$$

$\gamma(x_\alpha - x_\beta)$ is the variogram of the data. Because of the second-order stationarity, the variogram can be expressed as $C(0) - C(x_\alpha - x_\beta)$. μ^{OK} is the Lagrange parameter, that is needed to solve the system of equations for minimum variance (see appendix E.1).
Ordinary kriging gives the best estimate as a linear combination of all known points x_α. Unbiasedness is guaranteed by the constraint on the sum of the weights λ_α. The true value $Z(x_0)$ that is estimated by $Z^*(x_0)$ is expected to be within a certain range around $Z^*(x_0)$. In fact, the distance $Z(x_0) - Z^*(x_0)$ is normally distributed around $Z^*(x_0)$ with a variance σ^2_{OK}. This variance is independent from all values Z^* and $Z(x_\alpha)$ and given by

$$\sigma^2_{OK} = \begin{pmatrix} \lambda_1^{OK} \\ \vdots \\ \lambda_n^{OK} \\ \mu^{OK} \end{pmatrix}' \begin{pmatrix} \gamma(x_1 - x_0) \\ \vdots \\ \gamma(x_n - x_0) \\ 1 \end{pmatrix}. \tag{5.17}$$

5.3.3 Example of Kriging

To clarify the estimation by Kriging, the example profile (given in figure 2.2) is kriged based on 8 randomly choosen points. For the correlation structure, the scale of fluctuation from figure 2.8 (θ=0.47m) is used together with the assumption of an exponential correlation structure. The variance scaling parameter is taken from figure 2.5 as $C(0)=\sigma^2=3.209$. This leads to a correlation structure

$$C(x_0, x_i) = 3.209\ exp\left(-\frac{2|x_0 - x_i|}{0.47}\right) \quad \gamma(x_0, x_1) = 3.209\left(1 - exp\left(-\frac{2|x_0 - x_i|}{0.47}\right)\right) \tag{5.18}$$

that is used for the weighting in the kriging operation. Both simple kriging and ordinary kriging are shown, together with their 95% confidence range and the variance.

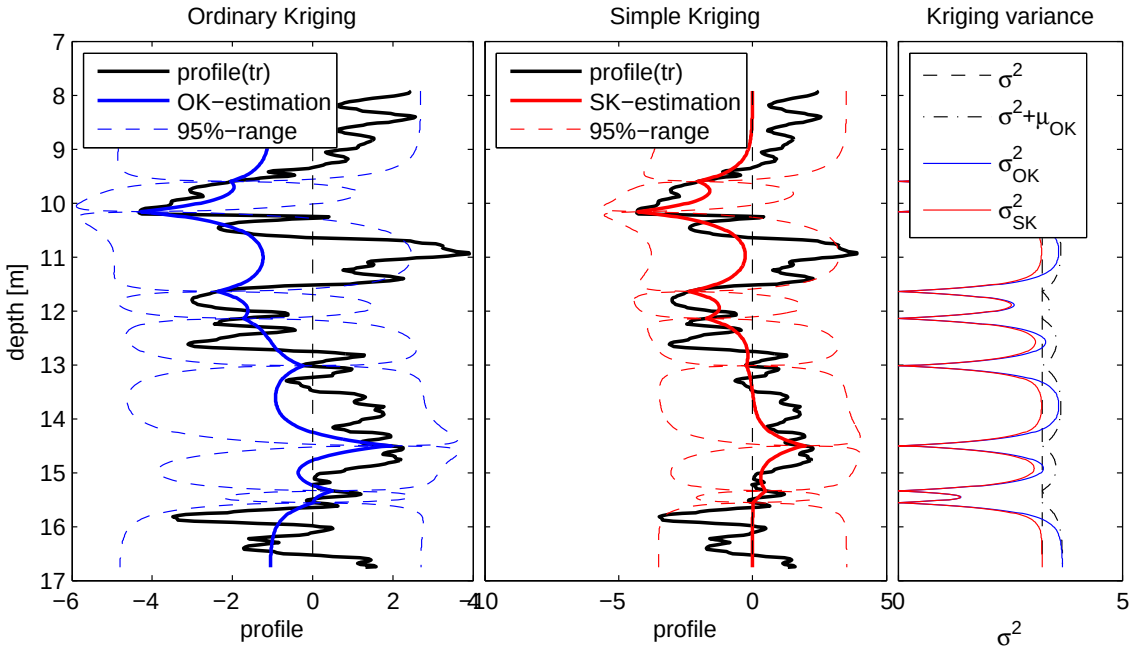

Figure 5.3: Example of kriging based on 8 random points of the profile. Statistical properties: θ=0.47m, σ^2=3.209, exponential correlation structure.

Although kriging gives the best estimation of the field that needs to be simulated, it does not provide the best simulation when the variability of the field is of interest. Kriging can only be used to estimate the mean and variance at field locations and to include the correlation structure of the generic field, other random field simulation techniques need to be used.

5.3.4 Computational expense of Kriging

This section covers the computation time of the kriging procedure. The computation time of the conditioning is of importance for the feasibility of the application of the conditioning in an engineering environment: when the conditioning takes a large amount of time compared to the improvement in the results of the analysis, it might not be interesting to use the conditioning at all. Because kriging uses the solution of a system of equations with the size of the number of the conditioning points, one of the important parameters in the computation time is the number of conditioning points. An other important parameter in the kriging is the number of points in the field that need to be kriged. The larger the field or the higher the field resolution, the longer the kriging will take. Therefore the kriging can be expected to take more time for larger number of points in the field and the number of conditioning points.

Despite the possible large computation time of the conditioning compared to the generation of the unconditioned random fields, a large computation time does not necessarily causes problems. When it is considered that the simulated fields are to be used in finite element analysis, the time for the conditioning of the random fields can be expected to be small compared to the time needed for the analysis with the finite element method.

As mentioned above, the use of the kriging methods involves the solution of the equation $\Gamma\lambda = \gamma$. When all conditioning points $Z_0(x_\alpha)$ are considered to contribute to the value of each point in the field to be kriged, the matrix Γ does not change during the entire operation. This means that matrix Γ has to be constructed and inverted only once. The size of Γ is $n \times n$ for n known conditioning points $Z(x_\alpha)$. Because $\gamma(x_i, x_0)$ changes for every point that needs kriging, $\Gamma\lambda = \gamma$ needs to be solved N times for a field of N points. For every point, Z^* is found by the multiplication of λ' by $Z(x_\alpha)$. In case of a larger distance between the conditioning points, the size of Γ can be reduced by only considering the conditioning points $Z_0(x_\alpha)$ that are correlated well enough to the point to be kriged. All points at distance $d \leq 3\theta$ for example can be used as a selection criteria for the neighbourhood. Because all points to be kriged have an other neighbourhood, the system $\Gamma\lambda = \gamma$ needs to be solved for all N points in the field. This method therefore can only be beneficial above including all conditioning points in case of the following cases:

- The number of field points N is not very large compared to the number of condition points n
- The conditioning points are distributed over a domain that is large compared to the scale of fluctuation to be able to ignore the bigger part of the conditioning points

Because in this report the simulated fields have a high resolution, n is small compared to N and the fields are not large compared to the scale of fluctuation, all conditioning points are used to krige every point in the fields. In this way, no decisions need to be taken in the selection of the appropriate search neighbourhood. The analysis of the computation time of kriging therefore relates to the kriging method in which all available conditioning points are taken into account over the entire field.

The time it takes to krige a full field depends on the process time of each individual step and the number of times each step has to be performed. The time it takes to perform a single step is usually a function of the matrix size n. For the general operations involved in the total kriging operation, the calculation time t can be given as a function of the number of known points n:

operation	time	operation
create $[n \times n]$	$t \propto n^2$	create square matrix
create $[n \times 1]$	$t \propto n^1$	create vector
$[n \times n] \backslash [n \times 1]$	$t \propto n^3$	solve system of equations
inv$([n \times n])$	$t \propto n^3$	invert square matrix
$[n \times n] * [n \times 1]$	$t \propto n^2$	matrix-vector product
$[1 \times n] * [n \times 1]$	$t \propto n^{1/2}$	vector product

Table 5.1: Theoretical calculation time for matlab operations, derived experimentally.

The relation between the known points n and the calculation time t is tested using vectors and matrices filled with random numbers. The results that support the calculation times for operators can be found in appendix E.3. The only operations for which the calculation time increases with the

number of points with the power 3 are the inversion of the square matrix Γ and the solution to the system of equations. The solution to the system of equations can be avoided in the kriging scheme when the inverse of the square matrix Γ is calculated once. The kriging scheme that is used in this case is given in table 5.2.

using all n known points $Z(x_\alpha)$	1 times
create $\Gamma(x_i, x_j)$	$c_1 n^2$
invert $\Gamma(x_i, x_j) \rightarrow \Gamma^{-1}$	$c_2 n^3$
for all N field points to be estimated	N times
create $\gamma(x_i, x_0) \rightarrow \gamma$	$c_3 n$
determine $\lambda = \Gamma^{-1}\gamma$	$c_4 n^2$
determine $Z^* = Z(x_\alpha)\lambda$	$c_5 n^{1/2}$

Table 5.2: Operation scheme for kriging. Approximate function of calculation is given as cn^k. The difference between matrix size n and $n+1$ (for Ordinary Kriging) is neglected.

The sum of all operation times in the scheme gives an estimation of the total operation time for the kriging of a N-point field conditioned by n known points as given by equation 5.19.

$$\begin{aligned} t(n,N) = &\quad c_2 n^3 + [c_1 + c_4 N]\, n^2 + (c_3 n + c_5\sqrt{n})N \\ = &\quad [c_3 + c_4 n]\, nN + c_5\sqrt{n}N + (c_2 n + c_1)n^2 \end{aligned} \tag{5.19}$$

For large n and N, the lower-order terms drop out and the calculation time t converges to

$$t(n,N) = c_4 N n^2 + c_2 n^3. \tag{5.20}$$

When $N >> n$ (which is usually the case, because otherwise no kriging is needed), the calculation time t can be further reduced to

$$t(n,N) = c_4 N n^2 = cNn^2. \tag{5.21}$$

5.3.5 Uncertainty of the Kriged fields

Kriging is an estimation with the lowest variance in the error that can be expected in the estimation. Considering the application of kriging in the conditioning of the random fields, it it desired to quantify this kriging error. In section 5.4 it will be explained that the kriging error is the same as the error in final conditioned field. In this report the error ϵ is defined as $\sqrt{\sigma_K^2/\sigma^2}$. This error ϵ is the expected absolute difference between the true field Z and the kriged field Z^* divided by the standard deviation of the original field σ. For ordinary kriging, the method that will be used for the conditioning, the definition of the error ϵ is given by

$$\epsilon = \frac{E[|Z - Z^*|]}{\sigma} = \frac{\sigma_{OK}}{\sigma}. \tag{5.22}$$

The ordinary kriging variance σ_{OK} equals zero at any point $x_0 = x_i$, for $x_i \in x_\alpha$ and increases with the distance $|x_0 - x_i|$. The maximum variance for ordinary kriging can be derived from equation 5.17 as $C(0) + \mu_{OK}$. The size of the Lagrange multiplier μ_{OK} depends on the number and spatial distribution of the known points $Z(x_\alpha)$. The more points available and the better their distribution over the domain, the smaller the Lagrange parameter will be. The Lagrange parameter μ is not a constant, but changes over the field. The maximum value for the Lagrange parameter can be found at an infinite distance from the conditioning points. In practice, the Lagrange parameter is at the maximum in the domain that has no conditioning locations x_α within the maximum correlation distance.
The estimation error in Ordinary Kriging consists of two parts. When the error is expressed as the variance of the difference between $Z^*_{OK}(x_0)$ and $Z(x_0)$ it is the sum of the simple kriging variance

(based on a known mean) and the uncertainty about the true mean. The uncertainty about the mean is a function of the Lagrange multiplier μ_{OK} and the simple kriging weights λ_α^{SK} [Wackernagel, 1998].

$$\sigma_{OK}^2 = \sigma_{SK}^2 + \left(1 - \sum_{\alpha=1}^{n} \lambda_\alpha^{SK}\right)^2 \mu_{OK} \tag{5.23}$$

The error can be expected to be larger at locations further away from the known point. For distances $x_0 - x_{\alpha,i} \gg x_{\alpha,i} - x_{\alpha,j}$ the simple kriging weights will tend to 0 because the expectation is no longer dependent on the known points and equals the mean. This means that for larger distances, the ordinary kriging variance tends to the form

$$\sigma_{OK}^2 = \sigma^2 + \mu^{OK} \tag{5.24}$$

because all terms that include simple kriging weights λ^{SK} will tend to zero. The Lagrange multiplier does not necessarily converge to a certain constant value, because of the constraint on the sum of the weights. The value for μ_{OK} is still dependent on the mutual distances between the known points. The upper and lower boundary for μ_{OK} can be found by:

If $\lvert x_{\alpha,i} - x_{\alpha,j}\rvert \ll \theta$	and	$\lvert x_{\alpha,i} - x_0\rvert \gg \theta$	$\mu^{OK} \approx \sigma^2$
If $\lvert x_{\alpha,i} - x_{\alpha,j}\rvert \gg \theta$	and	$\lvert x_{\alpha,i} - x_0\rvert \gg \theta$	$\mu^{OK} \approx \sigma^2/n$

This means that at kriging locations far from the known points, the domain of the kriging error is given by $\sqrt{\frac{n+1}{n}}\sigma \leq \epsilon \leq \sqrt{2}\sigma$. This means that the expected error is larger than $C(0)$ at larger distance due to the uncertainty in the kriging estimation of the mean.

To be able to quantify the performance of the full kriged field, an expression of the expected error in the kriged field is desired. Imagine an unknown normal distribution field with second-order stationarity for which the mean and the correlation structure $C(h)$ are known. All possible realisations for the simulation of this field by random fields are expected to be in a certain range around the mean. This range is given by the standard deviation of the field $\sigma = \sqrt{(C(0))}$; 95% of the simulated points are expected to be in the range $\mu \pm 1.96\sigma$. Within this range an infinite number of different realisations of simulations of the actual field are possible. The expected value of every simulation is the mean and the best estimate of the field therefore is the mean μ itself.

When a certain number of points of the actual field are known, the estimation can be conditioned by these conditioning points using kriging estimation. Conditioning of the estimation narrows down the number of possibilities of simulated random fields; the uncertainty is given by the kriging estimator σ_K that constrains the range of uncertainty to zero at the conditioning points. The 95% certainty domain in which the actual field can be expected is narrowed down by the conditioning of the kriging estimation; the more conditioning points that are available, the smaller the uncertainty of the estimation of the actual field is. The domain in which 95% of the actual field can be expected is reduced to $\mu \pm 1.96\sigma_{OK}$. An example of the uncertainty is given in figure 5.4. Because the kriging variance $\sigma_O K^2$ is not constant but location-dependent, the uncertainty over a full domain D has to be averaged over the domain. To quantify the uncertainty, a new variable 'total uncertainty' u is introduced. The definition of the total uncertainty u is chosen to be

$$u = \frac{1}{\sigma D} \int^{D} \sigma_{OK} \delta A, \tag{5.25}$$

which makes it the ratio between the average of the ordinary kriging standard deviation σ_{OK} and the initial standard deviation σ. Unconditioned fields for this reason have a total uncertainty of 1, the limit of total uncertainty is 0 for a field that is conditioned on each field point.

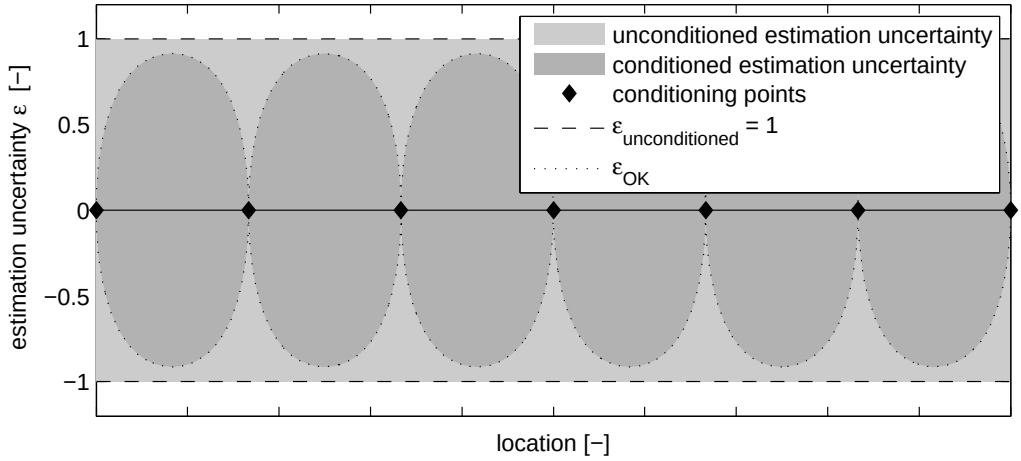

Figure 5.4: Example of uncertainty of an unconditioned estimation against the uncertainty of a conditioned estimation; total uncertainty can be interpreted from the surface under the graphs (conditioned/unconditioned=0.768/1), maximum uncertainty is the maximum of the graph (conditioned/unconditioned=0.913/1). An exponential correlation structure is assumed.

The reduction of uncertainty increases with increasing number of conditioning points (or decreasing distance between the conditioning points). Therefore, it would be an advantage to include as many conditioning points as possible. However, the more conditioning points are included, the more computationally expensive the process will become. When a large number of conditioning points are available (for example in the case of a CPT profile in a 2D field) it might be unnecessary to include all points because of the correlation between the conditioning points. In the case of clustered conditioning points points (like a CPT profile in a 2D or 3D field) the uncertainty does not continue to decrease with the increase of conditioning points. The efficiency of the conditioning of the field comes into play at the moment that the reduced uncertainty is compared with the calculation time. The next sections will discuss the different factors that influence the efficiency.

To investigate the effectiveness of the number of conditioning points in the field, the total uncertainty u as a function of the distance between the conditioning points is looked at. The first estimation is done in 1D. Based on the assumption of an exponential correlation structure, normal distribution and unit field statistics μ=0, σ^2=1 and θ=1, the kriging variance σ_K^2 is determined for a kriging estimation between 20 points. The spacing between the points is varied between 100θ and 0.01θ. Both simple kriging and ordinary kriging are applied and both the maximum uncertainty $\sigma_{K,max}$ and the total uncertainty u are determined. The results of this analysis are gathered in figure 5.5, clarifying that the uncertainty decreases with the square root of the distance between the conditioning points.

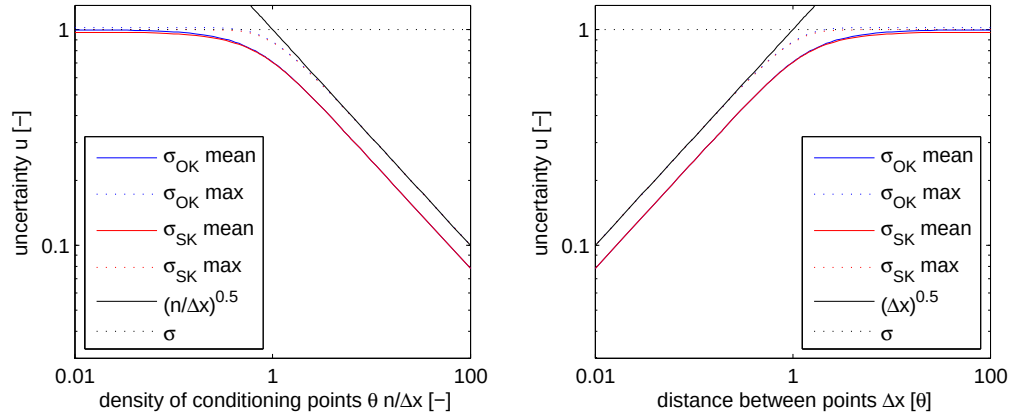

Figure 5.5: Kriging uncertainty in 1D as a function of the number of conditioning points; uncertainty decreases with the square root of the number of points for spacing smaller than scale of fluctuation θ

The uncertainty in figure 5.5 is the uncertainty in 1D. The same analysis can be performed in 2D, using an isotropic correlation structure ($\theta_x = \theta_y, C(h) = C(\sqrt{x^2 + y^2})$) and a field constrained by 4×4 constraining points as given in figure 5.6. again the total uncertainty u is the integral over the square root of the kriging variance divided by the domain size. The result shown in figure 5.6 is very similar to the 1D result.

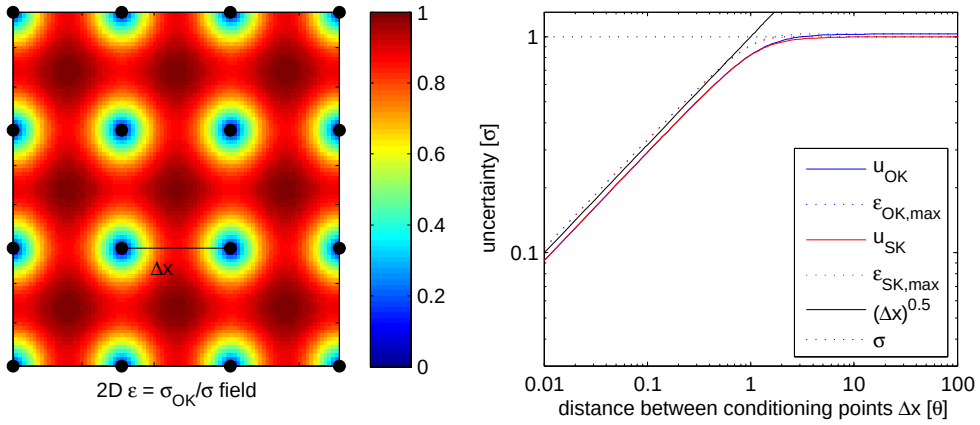

Figure 5.6: Kriging uncertainty in 2D as a function of the distance between conditioning points in two directions; uncertainty is similar to the 1D case. The correlation structure is assumed to be exponential and isotropic.

Because the desired application of the kriging estimation involves CPT-profiles in 2D or 3D fields, the influence of conditioning point spacing in a line on the uncertainty of a 2D field has to be looked at. The same method as for the 2D 4×4 field is used. Over a line of 8 times the scale of fluctuation, the conditioning points are divided equally. The number of conditioning points is then changed to see the influence on the total uncertainty, for which the boundary effects are ignored. The uncertainty is determined over a distance up to 3 times the scale of fluctuation from the line of conditioning points. The result is given in figure 5.7.

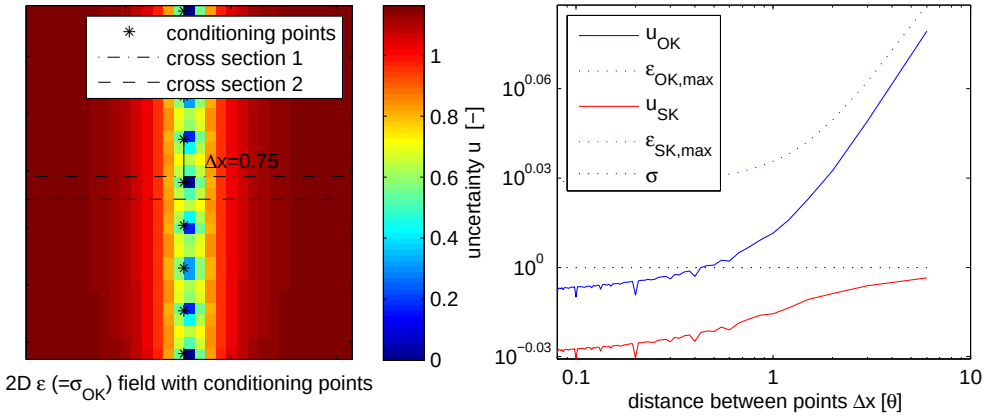

Figure 5.7: Kriging uncertainty in 2D with conditioning points on a line. The width of the field is 6 times the scale of fluctuation θ. *Cross sections 1* and *cross section 2* are used in the following graphs.

Because the domain of the field over which the uncertainty is determined in figure 5.7 influences the result (points further away from the line will have a high uncertainty, independent from the number of points on the line). The wider the chosen domain, the less the total uncertainty will be affected by the number of conditioning points. To be able to better visualise the influence of the conditioning point spacing, the kriging error ϵ along the cross sections indicated in figure 5.7 are plotted for different numbers on conditioning points. These cross sections are the upper and lower case of uncertainty, the first being located as far away as possible from the conditioning points, the second drawn across the center conditioning point. The result is a kriging error graph that looks like the 1D kriging error of kriging of a single point.

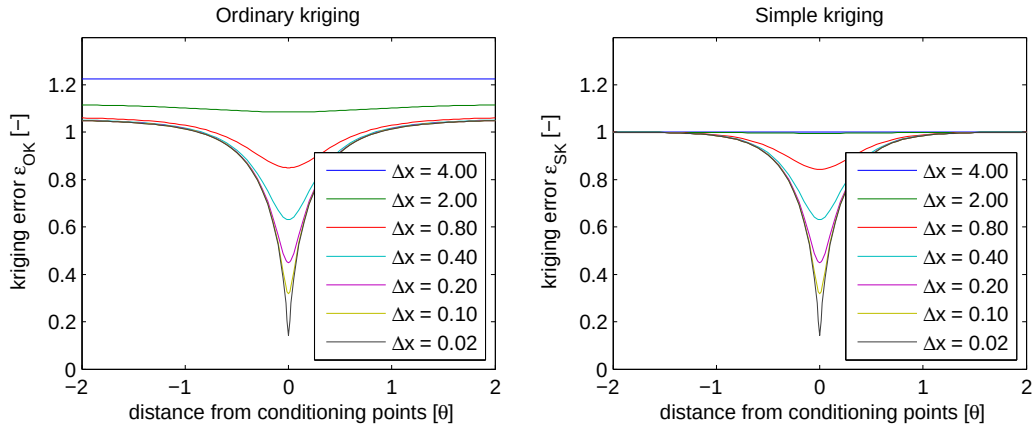

Figure 5.8: Kriging error ϵ along cross section 1 for different distances between the conditioning points.

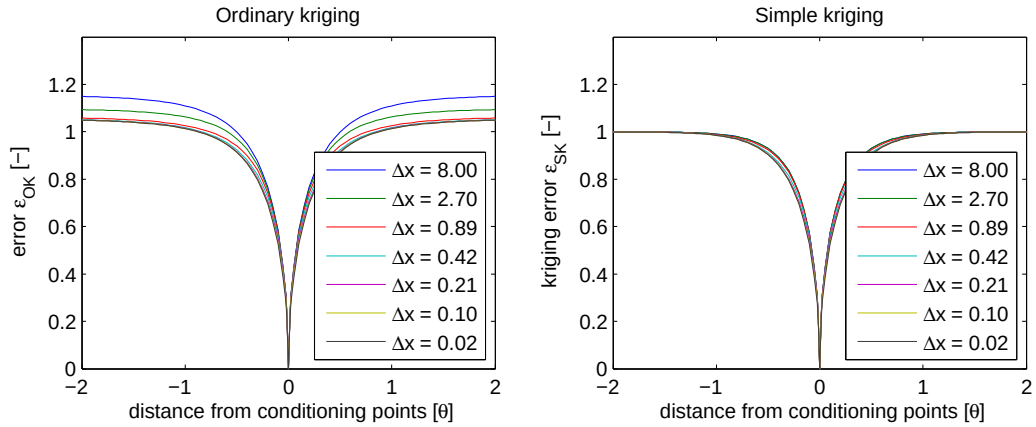

Figure 5.9: Kriging error ϵ along cross section 2 for different between the conditioning points.

Instead of one line of conditioning points, the same analysis can be done for two or more lines of constraining points. With the configuration as shown in figure 5.10, the same analysis that was done for figures 5.8 and 5.9was done, but with two lines of constraining points at a distance of four times the scale of fluctuation θ.

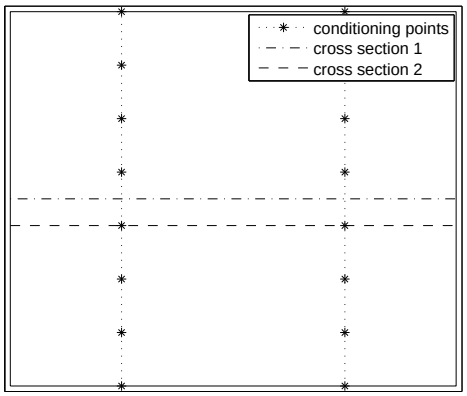

Figure 5.10: Outline of *cross section 1* and *cross section 2* as an example for 8 conditioning points.

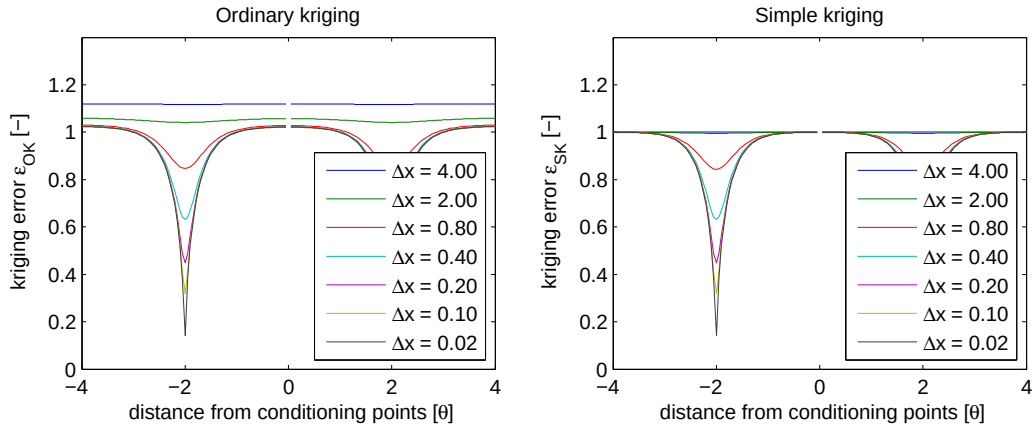

Figure 5.11: Kriging uncertainty along cross section 1 for different distances between the conditioning points.

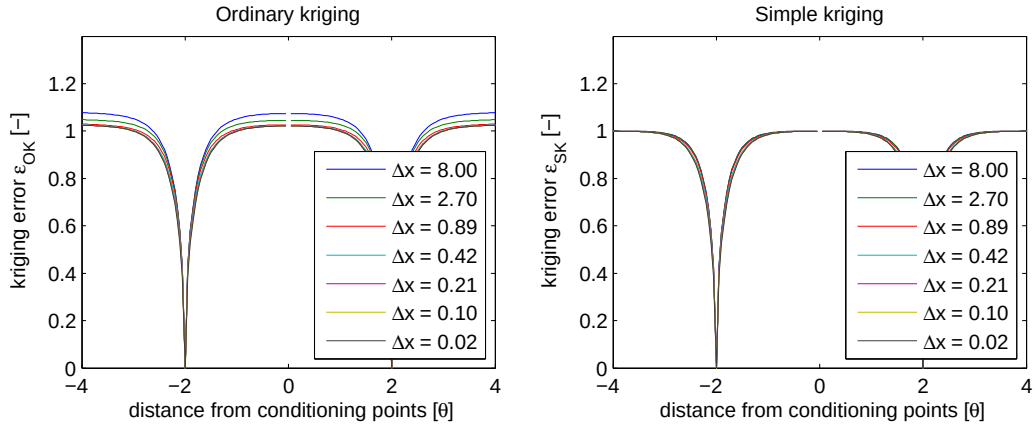

Figure 5.12: Kriging uncertainty along cross section 2 for different distances between the conditioning points

The application of the kriging procedure will be the kriging of fields conditioned by CPT profiles. Because CPT-profiles are semi-continuous with their spacing of 2cm, it is expected to be unnecessary to use all individual readings in the profile as individual conditioning points. From figures 5.8-5.12, the desired level of uncertainty can be determined when combined with the expected calculation time given by equations 5.19-5.21. A trade-off between reduction of uncertainty and calculation time has to be made. The reduction for total uncertainty u as a function of the conditioning point spacing will be influenced by the ratio between scale of fluctuation θ and the distance between the CPT-profiles. A more complete analysis, more specific to the case of 2D fields conditioned by CPT-profiles, is given in section 5.4.8.

5.4 Conditioning of the random field

The sections above all describe kriging theory and applications, which is an estimation technique instead of a stochastic process. The purpose of the report is to generate random fields, with correct statistical properties and conditioned by the measurements instead of a best estimate of the field. The conditioning within the generation of the random field is discussed in section 5.2.3 and proven to be too difficult to derive. Instead of this internal conditioning, post-processing a generated random field with the help of kriging can constrain the field to the known conditioning points. The method is described by Journel and Huijbregts [1978] and makes use of the independency of the kriging error with relation to the values of the conditioning points. The method was used by Frimpong and Achireko [1998] to simulate ore reserves.

The field simulations in this report are all simulations of fields of the state parameter. The tip resistance profiles are not used for the generation of simulations. The procedure to generate fields of

tip resistance is exactly the same as the procedures described and applied to state parameter fields in this chapter, with the only difference being the . The method of conditioned simulation of soil property fields is described in the following section.

The transformation of the original profile into the final simulation is a process that involves removing and adding trends and evaluating the zero-mean stationary (trend-removed) simulations. To distinguish between the fields in different stages of the conditioning process, the following notations will be used in this chapter:

$P(y)$:	original CPT profile, $P(y) = b + ay + Z_0(y)$
$T(x, y)$:	trend field described by $a(x, y)$ and $b(x)$
$F_0(x, y)$:	actual field to be simulated; $P(y)$ is a sample from F_0
$Z_0(x, y)$:	trend-removed (stationary) actual field; $F_0 - T$
$Z_0(\mathbf{x}_\alpha)$:	conditioning points; trend removed CPT profile (stationary)
$Z_0^*(x, y)$:	expected trend removed field: Kriging estimate of Z_0
$Z_CS(x, y)$:	trend removed conditional simulation; zero-mean stationary field conditioned by profiles $Z_0(y)$
$Z_S(x, y)$:	unconditioned random field realisation
$T(x, y)$:	trend field as a function of a and b
$F_0^*(x, y)$:	expected field: $F_0^* = T + Z_0^*$
$F_{CS}(x, y)$:	conditional simulation: $F_{CS} = T + Z_{CS}$; conditioned by profiles $P(y)$
$\boldsymbol{x}$:	coordinate; (x,y), x = lateral position, y = depth

Method of conditioning: The conditioning of random fields is a process that uses an unconditioned random field with the same characteristics as the conditioning data. This unconditioned random field is post-processed in order to condition it on the known conditioning points. An example of the conditioning of a random field in 1D is given in figure 5.13. For this example, the correlation structure is assumed to be exponential, the scale of fluctuation θ is 1.0m and the variance σ^2 is 1. The explanation of the conditioning method that follows refers to this example figure.

Imagine an unknown stationary field Z_0 of which a limited number of points $Z_{0,\alpha}$ at $\mathbf{x}_{0,\alpha}$ is known. $Z_{0,\alpha}$ are the conditioning points for the field Z_0 that is to be simulated. The correlation structure of Z_0 is known (or estimated from $Z_{0,\alpha}$) and a random field is desired to give a possible realisation of this unknown field Z_0. In the realisation the points $Z_{0,\alpha}$ need to be present.

A The first step is to give the best estimate of the field by kriging the field using the conditioning points (*). In this way the best estimate Z_0^* (blue line) is generated.

B The next step is to simulate a zero-mean random field Z_S (red) based on the correlation structure equal to that of the field Z_0. Values Z_{0S} at points $\mathbf{x}_{0,\alpha}$ in field Z_S (•) are taken to krige the simulated field to obtain Z_S^* (blue dashed). The variances of both kriged fields, Z_0^* and Z_S^* ($\sigma^2_{0,OK}$ and $\sigma^2_{S,OK}$), are equal because they are both a function of $\mathbf{x}_{0,\alpha}$ and the correlation structure.

C The expected difference between fields Z_0 and Z_0^* is given by the kriging estimation error and is equal to $Z_S - Z_S^*$ (red).

D The last step is mapping the difference $Z_S - Z_S^*$ on the best estimate of the field Z_0^* (blue) to generate the conditioned random field $Z_{CS} = Z_0^* + (Z_S - Z_S^*)$ (green). The produced field Z_{CS} is the conditioned simulation of field Z_0 and honours the mean and correlation structure.

The conditioning in 2D and 3D goes in the exact same way, with the only difference that a 2D or 3D random field generator has to be used and that the kriging estimation is based on scales of fluctuation that can be different in horizontal and vertical direction.

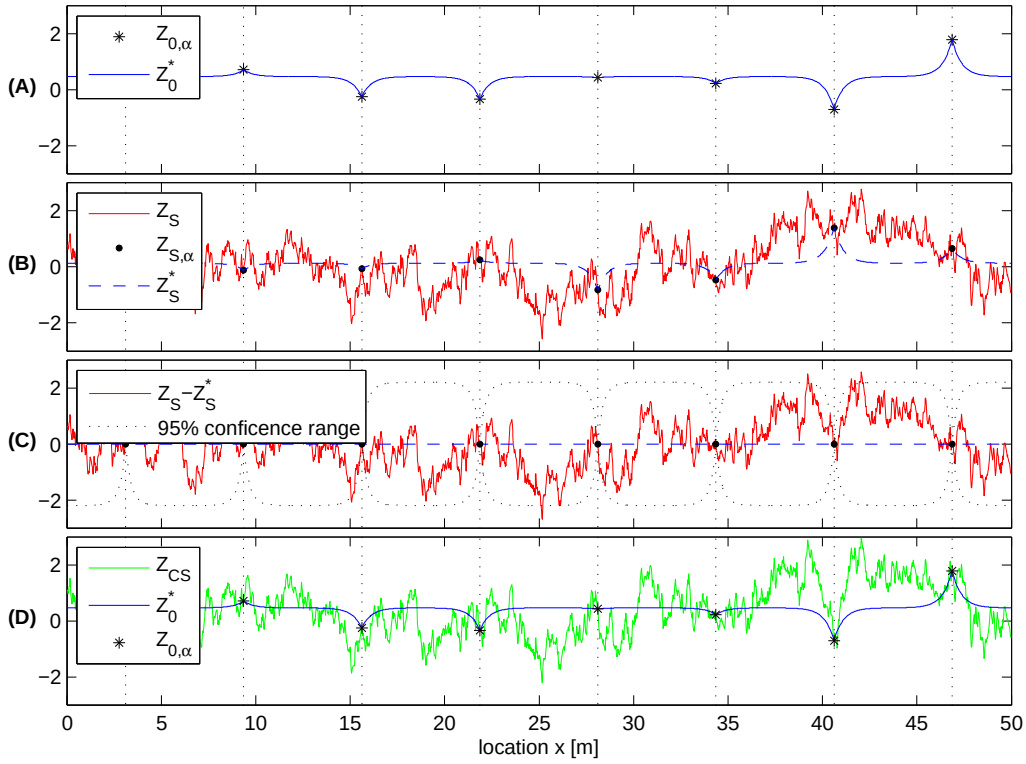

Figure 5.13: Example of 1D random field conditioning to clarify the conditioning procedure described above. Conditioning points is a randomly generated example, matching the correlation structure that is used.

To check the consistency of the simulated conditioned fields, the correlation structure is reproduced from 5000 simulations (figure 5.14). The correlation structure that has been used for the kriging is compared with the correlation structure of the conditioned simulations. The correlation structure of unconditioned random fields is given as well to indicate the relative error of the conditioning against the error in the simulation procedure of unconditioned fields itself. To generate the unconditioned random fields in this example, a 1D LAS random field generator with 9 levels of subdivision is used. This random field generator is written by the author. The difference between the correlation structures of the conditioned and unconditioned fields is small compared to the difference between the original and reproduced correlation structures.

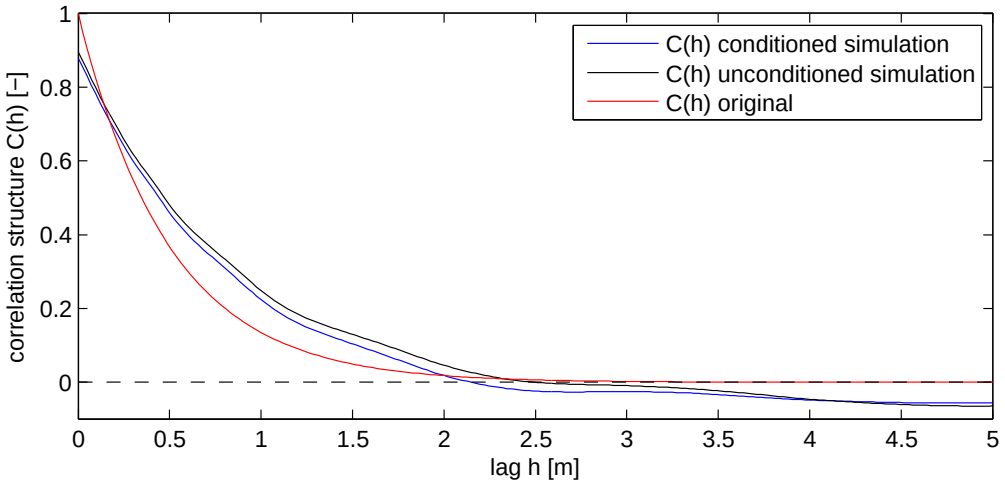

Figure 5.14: Theoretical correlation structure compared with the correlation structure derived from unconditioned and conditioned simulations. Correlation structures for conditioned and unconditioned fields are determined individually

For the analysis of the conditioning performance given in figure 5.14, the same field as given in example figure 5.13 is used. For each of the 5000 fields, new conditioning points are determined from separate realisations of random fields to avoid the possible biasedness of a single realisation of conditioning points. The simulated fields are both generated and analysed over the domain of 50m, which will be the cause of a small error due to the boundary effects in the generation of the fields.

The exact shape of the correlation structure is of importance for the conditioning of the random fields, because the correlation structure of the simulated fields is used in the kriging. Adding up and subtracting the kriged and simulated fields is only valid in the case of a consistent correlation structure in both the kriging and the unconditioned field generator.

Conditioning in 2D To apply the conditioning in 2D, Sim2D is used as random field generator. Because in Sim2D the approximate exponential correlation structure (equations 2.24 and 2.24) is used, the approximate correlation function is used from now on for all conditional simulations that use Sim2D. To show the influence of the different correlation structures on the random fields, the correlation function is back figured from 50 realisations of random fields. The result is depicted in figure 5.15.

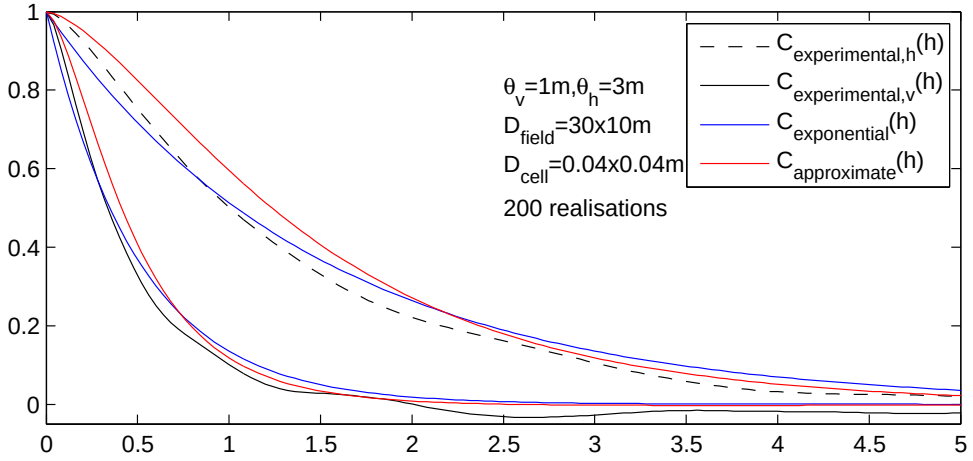

Figure 5.15: Horizontal and vertical covariance function determined from 50 unconditioned random fields generated with 'Sim2D'. 30*10m fields with cell domains of 4x4cm are used. Scale of fluctuations: $\theta_v = 1m, \theta_h = 3m$, $\sigma = 1$.

There certainly is a difference between the theoretical correlation structure and the correlation structure that was back figured from Sim2D. Part of this will be the effect of the difference between

the local averaging (as produced from by Sim2D) and the point statistics (as assumed to determine the covariance function). The other, probably smaller, part of the difference will be the effect of a small sample size from which the correlation structure is back figured. The influence of the small sample size is not a problem of accuracy of the actual procedure but a problem in back figuring the correlation structure. The influence of limited domain to be analysed and a limited number of subdivisions is something that needs to be accepted and can not be changed without increase of computations. For this reason the effect of the error in the LAS procedure is ignored in this analysis.

5.4.1 Type of kriging for the conditioning

The type of kriging that is to be used for the conditioning can be chosen based on the known information of the field that needs kriging. In the case of second order stationarity and a known mean, simple kriging will give the lowest kriging variance and therefore the lowest uncertainty in the conditional simulation. The assumption of known mean however is not trivial. The profiles that are used for the conditioning might have a zero mean, the reduction of the number of conditioning points can change the exact mean. In addition to this, large-scale variations, that are not described by the correlation structure when it is modelled by the exponential correlation structure, can be maintained by estimating the mean with ordinary kriging. For this reason, ordinary kriging is used in the conditioning.

Implication of using ordinary kriging for the conditioning is that the variance of the ordinary kriging estimation will determine the expected simulation error. Because this variance takes the estimation of the mean (the Lagrange parameter μ_{OK}) into account in addition to the simple kriging variance, the kriging variance can be larger that the variance in the correlation structure. This means that estimating the mean gives a higher variance than determined by the statistical interpretation of all profiles as a price for estimating the mean from the conditioning points.

5.4.2 Horizontal scale of fluctuation

For the simulation of 2D fields of the test site, the horizontal scale of fluctuation θ_h is required. The ratio between horizontal and vertical scales of fluctuation, the anisotropy $\xi = \theta_h/\theta_v$ is usually between 5/1 and 25/1 (e.g. Hicks and Samy [2002],Hicks and Onisiphorou [2005]). For the test site, this means that the expected horizontal scale of fluctuation is between 3m and 16m. Because the minimum distance between the CPT's is 25m, the scale of fluctuation in horizontal direction might have to be assumed.

It is tried to determine the horizontal scale of fluctuation based on the CPT's (figure 5.16). At every level (every 2 cm) the correlation between the different CPT's was determined. The expected correlation function is then found by the mean of all correlation functions. An exact exponential correlation function is fitted to the experimental result to give an indication of the scale of fluctuation of the data. A scale of fluctuation of 30m fits best to the experimental correlation function, but is considered to be incorrect due to the effect of the large distance between the CPT's relative to the scale of fluctuation. To accurately determine the horizontal scale of fluctuation, closely-spaced CPT's are needed.

To define the horizontal scaler of fluctuation, the anisotropy $\xi = \theta_h/\theta_v$ is used. In the following sections, ξ is assumed to be 5, 10, 20 or 50.

5.4.3 Defining the conditioning points; averaging and conditional statistics

Ordinary kriging is a kriging estimation method to estimate point values at location x_0 as a linear combination of known conditioning points at location x_α, without the prior knowledge of the field mean. The LAS method produces values that represent the average over cell domain D_{cell}. For a small cell domain D_{cell} (when the domain sizes are small compared to the scale of fluctuation) the values produced by the LAS method are similar to the point values of the cells centre. This is because the variation within cell domain D_{cell} is small for small cell domains.

In this report the conditioning points and the points in the field are expected to represent the point values; the average over the cell domain is expected to be the same as the center of the cell and therefore represents the point value accurately enough. In this way ordinary kriging can be used for the conditioning. For larger cell domains the difference between the statistics of points in the field will differ more from the statistics of the fields produced with the LAS method. The difference between

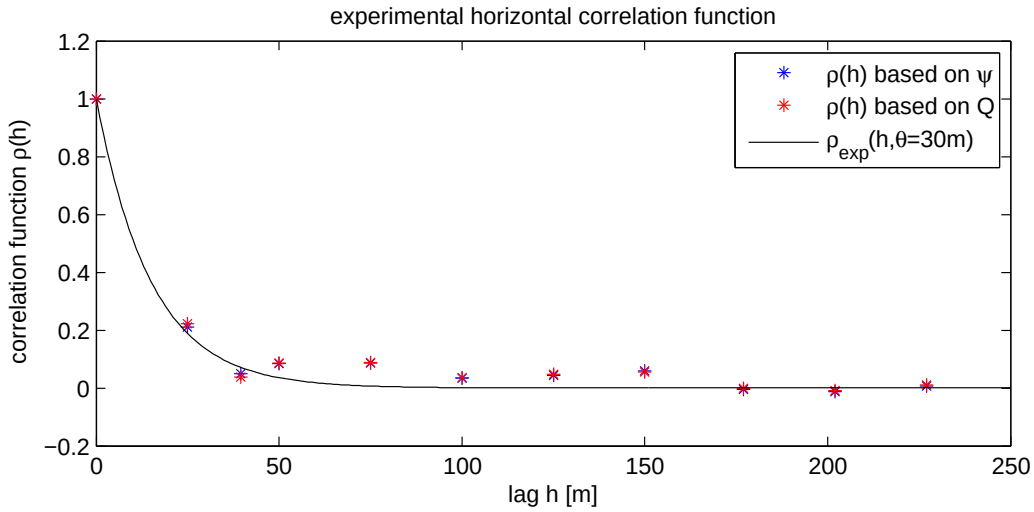

Figure 5.16: Attempt to determine the horizontal scale of fluctuation by regenerating the horizontal correlation function. A fit of an exponential correlation function to the experimental correlation function gives a horizontal scale of fluctuation θ_h=30m which is expected to be a unreliable result.

the two is described by the (conditional) variance function. In tis report the cell domain is kept as small as reasonably possible to avoid this difference as much as possible.

Because of the computational expense, not all points in the CPT profile can be used to directly condition the simulated fields. The number of points therefore needs to be reduced. For the reduction of the conditioning data different procedures can be worked out. Essential in this reduction is to give a reduced version of the original profile with the same statistics as the original CPT profile. For this report it is decided to avoid interference with the statistics of the conditioning profiles as much as possible for the following reasons;

- points in CPT profiles are already moving average representations of the soil. The exact form of the moving averaging function might not be uniform and therefore the influence of averaging over the points once more is unknown.
- averaging the conditioning points will influence the statistics (σ and θ) of the profile. This has to be corrected for, but since the influence is unknown this correction will be dificult.

To reduce the number of points in the conditioning profiles, samples are taken at regular intervals over the profile. In this way the statistics of the conditioning points is not influenced by the reduction, because the expected statistics of a sample of a data series is the same as the statistics of this series. This holds for mean, standard deviation and scale of fluctuation, but only for point statistics. By taking samples in this way, the statistics of the full conditioning profile is (expected to be) maintained, although some information of the conditioning profiles will not be used.

The variation of the conditioned field close to the conditioning points is smaller than farther away from the conditioning points. Points in the conditioned fields that are located at the exact same location as one of the conditioning points will show zero variation. This only holds for fields that contain point values or field cell domains with the same dimensions as the conditioning cell domains. Because the method aplied in this report assumes that the local average values, as produced by the LAS, can be used as point values for small cell sizes, some variation can exist. Because the cells in the simulated fields are not always located at the exact same location as the conditioning points, the variation in the conditioned fields at the exact conditioning points will not always be zero. The difference between the estimated field Z_0^* and the simulated field Z_{CS} will therefore not be exactly zero at all conditioning points.

The conditioning of local average cells by conditioning points will never reproduce a zero-variance estimation of the local average of the cell. This is the effect of the expected variation in the local average from a known point within this cell, even when it is located at the exact center of the cell domain. As mentioned before, in this report the cel domains are taken as small as possible to avoid the difference between local average and point satistics.

5.4.4 Dealing with trends

To determine the vertical scale of fluctuation for each profile, the trend of each profile has been removed to obtain first order stationarity. For the trend removal, the profile $P(y)$ is assumed to be of the form $a+b*y+Z(y)$, in which y is the depth and $Z(y)$ the trend-removed profile (the random function) from which the scale of fluctuation is determined. Motivation for restricting the trend to a linear shape are the average CPT profile (figure 4.4) and the average state parameter profile (figure 4.5), that both look linear as a function of depth. A realisation of a (conditioned) simulation $Z_{CS}(x,y)$ can be transformed into a (conditioned) simulation $F_{CS}(x,y)$ by mapping $Z_{CS}(x,y)$ on top of the trend $T(x,y)=a+b*y$. When in a 2D field $Z_{CS}(x,y)$ more than one profile is used for the conditioning, mapping the field on the trend is difficult. Because the trends that are removed differ from profile to profile, the field trend on which the stationary field is plotted is not only depth-dependent, but can vary in lateral direction as well. The lateral variation of the trend is unknown, only the trend at the locations of the profiles are known.

In this report the depth trend in the field $T(x,y)$ is restricted to a linear interpolation between the depth trends in the profiles $P(y)$. This linear interpolation is a restriction in the variability, but for the time being is considered as the best option to incorporate a stationary zero-mean conditioned random field Z_{CS}. The stationary zero-mean conditioned random field $Z_{CS}(x,y)$ is added to the linear interpolated trend field $T(x,y)$. In this way the trend at the profiles is correct and the simulated field F_{CS} is conditioned by the profiles $P(y)$.
More on the possibilities of the lateral variation in the depth trend can be found in appendix E.5.1.

5.4.5 Programming the conditioned simulation

To be able to realise conditional simulations of the site, the conditioning procedure needs to be programmed. Similar to all programming in this report, this has been done in Matlab. The exception to this is the simulation of the unconditioned random fields which is done outside Matlab by 'Sim2D'. The generation of the conditioned random fields is build into a Matlab function file 'Conditional_simulation_function.m'. This function file requires an input of conditioning points (x_α,y_α,$Z_0(x_\alpha,y_\alpha)$), the field statistics (σ,θ_v,ξ) and the field geometry parameters (D_{cell}, x_{min}, x_{max}, y_{min}, y_{max} and k) for which k represents the number of fields to be generated. Additional to these parameters an option *opt* is put in the function to choose between the exponential correlation structure ($opt=1$) and approximate exponential function ($opt=2$). Conditioning data x, y and z are equally sized matrices, whereas geometry parameters are scalars, determining the boundaries of the fields to be conditioned.
The function internally calls the executable 'Sim2D' and uses different function files as subroutines for the conditioning. No special effort has been put into the development of a script that works in the fastest way possible, and the script is kept as short as possible. The function looks as follows;

```
[X,Y,s2,Z_CS,Z_OK]=conditional_simulation_function(x,y,z,dy,x_min,x_max,...
...y_min,y_max,theta,c_0,xi,k,opt)
```

In this way the field Z_{CS} at locations (X,Y) is generated together with the estimation of the field Z_0^* and the estimation variance field σ^2. A subroutines that is used by the conditioning function that is not default a Matlab function is:

-'OKrige2D.m'

The k simulated fields Z_{CS} that are generated are saved as text files with filenames 'field1.txt'... 'field$k$.txt'.

5.4.6 Results of conditioned simulation of the test site

The conditioning is applied to the CPT-profiles to set up a random field conditioned by the profiles. The statistical properties of the field are taken from the average over all individual profile results:

- $\theta_v = 0.63$m

- $\sigma = 0.038$

Because no certainty about the horizontal scale of fluctuation or the exact shape of the correlation structure exists, the following assumptions are made:

- correlation structure is exponential (equations 2.22, 2.23)
- correlation structure is approximated by the approximate exponential correlation structure (equations 2.24, 2.25)
- $\xi = 5, 10, 20, 50$

For consistency in the conditioning, the kriging that is applied in combination with the fields generated by 'Sim2D' is done with the approximate exponential correlation structure as used by 'Sim2D'.

Conditioning to two stationary CPT profiles: To demonstrate the conditional simulation of the site, a 2-D simulation conditioned by 2 CPT-profiles is performed. For the conditioning, two CPT's at a distance of 25m that have no depth trend are chosen. In this way, the problem of mapping the zero-mean conditioned field Z^* on top of the depth trend is avoided. The mean of the two profiles is not exactly the same, but the influence of this is ignored for now; the kriging will deal with the trend in the horizontal direction and give the best estimation of the mean depending on the location relative to the two profiles. It has to be noticed that this is an estimation of the mean and not a stochastic simulation; the variations around the estimated trend are based on the assumption of stationarity in horizontal direction. Therefore the variability will be smaller than it should be.
For the simulation, an assumed anisotropy ξ of 5, 10, 20 and 50 is used. Two fields are generated, from which the difference is determined to check the conditioning of the field at the conditioning points. When the difference between the two simulations at the conditioning points is zero, the fields are indeed conditioned. To show the distribution of the uncertainty left in the simulated fields, the simulation standard deviation (from which the integral oven a domain D represents the uncertainty u_D of domain D) is given. To visualise the expectation of the simulations, the expected field Z_0^* is presented as well (figure 5.18).
The geometry for the simulations is as follows:

- cell domain:	0.02*0.02m^2	
- conditioning spacing:	0.20m	
- θ_v:	0.63m	
- ξ:	5,10,20,50	The results are discussed based on the case of ξ=20
- σ:	0.038	
- field domain	(-20;-10.6) (20;-2.4)	
- conditioned by CPT's:	$S51.18, S51.20$	

(figures 5.17 to 5.20).

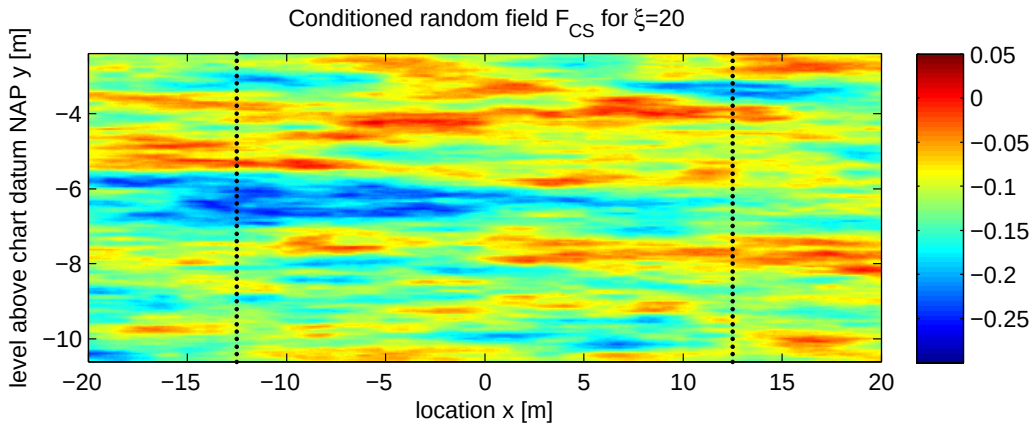

Figure 5.17: Application of the conditional simulation of two profiles that by themselves have no depth trend

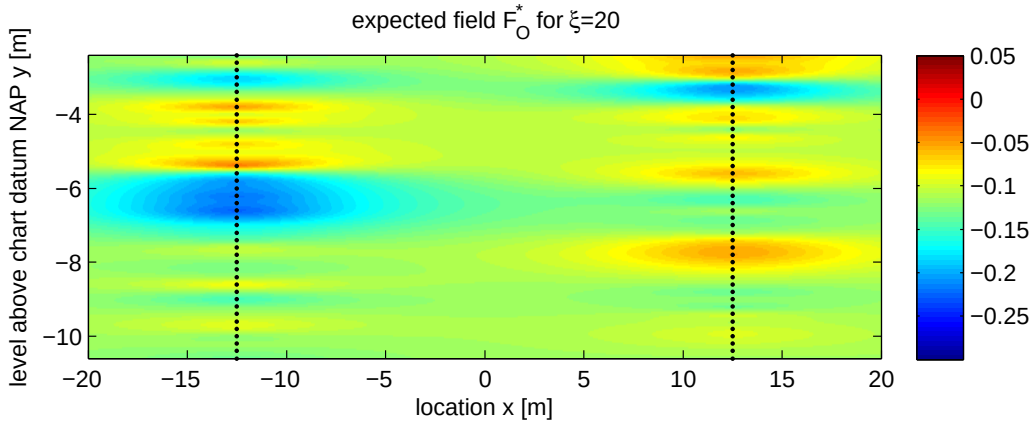

Figure 5.18: Application of the conditional simulation of two profiles that by themselves have no depth trend

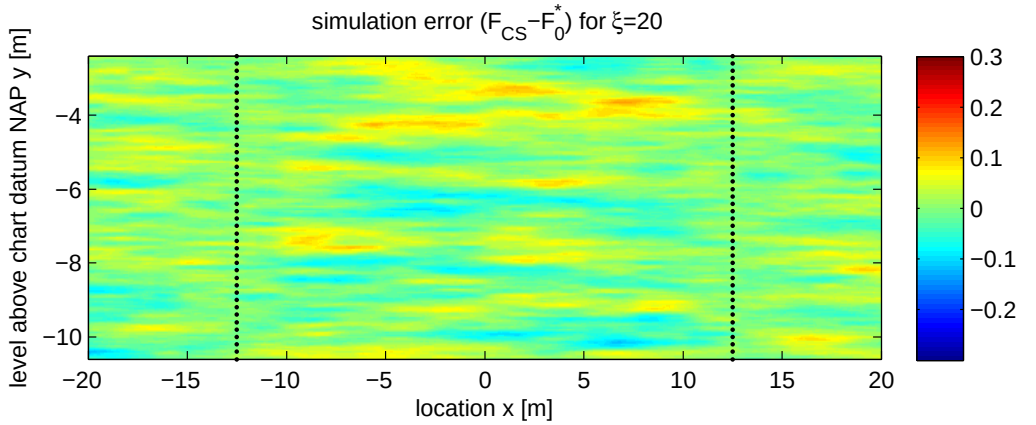

Figure 5.19: Application of the conditional simulation of two profiles that by themselves have no depth trend

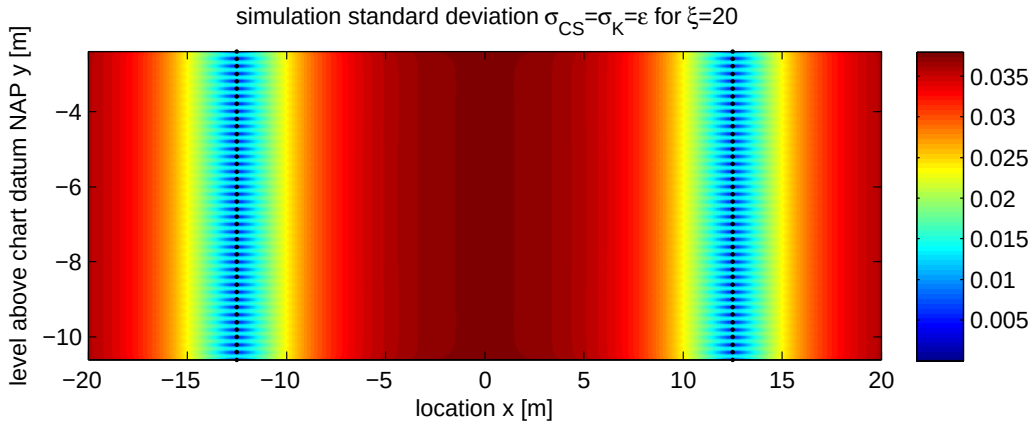

Figure 5.20: Application of the conditional simulation of two profiles that by themselves have no depth trend

Conditioning to 4 profiles with depth trend: To demonstrate conditioning of a field by multiple profiles with different depth trends, the trend that is removed to determine the statistics is interpolated between the CPT's and mapped over the zero-mean conditioned field. The interpolation method that is used is a linear interpolation between the trends in the different profiles. This method is chosen because it is straightforward and easy to implement in the code. The interpolation is an estimation method and therefore restricts the variability between the profiles. In other words, the trend might vary between the profiles and therefore the variability in the field is underestimated when the trend is interpolated. Possible suggestions for working with the trend are discussed in appendix E.5.1.
The geometry for the simulations is as follows:

- cell domain: $0.05*0.05m^2$
- conditioning spacing: 0.20m
- θ_v: 0.63m
- ξ: 5,10,20,50
- σ: 0.038
- field domain (-40;-10.6) (40;-2.4)
- conditioned by CPT's: S51.01, S51.03, S51.01, S51.03

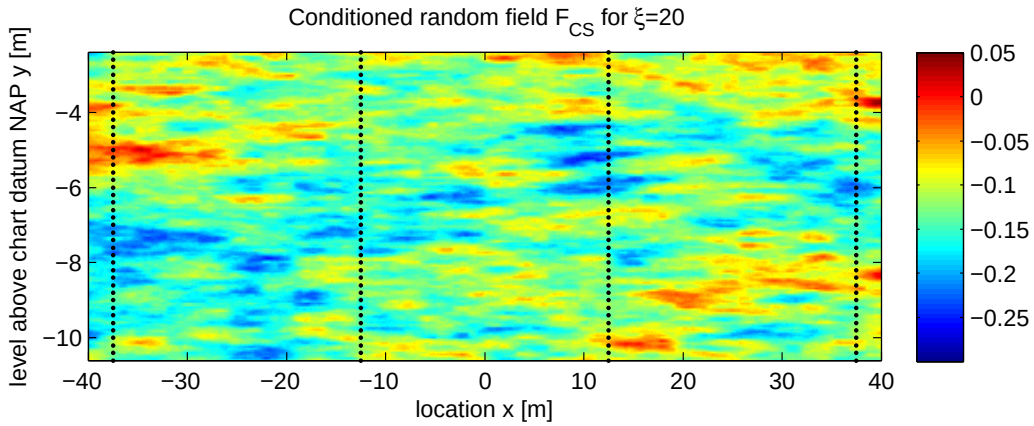

Figure 5.21: Simulation of the first part of section 5.1, conditioned by CPT profiles $S51.01$, $S51.03$, $S51.05$, $S51.07$. Depth trend is linearly interpolated between the profiles.

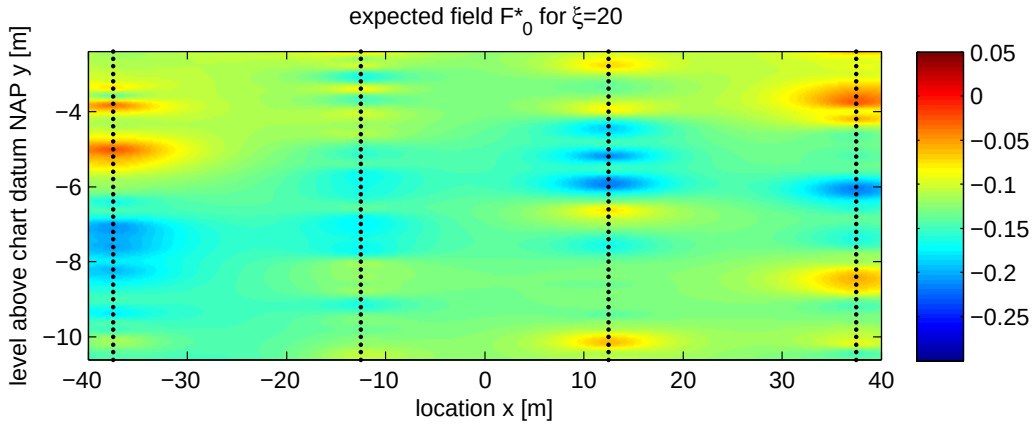

Figure 5.22: Expectation of the field simulated in figure 5.21

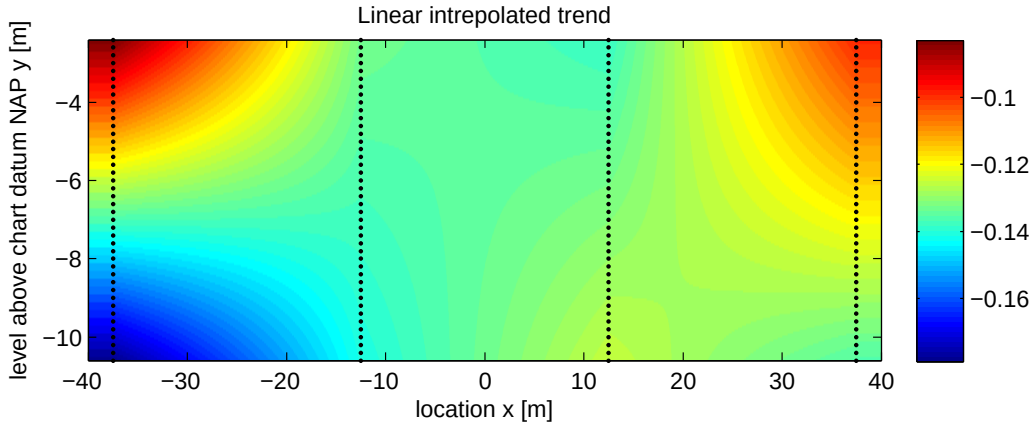

Figure 5.23: Linear interpolated trend of CPT profiles $S51.01$, $S51.03$, $S51.05$, $S51.07$ This is the underlying trend of figure 5.21. Note that color scales is not the same in both figures

5.4.7 Consistency of conditioning

To check if the statistical properties of the random fields are maintained during conditioning, the distribution and covariance function of conditional simulations of figure 5.21 are determined. Over 100 realisations of conditioned simulations, the experimental covariance function is determined and the distribution function is compared with its theoretical shape. The horizontal and vertical covariance functions are given in figures 5.24 and 5.25. The figures show that the correlation structure of the conditioning points that are used for the conditioning, influences the correlation structure of the simulated fields: The correlation structure of the simulated fields do not fully satisfy the theoretical correlation structure. This is the result of the simulated field satisfying the correlation structure of the conditioning points at locations close to these points. The covariance function therefore can always be expected between the covariance function of the conditioning points and the theoretical covariance function. Because the experimental covariance function is located close to the theoretical function or between the theoretical function and the conditioning points covariance function in figures 5.24 and 5.25, the consistency of the conditioning is considered to be demonstrated.

Some periodicity is present in the four conditioning profiles (the covariance is negative around h=2.5m). The experimental vertical covariance function (the black line in figure 5.25) shows some this periodicity as well because the conditioned field matches the conditioning points. However, the periodicity is not present in the entire field because of the use of the theoretical correlation structure that does not contain this periodicity.

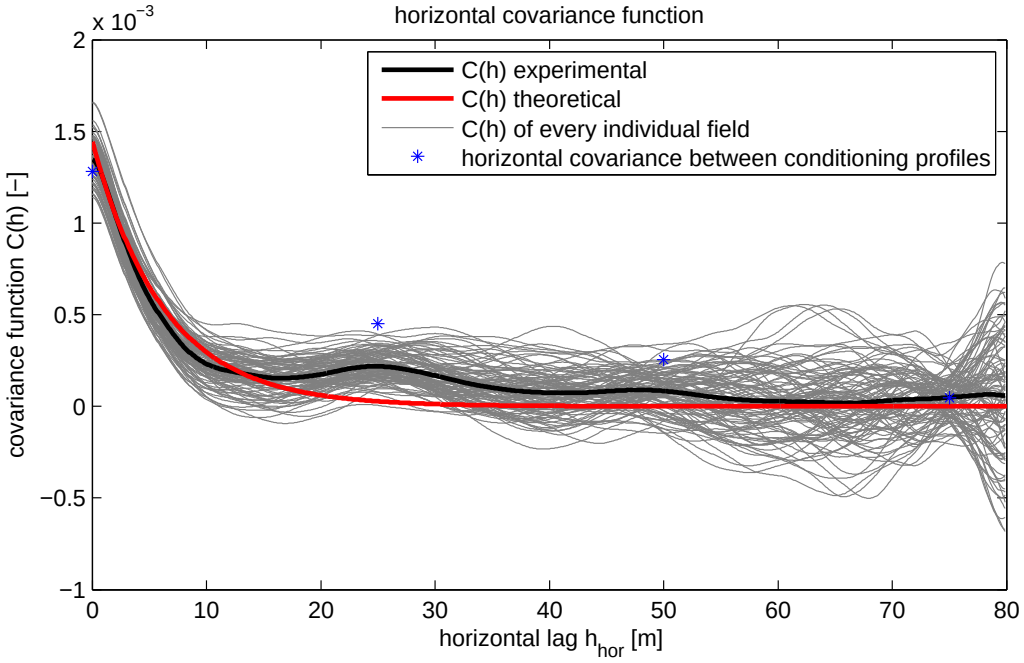

Figure 5.24: Experimental covariance function determined from 100 realisations of figure 5.21. The experimental covariance function seems to be located between the theoretical field covariance function and the covariance function of the conditioning points that were used for the conditioning.

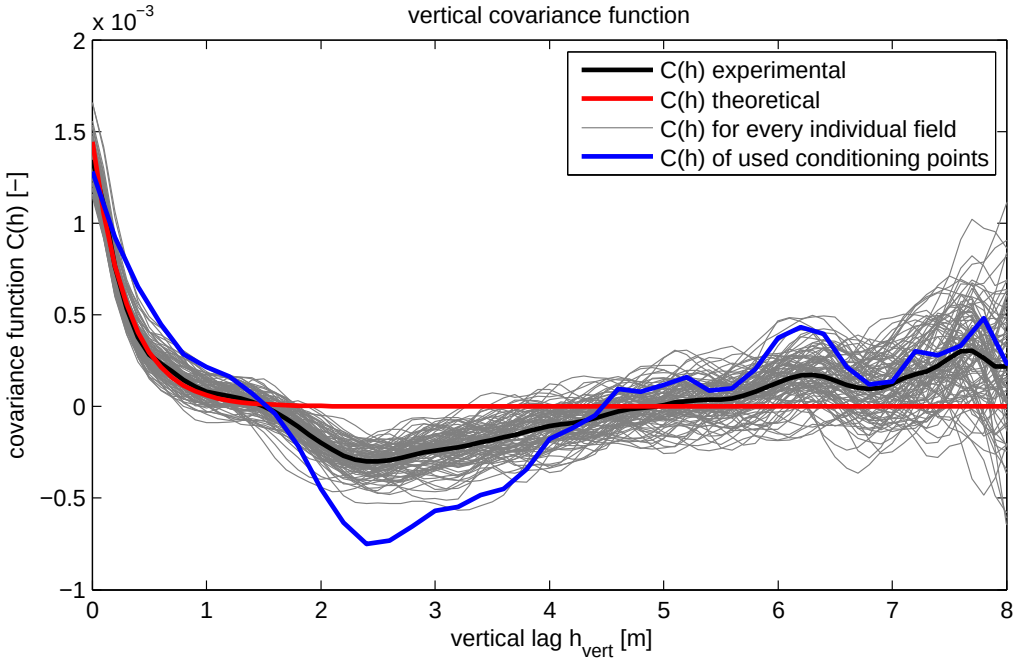

Figure 5.25: Experimental covariance function determined from 100 realisations of figure 5.21. The experimental covariance function seems to be located between the theoretical field covariance function and the covariance function of the conditioning points that were used for the conditioning.

To examine the consistency of the conditioning with respect to the distribution function, the shape of the experimental distribution function is looked at. It is found that the shape of the experimental distribution function is normal, as it can be expected from the generation of the random field by the LAS method. The experimental distribution parameters (mean and standard deviation) are determined from the 100 simulated fields and given in table 5.3. The experimental variance is between

the theoretical and conditioning variance as. This demonstrates the consistancy in the distribution function for the conditioning algorithm.

parameter	theoretical (input)	conditioning points	experimental
σ	0.038	0.0359	0.0367
σ^2	0.00144	0.00129	0.00135
μ	0	$5.99 \cdot 10^{-4}$	$6.24 \cdot 10^{-4}$

Table 5.3: Backfigured statistics from the conditional simulation.

5.4.8 Conditioning performance

For the situation of 2D fields conditioned by equally spaced CPT-profiles, the uncertainty u depends on the following parameters:

A $\Delta x/\theta_h$: lateral distance between profiles

B $\Delta y/\theta_v$: vertical spacing of conditioning points

C D_v/θ_v: length of profiles,vertical domain size

All three parameters are made unitless with respect to the horizontal and vertical scale of fluctuation. Parameters 2) and 3) together determine the total number of conditioning points n. Together with the number of points in the desired field N, n determines the time to generate a conditioned simulation of the field (see section 5.3.4). In general, the vertical spacing of conditioning points is the only true variable available to decrease the uncertainty to a desired level. The lateral spacing of CPT-profiles has to be chosen before the scales of fluctuation are determined. Therefore, the exact relative profile spacing can only be back figured after statistical analysis of the CPT profiles. The domain is determined by the geometry of the test site.

To show the effectiveness of the conditioning, the total uncertainty u is determined for the case of equally spaced CPT's in a 2D field. To simulate this, 4 theoretical CPT's with a length of 10 times the vertical scale of fluctuation are used to simulate a theoretical field. The uncertainty in 3 zones in this field is analysed (see figure 5.26). The total uncertainty in field $f1$, $u(f1)$, is determined as a function of the relative vertical spacing of conditioning points $\Delta y/\theta_v$ along the profiles. The determination of the uncertainty uses the kriging standard deviation field (see equation 5.25), analytically derived from the theoretical conditioning points by the kriging equations. This is done for a range of anisotropy factors to simulate the relative distance between the profiles $\Delta y/\theta_h$. The cell domain is kept constant at 0.167*0.167m^2, which implies a fixed number of cells $N = 2700$ in the analysed fields $f_{1,2,3}$. The effect that the fixed cell domain with changing anisotropy might have on the computational accuracy of the total uncertainty is ignored for now. The result is given in figure 5.27. The figure can be used to estimate the uncertainty for a given lateral spacing $\Delta x/\theta_h$ and vertical spacing of conditioning points $\Delta y/\theta_v$.

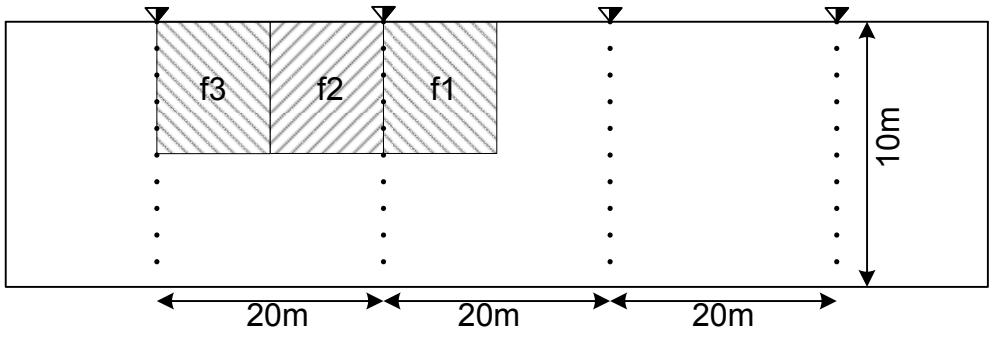

Figure 5.26: Geometry that is used for the analysis of figure 5.27. Cell domain is 0.166*0.166m, which means N=2700 cells to be evaluated in total.

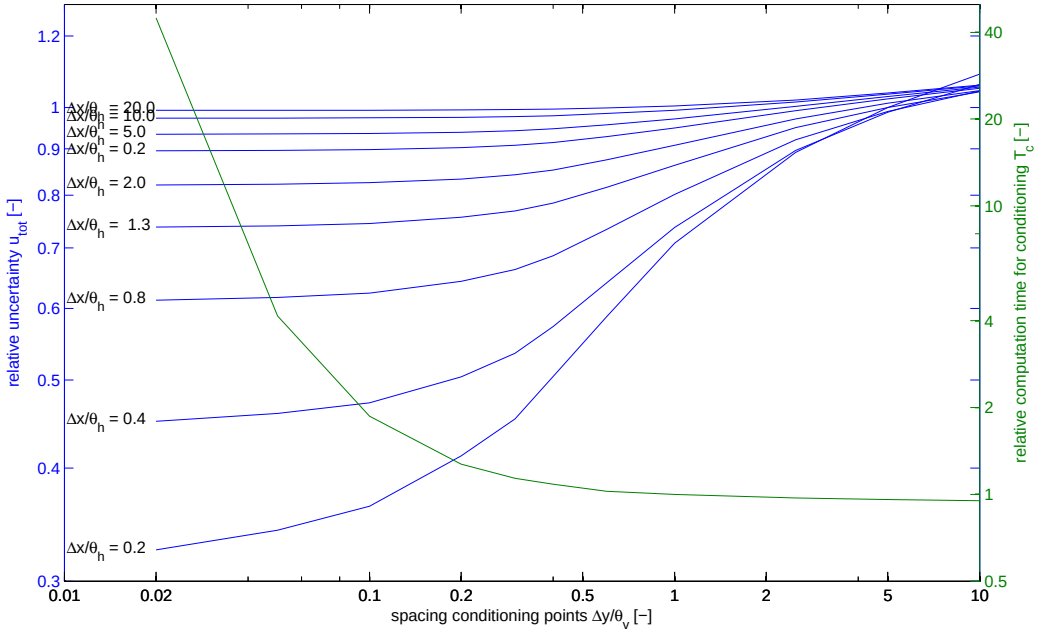

Figure 5.27: Effectiveness of the conditioning of 2D random field by equally-spaced CPT-profiles. On the horizontal axis, the distance between the interpolation points in the vertical direction $\Delta y/\theta$ is plotted. The total uncertainty u is determined for different distances between $\Delta x/\theta$. The absolute distance is kept constant at 20m and the anisotropy ξ is changed to simulate the difference in distance between the conditioning profiles. The relative uncertainty is larger than one as an effect of the use of ordinary kriging. Correlation function in the form of equation 2.25

To show that 4 CPT's is enough to simulate field $f1$ accurately enough compared to the case in which all CPT-profiles are included, the total uncertainty found in field $f1$ is compared with the uncertainty in field $f3$. In case the uncertainty of these two fields is the same, the uncertainty of field one is supposed not to be influenced by profiles that are further away than the four closest profiles.

All analyses that are used to generate figure 5.27 are used to determine the uncertainty in fields $f1$ and $f3$. This means that for a variety of anisotropy factors ξ and conditioning point spacings $\Delta x/\theta_v$ the ratio between $u(f1)$ and $u(f2)$ can be determined. Figure 5.27 shows that there is only a very small difference between the $u(f1)$ and $u(f3)$. This indicate that the uncertainty of a 2D field between two profiles is not influenced by the presence of more conditioning profiles further away. It therefore might be considered to leave out the CPT-profiles that are located further away from the point of interest. This will probably not lead to any differences in accuracy and will significantly decrease the computation time for the conditioning. This is in fact the introduction of a horizontal search neighbourhood. More on this is given in the recommendations in chapter 7

To evaluate the dependency of the calculation time, the time needed for the conditioning, as shown in figure 5.27 (for a field of N=2700 points), is presented as a function of the number of conditioning points n. The upper graph of this figure shows that for small numbers of conditioning points the computation time is linear dependent on the number of conditioning points. This is not in line with the equations determined for the theoretical calculation time. The lower graph shows that for a larger number of conditioning points n the calculation time converges to the form of $t = c * n^3$, which means that the solution of the system of equations becomes dominant for the calculation time. This is in line with equation 5.20.

The effect of the number of points in the field N is not evaluated. It is assumed to be trivial that the calculation time is linear dependent on the number of cells in the field N.

Uncertainty in simulations of the test site To quantify the reduction of uncertainty in for the simulations of the test site, the uncertainty is determined for the realisations in section 5.4.6 (see graphs in appendix E.5). The uncertainty is determined in the zone between the two center profiles and is assumed to represent the uncertainty of a field conditioned by a large number of equally space CPT profiles as shown before. The uncertainty for the different horizontal scales of fluctuation are:

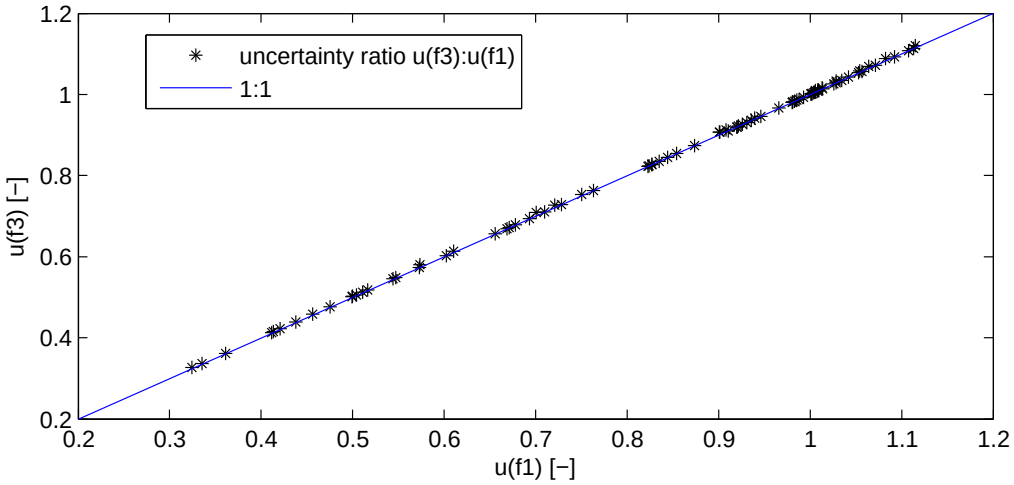

Figure 5.28: Difference between total uncertainty u of fields $f1$ and $f3$ for all points used for the analysis of figure 5.27. No significant difference between the total uncertainty can be observed.

ξ	$u \cdot \sigma$	u
unconditioned	0.038	1
5	0.0364	0.9580
10	0.0344	0.9062
20	0.0305	0.8033
50	0.0210	0.5526

Table 5.4: Uncertainties in the condition simulation of the test site.

Table 5.5: Table of uncertainties for the conditioned simulations of the site 2D field. CPT-spacing is 25m, θ_v=63cm, vertical spacing conditioning points = 20cm. The uncertainty is in line with the graph given in figure 5.27

5.4.9 Assumptions for the conditional simulation

To complete this chapter on the conditioning of the random fields, an overview is given of the assumptions that are made in order to be able to condition the local average random fields. The conditional simulation of the variability in the state of sand has been shown to be possible unter the following assumptions and generalisations;

- Decreasing the number of conditioning can be done by selecting a measurement point at a regular interval without averaging taking into account the conditional variance
- Data is normally distributed (correct assumption for state parameter)
- The correlation structure is exponential or approximately exponential
- Influence of difference between local average statistics (LAS) and point statistics (Ordinary Kriging) is negigible for the cell domains that are used
- Gain in accuracy can be measured by the average of the reduction in standard deviation
- The analysed field has a linear trend with depth and trend-removed profiles have second-order stationarity

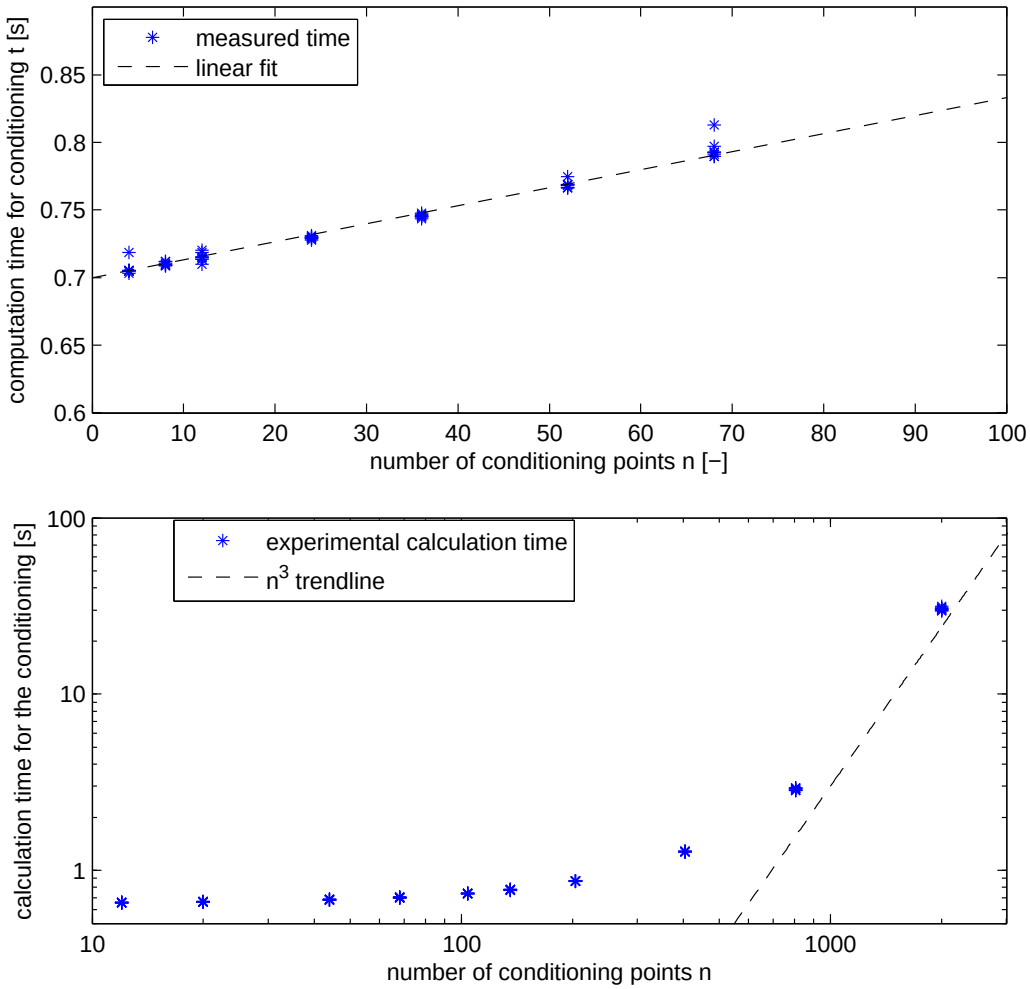

Figure 5.29: Calculation time for the conditioning of the fields used for the analysis of figure 5.27. Upper graph shows that for small numbers of

Chapter 6

Conclusions

This report describes a method for conditional simulation of the variability of sand state fields. The described method has been tested on consistency, accuracy and efficiency. To illustrate the method, part of a test site has been characterised using the conditional simulation method. The report is written to answer the following research questions:

- How can random fields be conditioned by CPT profiles?
- How does the conditioning of the random fields decrease the range of possible simulations?
- What are the requirements for site investigation for the conditioning to be useful?
- Can the conditioning be applied to a test site?

To answer these questions: It has been shown that random field simulations can be conditioned by cone penetration test profiles by using a post-processing conditioning algorithm that uses kriging estimation. The reduction of the range of possible realisations of the simulation is evaluated and it is demonstrated that the range of possible solutions does indeed decrease. The algorithm produces simulations that are consistent with the statistics and the conditional data. The decrease of possible solutions in case of conditioning by cone penetration test profiles is shown to depend mainly on three parameters: the horizontal scale of fluctuation, the lateral distance between conditioning profiles and the number of conditioning points in the profile used for conditioning. The dependency of the reduction in uncertainty on the distance between the cone penetration test profiles indicates that the site investigation plan partly determines the effectiveness of conditioning. It is derived that for an aimed reduction of uncertainty, the spacing between cone penetration test profiles for the site investigation can be determined based on the horizontal scale of fluctuation. The horizontal scale of fluctuation needs to be known or assumed for this. Application of this algorithm on the test site data has demonstrated that conditional simulation can be applied in practice. The reduction in the range of possible realisations is found to be between 5% and 45% for the site investigation performed at the test site, depending on the anisotropy of the variability.

In general, it can be stated that the research questions have been answered. The algorithm for the conditioning is programmed in Matlab and with this the objective of development of an algorithm for conditioning is reached in general as well, but it is far from complete. There are many possibilities for improvement in both efficiency and accuracy of the algorithm.

Other conclusions that can be drawn from this report are:

- For the calibration of the critical state stress ratio M and the parameter for the stress dilation ratio N, the Bishop Method was found to be the most suitable calibration method when triaxial tests of mainly dense drained samples are available.
- For the calibration of the critical state line parameters Γ and λ_{cs}, the triaxial approach and assumed chi method were demonstrated to be suitable calibration methods when only drained triaxial tests are available. The triaxial approach requires loose drained samples for a reliable result. The assumed chi method is found not to depend significantly on the assumed value of chi. The most likely point for cross-sections for this method can best be determined by the minimum

in standard deviation between the lines in the graph in horizontal and vertical direction, described as the 'assumed chi least standard deviation' method in the report.

- The result that is found for the hardening modulus H proved to be the most unreliable NorSand parameter that was calibrated. This is expected to be caused mainly by the assumption of correct deterministic descriptions of all other parameters. These parameters were used to simulate the triaxial compression response in order to calibrate H.

- From material properties found in literature, the calibrated material properties of the North Sea sand show the most resemblance with Erksak sand.

- For the statistical interpretation of the profiles it was found that the scale of fluctuation is not affected by the transformation from tip resistance to state parameter. A difference in scale of fluctuation in the range of 1% was found, which suggests that the scale of fluctuation is hardly affected by a transformation of distribution function. This validates the option of distribution transformation prior to the determination of correlation structure and conditional simulation.

- The best distribution to describe state parameter and tip resistance determined by the chi square goodness of fit for individual profiles shows no clear differences between Normal, Beta and Gamma distributions. Normal and Beta seem to be equally favourable. The best distribution of all data together is clearly Normal for the state parameter and Beta or Gamma for the tip resistance. Therefore the normal distribution is used as the distribution function of the data.

- It is found that internal conditioning of the Local Average Subdivision method was too complex to implement. Therefore, and because of other methods were available, the conditioning is performed as a post-processing algorithm.

- The application of the algorithm on local average random fields is valid in case the cell domain is small relative to the scale of fluctuation. In case the cell domain of the local average random fields becomes larger, the application of the conditioning algorithm is no longer valid and alternative versions of the algorithm have to be used.

- The conditional simulation produces fields that have a correlation structure that is similar to the theoretical correlation structure that is used and the experimental correlation structure of the conditioning points. It is experimentally shown that the statistics (distribution function and correlation structure) that are used as input are honoured.

- The reduction in uncertainty that can be achieved by conditional simulation is demonstrated to be in the order of 50%, depending on the scales of fluctuation and the density of available cone penetration test profiles. For the test site, the reduction of uncertainty is between 5% (for $\xi = 5$) and 45% (for $\xi = 50$), when conditioning points along the cone penetration test profiles at 20cm intervals are used.

- The calculation time involved in the conditioning algorithm is theoretically derived as a function of the number of conditioning points n and the number of field points N. When N is much larger than n the time it takes to condition a field is linear proportional to the number of points in the field N. When n is large compared to N, the conditioning time increases with n^3.

Chapter 7

Recommendations

As mentioned in the conclusion, the algorithm that was developed for the conditioning is far from complete. A number of improvements have to be made to work out all the details. Some of these improvements are discussed in this section as recommendations for further work. Recommendations regarding the other parts of this report are mentioned as well.

- To be useful in the numerical analysis of slope stability, the conditioning needs to be applied in 3D; the conditioning in 3D is nothing more than changing the coordinates from (x,y) to (x,y,z). An increase in calculation time can be expected to be similar to the 2D case; depending mainly on the number of field cells and the number of conditioning points. The only difference is the location of the cells to be conditioned. The change from 2D to 3D will have it's influence on the possibilities of restriction of number of conditioning points by a search neighbourhood.
- The decrease in uncertainty is shown as the function of number and location of the conditioning points with respect to the scales of fluctuation. The quality of this reduction with respect to the reduction of uncertainty in design is not shown. To quantify the true reduction in uncertainty, the conditional simulated fields need to be evaluated in a structure response. Next step therefore is to incorporate the conditional simulations in structure response analysis to compare the uncertainty in the results with the uncertainty in the analysis of unconditioned simulations.
- The effect of the assumption that the fields produced with the LAS method present point statistics needs to be validated when larger field cells are generated. The effect of the assumption that the difference between local average statistics and point statistics can be ignored needs to be quantified as a function of relative field cell size. A possible consequence is that the kriging procedure that is used has to be changed from ordinary kriging (kriging point values) to block kriging (kriging the average over a cell domain). It should be checked if the algorithm for conditional simulation still hold when block kriging is used for the estimation.
- Problems with the chi-square goodness of fit to determine the most likely probability function to describe distribution of the data are mentioned in this report. No further effort has been made to propose alternative methods of testing the distribution function. An evaluation of possible test methods might be needed to check the accuracy of the chi square method. The transformation of the generic distribution to a normal distribution before the analysis and conditional simulation, to back transform the normally distributed conditional simulation into the generic distribution, might be an alternative to deal with non-Gaussian distributions.
- In a full probabilistic approach the calibrated constitutive model parameters can not be used in the way they are used in this report. Although it has been proven that the scale of fluctuation is hardly affected by the transformation from tip resistance to state parameter, the mean and standard deviation in the state parameter are influenced by the result of the calibration. A more probabilistic approach in the calibration of the model parameters and the effect of uncertainty in these parameters with respect to the state parameter should be looked at.
- The reduction of the number of conditioning points in this report is achieved by simply selecting points in the profiles at a regular interval. This method avoids biased estimates, but because data is left out from the conditioning, uncertainty increases and selecting different points leads

to different conditioned random fields. Improvements in the procedure of reduction the number of conditioning points might be looked after in order to use more conditioning data without excessive increase of computation time.

- The evaluation that was done for the uncertainty in different locations of a field conditioned by four cone penetration test profiles has indicated that the region between two profiles is probably not much affected by regions that are located further away. This raises the question if these profiles need to be included in the conditioning of this region. The introduction of a search neighbourhood that determines the neighbourhood in which the relevant conditioning points are located should be considered. The introduction of a search neighbourhood however can be complicated and might have undesired effects on the estimation of the mean. Although the introduction of a search neighbourhood might look promissing in 2D due to the division of different parts of the field by the profiles, a search neighbourhood in 3D might be difficult to define due to the conditioning by profiles. Some comments on the search neighbourhood for kriging are given by Wackernagel [1998].

Bibliography

Siamak Bakhtiari. Statistical characterisation of spatial variability for a dredge excavation. Master's thesis, University of Manchester, 2006.

K. Been and Mike G. Jefferies. A state parameter for sand. *Géotechnique*, 35(2):99–112, 1985.

K. Been and Mike G. Jefferies. A state parameter for sand, reply. *Géotechnique*, 36:127–132, 1986.

K. Been, B.E. Lindau, J.H.A. Crooks, and B. Leach. Cone penetration calibration for erksak (beaufort sea) sand. *Canadian geotechnical journal*, 24:601–610, 1986.

G.D. Bouckovalas, K.I. Andianopoulos, and A.G. Papadimitriou. A critical state interpretation for the cyclic liquefaction resistance of silty sands. *Journal of Soil Dynamics & Earthquake Engineering*, 11 (1), 2002.

Johannes Bruining, Diederik van Batenburg, Larry W. Lake, and An Ping Yang. Flexible spectral methods for the generation of random fields with power-law semivariograms. *Mathematical Geology*, 29(6):823–848, 1997.

N. Cressie. The origins of kriging. *Mathematical Geology*, 22(3):239–252, 1990.

Gordon A. Fenton and D.V. Griffiths. Random field generation and the local average subdivision method. *CISM International Centre for Mechanical Sciences*, 491, 2007.

Gordon A. Fenton and E.H. Vanmarke. Simulation of random fields via local average subdivision. *Journal of Engineering Mechanics*, 1(99), 1990.

Samuel Frimpong and Peter K. Achireko. Conditional las stochastic simulation of regionalized variables in random fields. *Computational Geosciences*, 2:37–45, 1998.

Inna Gitman. Internal report, university of manchester, 2006.

M.A. Hicks and C. Onisiphorou. Stochastic evaluation of static liquefaction in a predominantly dilative sand fill. *Géotechnique*, 55(5):123–133, 2005.

M.A. Hicks and K. Samy. Influence of anisotropic spatial variability on slope reliability. *Proceedings of the 8th int symp num models geomech, Rome*, 29(6):535–9, 2002.

M.A. Hicks and W.A. Spencer. Influence of heterogeneity on the reliability and failure of a long 3d slope. *Computers and Geotechnics*, 37:948–955, 2010.

M. G. Jefferies. Nor-sand: A simple critical state model for sand. *Géotechnique*, (43):91–103, 1993.

M. G. Jefferies and D. A. Shuttle. Norsand: Features, calibration and use. *Geotechnical special publication*, (128,Soil Constitutive Models: Evaluation, Selection and Calibration):204–236, 2005.

Mike G. Jefferies and Ken. Been. *Soil liquefaction: a critical state approach*. Taylor and Francis, 2006.

A.G. Journel. Conditional simulation of gelogically averaged block permeabilities. *Journal of hydrology*, 183:23–35, 1994.

A.G. Journel and Ch. J. Huijbregts. *Mining Geostatistics*. Acedemic Press, 1978.

T. Lunne, J.J.M. Powell, and P.K. Robertson. *Cone Penetration Testing in Geotechnical Practice*. Taylor and Francis, 1997.

D. Negussey, W.K.D. Wijewickreme, and Y.P. Vaid. Constant-volume friction angle of granular materials. *Canadian Geotechnical Journal*, 25:50–55, 1987.

Rijkswaterstaat. Waternormalen:waterstanden, 8 2010. http://www.rijkswaterstaat.nl/water/scheepvaartberichten_wate

D.A. Shuttle and M.G. Jefferies. Dimensionless and unbiased cpt interpretation i sand. *International Journal of Numerical and Analytical Methods in Geomechanics*, 22:351–391, 1998.

E.H. Vanmarcke. Probabilistic modeling of soil profiles. *Journal of the Geotechnical Engineering Div.*, 103(GT 11), 1977.

Erik H. Vanmarcke. *Random Fields: Analysis and Synthesis*. The MIT Press, 1984.

Hans Wackernagel. *Multivariate Geostatistics*. Springer-Verlag, 1998.

Damika Wickremesinghe and R.G. Campanella. *Scale of fluctuation as a descriptor of soil variability*. Balkema, in: probabilistic methods in geotechnical engineering, li & lo (eds) edition, 1993. ISBN 90 5410 303 5.

S.Y. Wong. *Stochastic Characterization and Reliability of Saturated Soils*. PhD thesis, University of Manchester, 2004.

Appendix A

Statistical distribution functions

This appendix describes the four statistical distribution functions that are used in this report.

Normal distribution; The normal distribution is determined by the parameters mean μ and standard deviation σ. These parameters lead to the probability density function with the following equation;

$$Normal: \ PDF(z|\mu,\sigma) = \frac{1}{\sigma\sqrt{2\pi}} e^{-\frac{1}{2}\left(\frac{z-\mu}{\sigma}\right)^2} \tag{A.1}$$

Examples of the nromal distribution finction are presented in figure A.1. The normal distribution can be reduced to standard normal distribution when the mean and the standard deviation are chosen to be 0 and 1. The probability density function in this case is given by:

$$PDF_{standard-normal}(z) = \frac{1}{\sqrt{2\pi}} e^{-\frac{1}{2}z^2} \tag{A.2}$$

The normal distribution is a non-skewed (symmetric) distribution which means that when the standard deviation is of the same order of magnitude as the mean, negative values can be obtained. This gives problems when, for example, pressures are described using the normal distribution. A skewed distribution guaranteeing only values larger than zero might be more suitable to use as distribution.

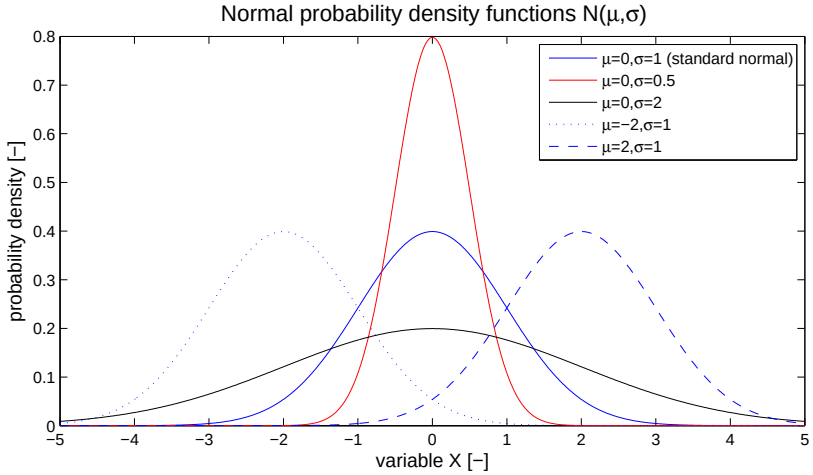

Figure A.1: Example of the Normal distribution

Lognormal distribution; A dataset can be described with the log-normal distribution when the logarithm of the dataset is normal distributed. In other words, the exponent of a normal distributed dataset is log-normal distributed. This means that the log-normal distribution is dependent on the

mean μ and standard deviation σ just like the normal distribution. The probability density function is given by equation A.3. The difference with the normal probability density function is the natural logarithm of x instead of x as the variable in the exponent. To correct for the change in probability density, the probability density function has to be scaled by $\frac{\delta ln(x)}{\delta x}$, which is the extra x in the denominator in front of the equation for the probability density function.

$$Lognormal: \ PDF(z|\mu,\sigma) = \frac{1}{z\sigma\sqrt{2\pi}} e^{-\frac{1}{2}\left(\frac{\ln(z)-\mu}{\sigma}\right)^2} \tag{A.3}$$

Because of the exponential behaviour with respect to the normal distribution, the lognormal distribution is always greater than 0. Also the log-normal distribution has a positive skewness (the mean is greater than the median). Examples of the lognormal distribution finction are presented in figure A.2.

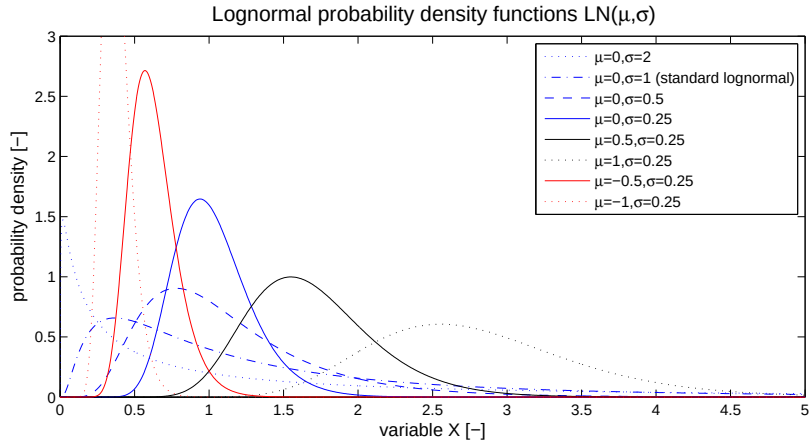

Figure A.2: Example of the Lognormal distribution

Beta distribution: The beta-distribution is a distribution that describes the likelihood of a value being present between the values 0 and 1. The Beta-distribution depends on parameters α and β and is defined over the domain [0;1]. The probabilitu density function is given by

$$Beta: \ PDF(x|\alpha,\beta) = \frac{x^{\alpha-1}(1-x)^{\beta-1}}{B(\alpha,\beta)} \tag{A.4}$$

with

$$B(\alpha,\beta) = \int_0^1 t^{\alpha-1}(1-t)^{\beta-1}dt. \tag{A.5}$$

The Beta-function $B(\alpha,\beta)$ in the denominator normalises the Beta-distribution to reach an area under the graph equal to 1. It is in fact the area under the full graph of $x^{\alpha-1}(1-x)^{\beta-1}$. The Beta-distribution can be both skewed ($\alpha \neq \beta$) and non-skewed ($\alpha = \beta$). Examples of possible probability density graphs are given in figure A.3. The Beta-distribution is a special case of the Gamma distribution.

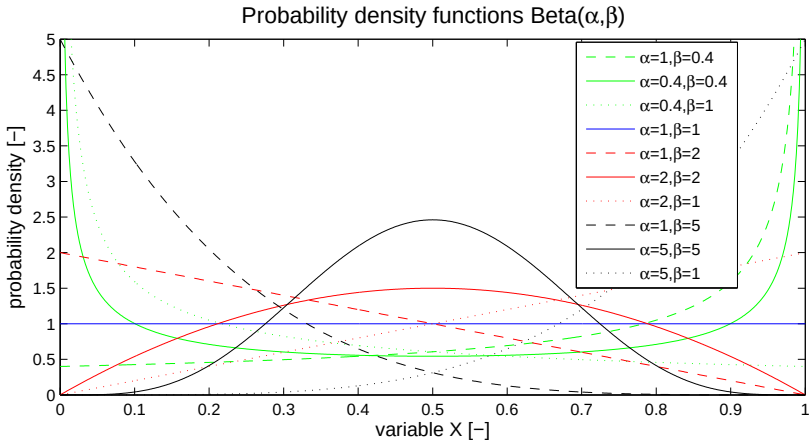

Figure A.3: Example of the Beta distribution

Gamma distribution: The Gamma-distribution depends on two parameters; shape parameter α and β. In some cases other symbols are used as parameters for the Gamma-distribution. Other symbols that can be found in literature are shape parameter $k = \alpha$ and scale parameter $\theta = \frac{1}{\beta}$. Examples of possible probability density graphs are given in figure A.3.

$$Gamma: \ PDF(x|\alpha,\beta) = \frac{\beta^{\alpha}}{\Gamma(\alpha)} x^{\alpha-1} e^{-\beta x} \tag{A.6}$$

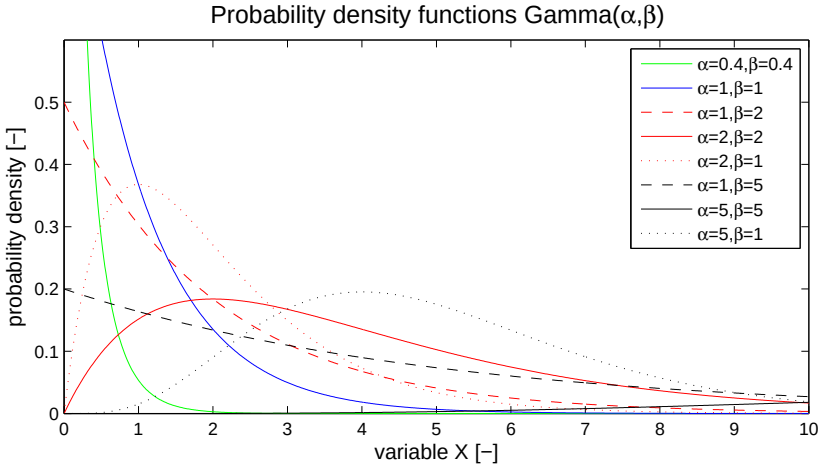

Figure A.4: Example of the Gamma distribution

Appendix B

Changes in the code for the statistical interpretation

To make the code that is used for the statistical characterisation [Gitman, 2006] compliant to the demands of usability and accessibility, some of the structures are rearranged and methods of input and output are changed to the author's liking. Most of the changes were made because of the analysis for multiple options in one go (state parameter, tip resistance, trend removed and not-removed at the same time). Input, analysis and output were split into separate parts of the code to ease future additions to the code. The method of presentation of the result is changed to satisfy the wishes of an overview that can be directly included into the report.
The actual codes are not fully discussed. This section discusses the changes in general.
While working with the code, it has been worked through to delete all unnecessary commands and change the sometimes extensive loops for Matlab build-in commands. This has reduced the length of the code (maybe not the overall running time) and increased the readability and clarity of the code. However, an increase in length of the code can be attributed to the commands that are needed to present all results in one page. The largest part of the code now consists of the definition of the layout for the result presentation.

B.1 Input

Original code The original code used text files with columns of the CPT-measurements as data input. All geometry data of the CPT-profiles (numbers, file names, output file names, depth, etc.) was put into a separate text file. Changing the profiles to be evaluated therefore was a tedious business, because all text files had to correspond to the evaluated profiles.

Changes made: CPT-data of this project are available in GEF-files (GEF = Geotechnical Exchange Format), a standard text file-format to store geotechnical measurements. Because most of the geometry information is stored in the headers of the GEF-files, the code is changed in such a way that it can use the GEF-files as input data files. To deal with the header files, the Matlab function file 'ReadData.m' is added to the code. This function file reads the available data in the header of the GEF file and stores it as variables in Matlab (X,Y,Z-coordinates, file-ID, profile length, profile values).

At this moment, this code only works for 5-column GEF-files; the code still needs some extension to be able to read all types of GEF-files. Reduction of the number of text files with parametric information is achieved by including the input of all constitutive model data in the main code file (direct input). The names and number of the GEF-files are determined by the code (INFO=GET(*.GEF)).

B.2 Parallel analysis

To avoid running the code for different parameters, analysis is done for tip resistance and state parameter, for the trend-removed and the original case, in one go. To be able to change the code into running the analysis for multiple datasets at the same time, some loops had to be inserted and the

order of different steps was changed at some parts of the code. Instead of vectors, the profile to be analysed was changed to a 6-column matrix (state parameter, friction ratio and tip resistance)(both original and trend removed) and the analysis was done for the full vector. In this way, the code does not have to be run several times for different parameters and options and the combination of results is easy to implement in the code. The results for the friction ration is not used in this report.

B.2.1 Plotting and gathering results

To ease the work of inserting all results in the report and give a clear overview of the results, all results from the individual CPT's are plotted on a one-page overview picture. Results are no longer stored in JPEG format but in postscript (.PS) format, to guarantee accessibility and readability. Instead of an individual file for each graph that is produced, all results of a single profile is stored in one single-page file that can be inserted in the report directly.

B.3 Chi square goodness of fit

Because of an error in the goodness-of-fit in the original code, the entire part of the code that evaluated the chi-square score was rewritten with the help of the build-in Matlab operator $chi2gof$.

Original code The sequence of observed bin counts O is divided by $N * binwidth$ in the original code by Gitman [2006]. In this way, a histogram of the probability density function is constructed (the area of the histogram is equal to 1). This is good when comparing the histogram with theoretical distributions, but incorrect when it is used for the chi-square goodness of fit. Because the chi-square probability is calculated for $\chi^2/(N*binwidth)$ instead of χ^2, the probabilities of finding a similar result or beter are extremely low (in the range of 10^{-8}).

```
   - The original code (variable names have been changed)  for i=1:N
   for j = 1:numberofbins
      if data(i)>=binedge(j) & data(i) < binedge(j+1)))
         O(j)=O(j) + 1
      end
   end
end
O = O/(N*binwidth)
chi-square=0
for j=1:numberofbins
   if E(j)>0.0001
      chi-square = chi-square+(O(j)-E(j))^2/E(j)
   end
end
```

Changes in the code To reduce the number of loops in the code, the built-in commands in Matlab are used where possible. The section of the original code above has been changed for the following line; `[H,P,STAT] = chi2gof(data,'edges',binedges,'expected',E,'emin',0,'nparams',2)`

The result of this command gives the probability P of generating the observed distribution or one that

has a higher χ^2 score. STAT is a summary of the statistical properties of the fit and contains the χ^2-score, the number of degrees of freedom, O, E and the edges of the bins. With 'emin' the minimal number of expected counts in each bin is defined. Bins with a smaller expected count are pooled with their neighbouring bin. If so, the number of degrees of freedom is reduced and changes in the bin edges are stored in 'STAT.edges'. With 'nparams' the number of estimated parameters is defined to be able to determine the number of degrees of freedom.
The effect of the changes is that the correct χ^2-scores are generated.

Appendix C

Calibration results

C.1 Calibration of M and N: Stress-strain curves

The Triaxial data is interpreted in accordance with the theory described in the report. The application of this theory on the data is done in Matlab. The full calibration process is stored in a command file that can be found ....[rreference to be added]

Lab B-data interpretation results

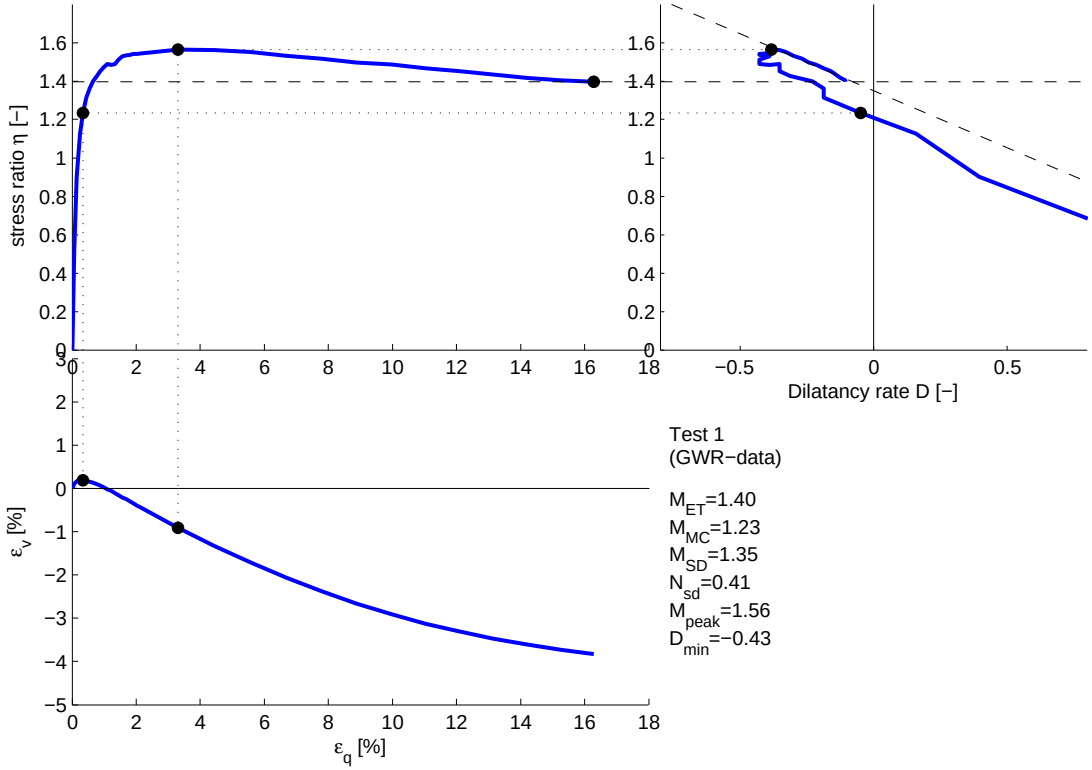

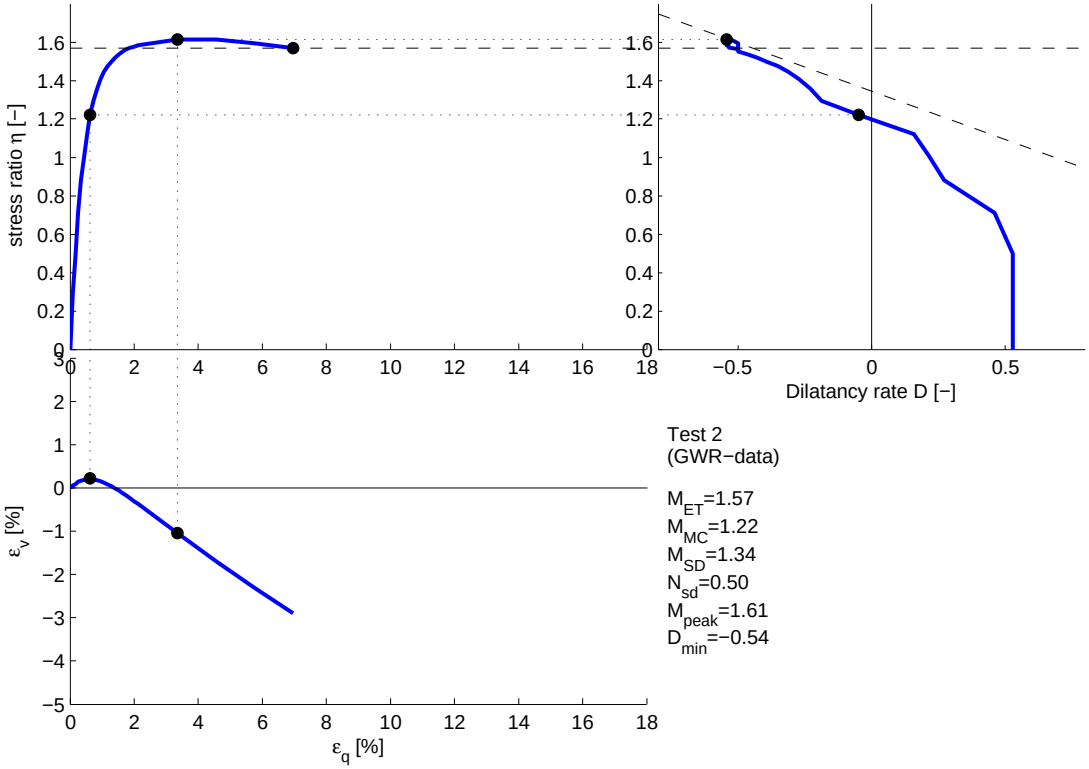
stress ratio η [−]
Dilatancy rate D [−]
εv [%]
εq [%]
Test 2
(GWR−data)
MET=1.57
MMC=1.22
MSD=1.34
Nsd=0.50
Mpeak=1.61
Dmin=−0.54

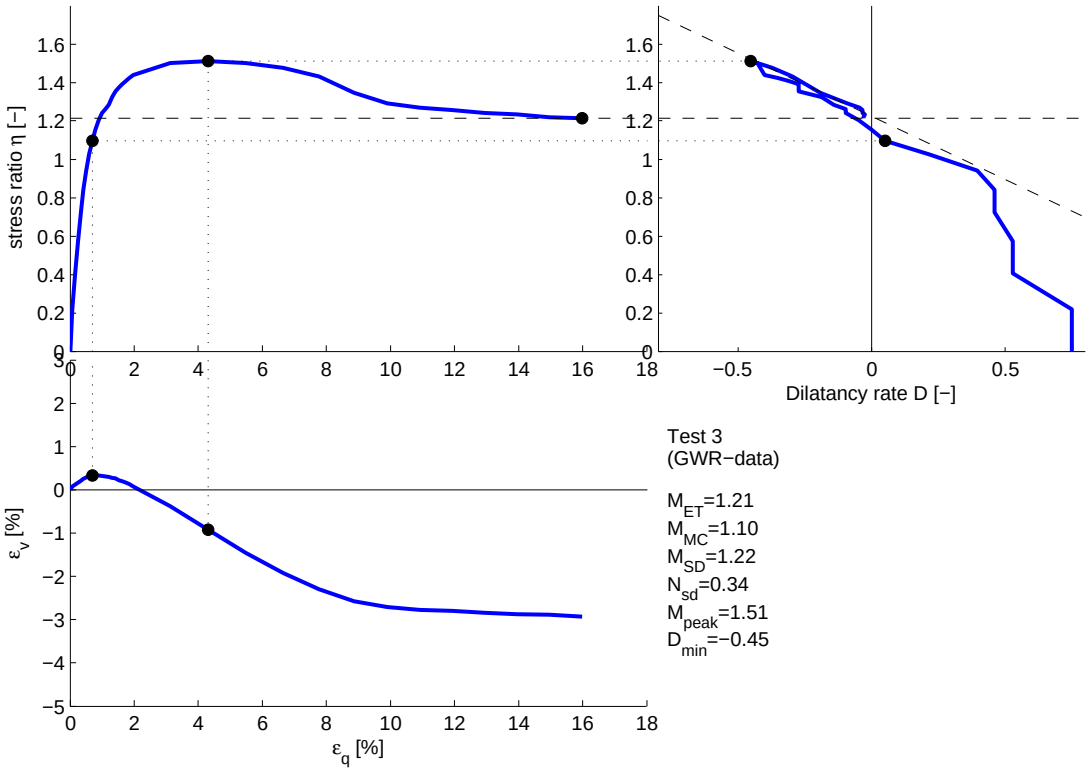
stress ratio η [−]
Dilatancy rate D [−]
εv [%]
εq [%]
Test 3
(GWR−data)
MET=1.21
MMC=1.10
MSD=1.22
Nsd=0.34
Mpeak=1.51
Dmin=−0.45

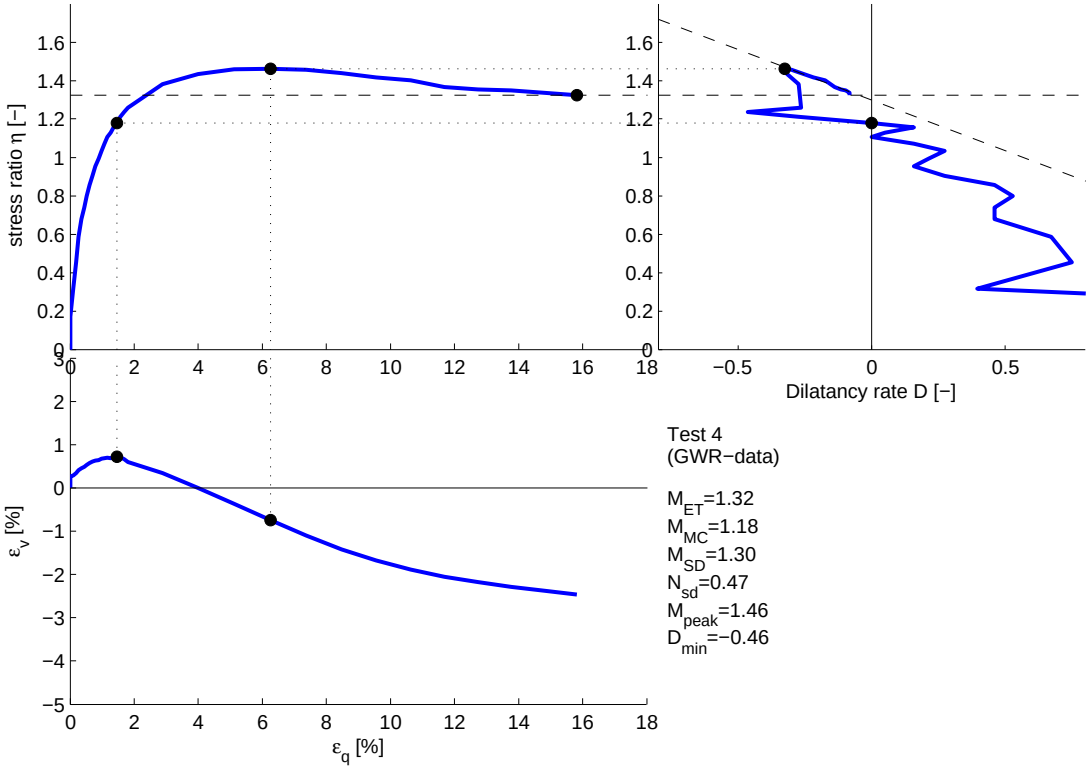
stress ratio η [−]
Dilatancy rate D [−]
ε_v [%]
ε_q [%]
Test 4
(GWR−data)
M_ET=1.32
M_MC=1.18
M_SD=1.30
N_sd=0.47
M_peak=1.46
D_min=−0.46

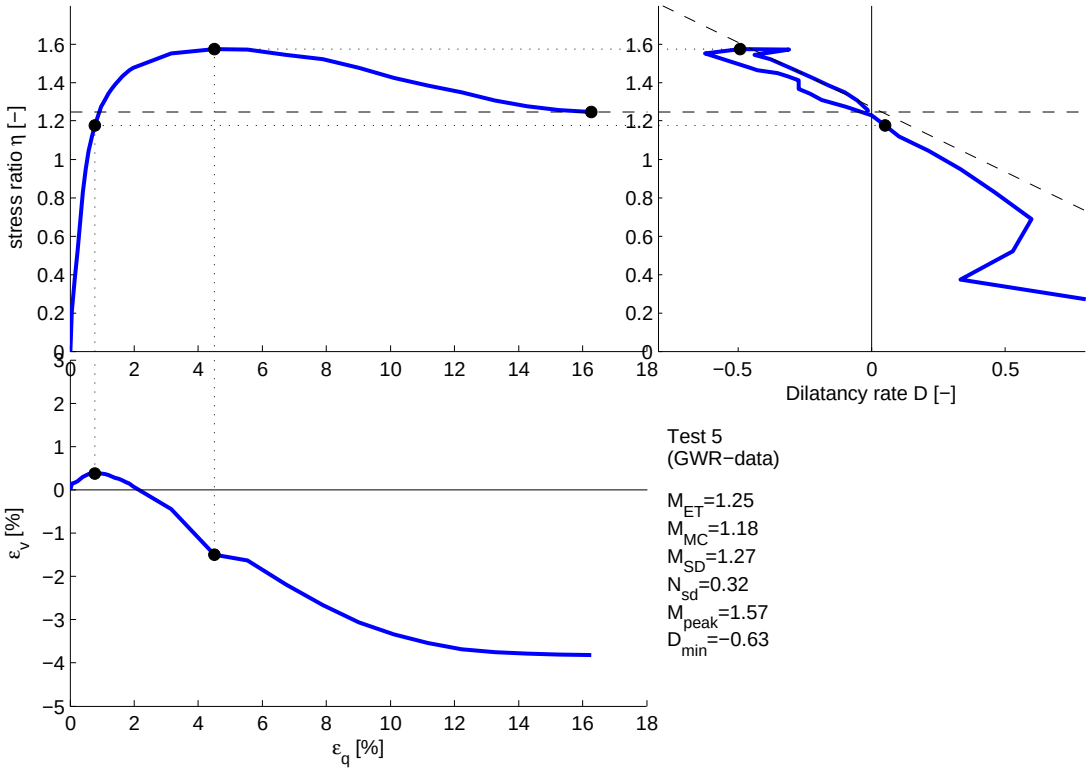
stress ratio η [−]
Dilatancy rate D [−]
ε_v [%]
ε_q [%]
Test 5
(GWR−data)
M_ET=1.25
M_MC=1.18
M_SD=1.27
N_sd=0.32
M_peak=1.57
D_min=−0.63

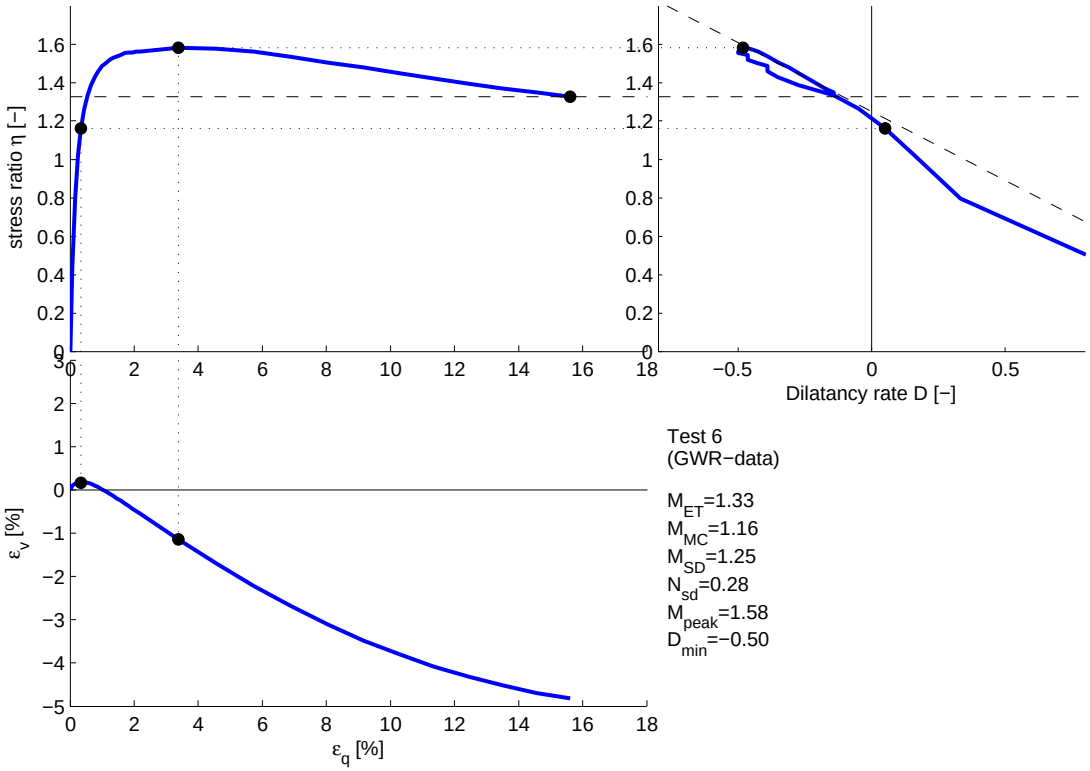
stress ratio η [−]
Dilatancy rate D [−]
ε_v [%]
ε_q [%]
Test 6
(GWR−data)
M_{ET}=1.33
M_{MC}=1.16
M_{SD}=1.25
N_{sd}=0.28
M_{peak}=1.58
D_{min}=−0.50

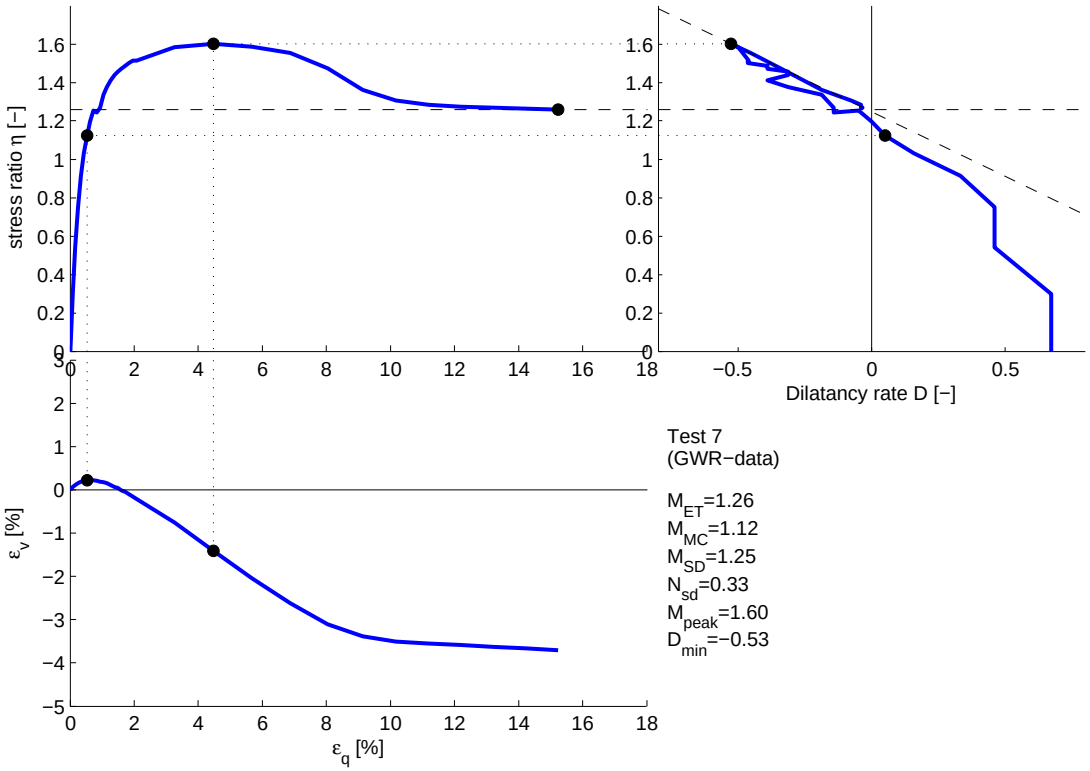
stress ratio η [−]
Dilatancy rate D [−]
ε_v [%]
ε_q [%]
Test 7
(GWR−data)
M_{ET}=1.26
M_{MC}=1.12
M_{SD}=1.25
N_{sd}=0.33
M_{peak}=1.60
D_{min}=−0.53

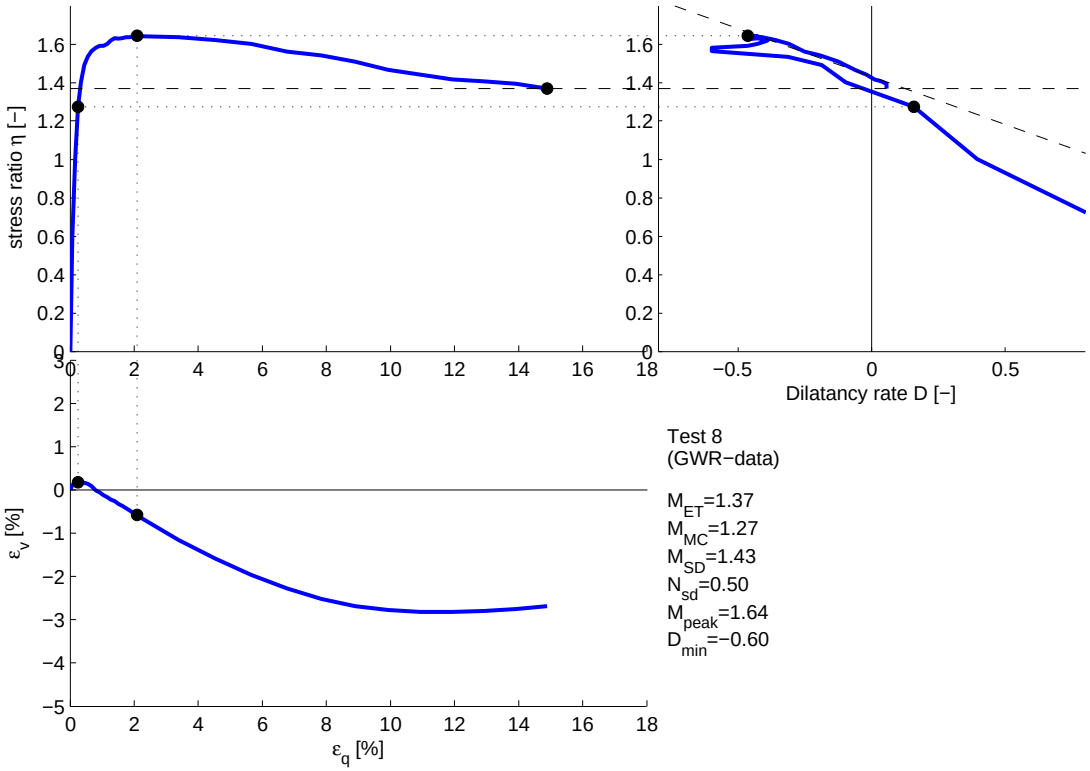
stress ratio η [−]
Dilatancy rate D [−]
ε_v [%]
ε_q [%]
Test 8
(GWR−data)
M_{ET}=1.37
M_{MC}=1.27
M_{SD}=1.43
N_{sd}=0.50
M_{peak}=1.64
D_{min}=−0.60

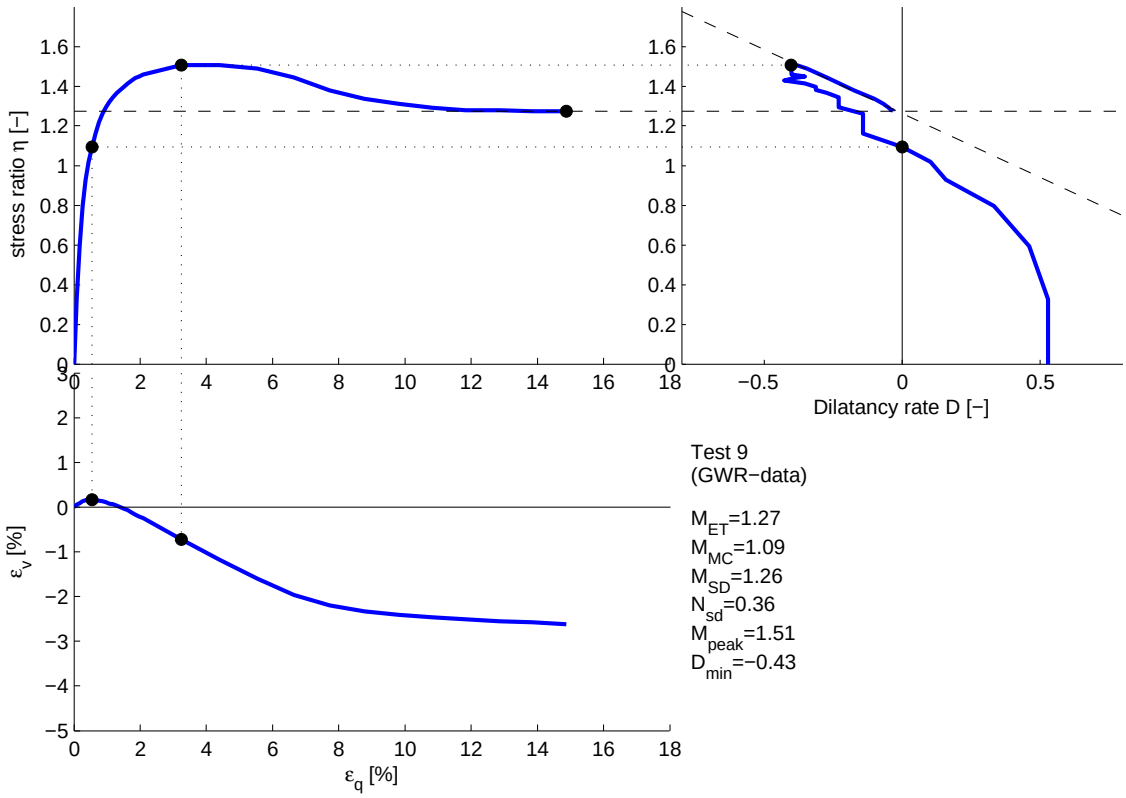
stress ratio η [−]
Dilatancy rate D [−]
ε_v [%]
ε_q [%]
Test 9
(GWR−data)
M_{ET}=1.27
M_{MC}=1.09
M_{SD}=1.26
N_{sd}=0.36
M_{peak}=1.51
D_{min}=−0.43

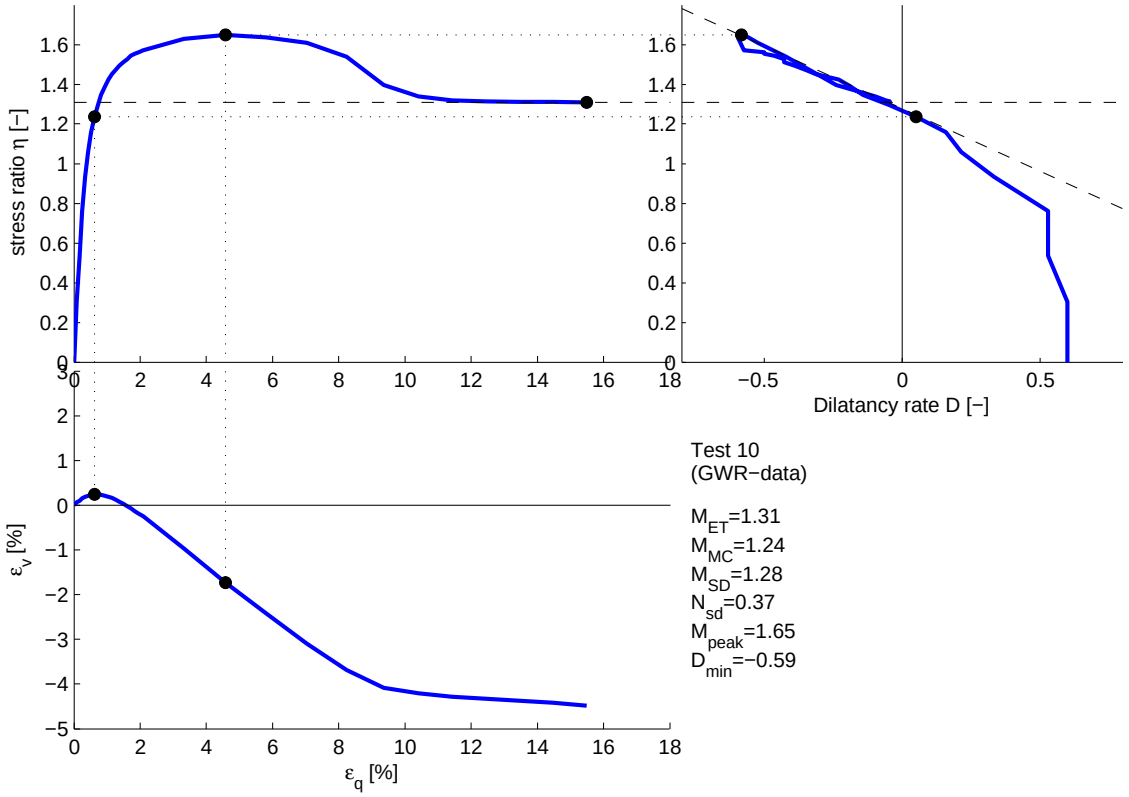
stress ratio η [−]
Dilatancy rate D [−]
ε_v [%]
ε_q [%]
Test 10
(GWR−data)
M_ET=1.31
M_MC=1.24
M_SD=1.28
N_sd=0.37
M_peak=1.65
D_min=−0.59

Lab A-data interpretation results

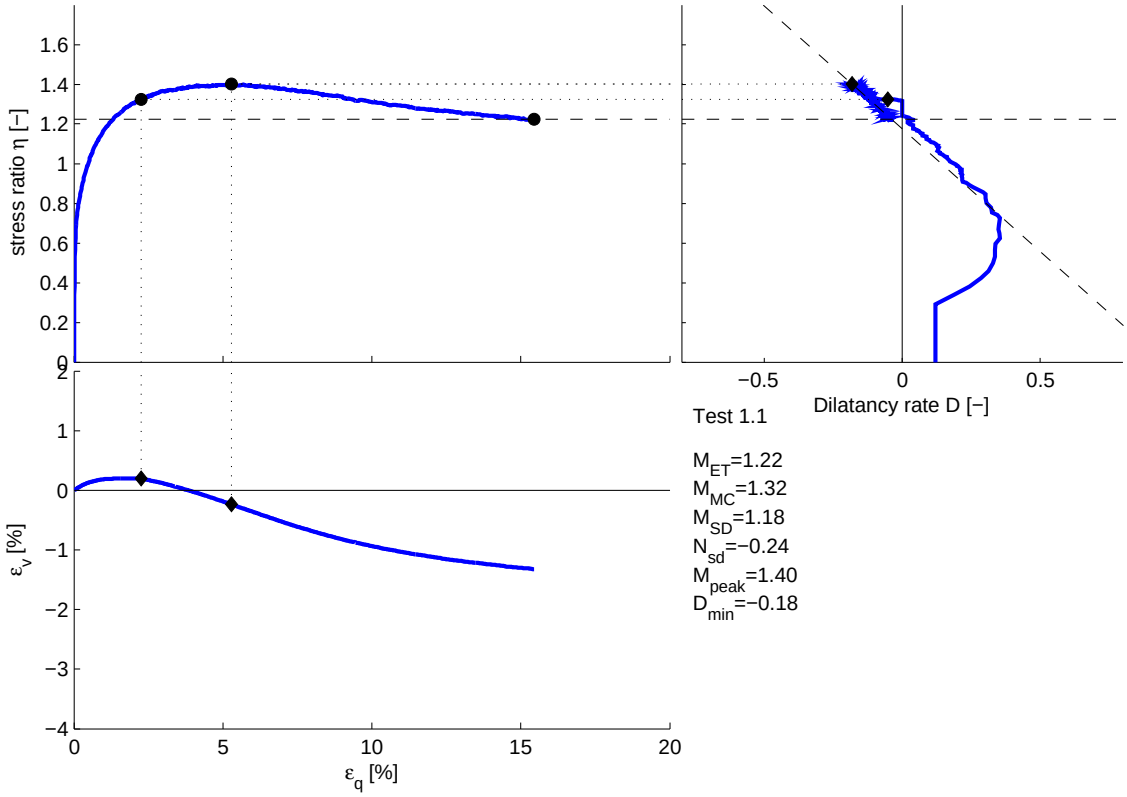
stress ratio η [–]
Dilatancy rate D [–]
Test 1.1
M_{ET}=1.22
M_{MC}=1.32
M_{SD}=1.18
N_{sd}=−0.24
M_{peak}=1.40
D_{min}=−0.18
ε_v [%]
ε_q [%]

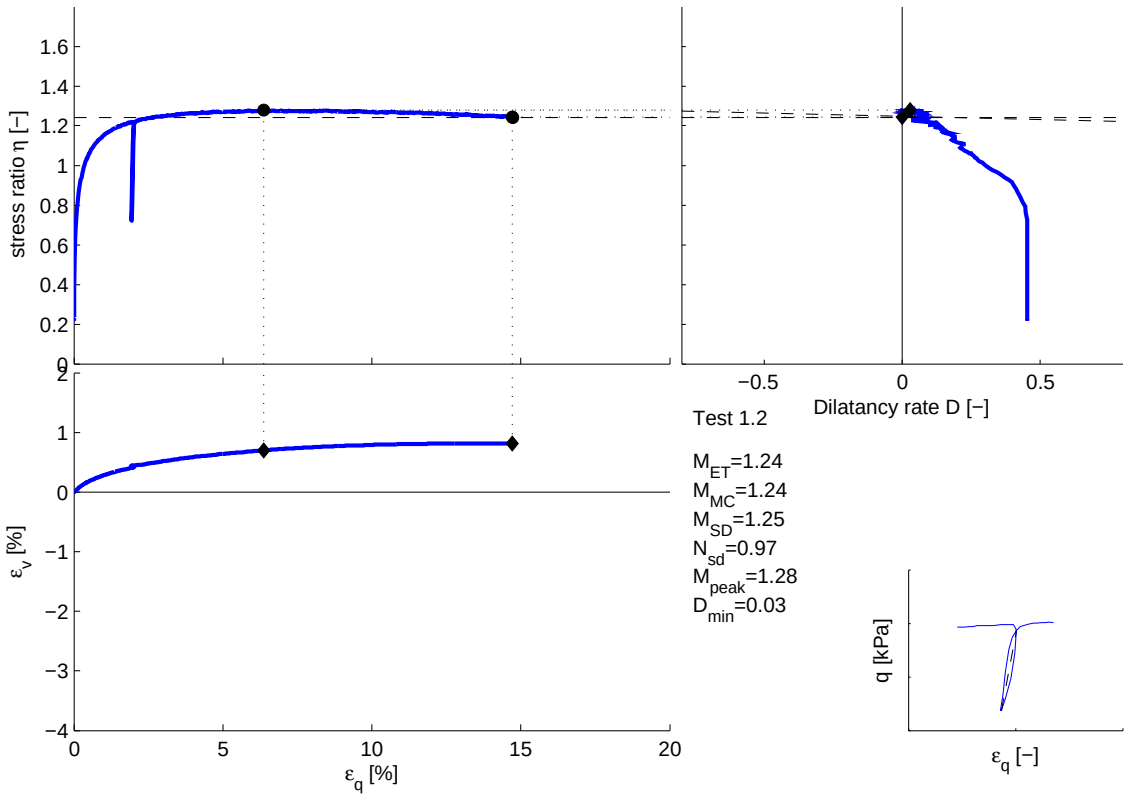
stress ratio η [–]
Dilatancy rate D [–]
Test 1.2
M_{ET}=1.24
M_{MC}=1.24
M_{SD}=1.25
N_{sd}=0.97
M_{peak}=1.28
D_{min}=0.03
q [kPa]
ε_q [–]
ε_v [%]
ε_q [%]

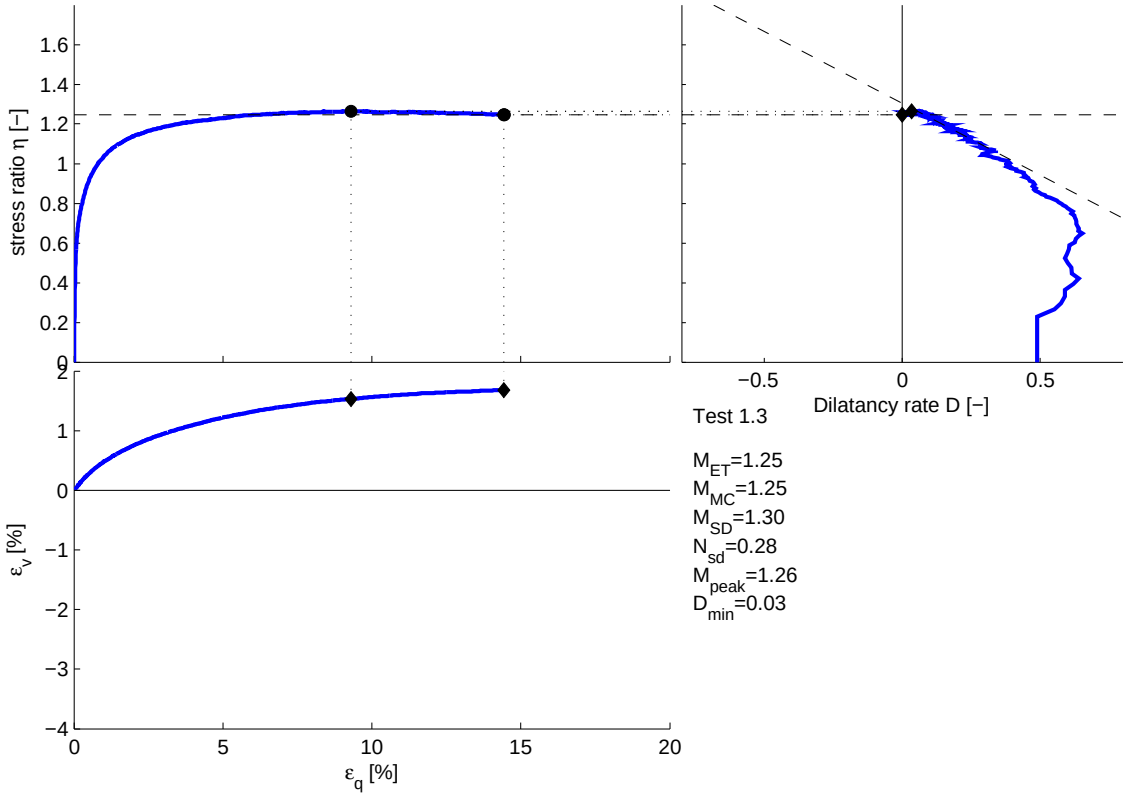
stress ratio η [–]
Dilatancy rate D [–]
Test 1.3
M_ET=1.25
M_MC=1.25
M_SD=1.30
N_sd=0.28
M_peak=1.26
D_min=0.03
ε_v [%]
ε_q [%]

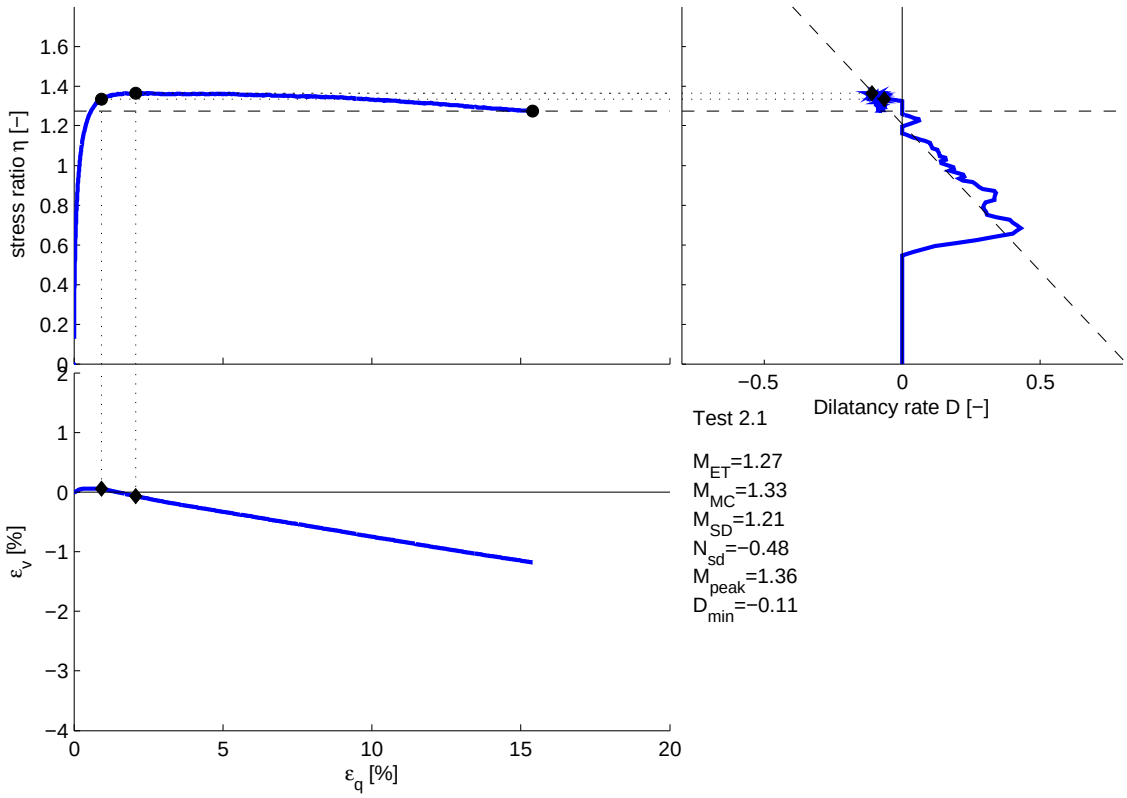
stress ratio η [–]
Dilatancy rate D [–]
Test 2.1
M_ET=1.27
M_MC=1.33
M_SD=1.21
N_sd=−0.48
M_peak=1.36
D_min=−0.11
ε_v [%]
ε_q [%]

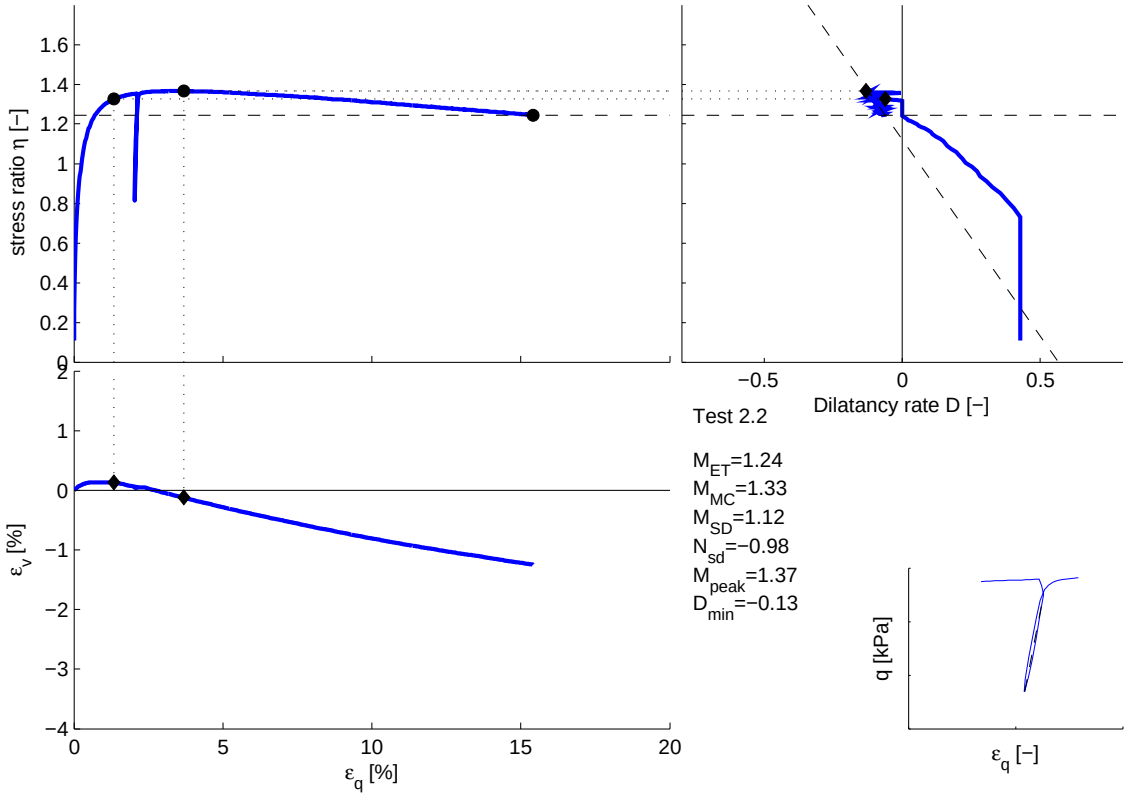
stress ratio η [−]
Dilatancy rate D [−]
Test 2.2
M_ET=1.24
M_MC=1.33
M_SD=1.12
N_sd=−0.98
M_peak=1.37
D_min=−0.13
ε_v [%]
ε_q [%]
q [kPa]
ε_q [−]

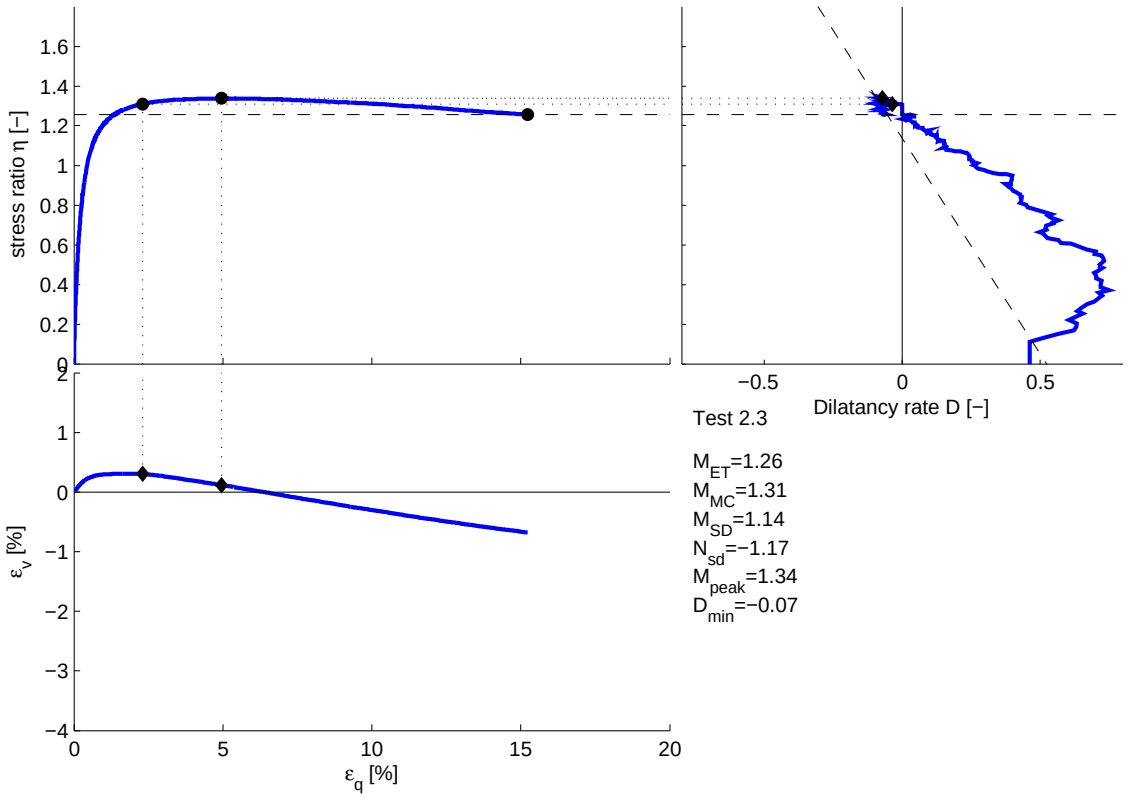
stress ratio η [−]
Dilatancy rate D [−]
Test 2.3
M_ET=1.26
M_MC=1.31
M_SD=1.14
N_sd=−1.17
M_peak=1.34
D_min=−0.07
ε_v [%]
ε_q [%]

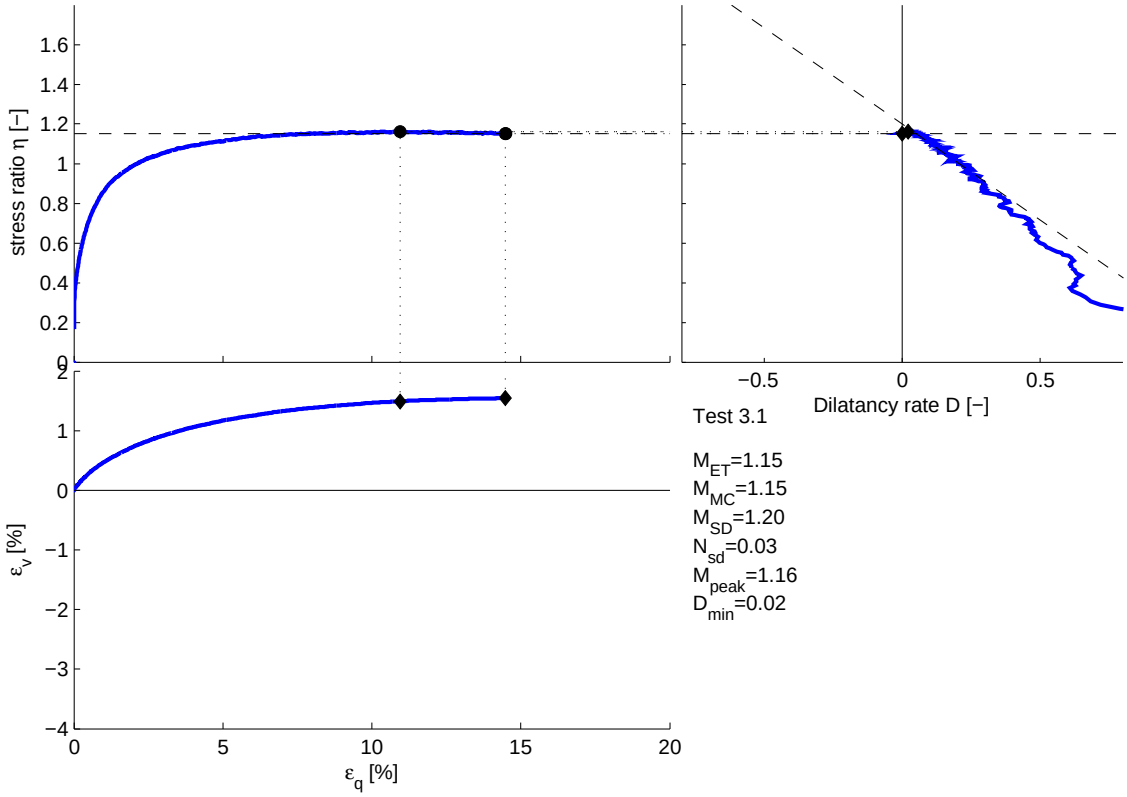
stress ratio η [−]
Dilatancy rate D [−]
Test 3.1
M_ET=1.15
M_MC=1.15
M_SD=1.20
N_sd=0.03
M_peak=1.16
D_min=0.02
ε_v [%]
ε_q [%]

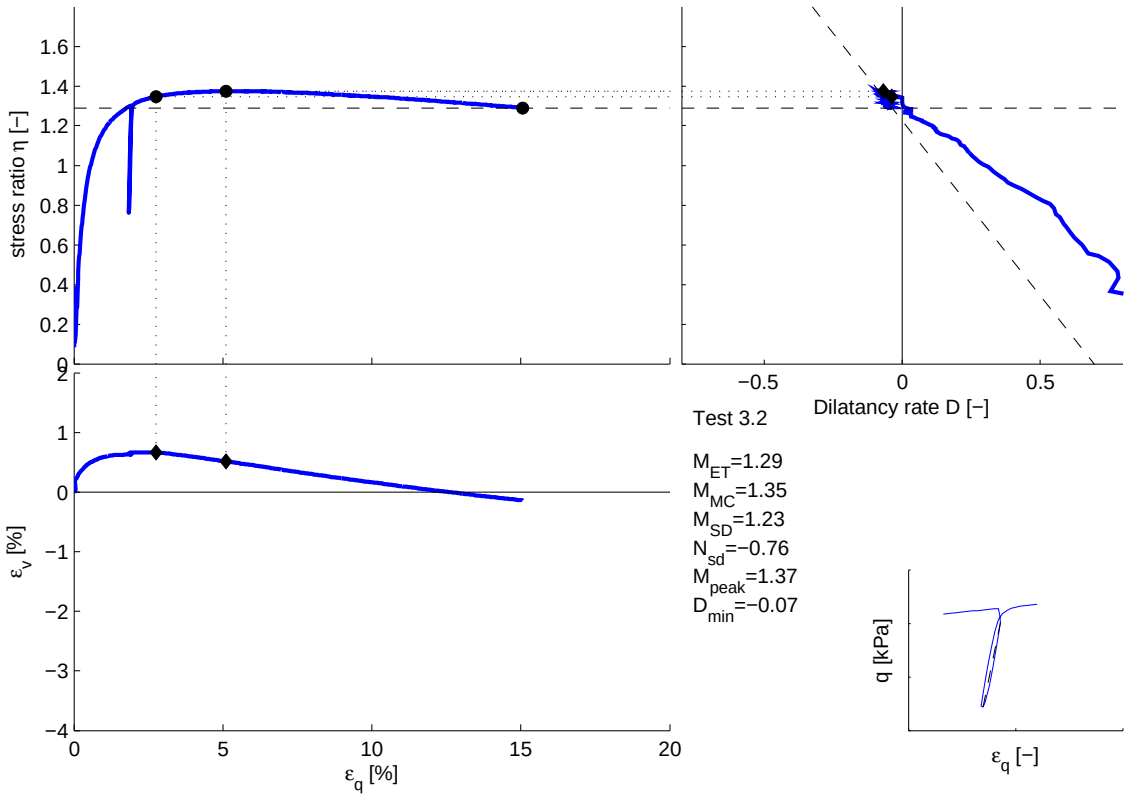
stress ratio η [−]
Dilatancy rate D [−]
Test 3.2
M_ET=1.29
M_MC=1.35
M_SD=1.23
N_sd=−0.76
M_peak=1.37
D_min=−0.07
ε_v [%]
ε_q [%]
q [kPa]
ε_q [−]

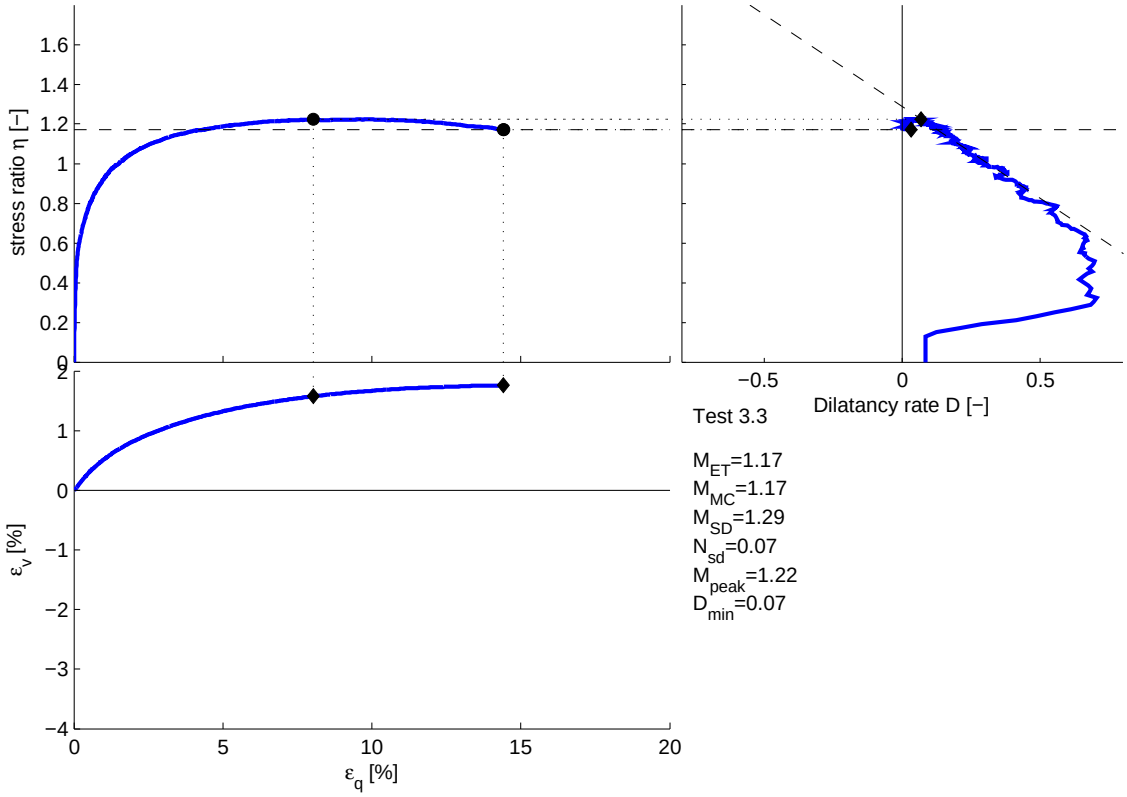
stress ratio η [–]
Dilatancy rate D [–]
Test 3.3
M_{ET}=1.17
M_{MC}=1.17
M_{SD}=1.29
N_{sd}=0.07
M_{peak}=1.22
D_{min}=0.07
ε_v [%]
ε_q [%]

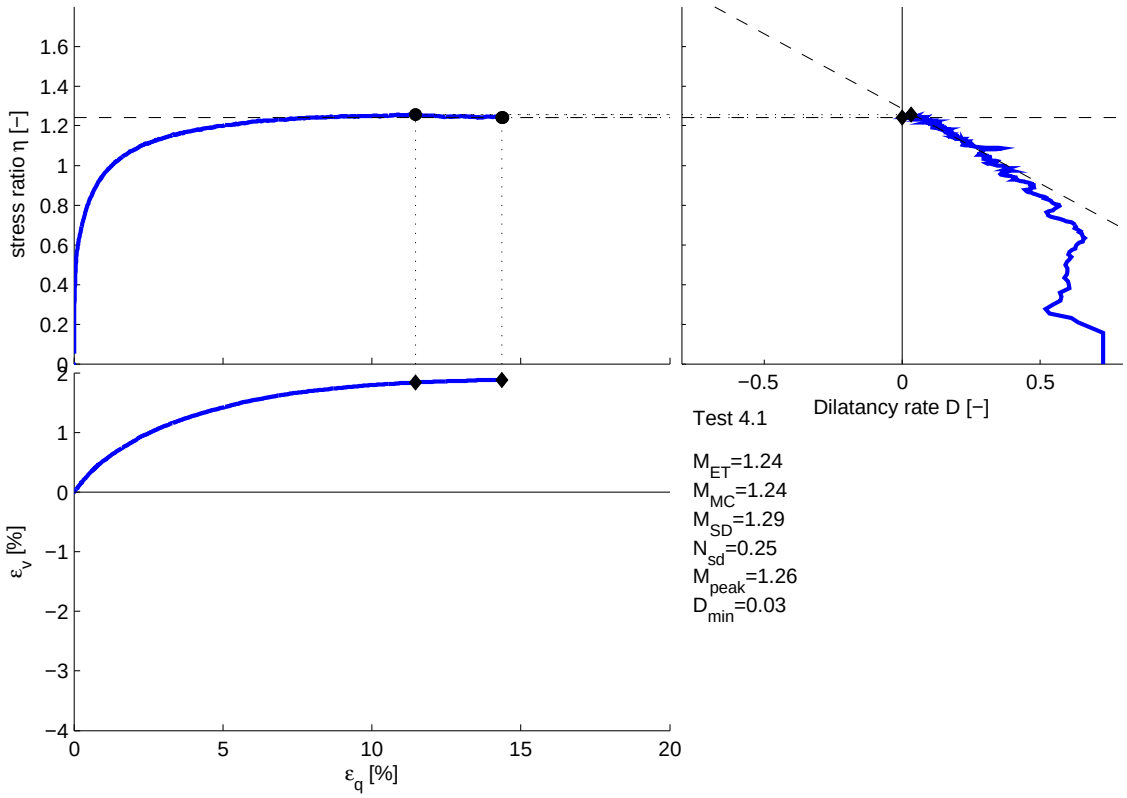
stress ratio η [–]
Dilatancy rate D [–]
Test 4.1
M_{ET}=1.24
M_{MC}=1.24
M_{SD}=1.29
N_{sd}=0.25
M_{peak}=1.26
D_{min}=0.03
ε_v [%]
ε_q [%]

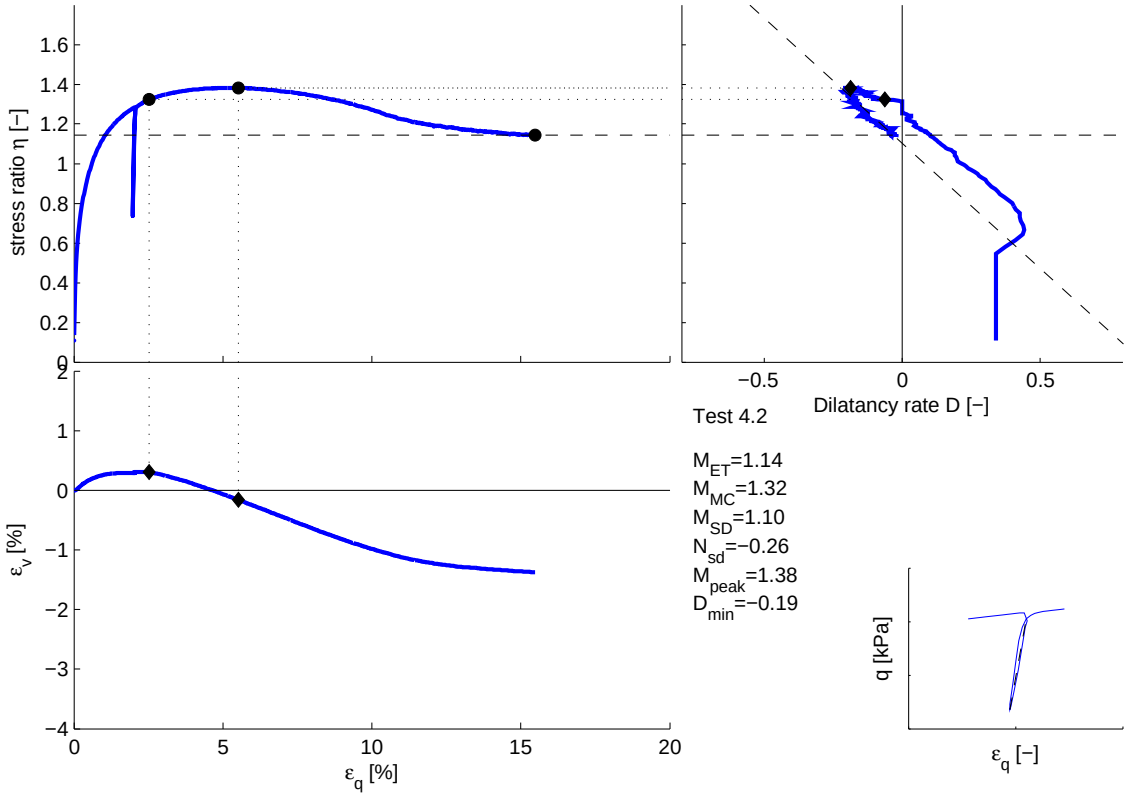
stress ratio η [−]
Dilatancy rate D [−]
Test 4.2
M_{ET}=1.14
M_{MC}=1.32
M_{SD}=1.10
N_{sd}=−0.26
M_{peak}=1.38
D_{min}=−0.19
ε_v [%]
ε_q [%]
q [kPa]
ε_q [−]

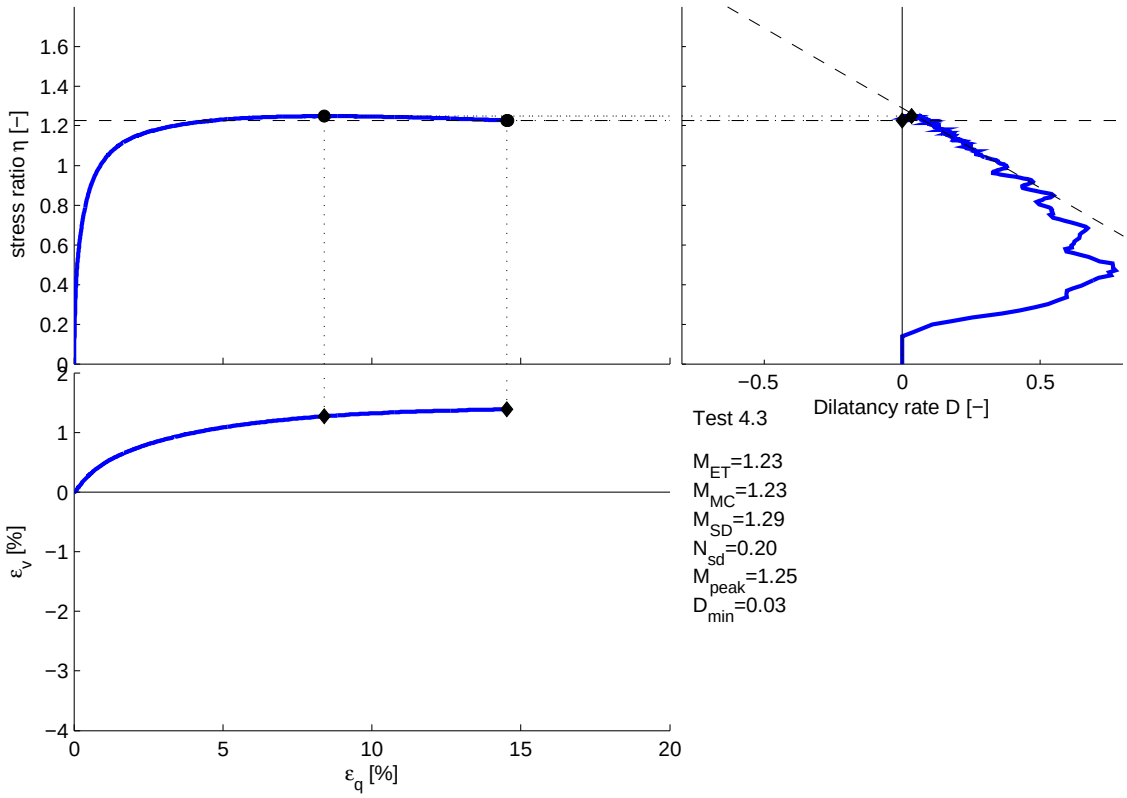
stress ratio η [−]
Dilatancy rate D [−]
Test 4.3
M_{ET}=1.23
M_{MC}=1.23
M_{SD}=1.29
N_{sd}=0.20
M_{peak}=1.25
D_{min}=0.03
ε_v [%]
ε_q [%]

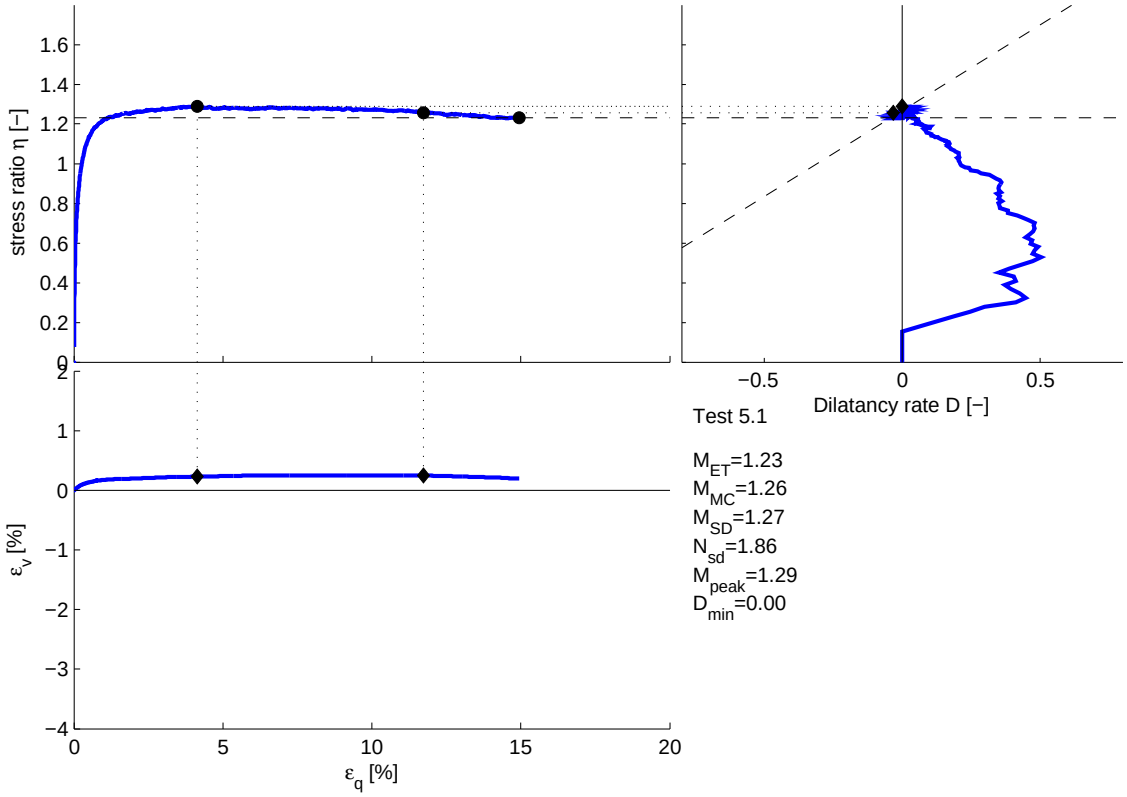
stress ratio η [–]
Dilatancy rate D [–]
Test 5.1
M_ET=1.23
M_MC=1.26
M_SD=1.27
N_sd=1.86
M_peak=1.29
D_min=0.00
ε_v [%]
ε_q [%]

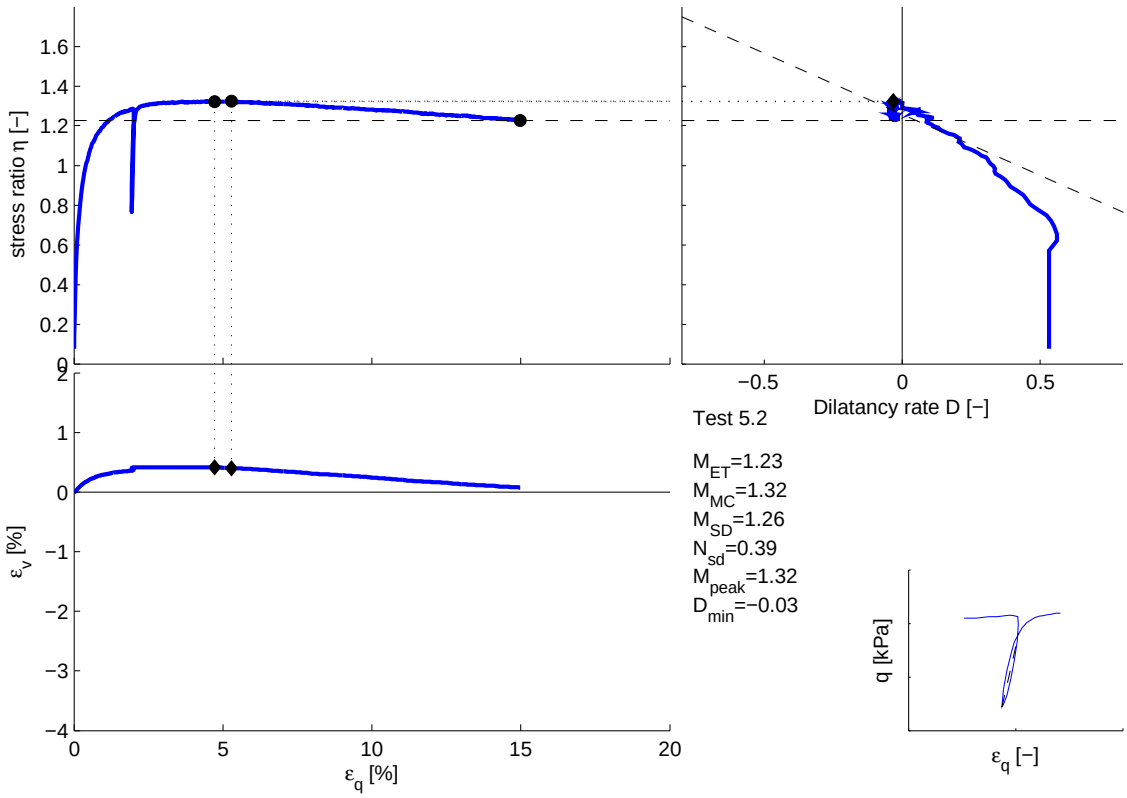
stress ratio η [–]
Dilatancy rate D [–]
Test 5.2
M_ET=1.23
M_MC=1.32
M_SD=1.26
N_sd=0.39
M_peak=1.32
D_min=−0.03
q [kPa]
ε_q [–]
ε_v [%]
ε_q [%]

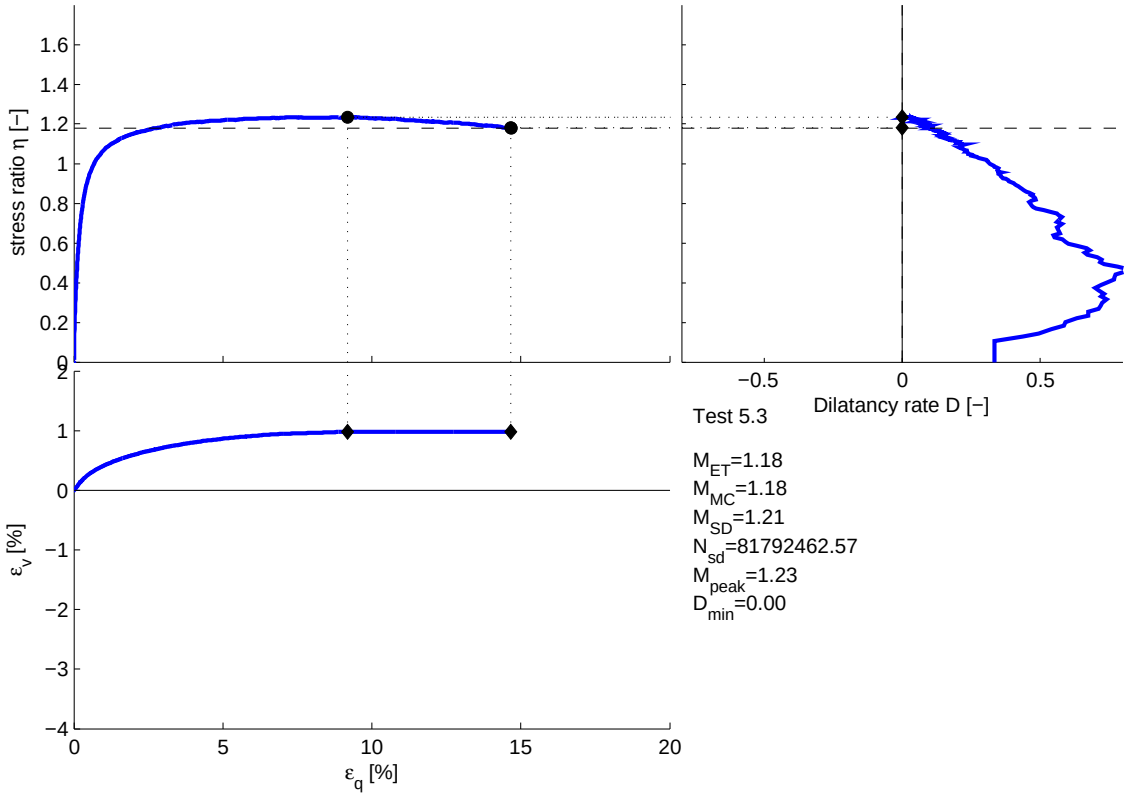
stress ratio η [–]
Dilatancy rate D [–]
ε_v [%]
ε_q [%]
Test 5.3
M_{ET}=1.18
M_{MC}=1.18
M_{SD}=1.21
N_{sd}=81792462.57
M_{peak}=1.23
D_{min}=0.00

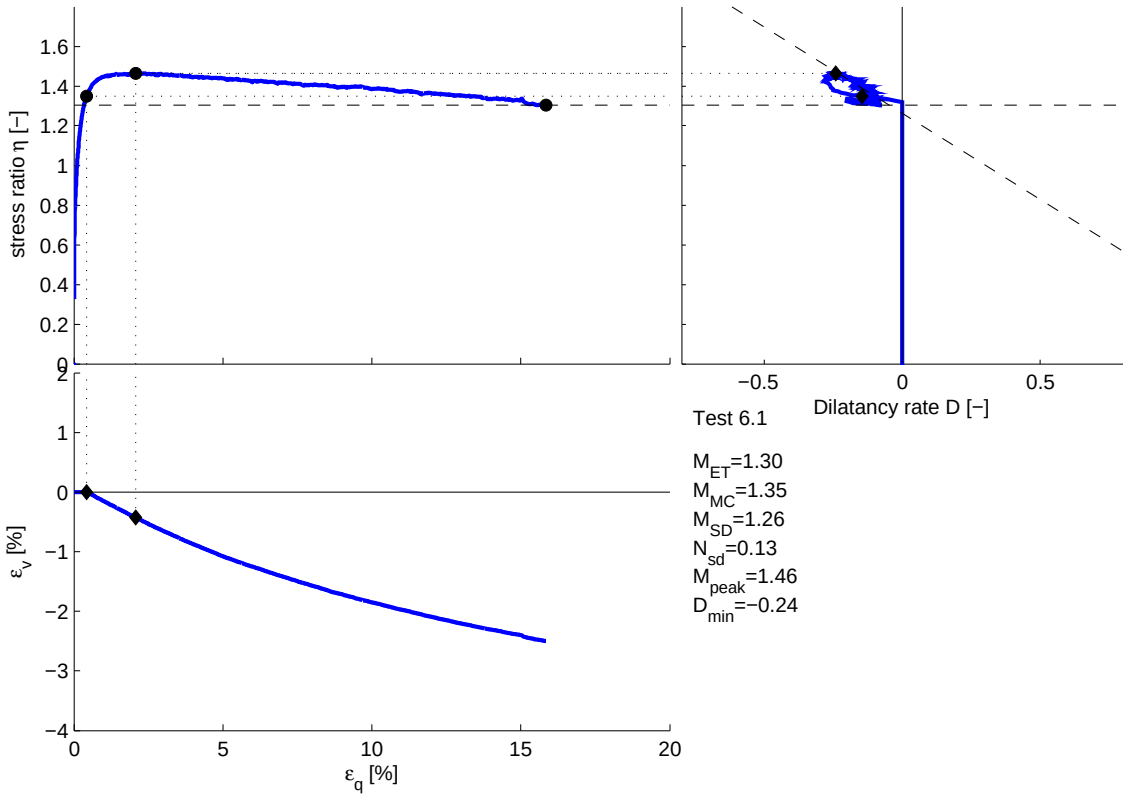
stress ratio η [–]
Dilatancy rate D [–]
ε_v [%]
ε_q [%]
Test 6.1
M_{ET}=1.30
M_{MC}=1.35
M_{SD}=1.26
N_{sd}=0.13
M_{peak}=1.46
D_{min}=−0.24

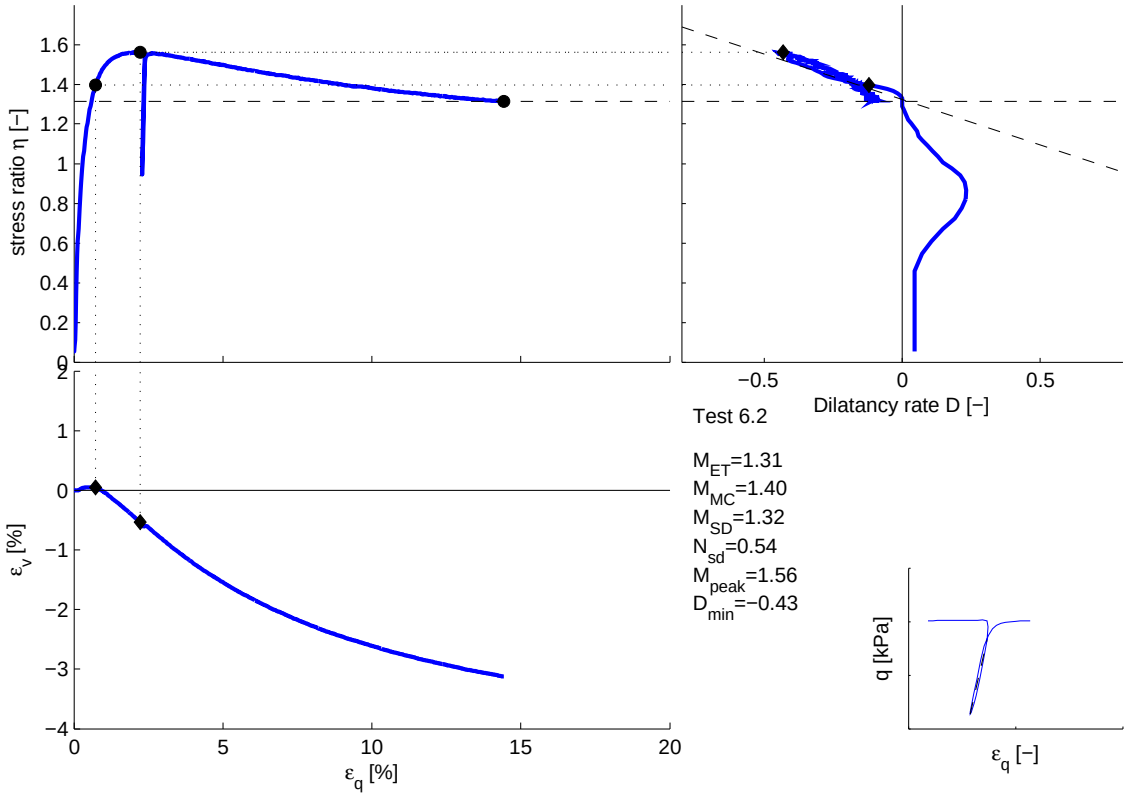
stress ratio η [–]
Dilatancy rate D [–]
Test 6.2
M_{ET}=1.31
M_{MC}=1.40
M_{SD}=1.32
N_{sd}=0.54
M_{peak}=1.56
D_{min}=−0.43
ε_v [%]
ε_q [%]
q [kPa]
ε_q [–]

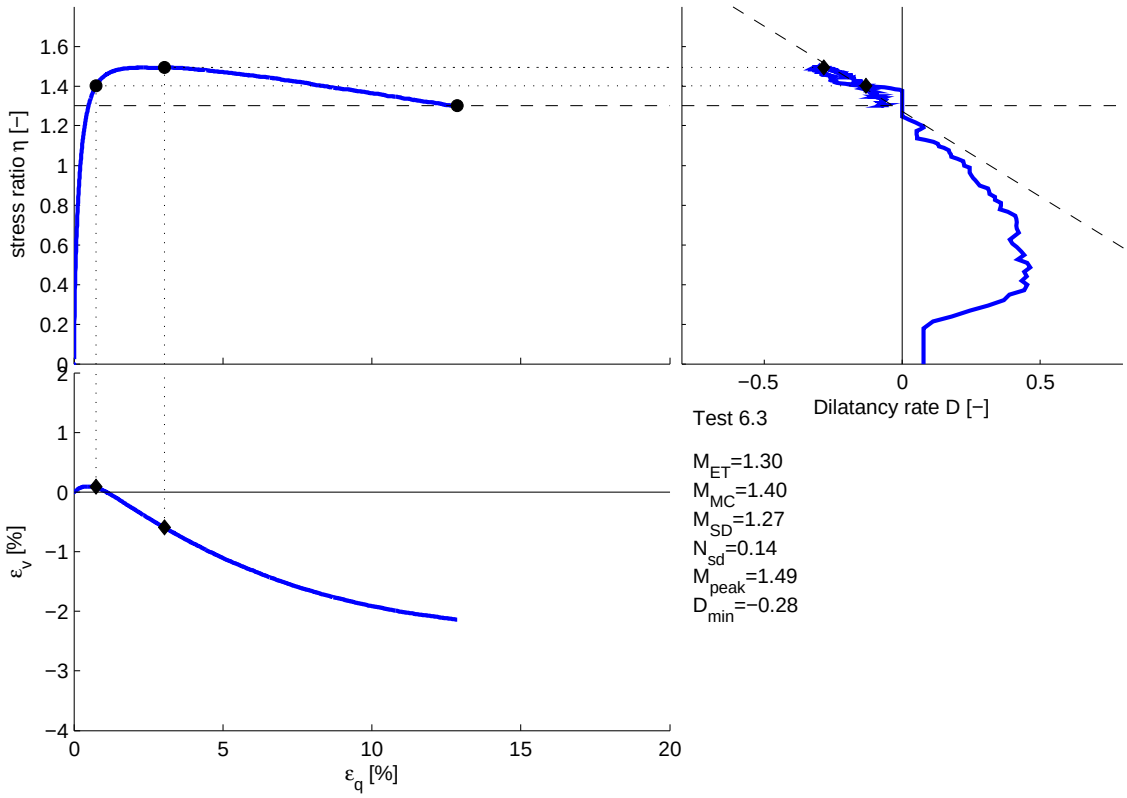
stress ratio η [–]
Dilatancy rate D [–]
Test 6.3
M_{ET}=1.30
M_{MC}=1.40
M_{SD}=1.27
N_{sd}=0.14
M_{peak}=1.49
D_{min}=−0.28
ε_v [%]
ε_q [%]

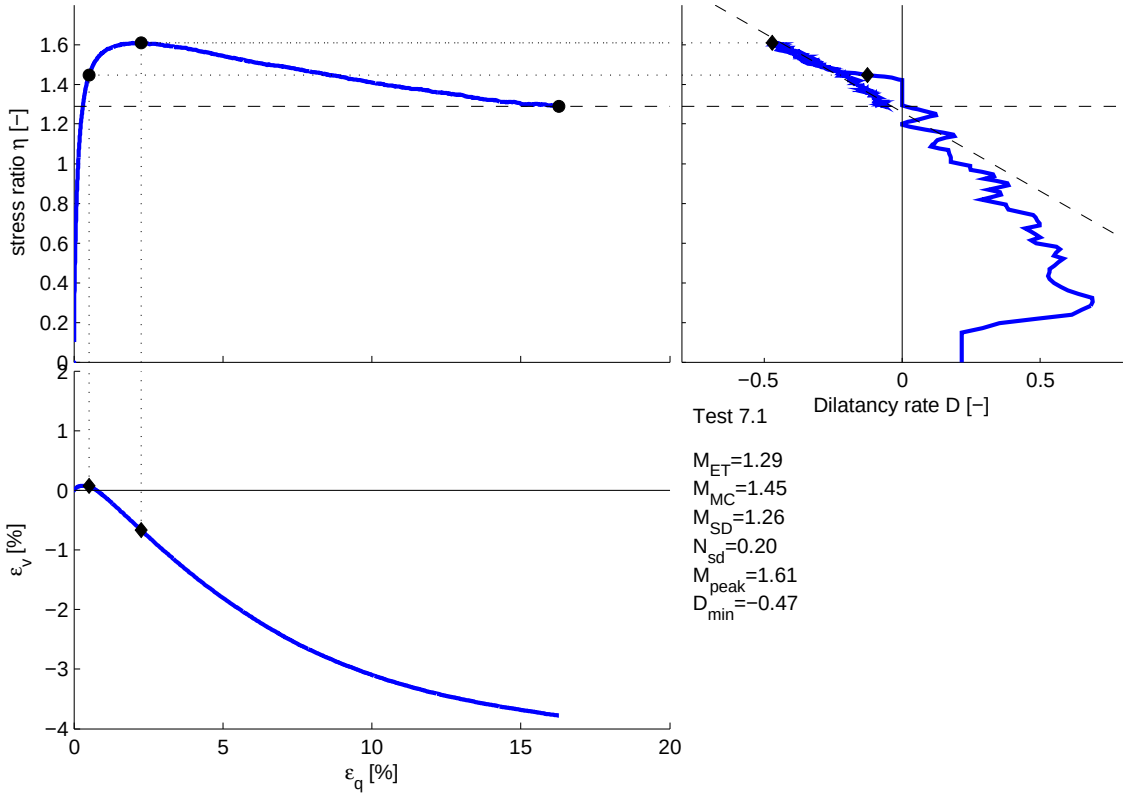
stress ratio η [–]
Dilatancy rate D [–]
Test 7.1
M_{ET}=1.29
M_{MC}=1.45
M_{SD}=1.26
N_{sd}=0.20
M_{peak}=1.61
D_{min}=−0.47
ε_v [%]
ε_q [%]

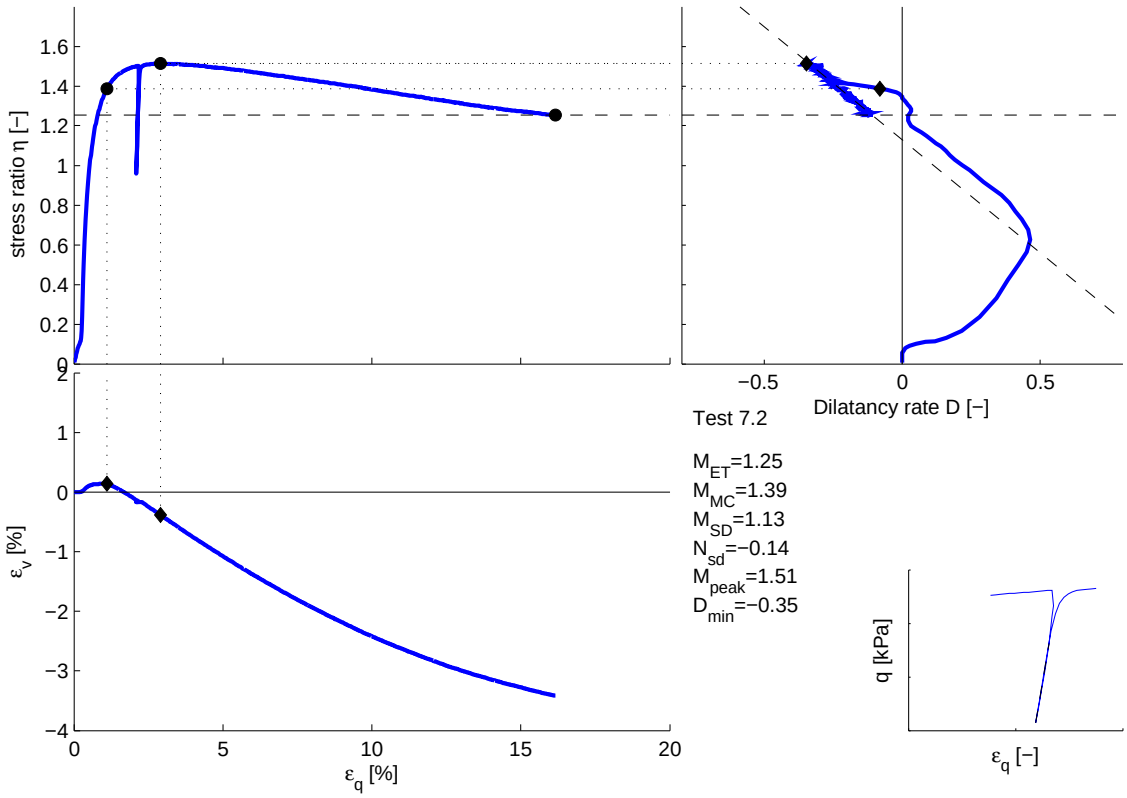
stress ratio η [–]
Dilatancy rate D [–]
Test 7.2
M_{ET}=1.25
M_{MC}=1.39
M_{SD}=1.13
N_{sd}=−0.14
M_{peak}=1.51
D_{min}=−0.35
q [kPa]
ε_q [–]
ε_v [%]
ε_q [%]

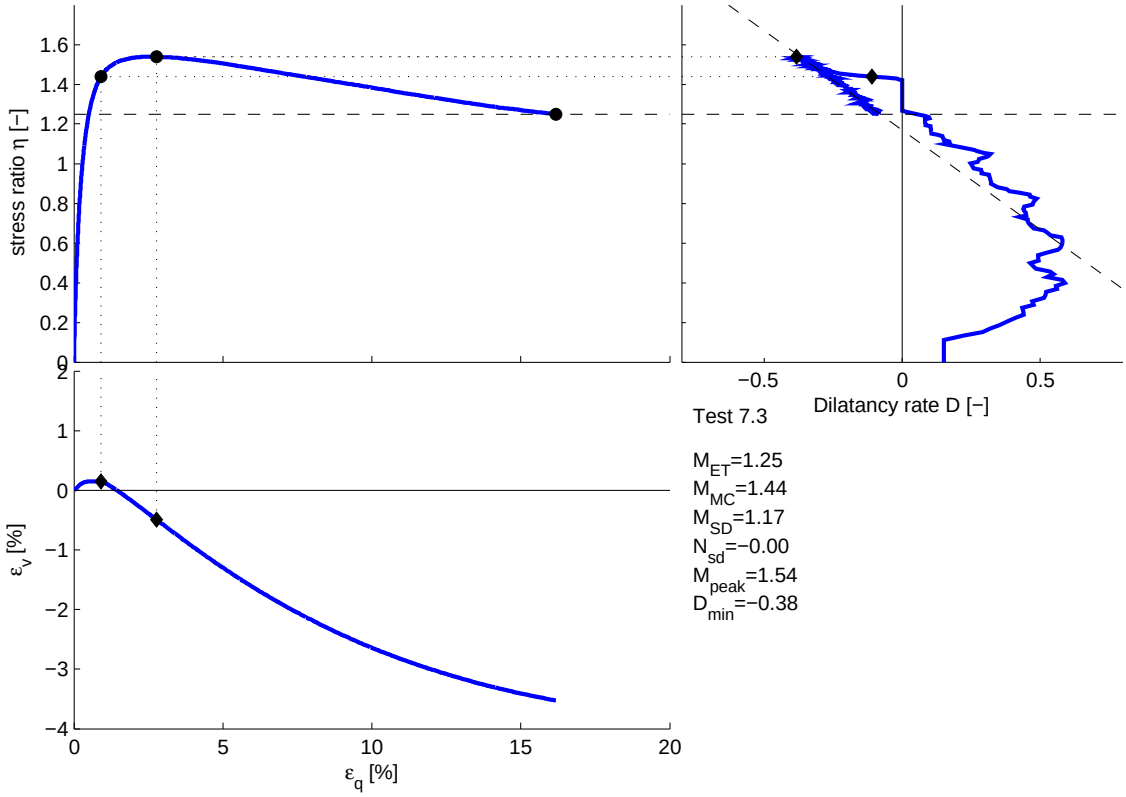
stress ratio η [–]
Dilatancy rate D [–]
Test 7.3
M_{ET}=1.25
M_{MC}=1.44
M_{SD}=1.17
N_{sd}=−0.00
M_{peak}=1.54
D_{min}=−0.38
ε_v [%]
ε_q [%]

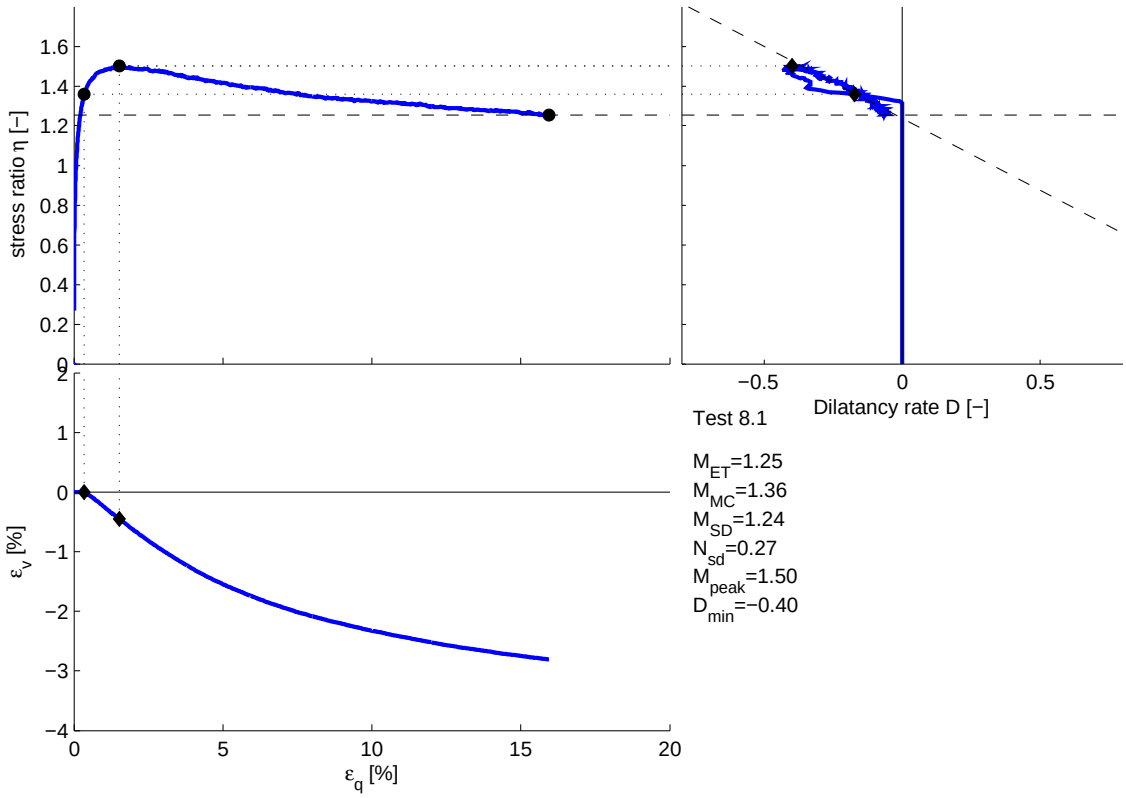
stress ratio η [–]
Dilatancy rate D [–]
Test 8.1
M_{ET}=1.25
M_{MC}=1.36
M_{SD}=1.24
N_{sd}=0.27
M_{peak}=1.50
D_{min}=−0.40
ε_v [%]
ε_q [%]

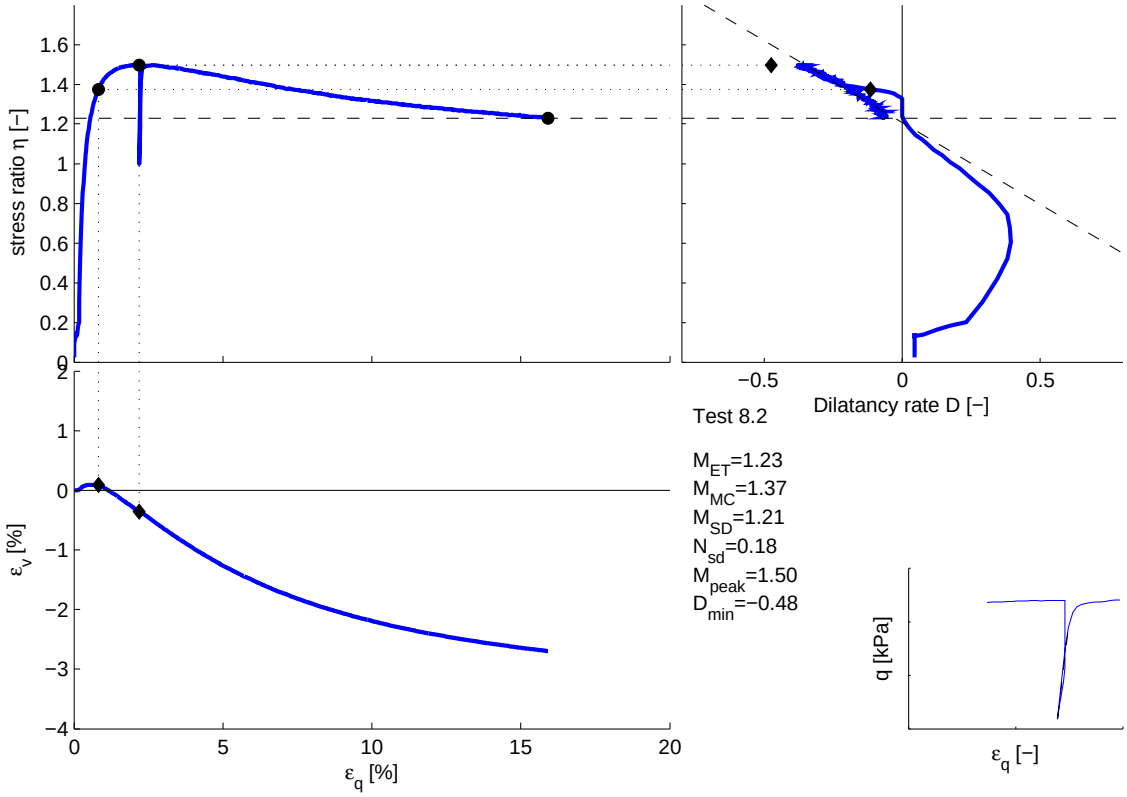
stress ratio η [−]
Dilatancy rate D [−]
Test 8.2
M_ET=1.23
M_MC=1.37
M_SD=1.21
N_sd=0.18
M_peak=1.50
D_min=−0.48
ε_v [%]
ε_q [%]
q [kPa]
ε_q [−]

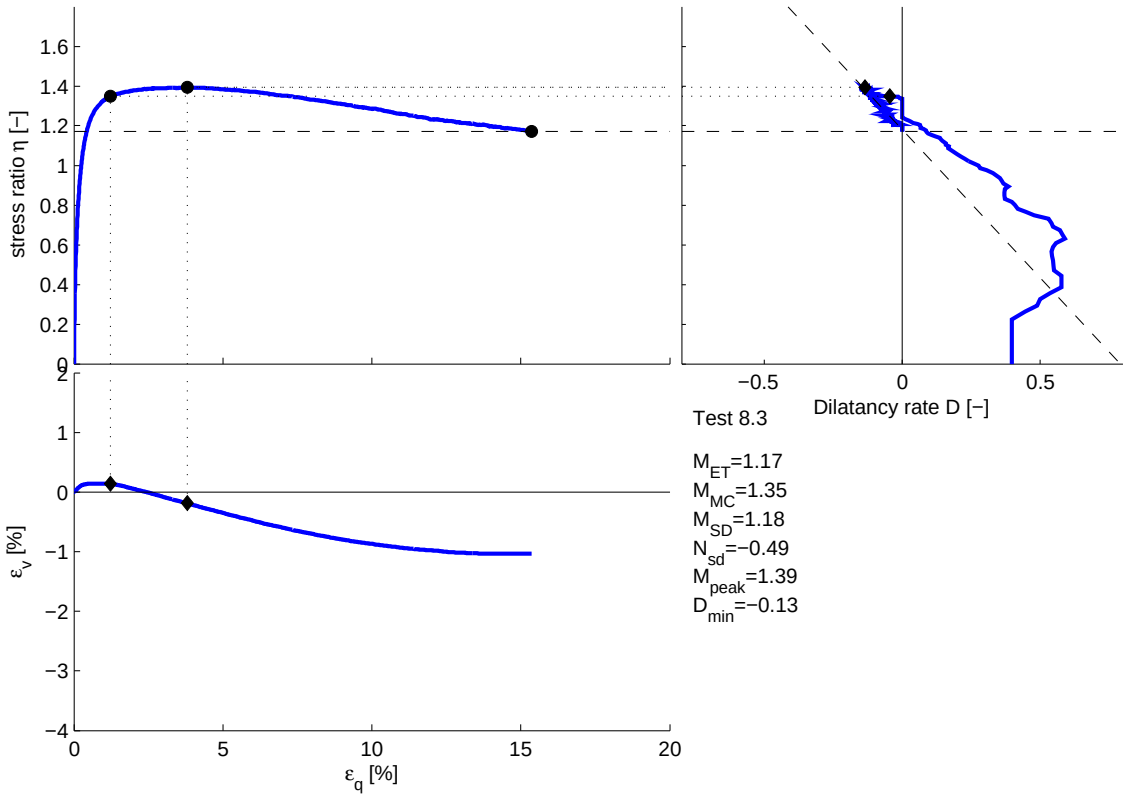
stress ratio η [−]
Dilatancy rate D [−]
Test 8.3
M_ET=1.17
M_MC=1.35
M_SD=1.18
N_sd=−0.49
M_peak=1.39
D_min=−0.13
ε_v [%]
ε_q [%]

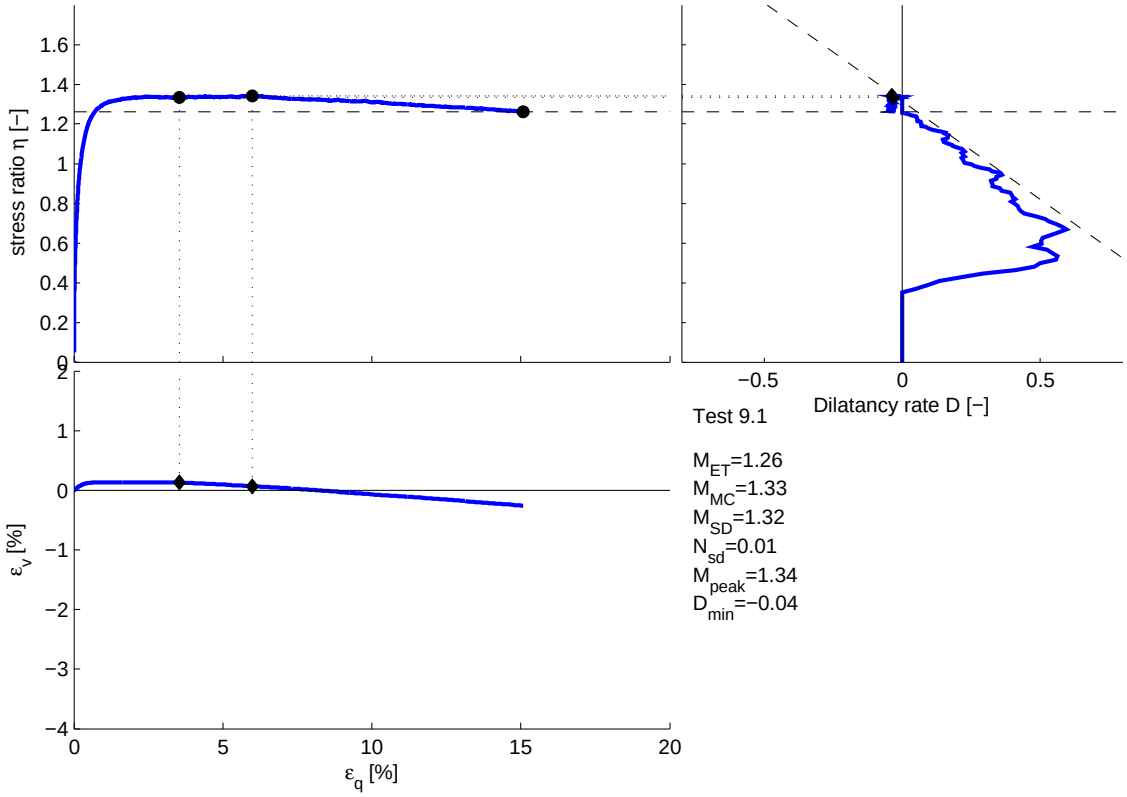
stress ratio η [−]
Dilatancy rate D [−]
ε_v [%]
ε_q [%]
Test 9.1
M_{ET}=1.26
M_{MC}=1.33
M_{SD}=1.32
N_{sd}=0.01
M_{peak}=1.34
D_{min}=−0.04

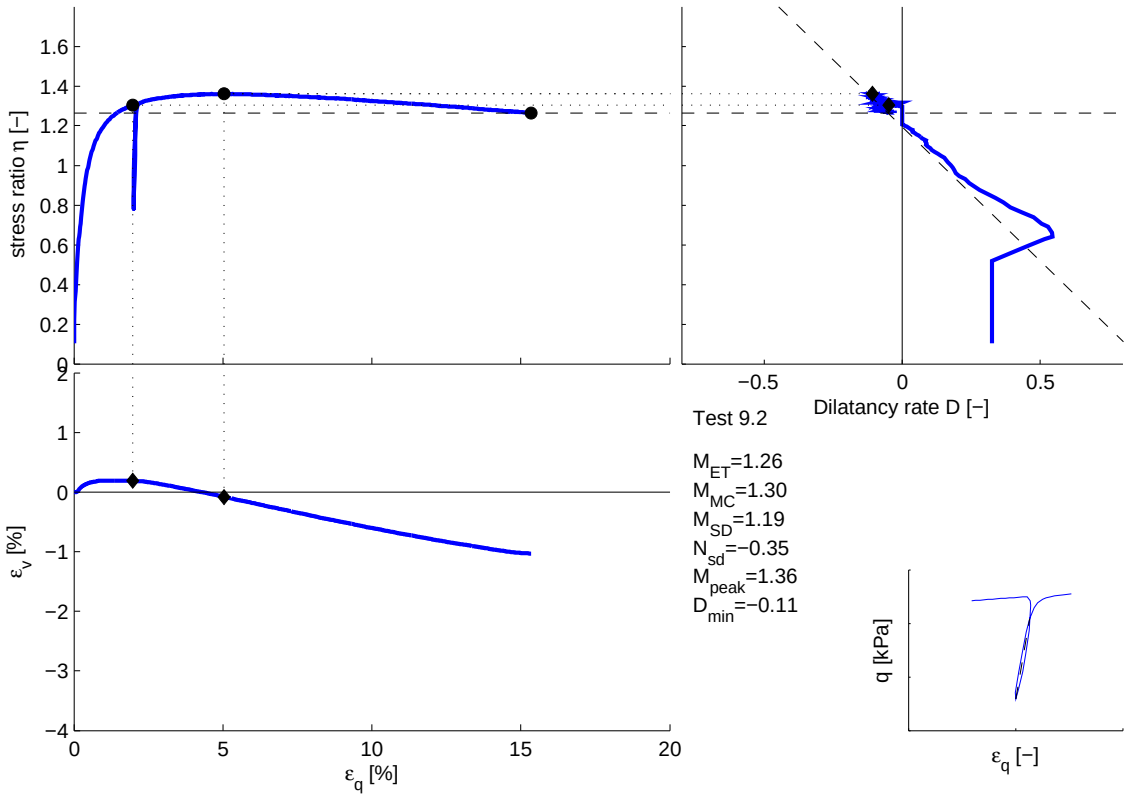
stress ratio η [−]
Dilatancy rate D [−]
ε_v [%]
ε_q [%]
Test 9.2
M_{ET}=1.26
M_{MC}=1.30
M_{SD}=1.19
N_{sd}=−0.35
M_{peak}=1.36
D_{min}=−0.11
q [kPa]
ε_q [−]

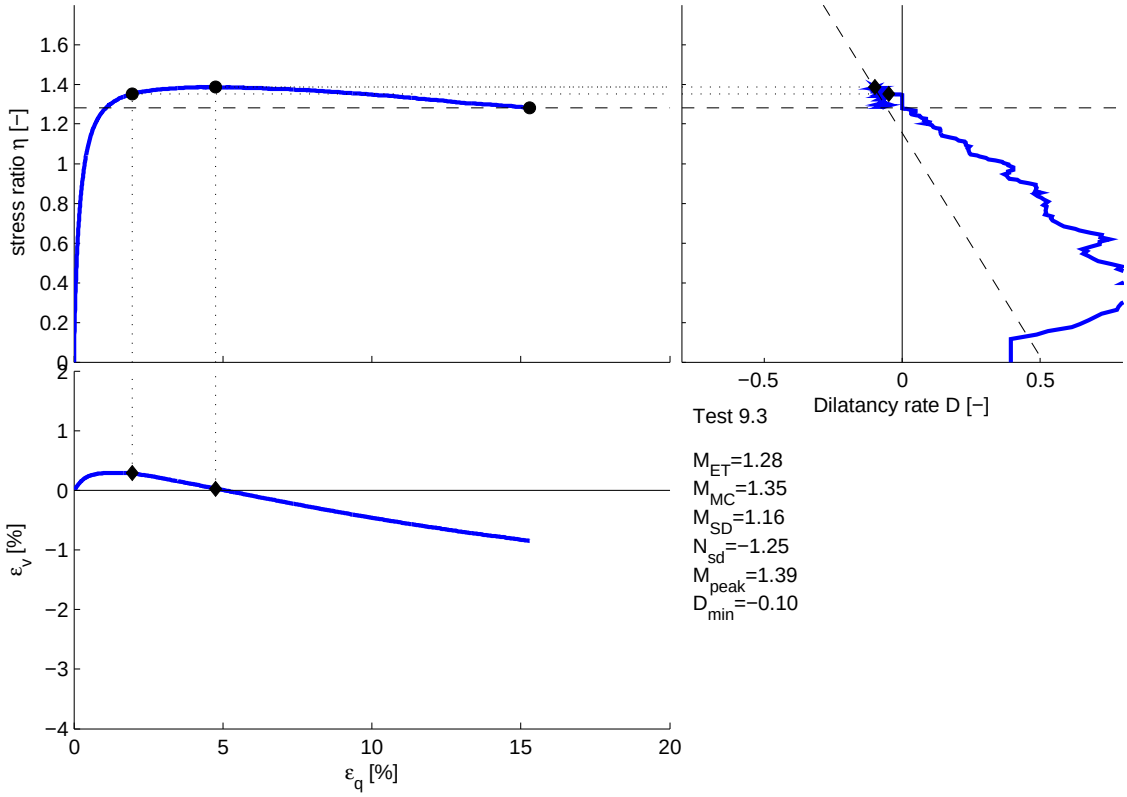
stress ratio η [–]
Dilatancy rate D [–]
Test 9.3
M_ET=1.28
M_MC=1.35
M_SD=1.16
N_sd=−1.25
M_peak=1.39
D_min=−0.10
ε_v [%]
ε_q [%]

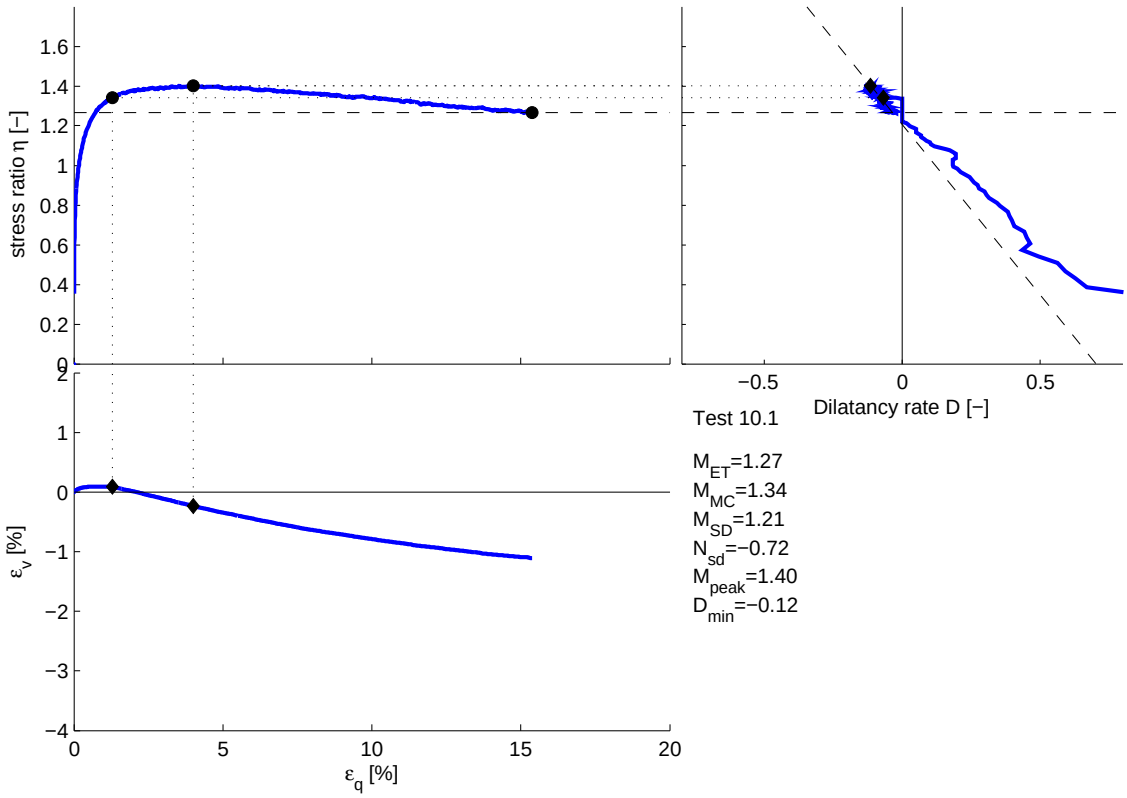
stress ratio η [–]
Dilatancy rate D [–]
Test 10.1
M_ET=1.27
M_MC=1.34
M_SD=1.21
N_sd=−0.72
M_peak=1.40
D_min=−0.12
ε_v [%]
ε_q [%]

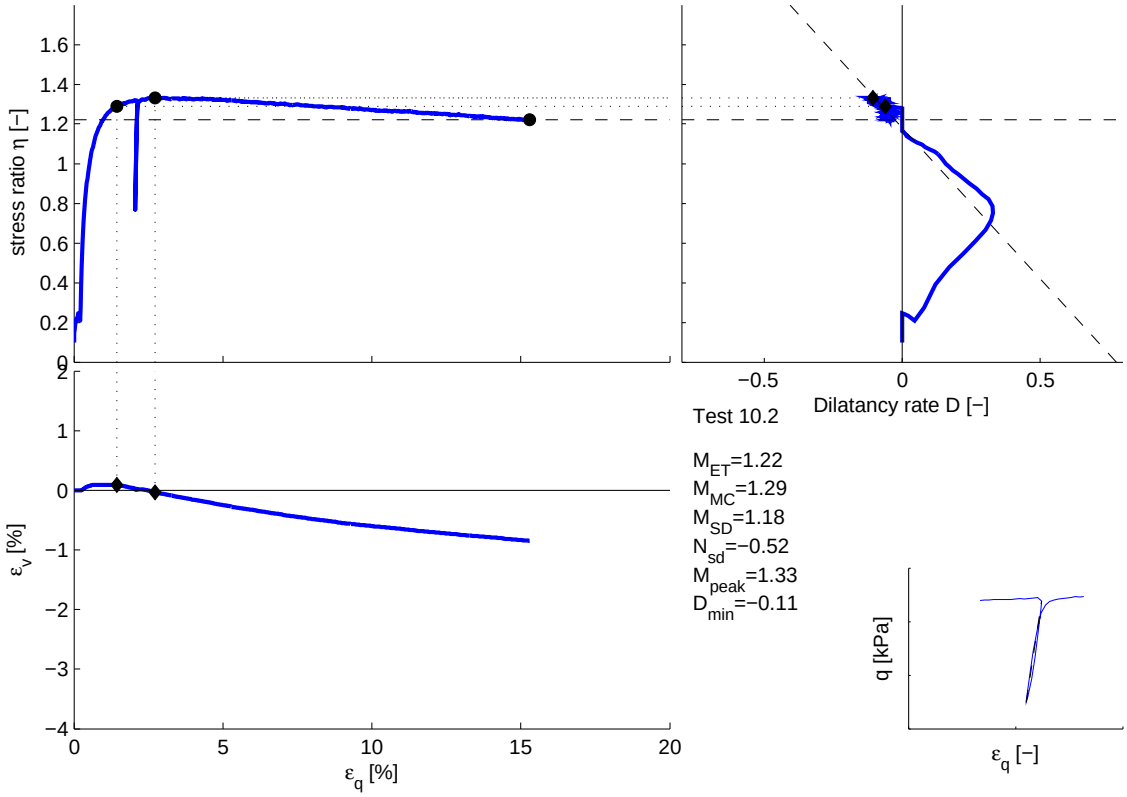
stress ratio η [−]
Dilatancy rate D [−]
Test 10.2
M_{ET}=1.22
M_{MC}=1.29
M_{SD}=1.18
N_{sd}=−0.52
M_{peak}=1.33
D_{min}=−0.11
ε_v [%]
ε_q [%]
q [kPa]
ε_q [−]

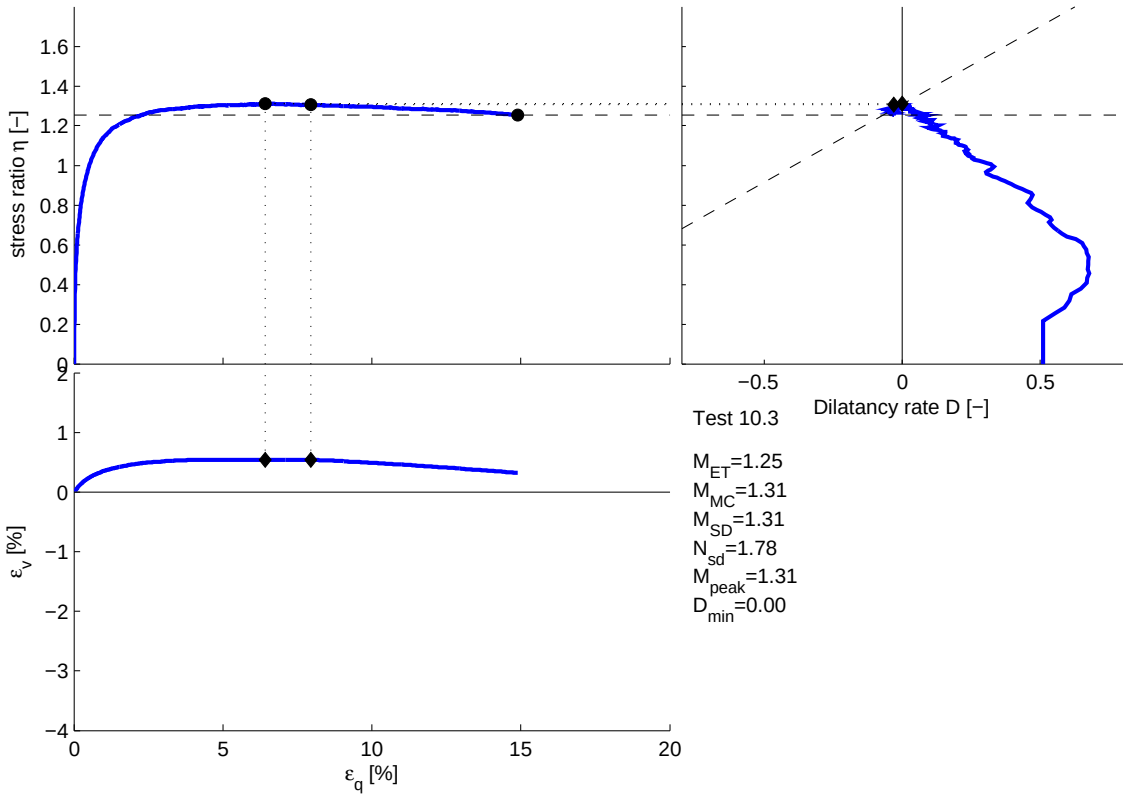
stress ratio η [−]
Dilatancy rate D [−]
Test 10.3
M_{ET}=1.25
M_{MC}=1.31
M_{SD}=1.31
N_{sd}=1.78
M_{peak}=1.31
D_{min}=0.00
ε_v [%]
ε_q [%]

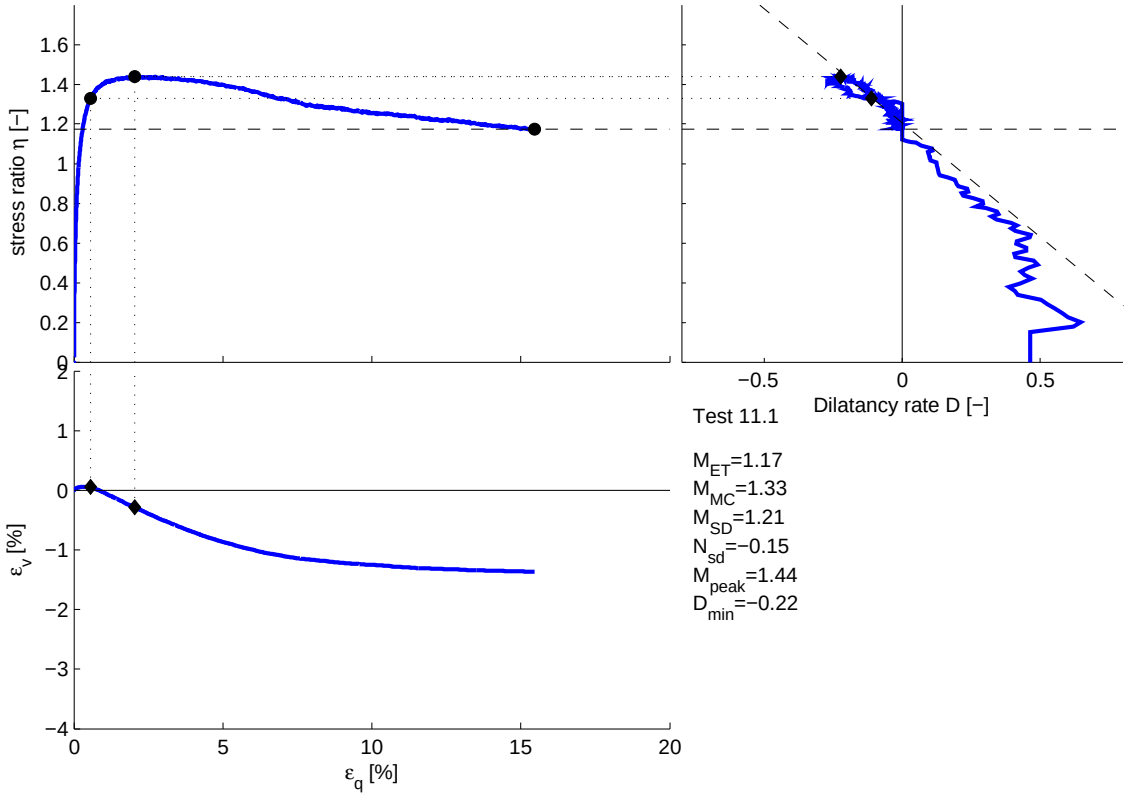
stress ratio η [–]
Dilatancy rate D [–]
Test 11.1
M_{ET}=1.17
M_{MC}=1.33
M_{SD}=1.21
N_{sd}=−0.15
M_{peak}=1.44
D_{min}=−0.22
ε_v [%]
ε_q [%]

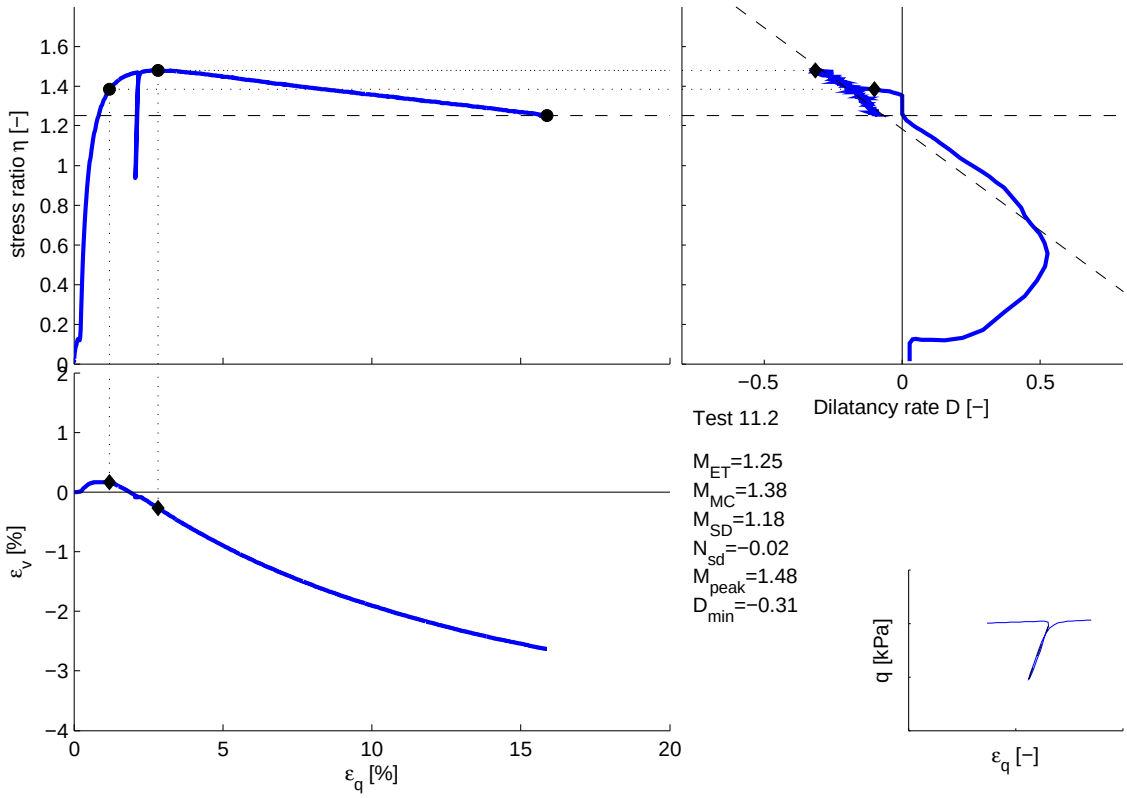
stress ratio η [–]
Dilatancy rate D [–]
Test 11.2
M_{ET}=1.25
M_{MC}=1.38
M_{SD}=1.18
N_{sd}=−0.02
M_{peak}=1.48
D_{min}=−0.31
q [kPa]
ε_q [–]
ε_v [%]
ε_q [%]

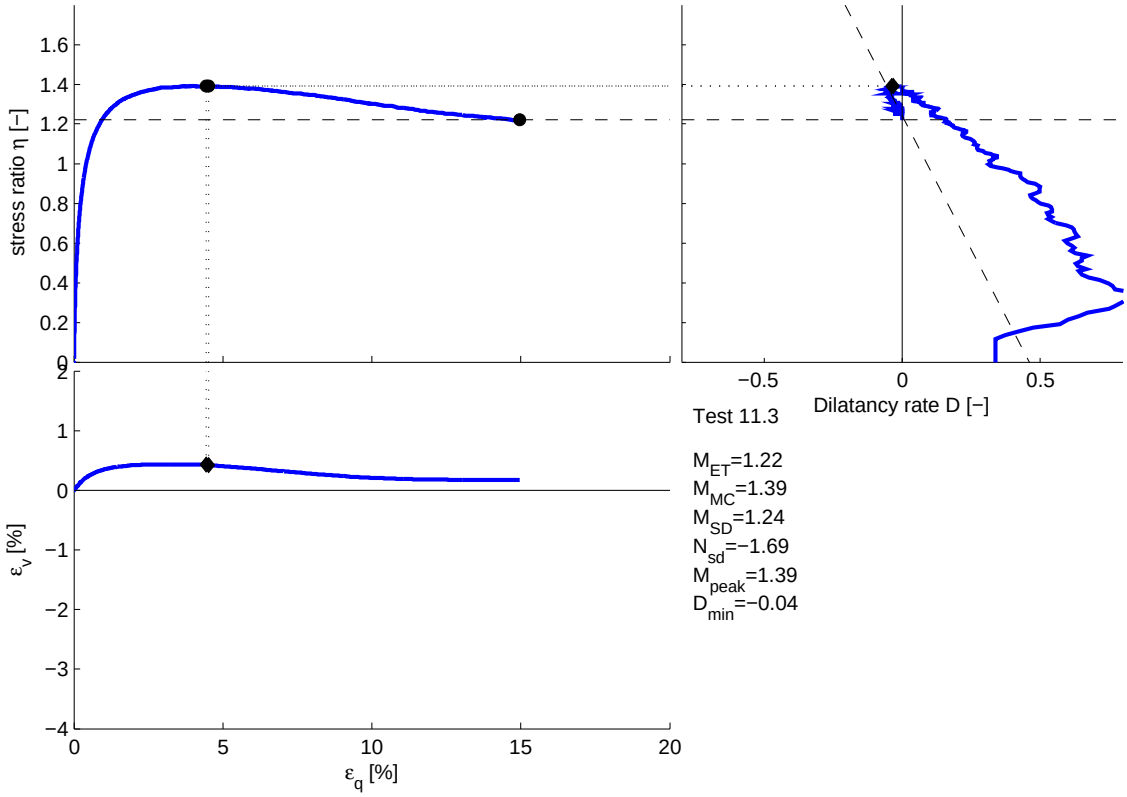
stress ratio η [–]
Dilatancy rate D [–]
Test 11.3
M_ET=1.22
M_MC=1.39
M_SD=1.24
N_sd=−1.69
M_peak=1.39
D_min=−0.04
ε_v [%]
ε_q [%]

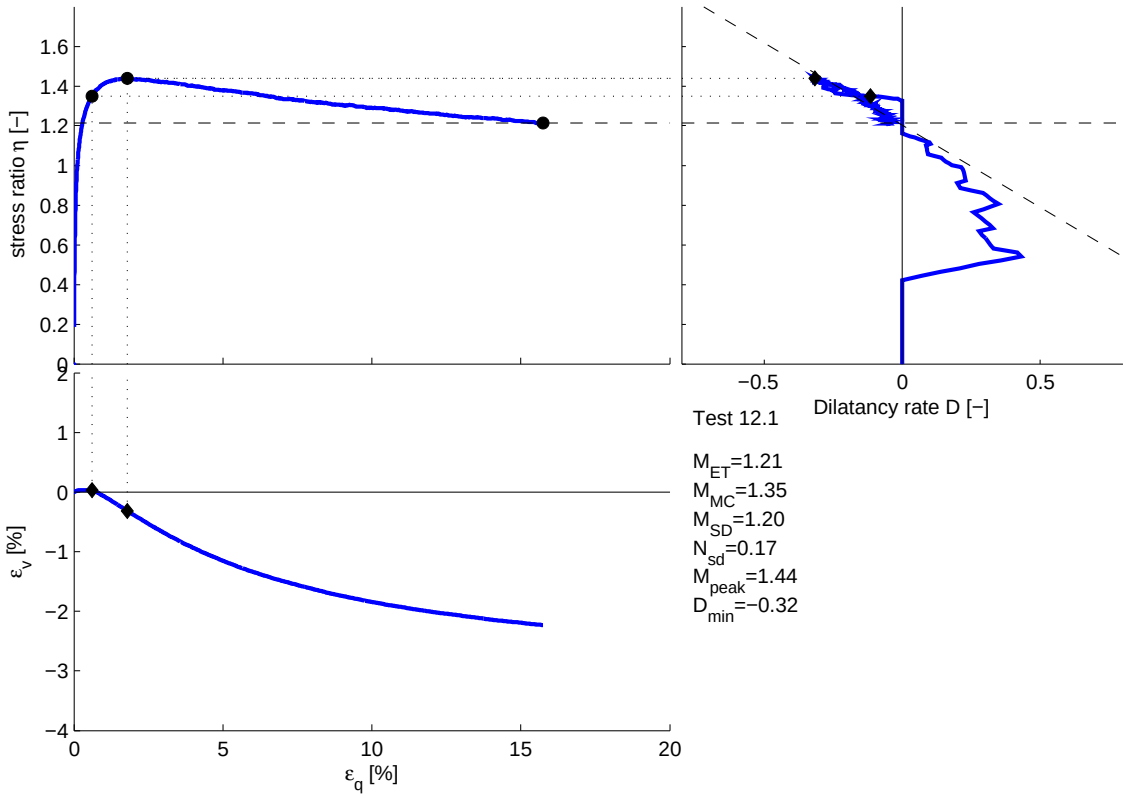
stress ratio η [–]
Dilatancy rate D [–]
Test 12.1
M_ET=1.21
M_MC=1.35
M_SD=1.20
N_sd=0.17
M_peak=1.44
D_min=−0.32
ε_v [%]
ε_q [%]

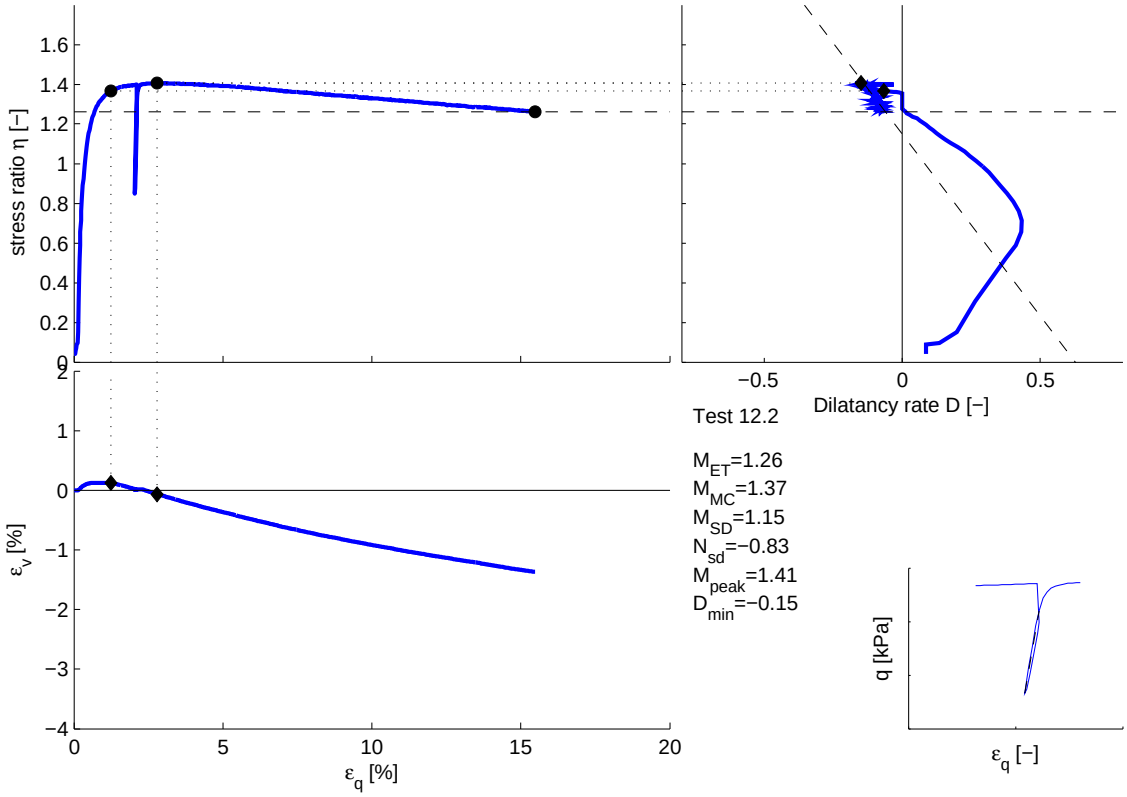
stress ratio η [−]
Dilatancy rate D [−]
Test 12.2
M_{ET}=1.26
M_{MC}=1.37
M_{SD}=1.15
N_{sd}=−0.83
M_{peak}=1.41
D_{min}=−0.15
ε_v [%]
ε_q [%]
q [kPa]
ε_q [−]

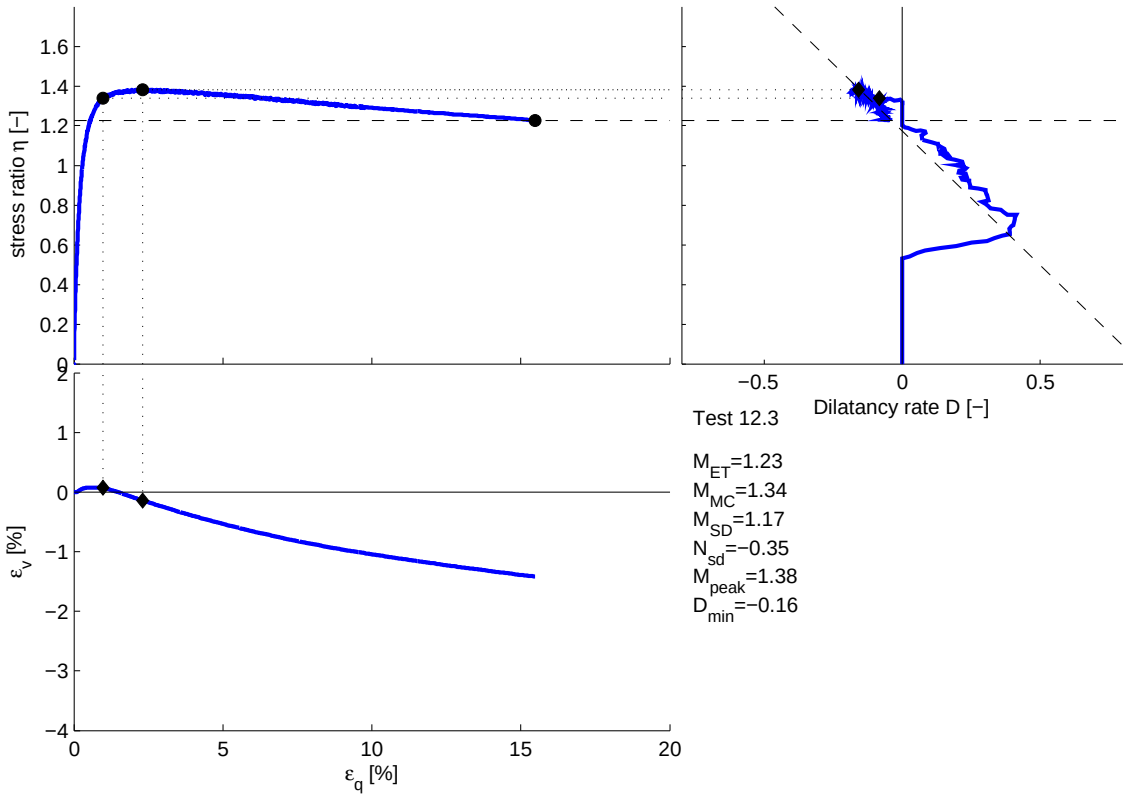
stress ratio η [−]
Dilatancy rate D [−]
Test 12.3
M_{ET}=1.23
M_{MC}=1.34
M_{SD}=1.17
N_{sd}=−0.35
M_{peak}=1.38
D_{min}=−0.16
ε_v [%]
ε_q [%]

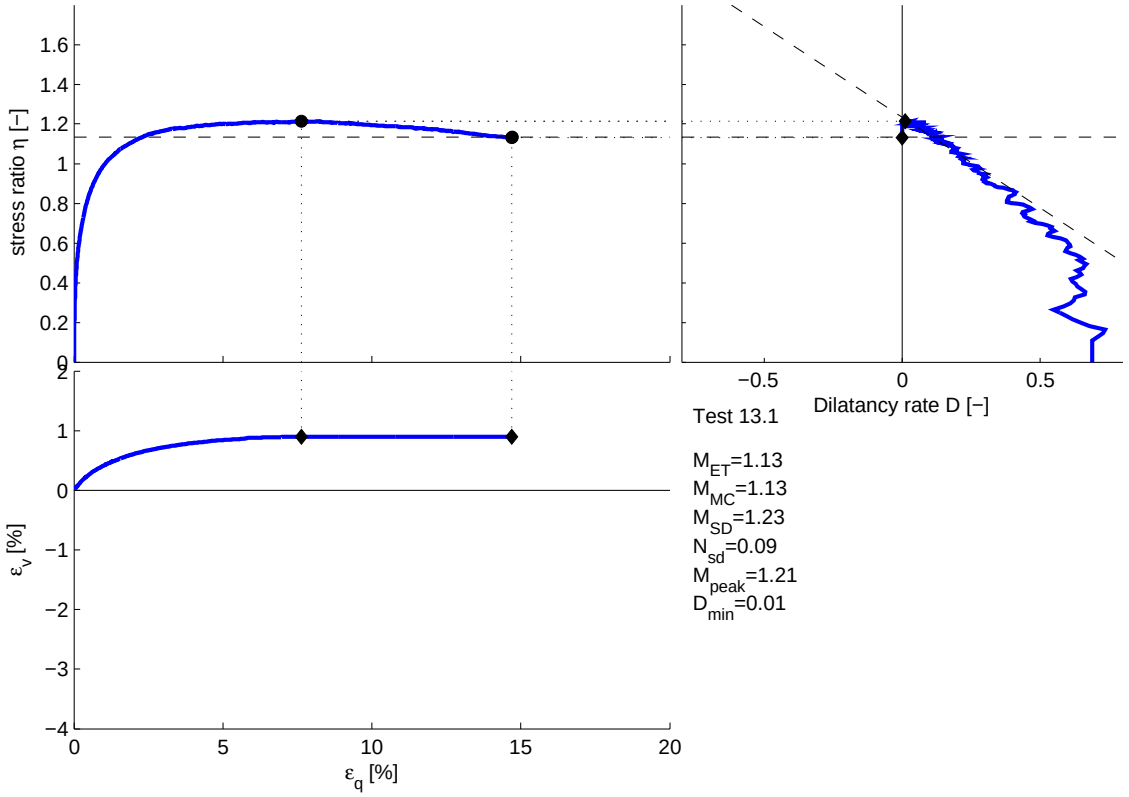
stress ratio η [–]
Dilatancy rate D [–]
Test 13.1
M_{ET}=1.13
M_{MC}=1.13
M_{SD}=1.23
N_{sd}=0.09
M_{peak}=1.21
D_{min}=0.01
ε_v [%]
ε_q [%]

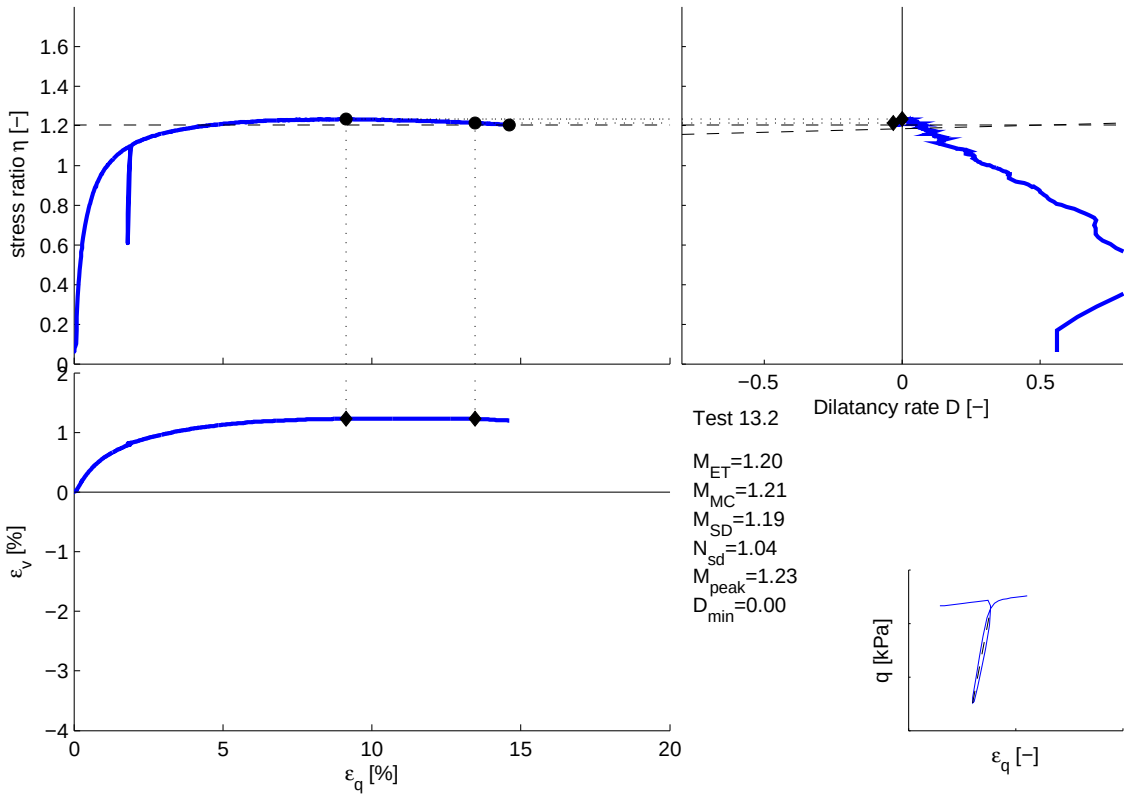
stress ratio η [–]
Dilatancy rate D [–]
Test 13.2
M_{ET}=1.20
M_{MC}=1.21
M_{SD}=1.19
N_{sd}=1.04
M_{peak}=1.23
D_{min}=0.00
q [kPa]
ε_q [–]
ε_v [%]
ε_q [%]

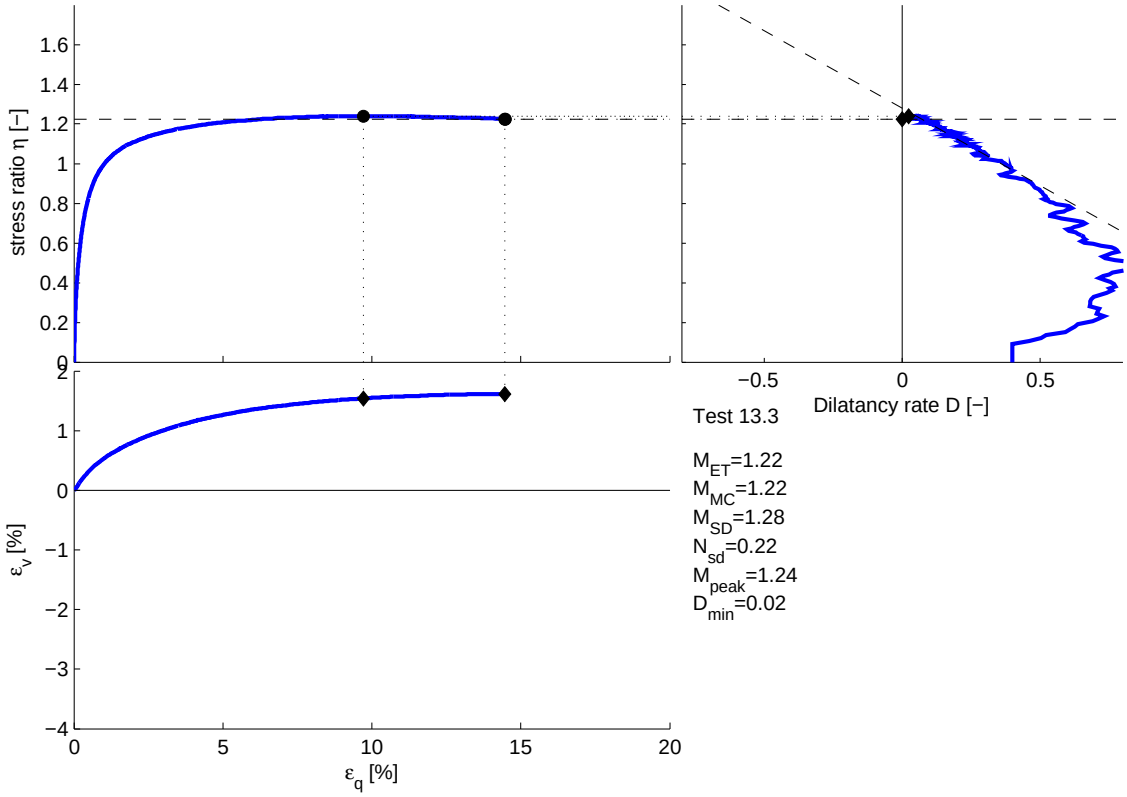
stress ratio η [–]
Dilatancy rate D [–]
Test 13.3
M_{ET}=1.22
M_{MC}=1.22
M_{SD}=1.28
N_{sd}=0.22
M_{peak}=1.24
D_{min}=0.02
ε_v [%]
ε_q [%]

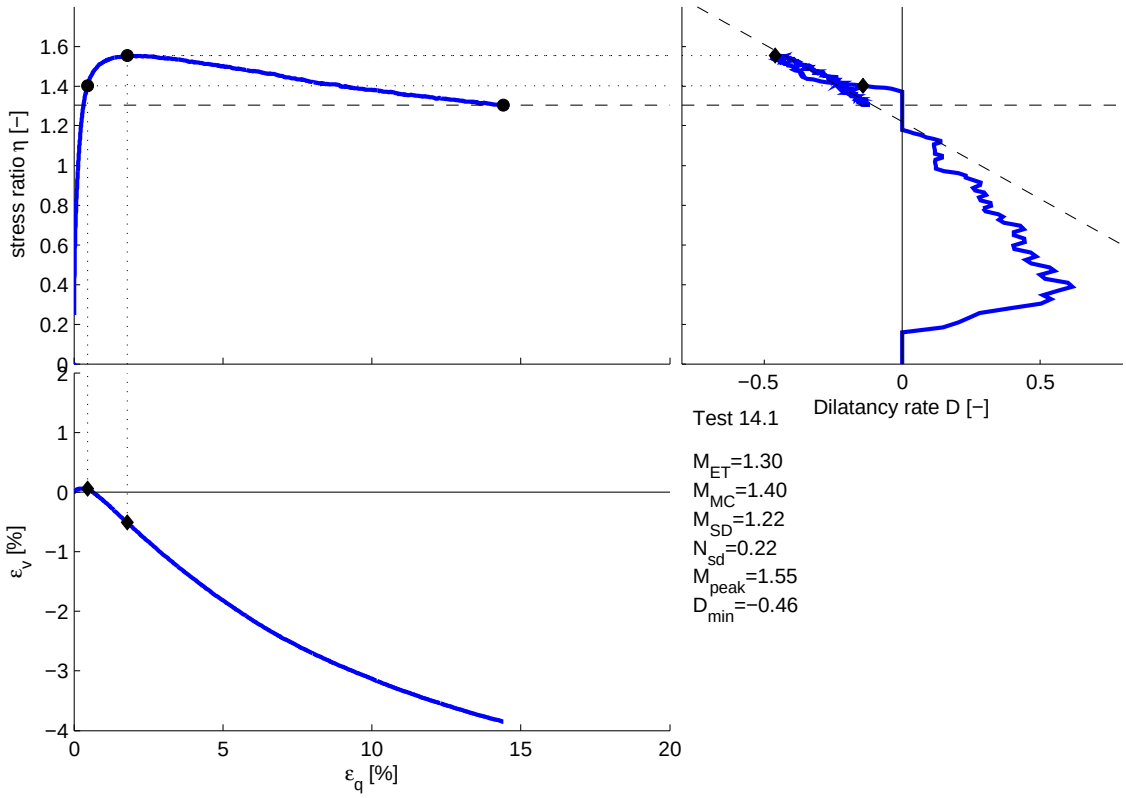
stress ratio η [–]
Dilatancy rate D [–]
Test 14.1
M_{ET}=1.30
M_{MC}=1.40
M_{SD}=1.22
N_{sd}=0.22
M_{peak}=1.55
D_{min}=−0.46
ε_v [%]
ε_q [%]

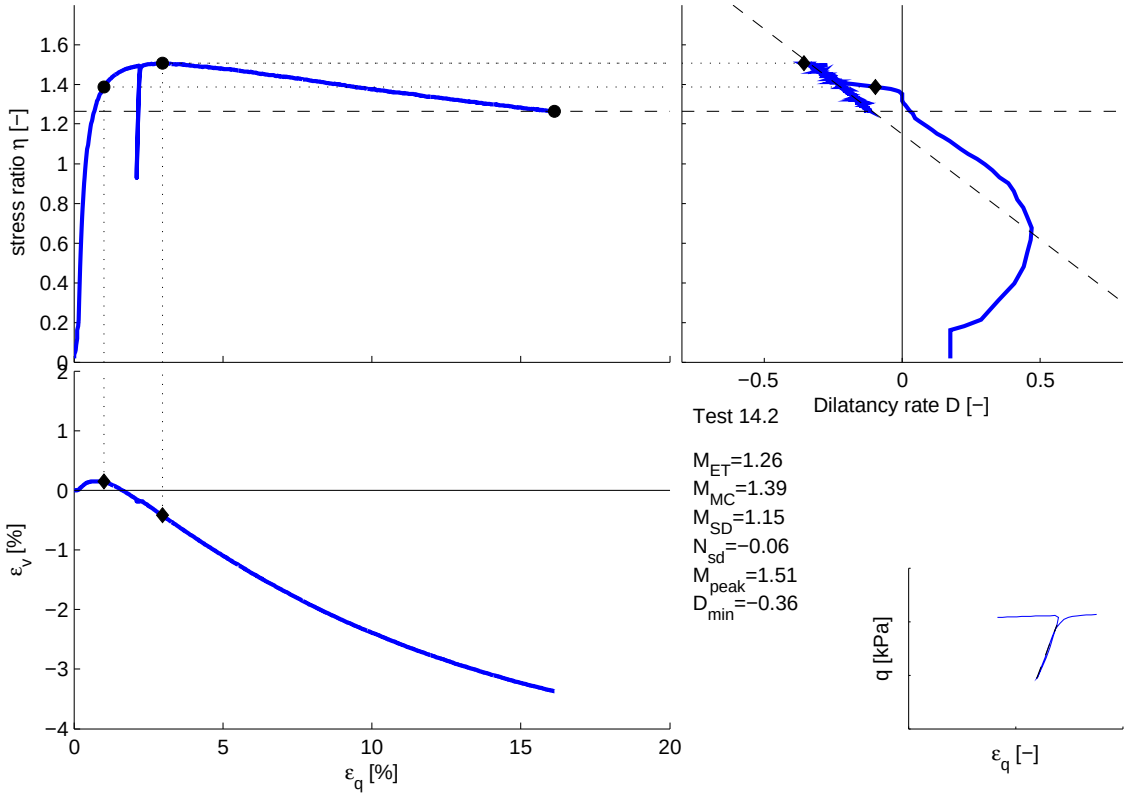
stress ratio η [–]
Dilatancy rate D [–]
Test 14.2
M_{ET}=1.26
M_{MC}=1.39
M_{SD}=1.15
N_{sd}=−0.06
M_{peak}=1.51
D_{min}=−0.36
ε_v [%]
ε_q [%]
q [kPa]
ε_q [–]

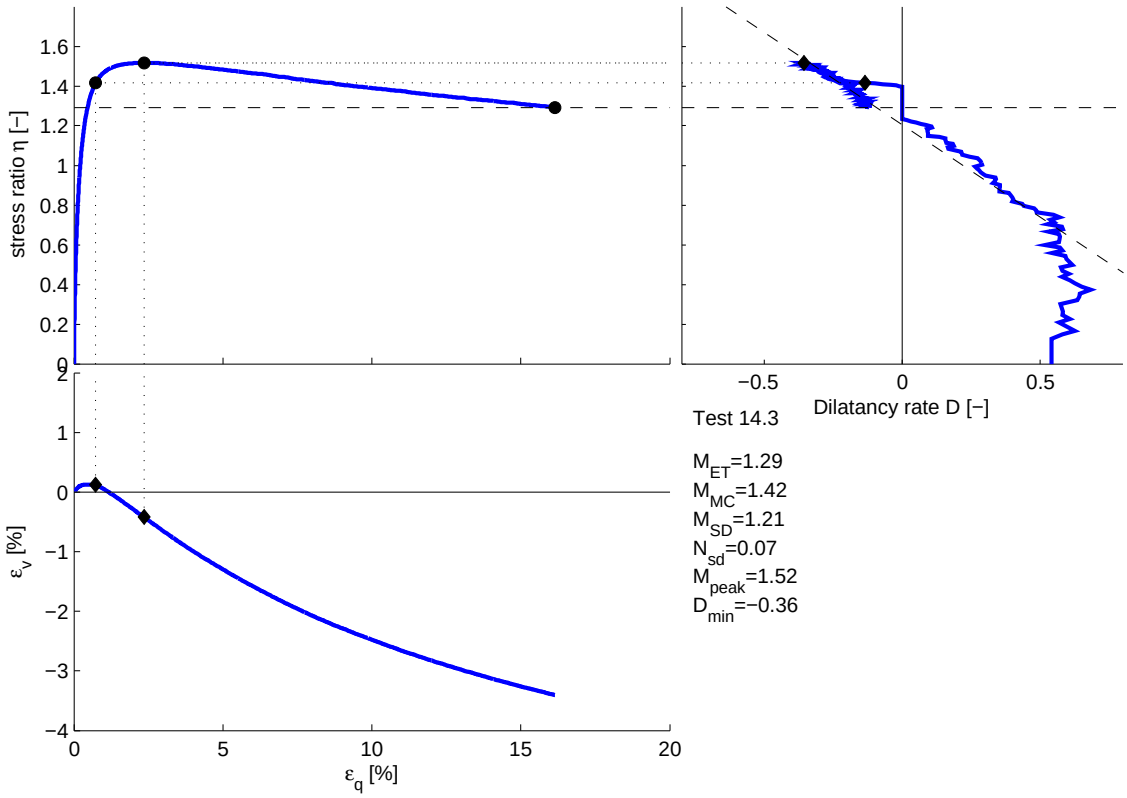
stress ratio η [–]
Dilatancy rate D [–]
Test 14.3
M_{ET}=1.29
M_{MC}=1.42
M_{SD}=1.21
N_{sd}=0.07
M_{peak}=1.52
D_{min}=−0.36
ε_v [%]
ε_q [%]

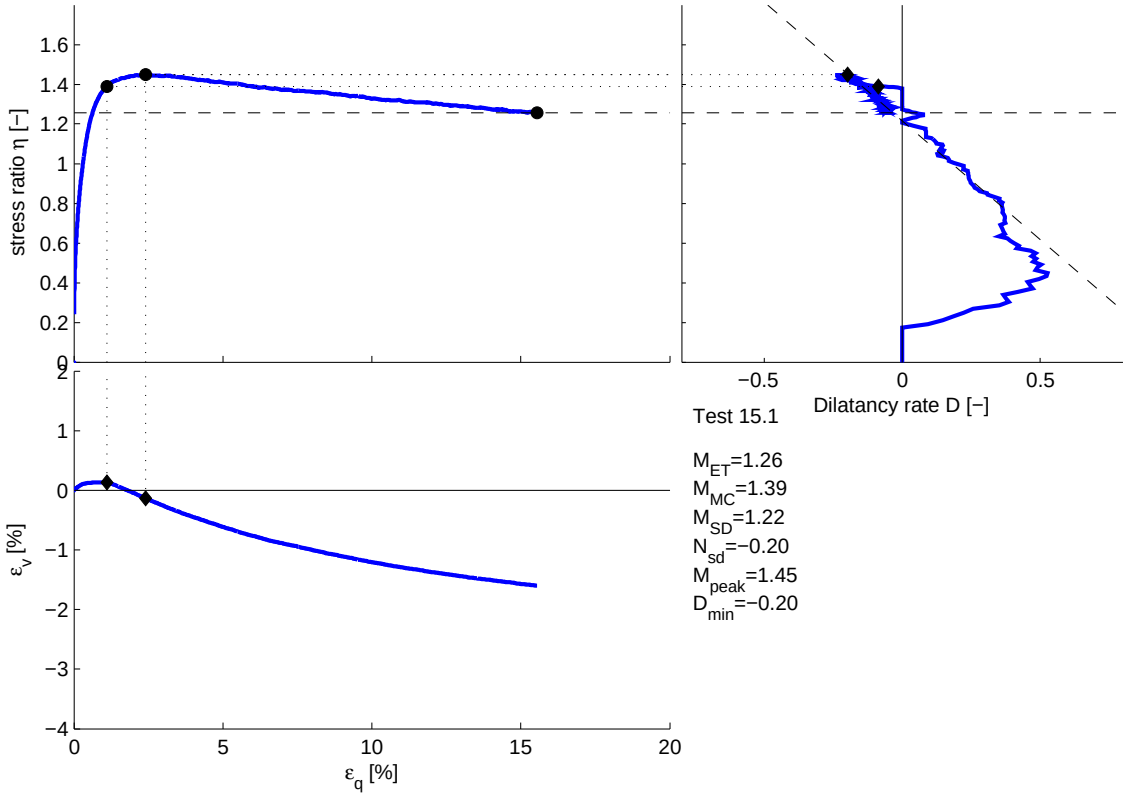
stress ratio η [–]
Dilatancy rate D [–]
Test 15.1
M_{ET}=1.26
M_{MC}=1.39
M_{SD}=1.22
N_{sd}=−0.20
M_{peak}=1.45
D_{min}=−0.20
ε_v [%]
ε_q [%]

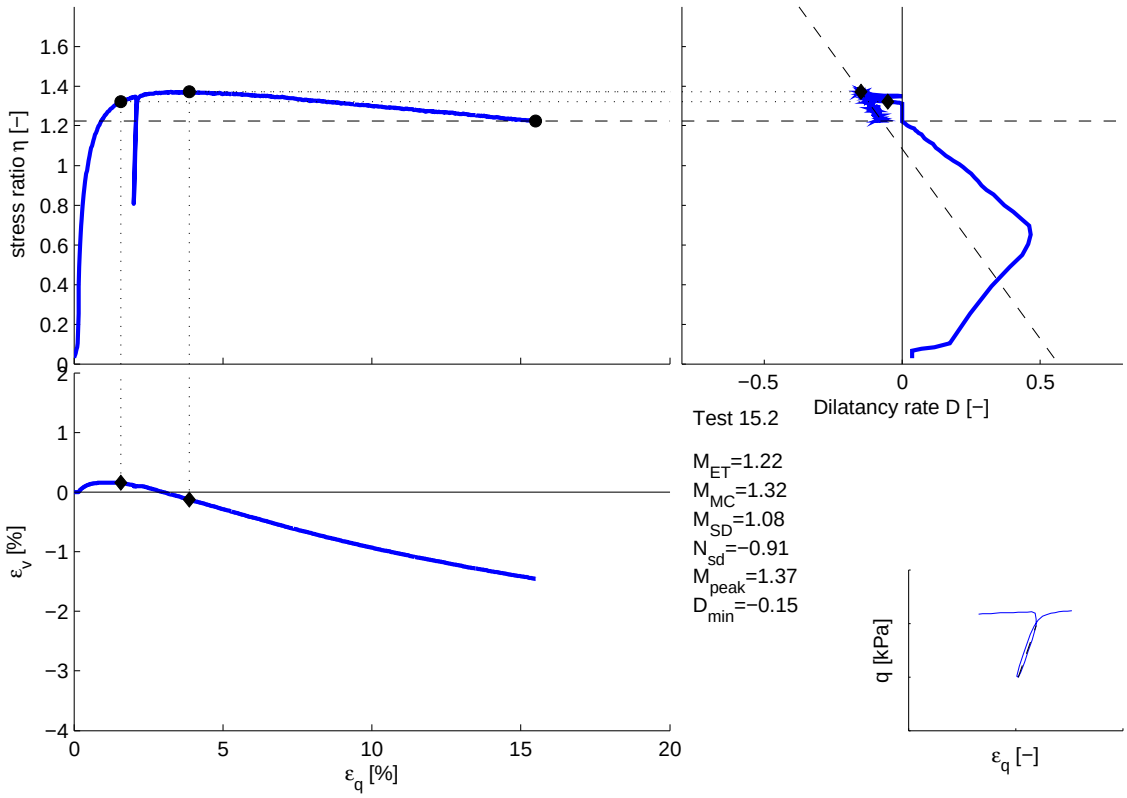
stress ratio η [–]
Dilatancy rate D [–]
Test 15.2
M_{ET}=1.22
M_{MC}=1.32
M_{SD}=1.08
N_{sd}=−0.91
M_{peak}=1.37
D_{min}=−0.15
q [kPa]
ε_q [–]
ε_v [%]
ε_q [%]

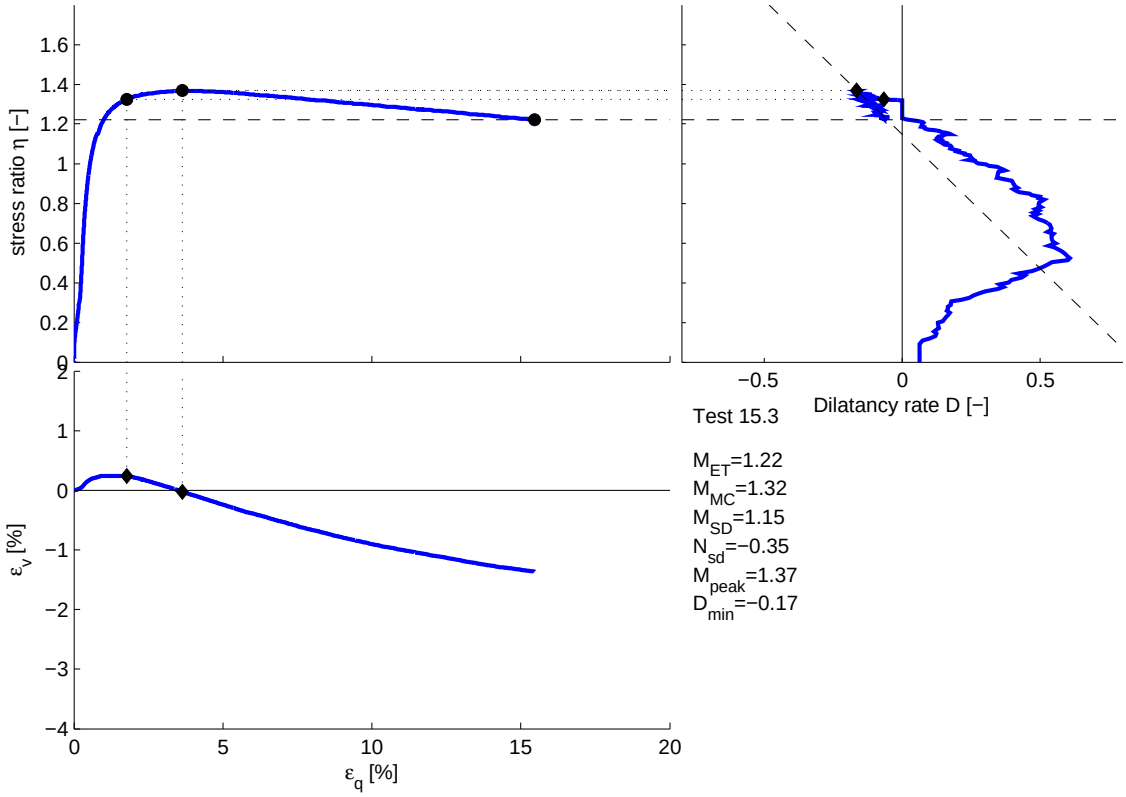
stress ratio η [–]
1.6
1.4
1.2
1
0.8
0.6
0.4
0.2
0
−0.5
0
0.5
Dilatancy rate D [–]
Test 15.3
M_ET=1.22
M_MC=1.32
M_SD=1.15
N_sd=−0.35
M_peak=1.37
D_min=−0.17
ε_v [%]
2
1
0
−1
−2
−3
−4
0
5
10
15
20
ε_q [%]

D.2 Calibration of H:

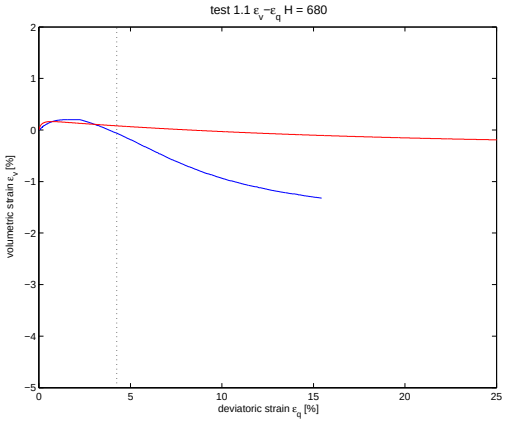

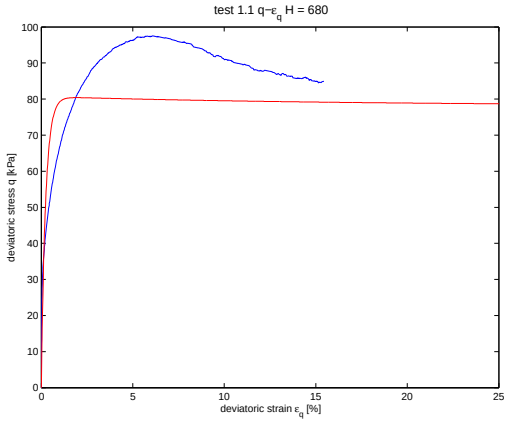

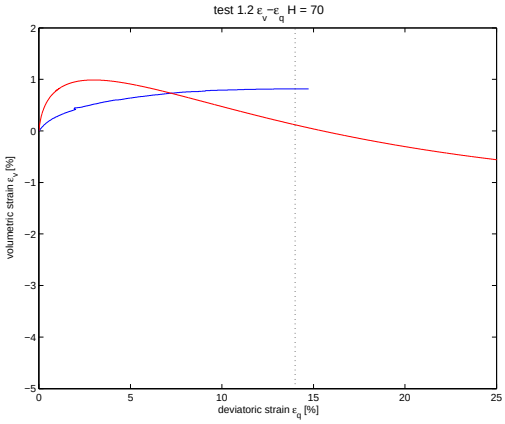

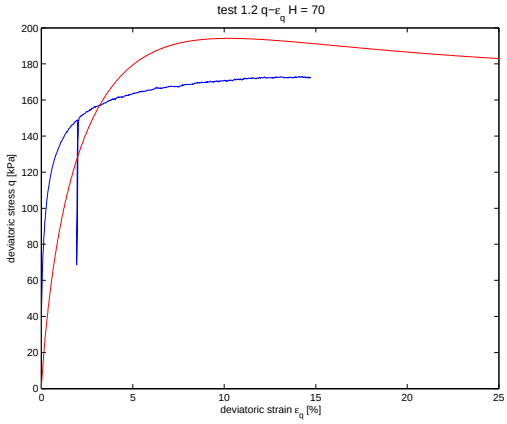

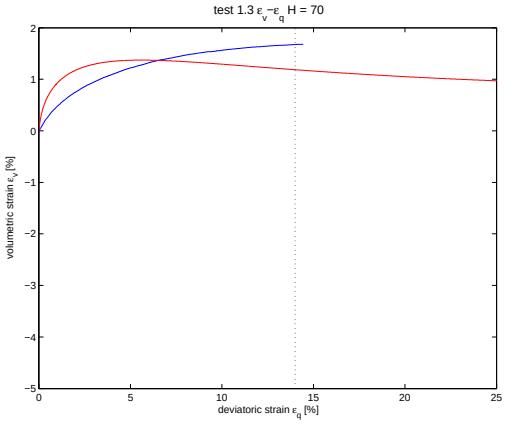

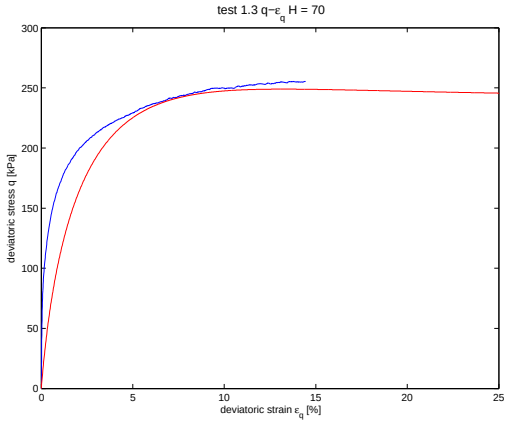

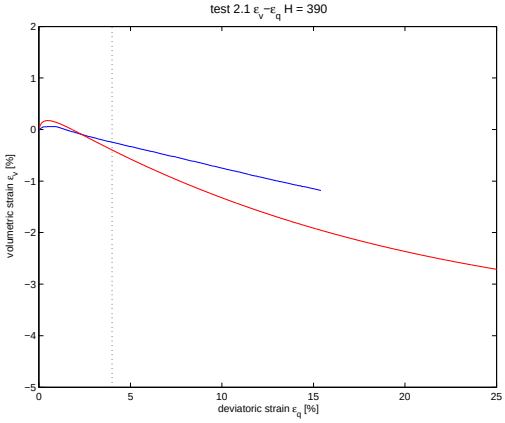
test 2.1 ε_v–ε_q H = 390
volumetric strain ε_v [%]
deviatoric strain ε_q [%]

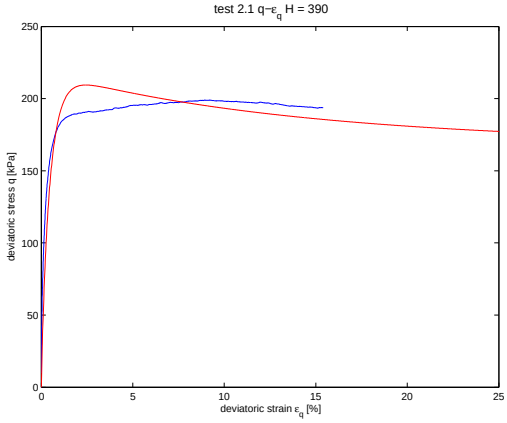
test 2.1 q–ε_q H = 390
deviatoric stress q [kPa]
deviatoric strain ε_q [%]

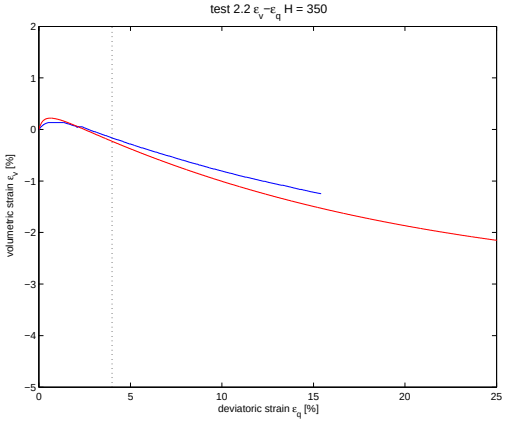
test 2.2 ε_v–ε_q H = 350
volumetric strain ε_v [%]
deviatoric strain ε_q [%]

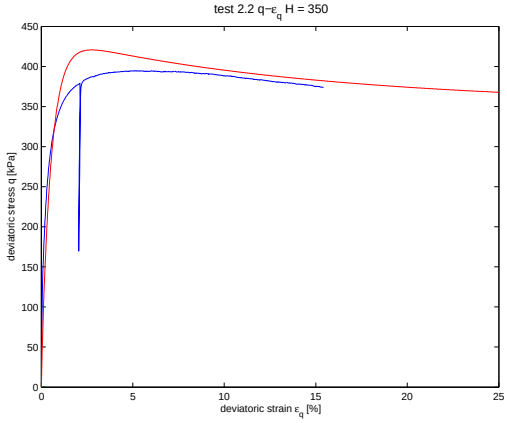
test 2.2 q–ε_q H = 350
deviatoric stress q [kPa]
deviatoric strain ε_q [%]

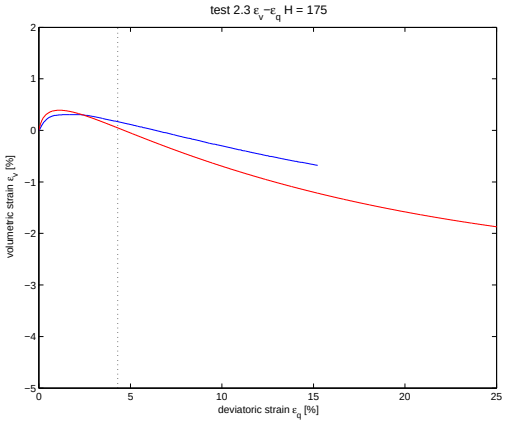
test 2.3 ε_v–ε_q H = 175
volumetric strain ε_v [%]
deviatoric strain ε_q [%]

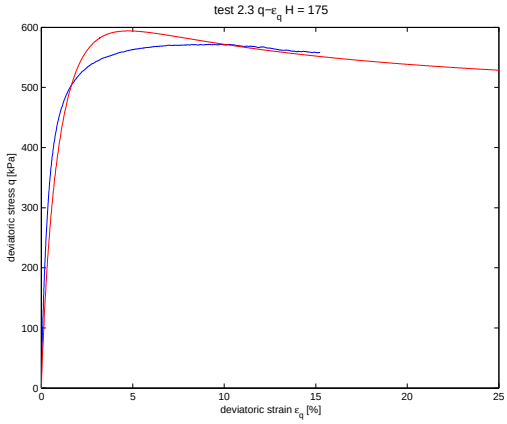
test 2.3 q–ε_q H = 175
deviatoric stress q [kPa]
deviatoric strain ε_q [%]

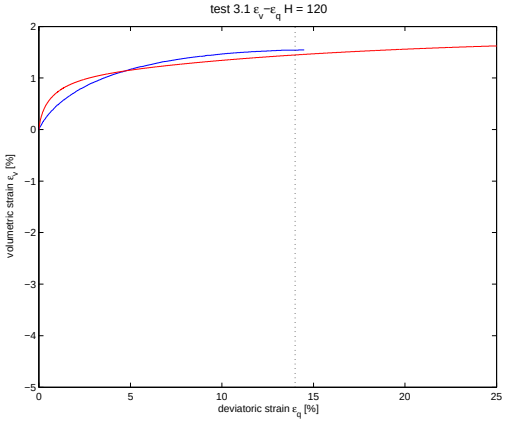
test 3.1 ε_v−ε_q H = 120
volumetric strain ε_v [%]
deviatoric strain ε_q [%]

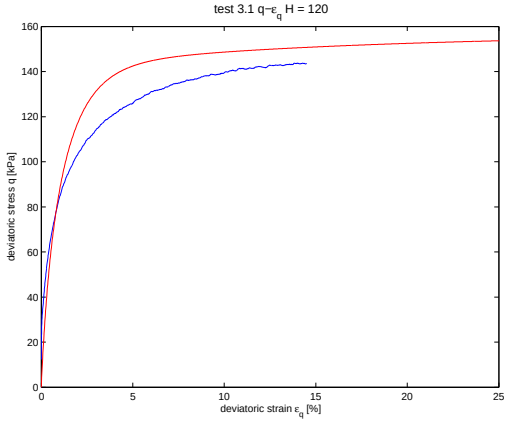
test 3.1 q−ε_q H = 120
deviatoric stress q [kPa]
deviatoric strain ε_q [%]

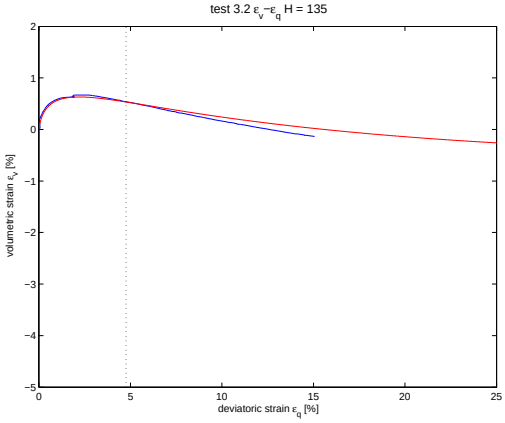
test 3.2 ε_v−ε_q H = 135
volumetric strain ε_v [%]
deviatoric strain ε_q [%]

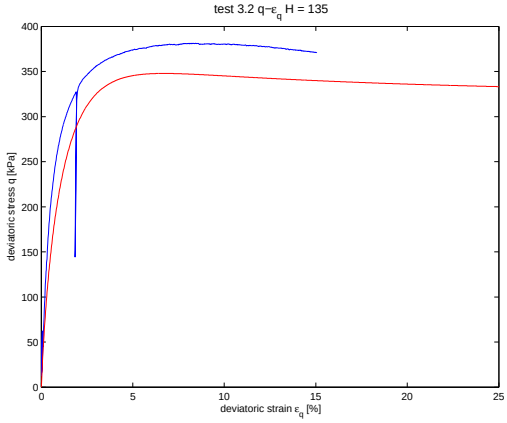
test 3.2 q−ε_q H = 135
deviatoric stress q [kPa]
deviatoric strain ε_q [%]

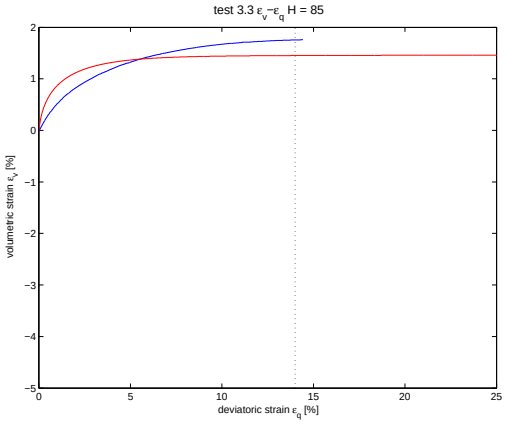
test 3.3 ε_v−ε_q H = 85
volumetric strain ε_v [%]
deviatoric strain ε_q [%]

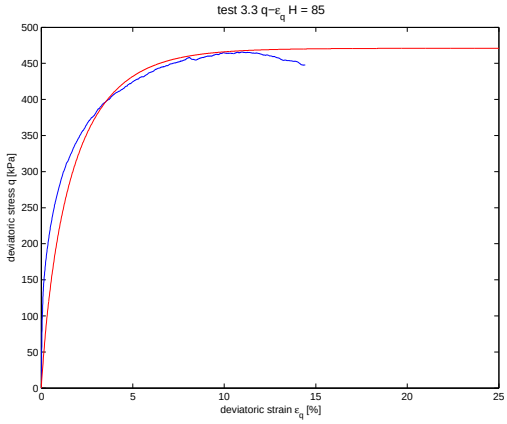
test 3.3 q−ε_q H = 85
deviatoric stress q [kPa]
deviatoric strain ε_q [%]

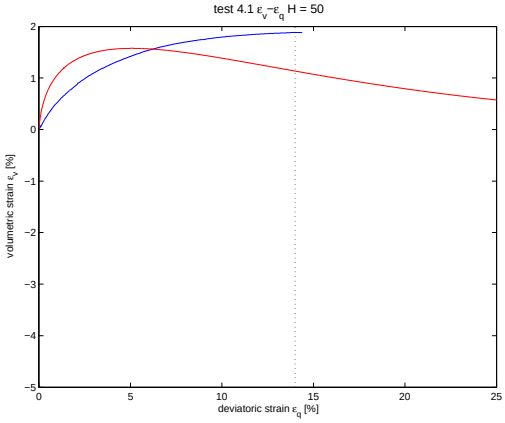
test 4.1 ε_v−ε_q H = 50
volumetric strain ε_v [%]
deviatoric strain ε_q [%]

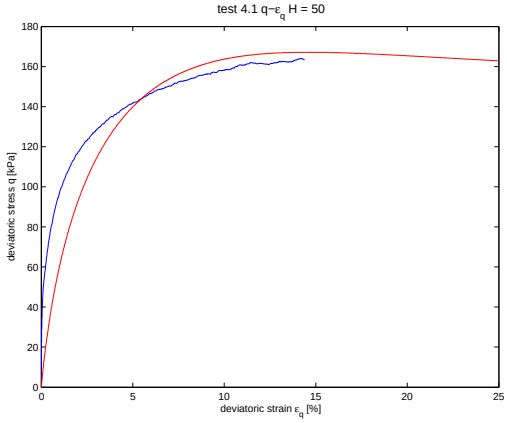
test 4.1 q−ε_q H = 50
deviatoric stress q [kPa]
deviatoric strain ε_q [%]

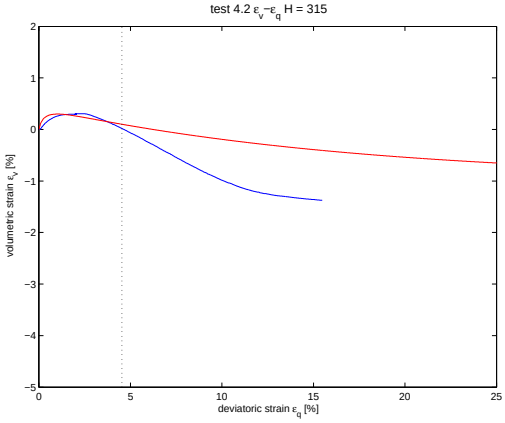
test 4.2 ε_v−ε_q H = 315
volumetric strain ε_v [%]
deviatoric strain ε_q [%]

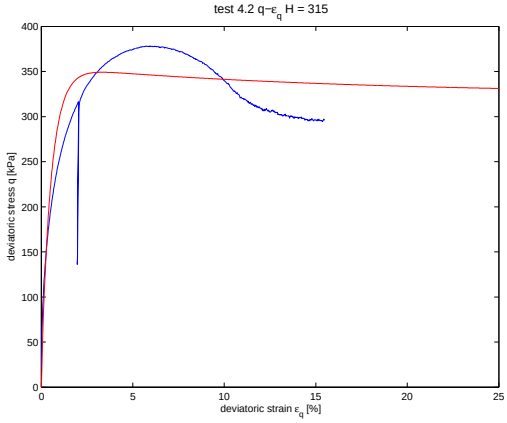
test 4.2 q−ε_q H = 315
deviatoric stress q [kPa]
deviatoric strain ε_q [%]

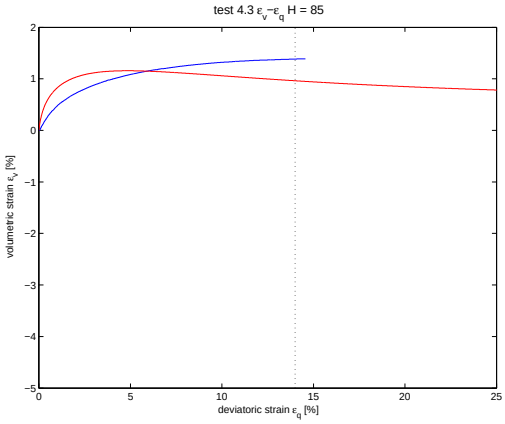
test 4.3 ε_v−ε_q H = 85
volumetric strain ε_v [%]
deviatoric strain ε_q [%]

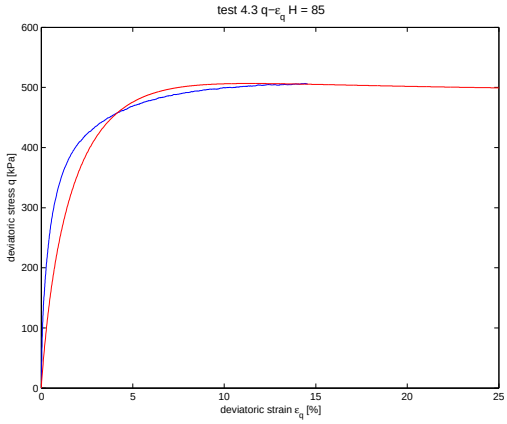
test 4.3 q−ε_q H = 85
deviatoric stress q [kPa]
deviatoric strain ε_q [%]

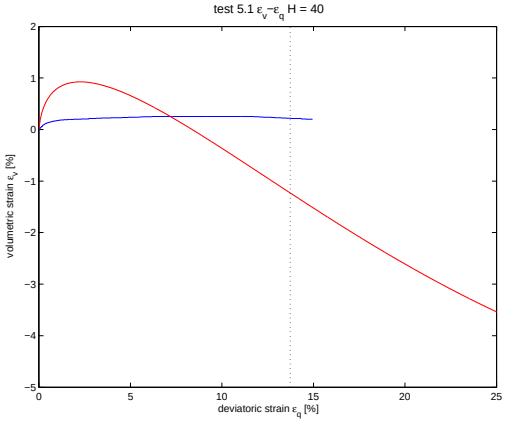
test 5.1 ε_v−ε_q H = 40
volumetric strain ε_v [%]
deviatoric strain ε_q [%]

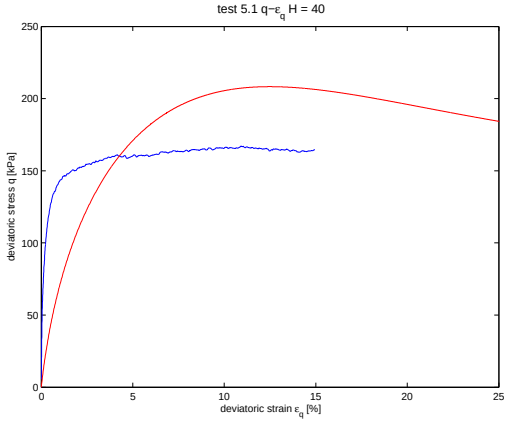
test 5.1 q−ε_q H = 40
deviatoric stress q [kPa]
deviatoric strain ε_q [%]

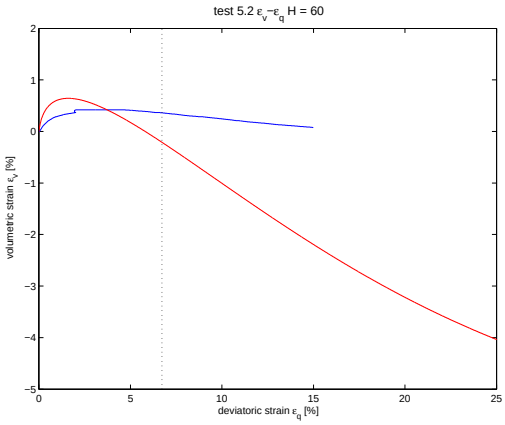
test 5.2 ε_v−ε_q H = 60
volumetric strain ε_v [%]
deviatoric strain ε_q [%]

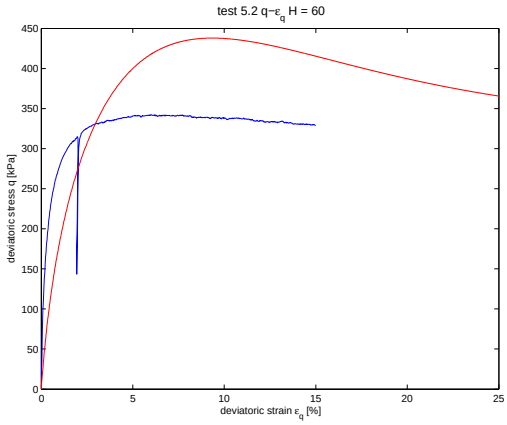
test 5.2 q−ε_q H = 60
deviatoric stress q [kPa]
deviatoric strain ε_q [%]

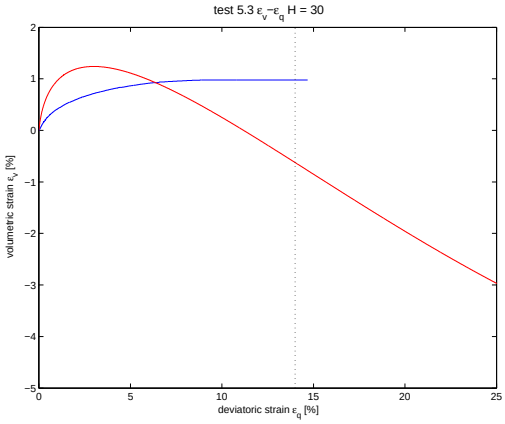
test 5.3 ε_v−ε_q H = 30
volumetric strain ε_v [%]
deviatoric strain ε_q [%]

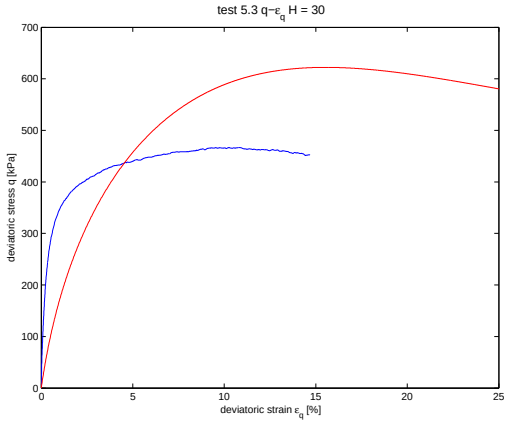
test 5.3 q−ε_q H = 30
deviatoric stress q [kPa]
deviatoric strain ε_q [%]

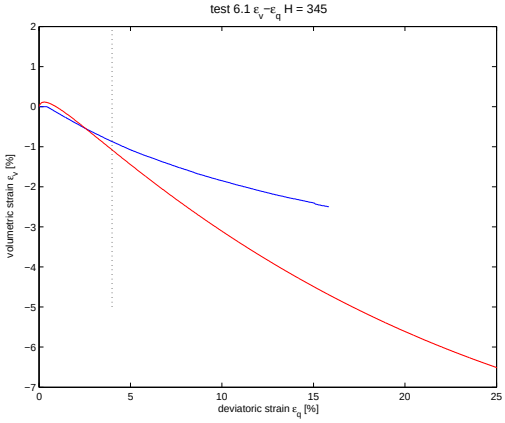
test 6.1 ε_v–ε_q H = 345
volumetric strain ε_v [%]
deviatoric strain ε_q [%]

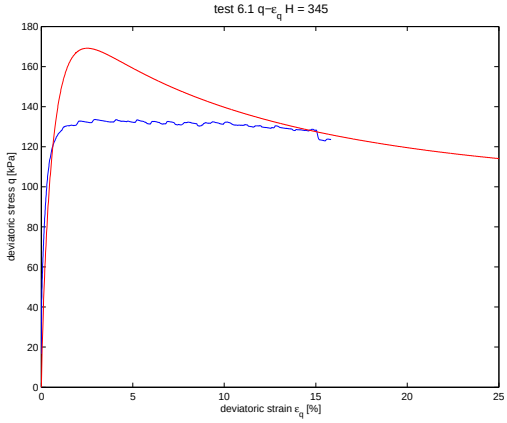
test 6.1 q–ε_q H = 345
deviatoric stress q [kPa]
deviatoric strain ε_q [%]

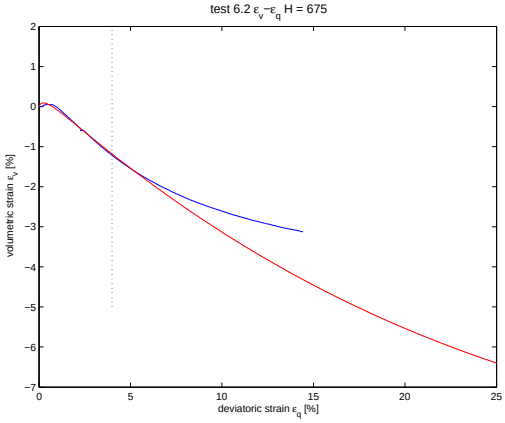
test 6.2 ε_v–ε_q H = 675
volumetric strain ε_v [%]
deviatoric strain ε_q [%]

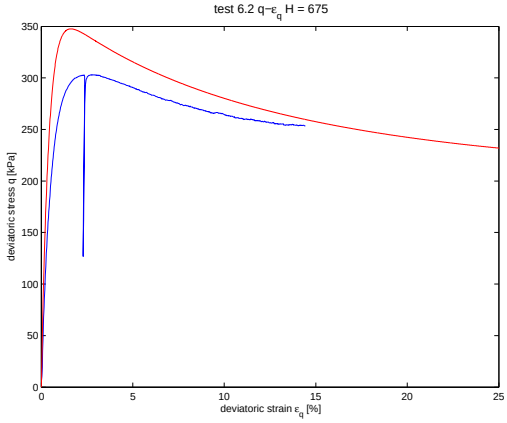
test 6.2 q–ε_q H = 675
deviatoric stress q [kPa]
deviatoric strain ε_q [%]

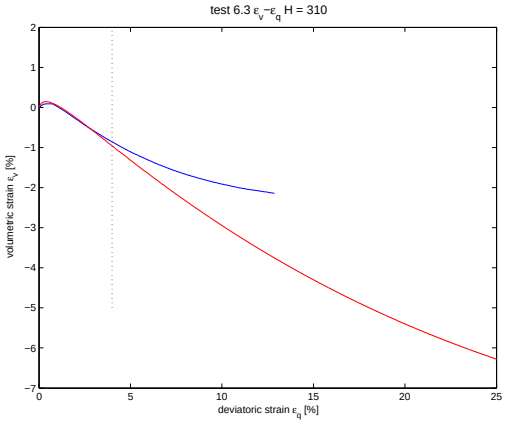
test 6.3 ε_v–ε_q H = 310
volumetric strain ε_v [%]
deviatoric strain ε_q [%]

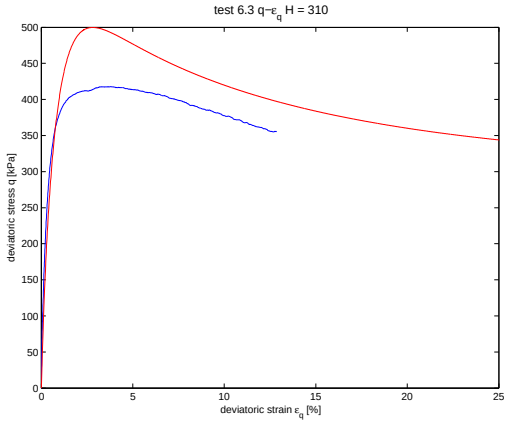
test 6.3 q–ε_q H = 310
deviatoric stress q [kPa]
deviatoric strain ε_q [%]

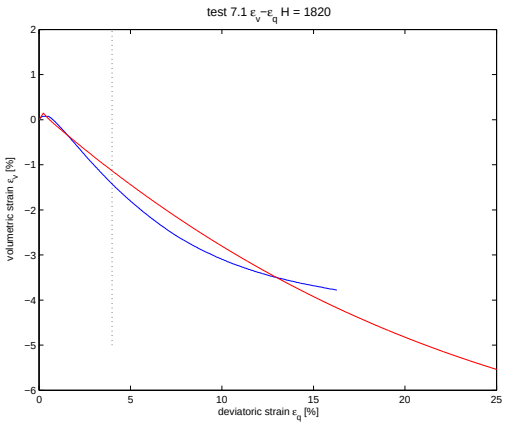
test 7.1 ε_v−ε_q H = 1820
volumetric strain ε_v [%]
deviatoric strain ε_q [%]

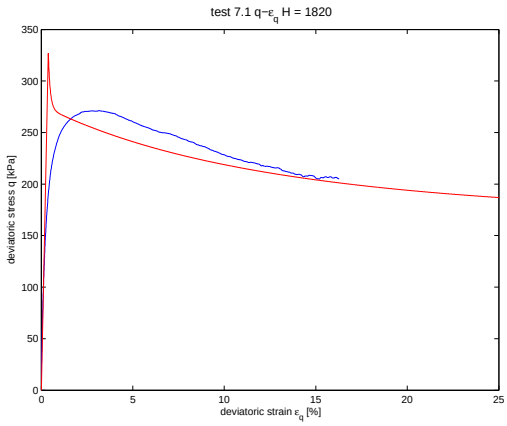
test 7.1 q−ε_q H = 1820
deviatoric stress q [kPa]
deviatoric strain ε_q [%]

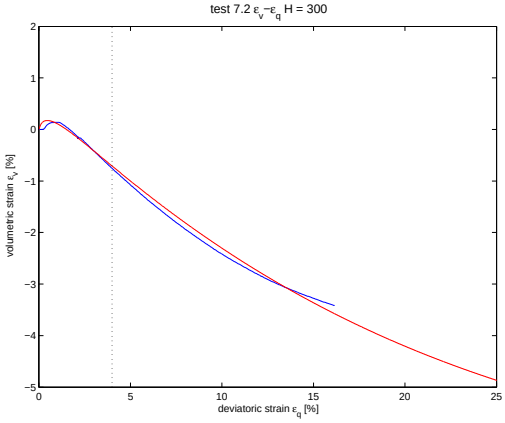
test 7.2 ε_v−ε_q H = 300
volumetric strain ε_v [%]
deviatoric strain ε_q [%]

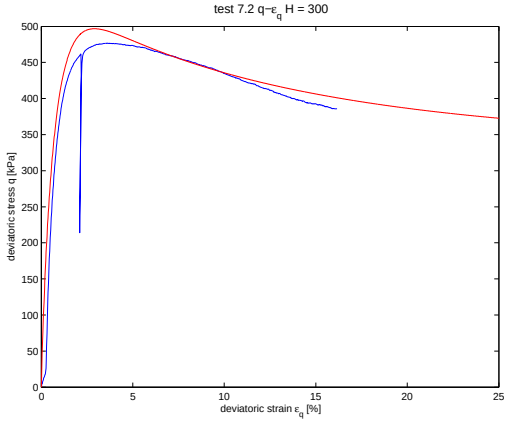
test 7.2 q−ε_q H = 300
deviatoric stress q [kPa]
deviatoric strain ε_q [%]

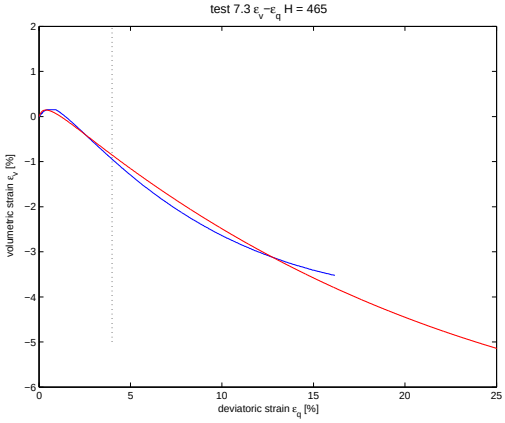
test 7.3 ε_v−ε_q H = 465
volumetric strain ε_v [%]
deviatoric strain ε_q [%]

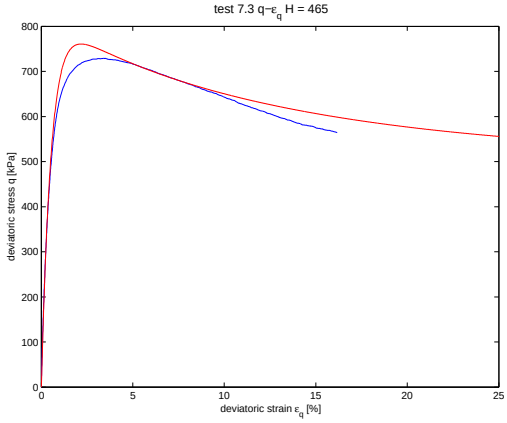
test 7.3 q−ε_q H = 465
deviatoric stress q [kPa]
deviatoric strain ε_q [%]

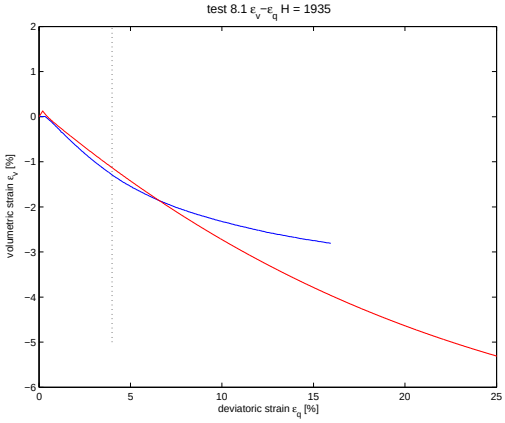
test 8.1 ε_v−ε_q H = 1935
volumetric strain ε_v [%]
deviatoric strain ε_q [%]

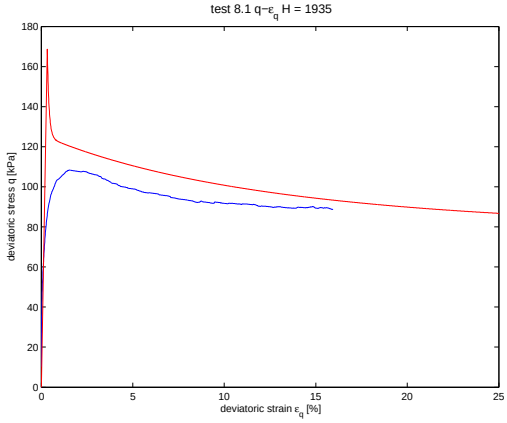
test 8.1 q−ε_q H = 1935
deviatoric stress q [kPa]
deviatoric strain ε_q [%]

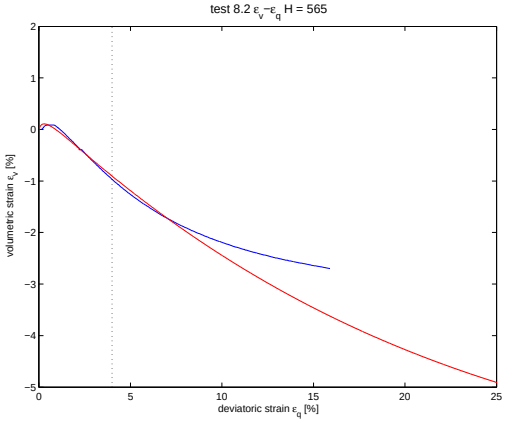
test 8.2 ε_v−ε_q H = 565
volumetric strain ε_v [%]
deviatoric strain ε_q [%]

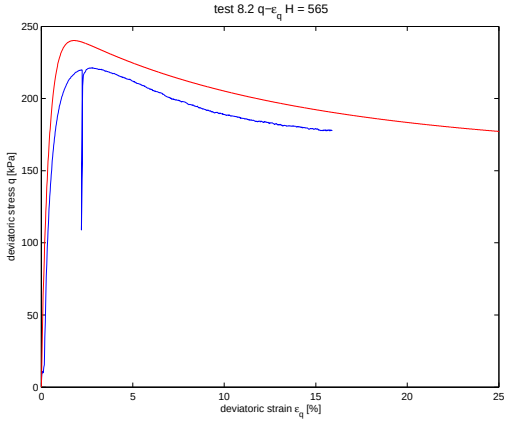
test 8.2 q−ε_q H = 565
deviatoric stress q [kPa]
deviatoric strain ε_q [%]

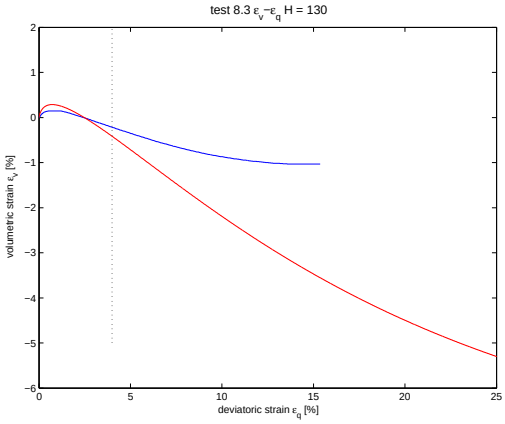
test 8.3 ε_v−ε_q H = 130
volumetric strain ε_v [%]
deviatoric strain ε_q [%]

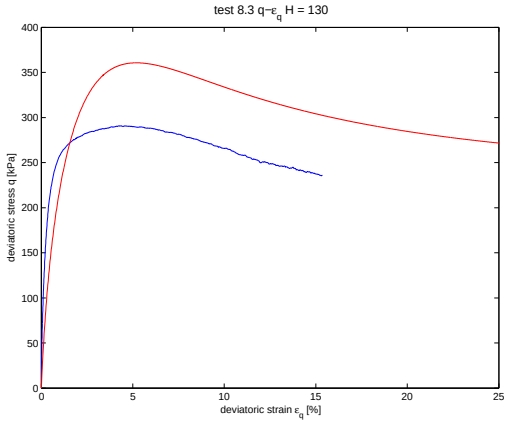
test 8.3 q−ε_q H = 130
deviatoric stress q [kPa]
deviatoric strain ε_q [%]

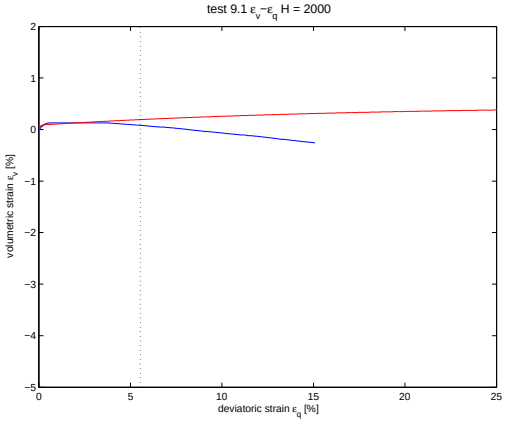
test 9.1 ε_v−ε_q H = 2000
volumetric strain ε_v [%]
deviatoric strain ε_q [%]

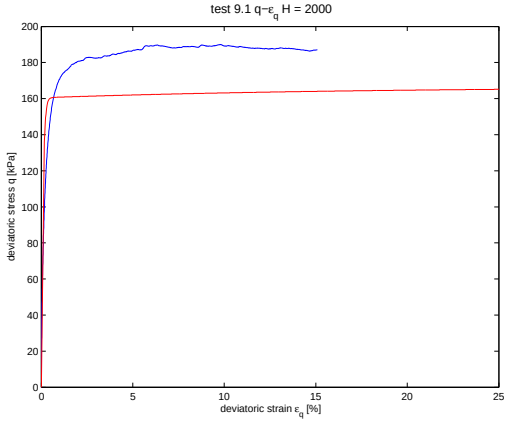
test 9.1 q−ε_q H = 2000
deviatoric stress q [kPa]
deviatoric strain ε_q [%]

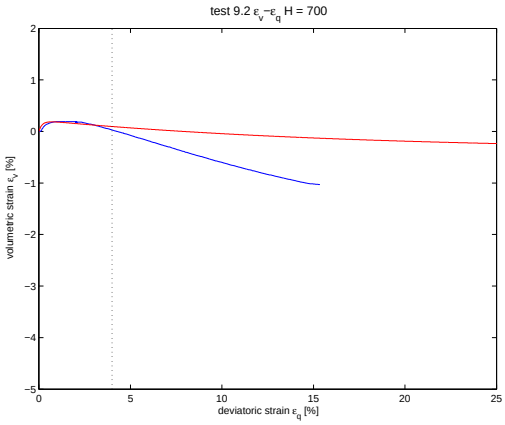
test 9.2 ε_v−ε_q H = 700
volumetric strain ε_v [%]
deviatoric strain ε_q [%]

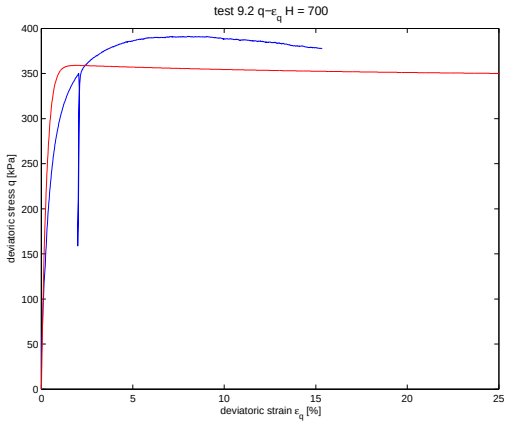
test 9.2 q−ε_q H = 700
deviatoric stress q [kPa]
deviatoric strain ε_q [%]

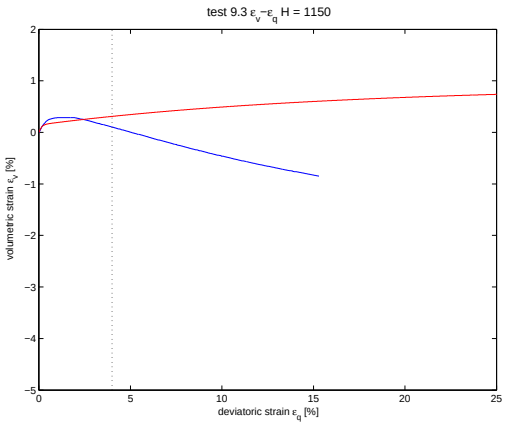
test 9.3 ε_v−ε_q H = 1150
volumetric strain ε_v [%]
deviatoric strain ε_q [%]

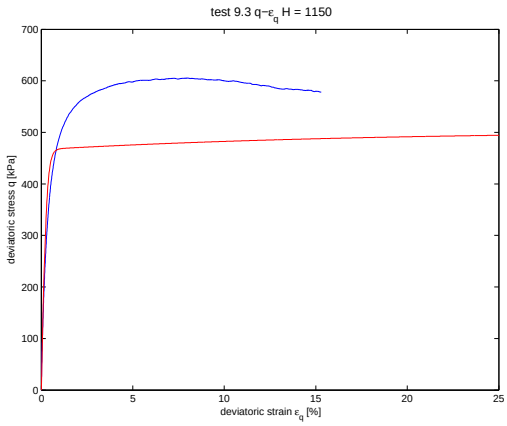
test 9.3 q−ε_q H = 1150
deviatoric stress q [kPa]
deviatoric strain ε_q [%]

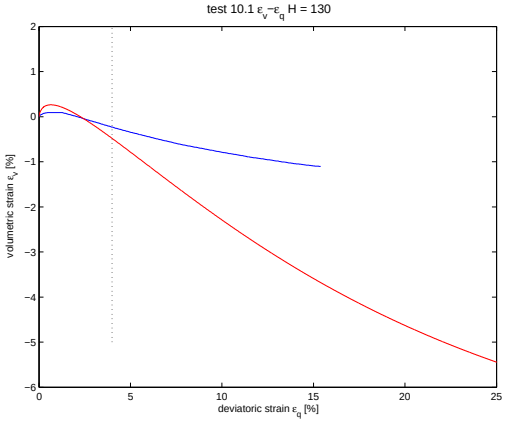
test 10.1 ε_v−ε_q H = 130
volumetric strain ε_v [%]
deviatoric strain ε_q [%]

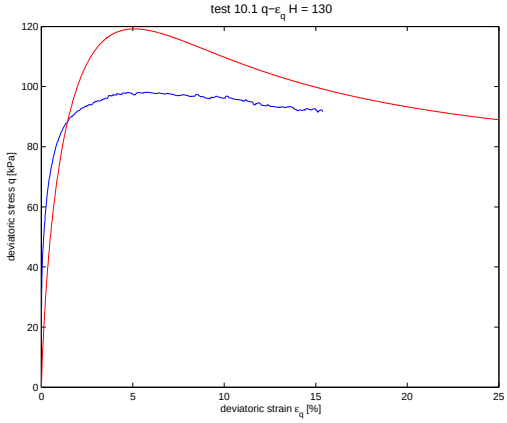
test 10.1 q−ε_q H = 130
deviatoric stress q [kPa]
deviatoric strain ε_q [%]

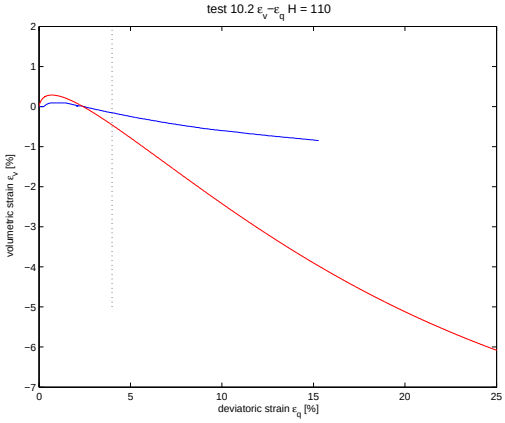
test 10.2 ε_v−ε_q H = 110
volumetric strain ε_v [%]
deviatoric strain ε_q [%]

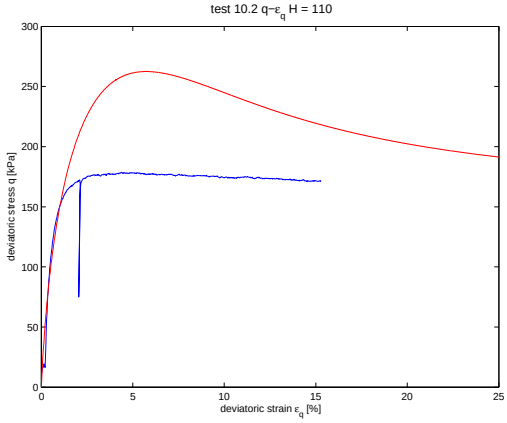
test 10.2 q−ε_q H = 110
deviatoric stress q [kPa]
deviatoric strain ε_q [%]

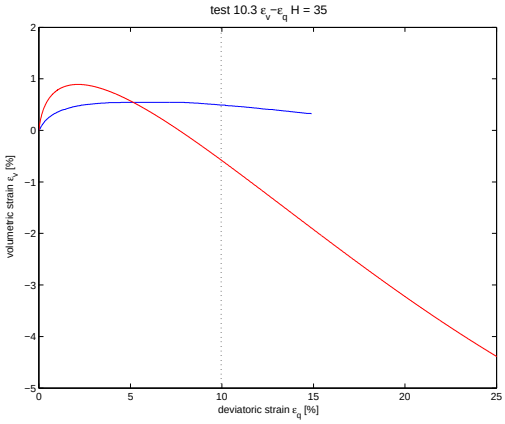
test 10.3 ε_v−ε_q H = 35
volumetric strain ε_v [%]
deviatoric strain ε_q [%]

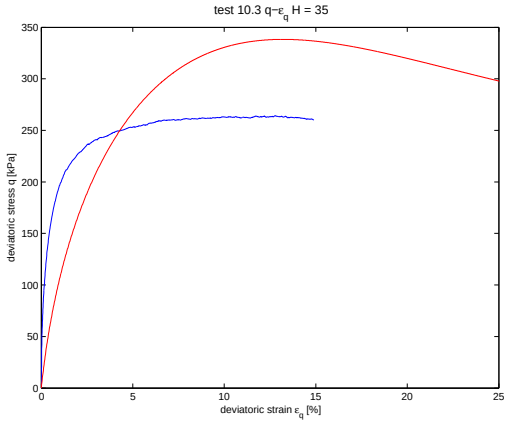
test 10.3 q−ε_q H = 35
deviatoric stress q [kPa]
deviatoric strain ε_q [%]

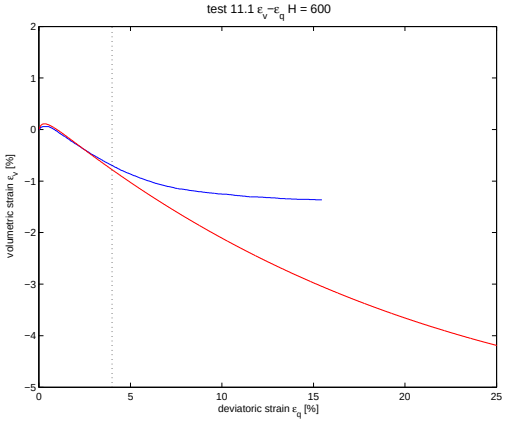
test 11.1 ϵ_v–ϵ_q H = 600
volumetric strain ϵ_v [%]
deviatoric strain ϵ_q [%]

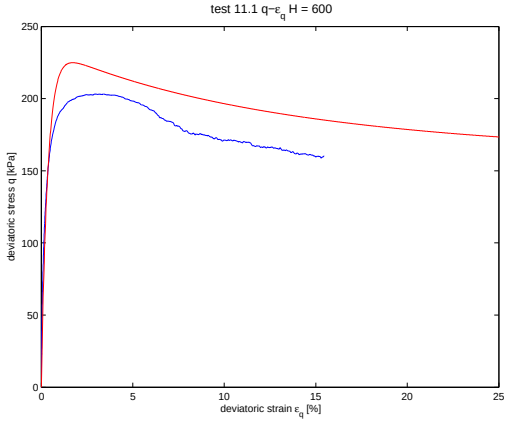
test 11.1 q–ϵ_q H = 600
deviatoric stress q [kPa]
deviatoric strain ϵ_q [%]

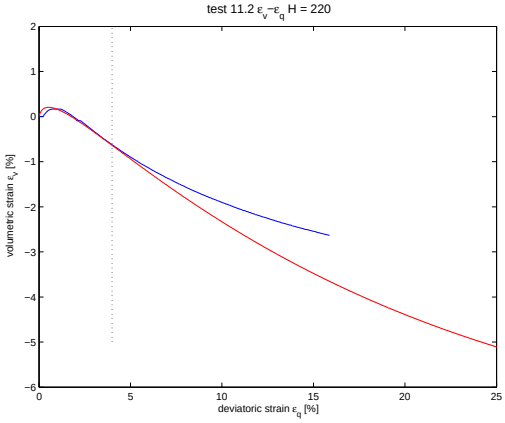
test 11.2 ϵ_v–ϵ_q H = 220
volumetric strain ϵ_v [%]
deviatoric strain ϵ_q [%]

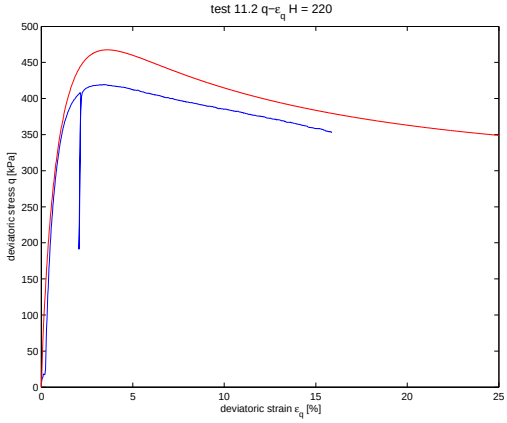
test 11.2 q–ϵ_q H = 220
deviatoric stress q [kPa]
deviatoric strain ϵ_q [%]

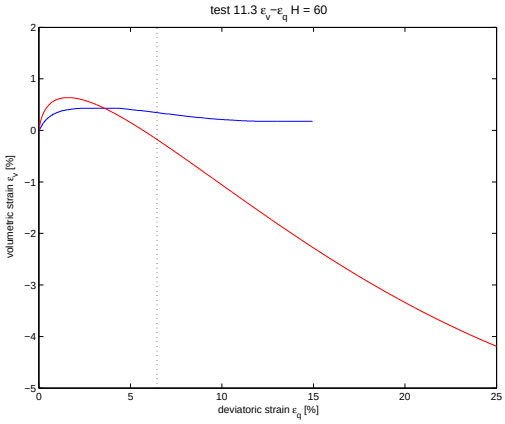
test 11.3 ϵ_v–ϵ_q H = 60
volumetric strain ϵ_v [%]
deviatoric strain ϵ_q [%]

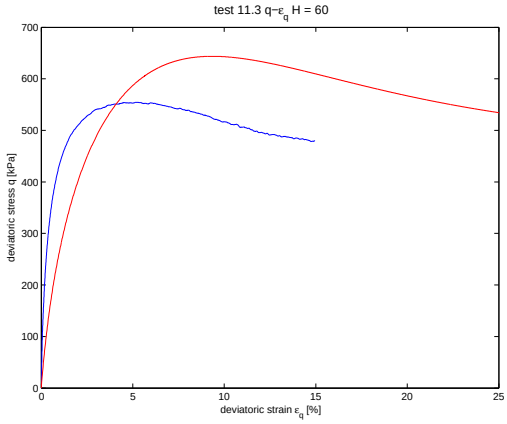
test 11.3 q–ϵ_q H = 60
deviatoric stress q [kPa]
deviatoric strain ϵ_q [%]

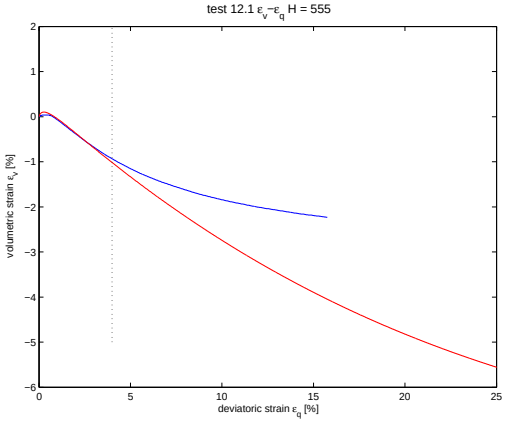
test 12.1 ε_v−ε_q H = 555
volumetric strain ε_v [%]
deviatoric strain ε_q [%]

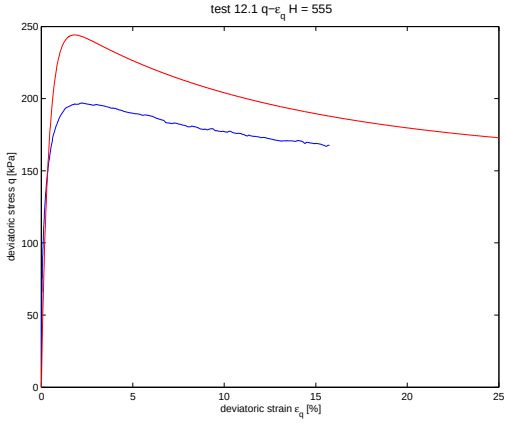
test 12.1 q−ε_q H = 555
deviatoric stress q [kPa]
deviatoric strain ε_q [%]

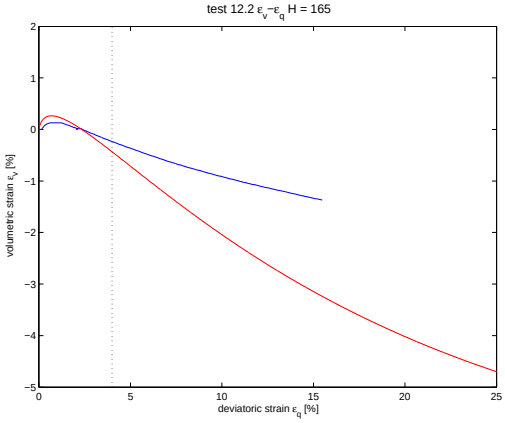
test 12.2 ε_v−ε_q H = 165
volumetric strain ε_v [%]
deviatoric strain ε_q [%]

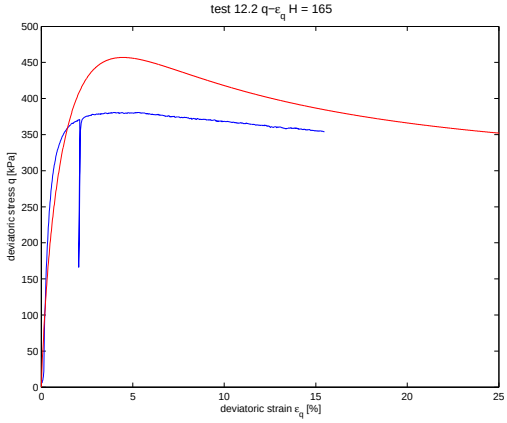
test 12.2 q−ε_q H = 165
deviatoric stress q [kPa]
deviatoric strain ε_q [%]

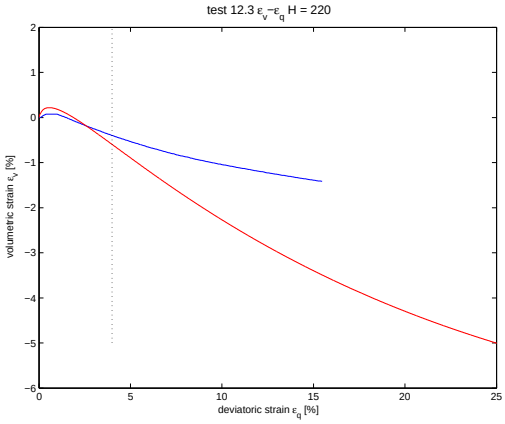
test 12.3 ε_v−ε_q H = 220
volumetric strain ε_v [%]
deviatoric strain ε_q [%]

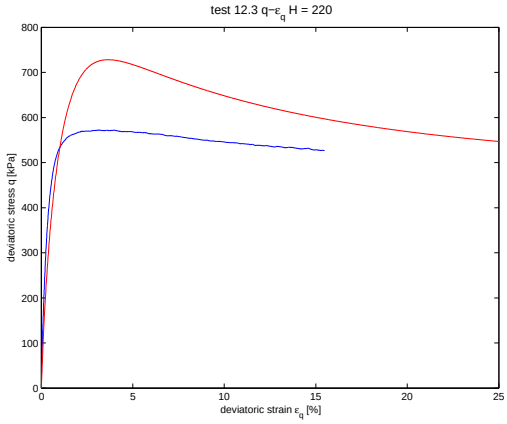
test 12.3 q−ε_q H = 220
deviatoric stress q [kPa]
deviatoric strain ε_q [%]

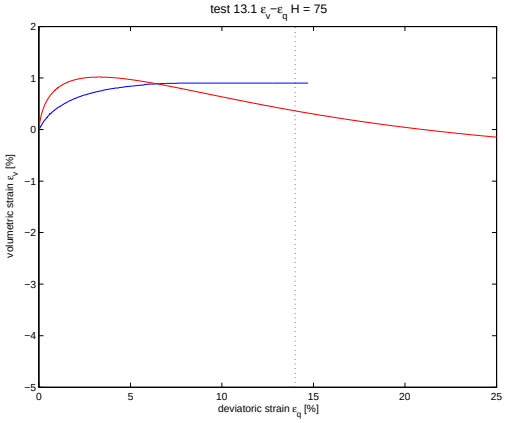
test 13.1 ε_v−ε_q H = 75
volumetric strain ε_v [%]
deviatoric strain ε_q [%]

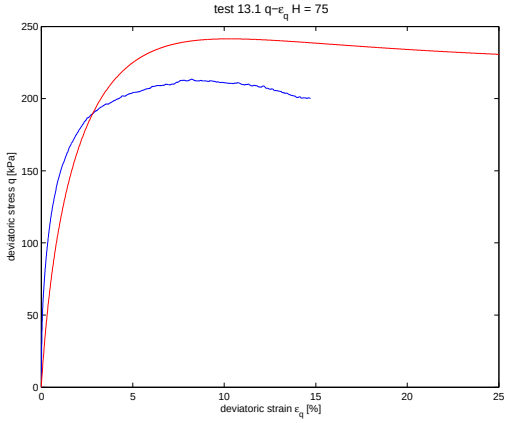
test 13.1 q−ε_q H = 75
deviatoric stress q [kPa]
deviatoric strain ε_q [%]

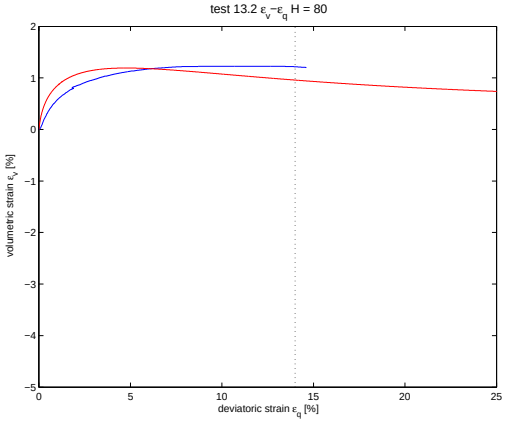
test 13.2 ε_v−ε_q H = 80
volumetric strain ε_v [%]
deviatoric strain ε_q [%]

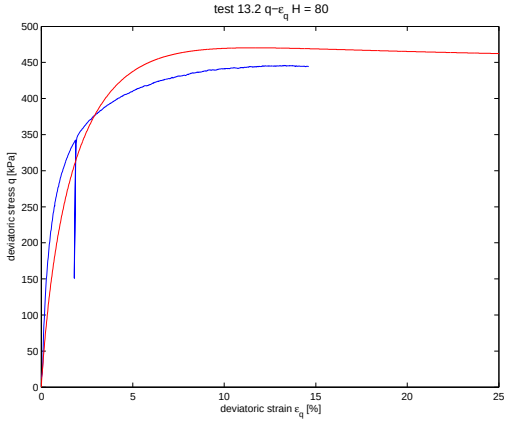
test 13.2 q−ε_q H = 80
deviatoric stress q [kPa]
deviatoric strain ε_q [%]

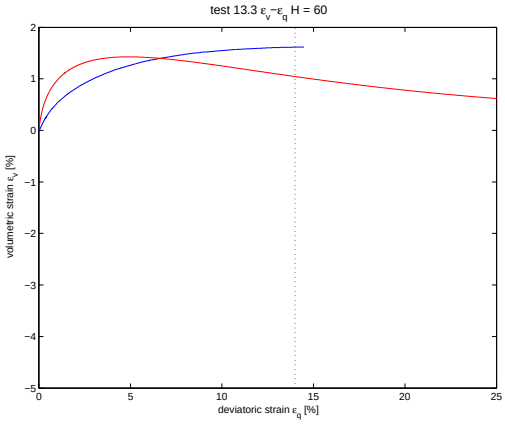
test 13.3 ε_v−ε_q H = 60
volumetric strain ε_v [%]
deviatoric strain ε_q [%]

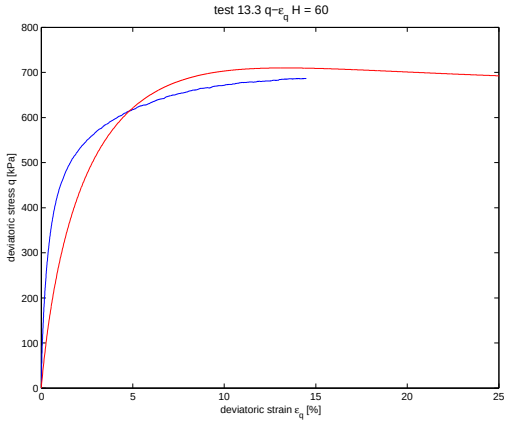
test 13.3 q−ε_q H = 60
deviatoric stress q [kPa]
deviatoric strain ε_q [%]

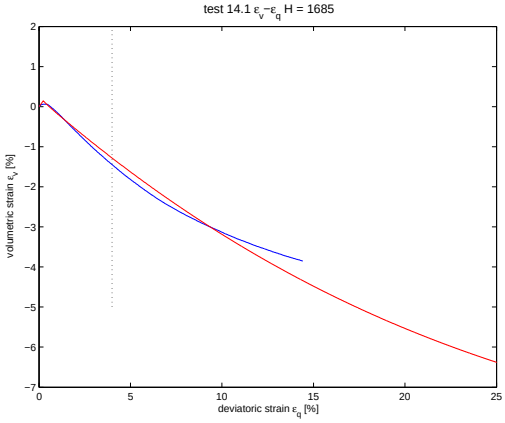
test 14.1 ε_v–ε_q H = 1685
volumetric strain ε_v [%]
deviatoric strain ε_q [%]

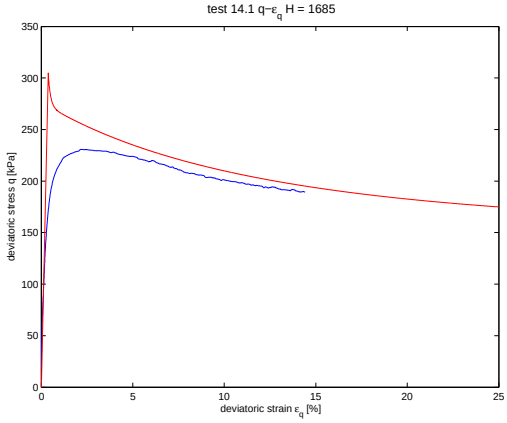
test 14.1 q–ε_q H = 1685
deviatoric stress q [kPa]
deviatoric strain ε_q [%]

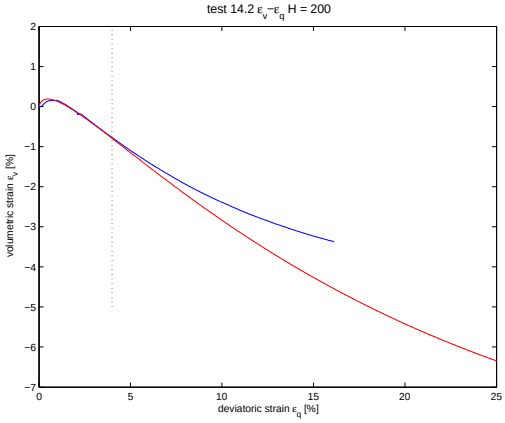
test 14.2 ε_v–ε_q H = 200
volumetric strain ε_v [%]
deviatoric strain ε_q [%]

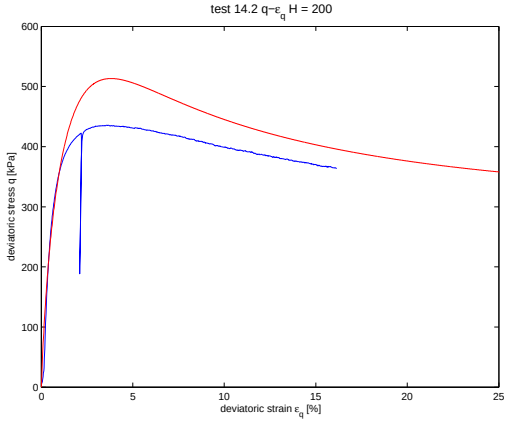
test 14.2 q–ε_q H = 200
deviatoric stress q [kPa]
deviatoric strain ε_q [%]

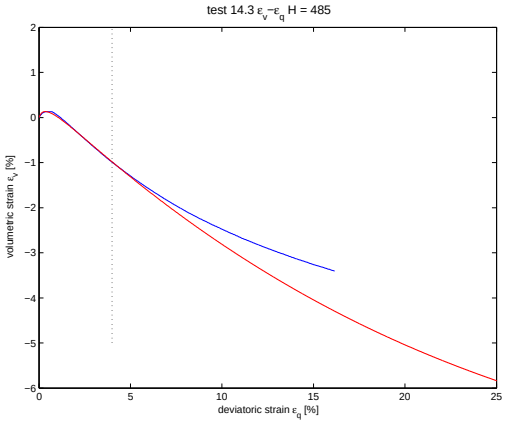
test 14.3 ε_v–ε_q H = 485
volumetric strain ε_v [%]
deviatoric strain ε_q [%]

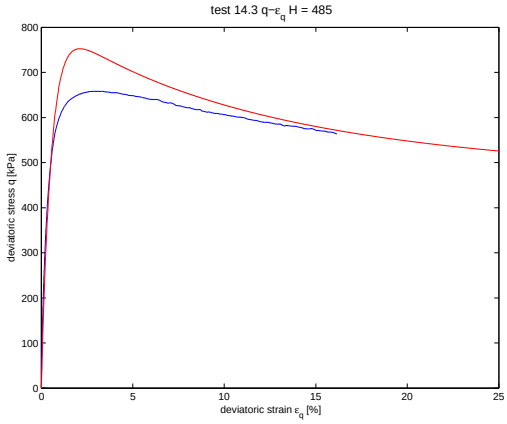
test 14.3 q–ε_q H = 485
deviatoric stress q [kPa]
deviatoric strain ε_q [%]

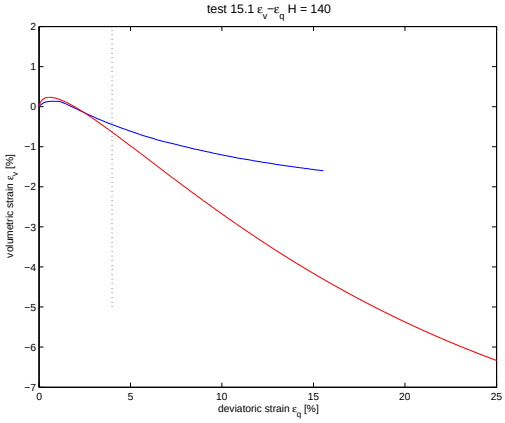
test 15.1 ε_v−ε_q H = 140
volumetric strain ε_v [%]
deviatoric strain ε_q [%]

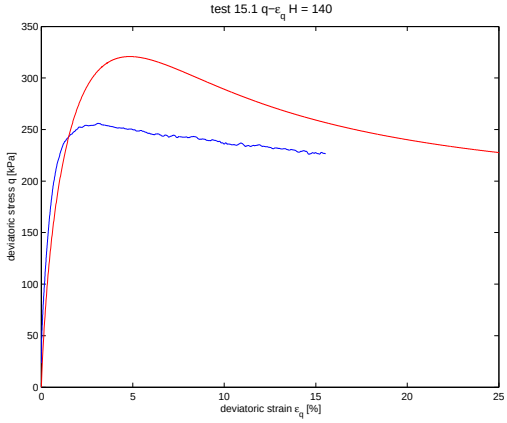
test 15.1 q−ε_q H = 140
deviatoric stress q [kPa]
deviatoric strain ε_q [%]

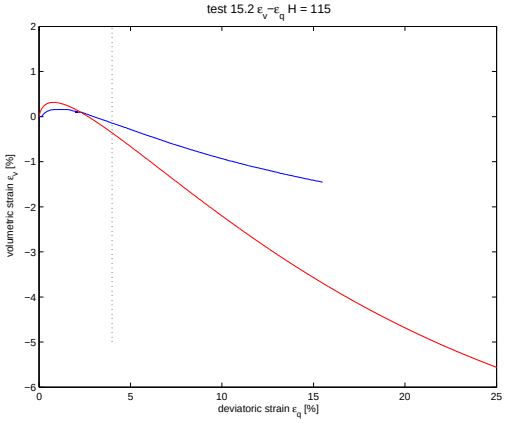
test 15.2 ε_v−ε_q H = 115
volumetric strain ε_v [%]
deviatoric strain ε_q [%]

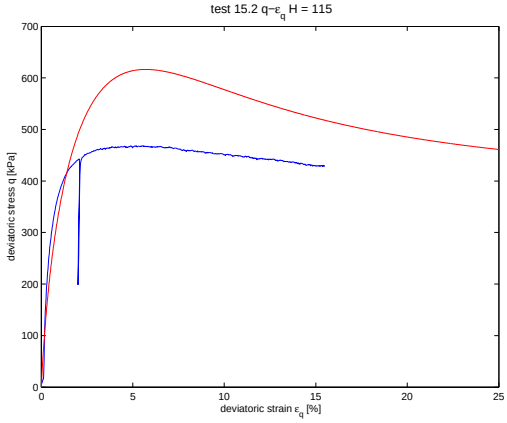
test 15.2 q−ε_q H = 115
deviatoric stress q [kPa]
deviatoric strain ε_q [%]

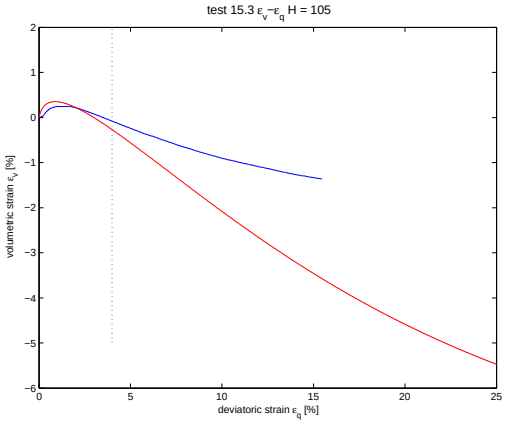
test 15.3 ε_v−ε_q H = 105
volumetric strain ε_v [%]
deviatoric strain ε_q [%]

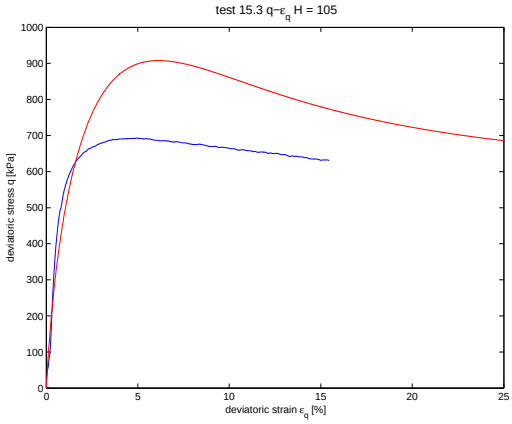
test 15.3 q−ε_q H = 105
deviatoric stress q [kPa]
deviatoric strain ε_q [%]

Appendix D

Statistical interpretation

D.1 Results of statistical interpretation for individual profiles

To decrease the size of the report, not all testresults are shown in this appendix. All 140 test results can be found on the data-CD. The 6 results that are shown here are the profiles that are used for the conditioning.

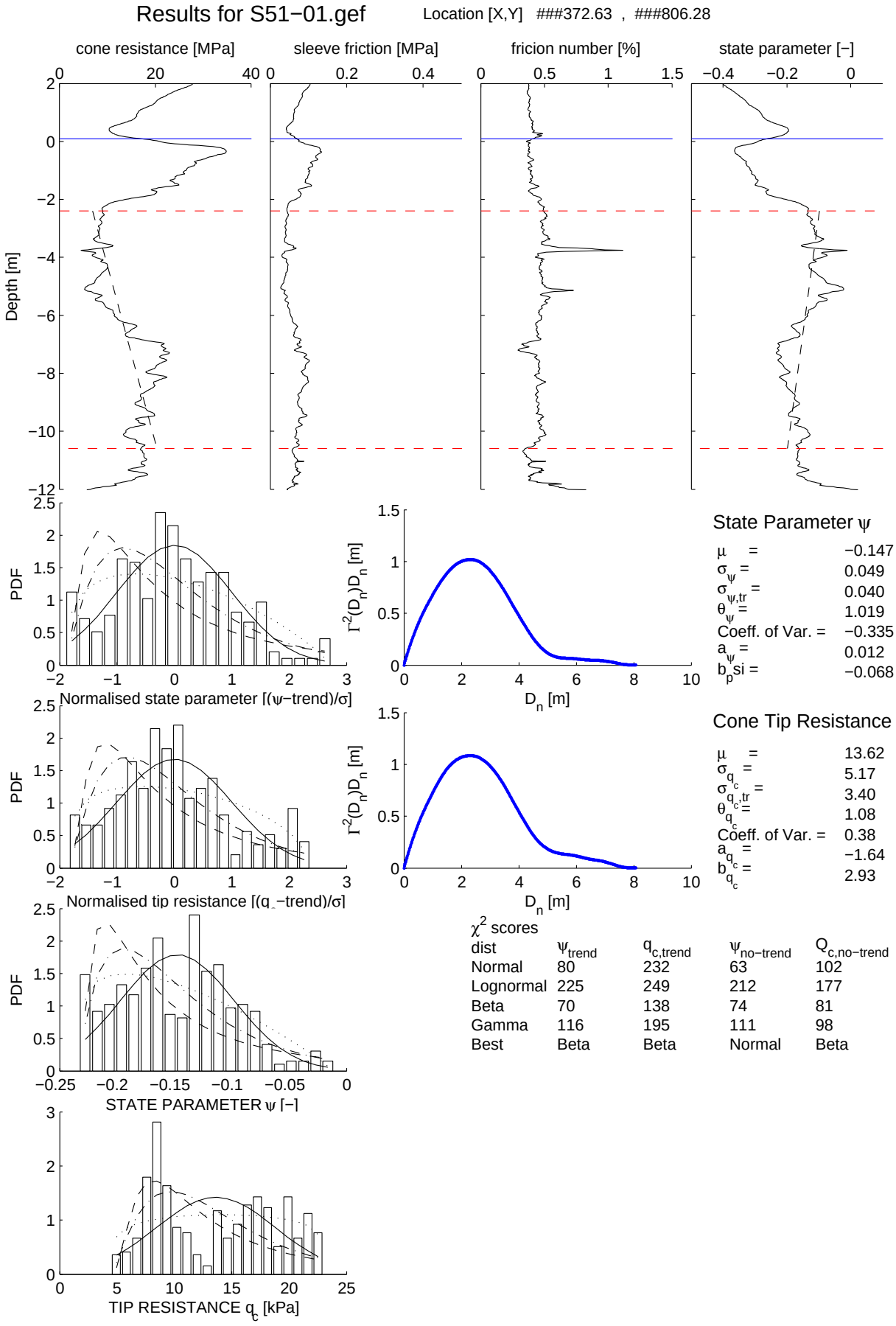
Results for S51−01.gef
Location [X,Y] ###372.63 , ###806.28
cone resistance [MPa]
sleeve friction [MPa]
fricion number [%]
state parameter [−]
Depth [m]
PDF
Normalised state parameter [(ψ−trend)/σ]
Normalised tip resistance [(q_c−trend)/σ]
STATE PARAMETER ψ [−]
TIP RESISTANCE q_c [kPa]
Γ²(D_n)D_n [m]
D_n [m]
State Parameter ψ
μ = −0.147
σ_ψ = 0.049
σ_ψ,tr = 0.040
θ_ψ = 1.019
Coeff. of Var. = −0.335
a_ψ = 0.012
b_psi = −0.068
Cone Tip Resistance q_c
μ = 13.62
σ_qc = 5.17
σ_qc,tr = 3.40
θ_qc = 1.08
Coeff. of Var. = 0.38
a_qc = −1.64
b_qc = 2.93
χ² scores
dist ψ_trend q_c,trend ψ_no−trend Q_c,no−trend
Normal 80 232 63 102
Lognormal 225 249 212 177
Beta 70 138 74 81
Gamma 116 195 111 98
Best Beta Beta Normal Beta

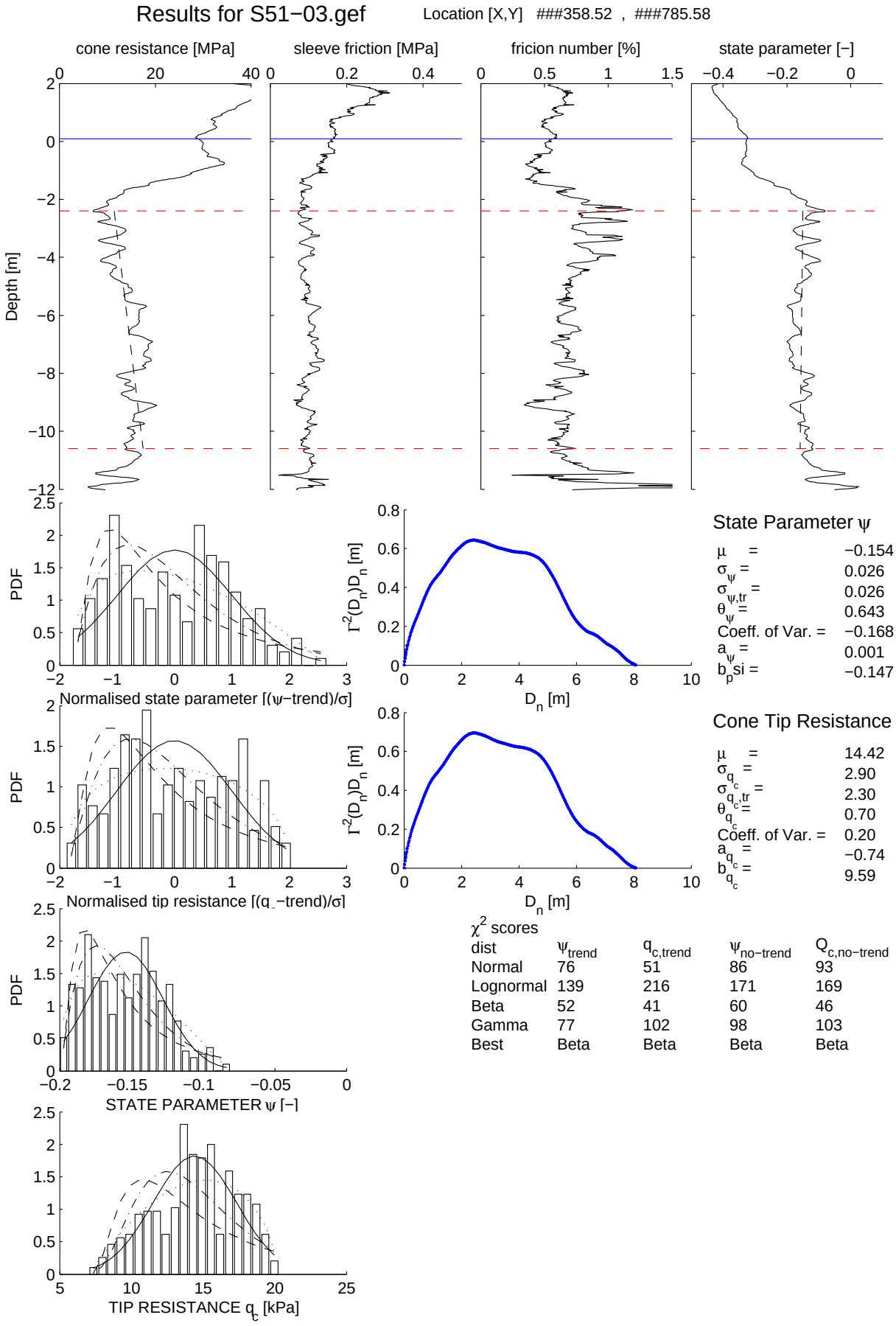
Results for S51−03.gef
Location [X,Y] ###358.52 , ###785.58
cone resistance [MPa]
sleeve friction [MPa]
fricion number [%]
state parameter [−]
Depth [m]
PDF
Normalised state parameter [(ψ−trend)/σ]
Normalised tip resistance [(q_c−trend)/σ]
STATE PARAMETER ψ [−]
TIP RESISTANCE q_c [kPa]
Γ²(D_n)D_n [m]
D_n [m]
State Parameter ψ
μ = −0.154
σ_ψ = 0.026
σ_ψ,tr = 0.026
θ_ψ = 0.643
Coeff. of Var. = −0.168
a_ψ = 0.001
b_psi = −0.147
Cone Tip Resistance q_c
μ = 14.42
σ_qc = 2.90
σ_qc,tr = 2.30
θ_qc = 0.70
Coeff. of Var. = 0.20
a_qc = −0.74
b_qc = 9.59
χ² scores
dist ψ_trend q_c,trend ψ_no−trend Q_c,no−trend
Normal 76 51 86 93
Lognormal 139 216 171 169
Beta 52 41 60 46
Gamma 77 102 98 103
Best Beta Beta Beta Beta

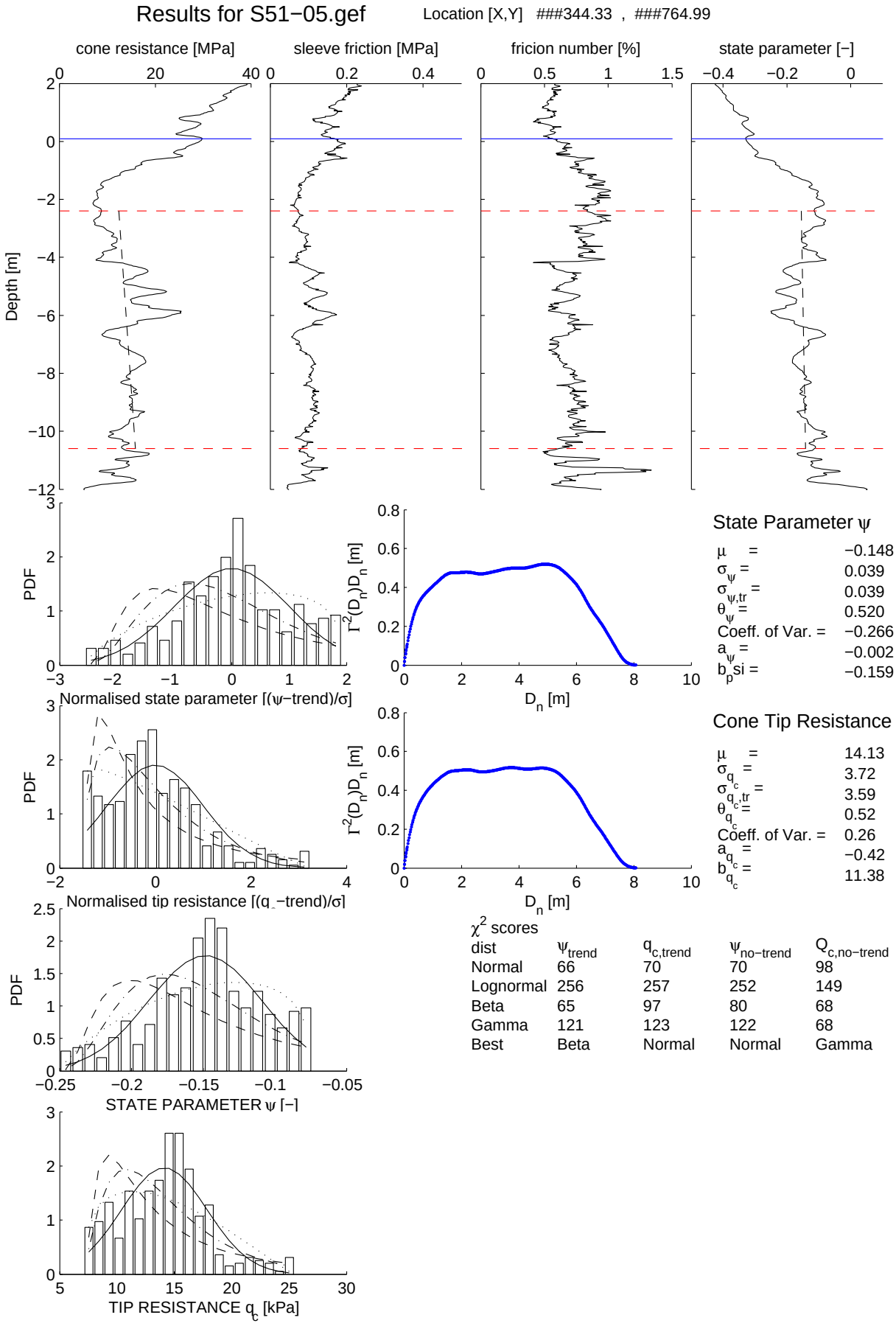
Results for S51−05.gef
Location [X,Y] ###344.33 , ###764.99
cone resistance [MPa]
sleeve friction [MPa]
fricion number [%]
state parameter [−]
Depth [m]
PDF
Normalised state parameter [(ψ−trend)/σ]
Γ²(D_n)D_n [m]
D_n [m]
State Parameter ψ
μ = −0.148
σ_ψ = 0.039
σ_ψ,tr = 0.039
θ_ψ = 0.520
Coeff. of Var. = −0.266
a_ψ = −0.002
b_psi = −0.159
Normalised tip resistance [(q_c−trend)/σ]
Cone Tip Resistance q_c
μ = 14.13
σ_qc = 3.72
σ_qc,tr = 3.59
θ_qc = 0.52
Coeff. of Var. = 0.26
a_qc = −0.42
b_qc = 11.38
STATE PARAMETER ψ [−]
TIP RESISTANCE q_c [kPa]
χ² scores
dist ψ_trend q_c,trend ψ_no−trend Q_c,no−trend
Normal 66 70 70 98
Lognormal 256 257 252 149
Beta 65 97 80 68
Gamma 121 123 122 68
Best Beta Normal Normal Gamma

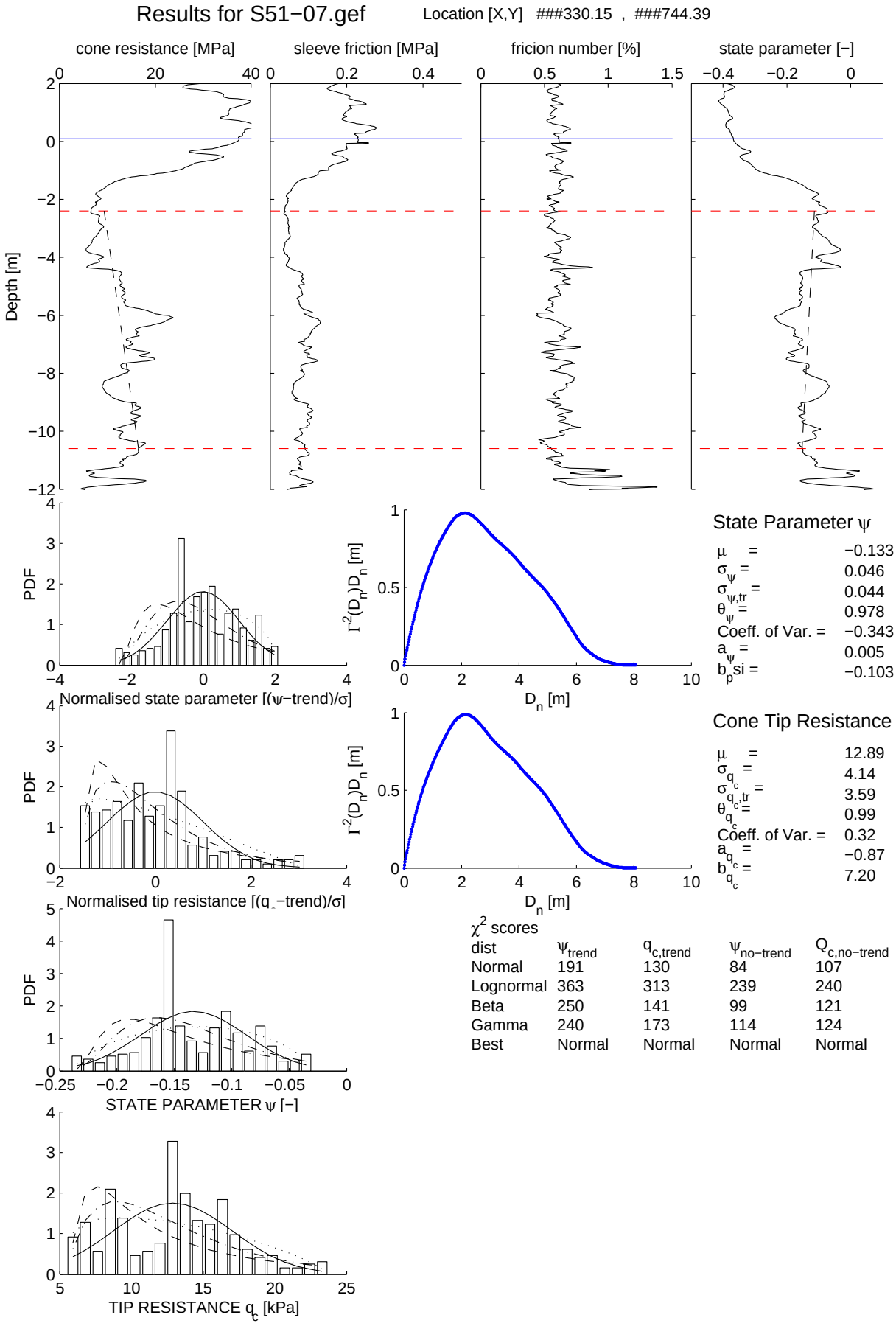

χ^2 scores

dist	ψ_{trend}	$q_{c,trend}$	$\psi_{no-trend}$	$Q_{c,no-trend}$
Normal	191	130	84	107
Lognormal	363	313	239	240
Beta	250	141	99	121
Gamma	240	173	114	124
Best	Normal	Normal	Normal	Normal

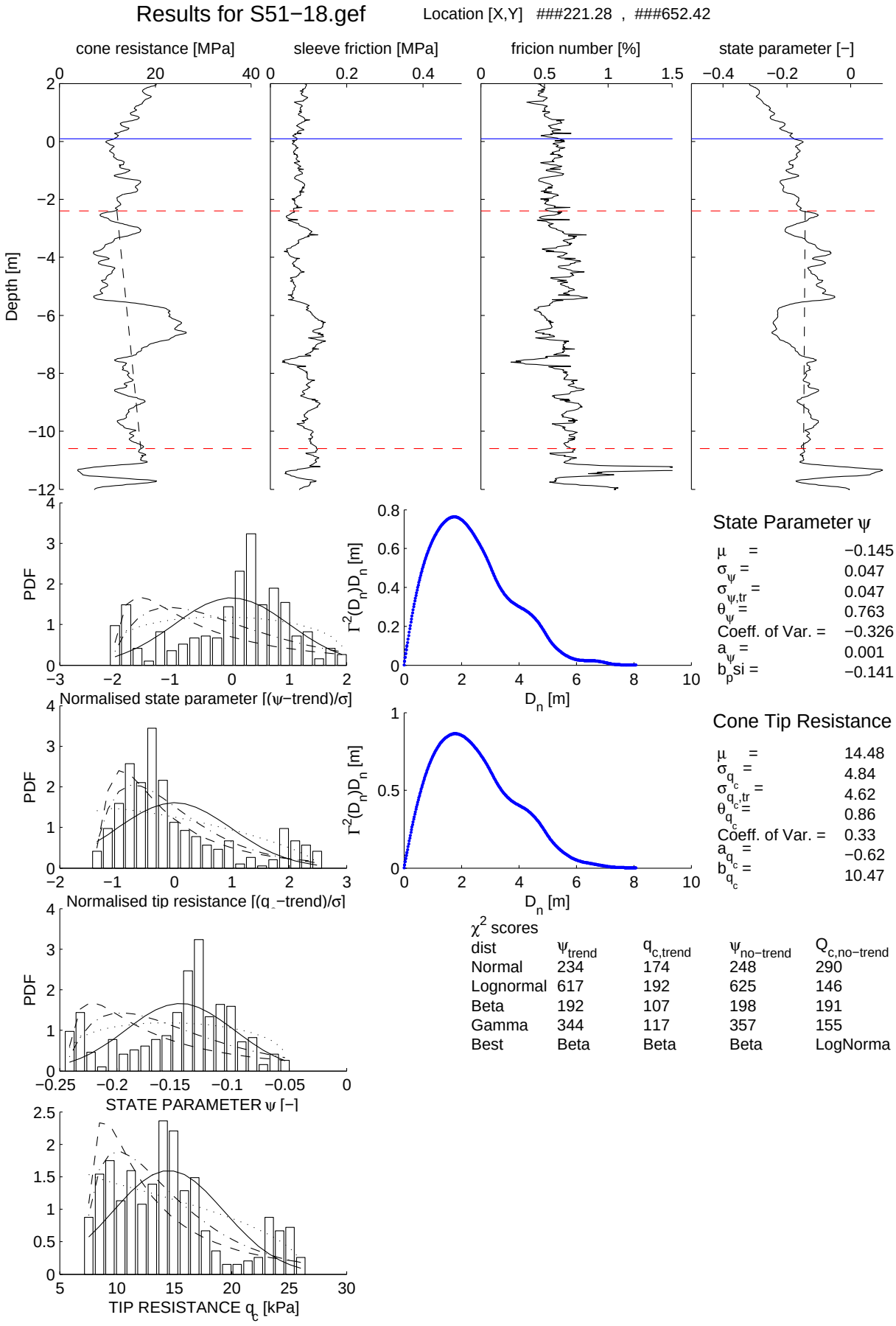

χ^2 scores

dist	ψ_{trend}	$q_{c,trend}$	$\psi_{no-trend}$	$Q_{c,no-trend}$
Normal	234	174	248	290
Lognormal	617	192	625	146
Beta	192	107	198	191
Gamma	344	117	357	155
Best	Beta	Beta	Beta	LogNorma

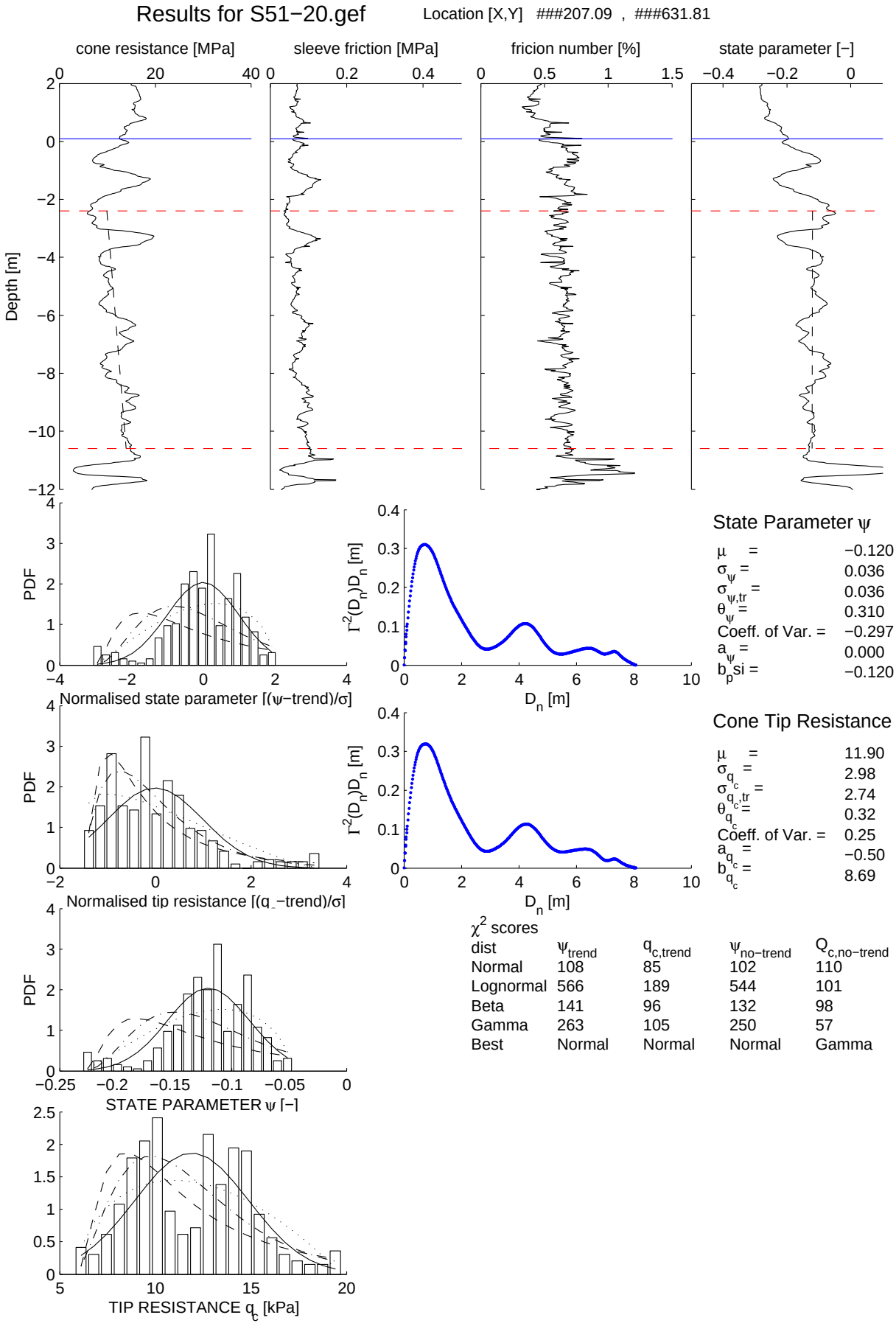
Results for S51−20.gef
Location [X,Y] ###207.09 , ###631.81
cone resistance [MPa]
sleeve friction [MPa]
fricion number [%]
state parameter [−]
Depth [m]
PDF
Normalised state parameter [(ψ−trend)/σ]
Normalised tip resistance [(q_c−trend)/σ]
STATE PARAMETER ψ [−]
TIP RESISTANCE q_c [kPa]
Γ²(D_n)D_n [m]
D_n [m]
State Parameter ψ
μ = −0.120
σ_ψ = 0.036
σ_ψ,tr = 0.036
θ_ψ = 0.310
Coeff. of Var. = −0.297
a_ψ = 0.000
b_psi = −0.120
Cone Tip Resistance q_c
μ = 11.90
σ_qc = 2.98
σ_qc,tr = 2.74
θ_qc = 0.32
Coeff. of Var. = 0.25
a_qc = −0.50
b_qc = 8.69
χ² scores
dist ψ_trend q_c,trend ψ_no−trend Q_c,no−trend
Normal 108 85 102 110
Lognormal 566 189 544 101
Beta 141 96 132 98
Gamma 263 105 250 57
Best Normal Normal Normal Gamma

D.2 Tabular results of individual statistical interpretation

Statistical interpretation is done based on the profiles of tip resistance q_c and state parameter psi. The following statistics can be found in the tables for both parameters:

CPT-ID	Name-tag of measurement
X [m]	Horizontal location coordinate
Y [m]	Horizontal location coordinate
Z [m]	Vertical location coordinate; surfacelevel (relative to NAP)
μ [-]	Average of the profile (trend not removed)
σ [-]	Standard deviation of the profile (trend not removed)
dist	Distribution fitting best to the points in the profile (trend not removed)
a_{tr} [m^{-1}]	Slope of the trend in the profile (trend=a*z+b, z=depth)
b_{tr} [-]	Trend at z=0(trend=a*z+b, z=depth)
σ_{tr} [-]	Standard deviation of the trend-removed profile
θ [m]	Scale of fluctuation
$dist_{tr}$	Distribution fitting best to the points in the trend-removed profile

Statistics for state parameter ψ

CPT-ID	X [m]	Y [m]	Z [m]	μ [-]	σ [-]	dist	a_{tr} [m^{-1}]	b_{tr} [-]	σ_{tr} [-]	θ [m]	$dist_{tr}$
S51-01.gef	##5372.63	##5806.28	4.63	-0.1309	0.0472	β	0.0117	-0.0551	0.0382	1.0196	N
S51-02.gef	##5334.72	##5817.13	5.29	-0.0942	0.047	Γ	-0.0067	-0.1374	0.0442	0.3534	N
S51-03.gef	##5358.52	##5785.58	5.27	-0.137	0.0247	β	0.001	-0.1306	0.0246	0.6423	β
S51-04.gef	##5320.54	##5796.54	5.16	-0.1248	0.0511	N	-0.0083	-0.1791	0.0471	1.1623	Γ
S51-05.gef	##5344.33	##5764.99	5.27	-0.1318	0.0377	N	-0.0016	-0.1421	0.0375	0.5196	N
S51-06.gef	##5306.36	##5775.95	5.3	-0.1361	0.036	N	-0.0065	-0.1785	0.0325	0.313	Γ
S51-07.gef	##5330.15	##5744.39	5.21	-0.1174	0.0436	N	0.0045	-0.0883	0.0423	0.9776	N
S51-08.gef	##5292.18	##5755.36	5.42	-0.1531	0.0416	β	-0.0055	-0.1891	0.0395	0.7875	N
S51-09.gef	##5315.97	##5723.79	5.24	-0.1304	0.0401	β	0.0011	-0.1232	0.04	0.5629	β
S51-10.gef	##5278.00	##5734.78	5.3	-0.1375	0.0555	β	0.0023	-0.1228	0.0552	0.8567	β
S51-11.gef	##5301.78	##5703.22	5.4	-0.1157	0.0283	β	0.0033	-0.0943	0.0272	0.1956	β
S51-12.gef	##5263.83	##5714.18	5.4	-0.1648	0.0439	N	-0.0069	-0.2098	0.0407	0.6465	β
S51-13.gef	##5287.62	##5682.63	5.6	-0.1332	0.0413	N	-0.0004	-0.1357	0.0413	0.3668	N
S51-14.gef	##5249.63	##5693.58	5.48	-0.1114	0.036	Γ	0.0057	-0.0745	0.0334	0.7845	Γ
S51-15.gef	##5273.44	##5662.03	5.57	-0.1086	0.0512	N	-0.0024	-0.124	0.0509	0.3306	N
S51-16.gef	##5235.46	##5673.01	5.57	-0.1284	0.0343	N	-0.0041	-0.1552	0.0329	0.2826	Γ
S51-17.gef	##5259.25	##5641.45	5.53	-0.1431	0.0354	N	-0.0052	-0.1768	0.0332	0.4367	N
S51-18.gef	##5221.28	##5652.42	5.53	-0.1286	0.0451	β	0.0006	-0.1244	0.0451	0.7631	β
S51-19.gef	##5245.09	##5620.84	5.51	-0.1563	0.0405	N	-0.0065	-0.1985	0.0375	0.4643	N
S51-20.gef	##5207.09	##5631.81	5.37	-0.105	0.0342	N	0	-0.1049	0.0342	0.3104	N
S51-21.gef	##5230.91	##5600.25	5.44	-0.1486	0.0463	β	-0.0155	-0.2496	0.0279	0.3647	N
S51-22.gef	##5192.93	##5611.23	5.51	-0.0959	0.0411	β	0.0087	-0.0393	0.0355	0.7548	N
S51-23.gef	##5216.79	##5579.74	5.43	-0.1332	0.0236	β	-0.0049	-0.1648	0.0206	0.2842	β
S51-24.gef	##5178.75	##5590.64	5.46	-0.1204	0.0266	N	0.0023	-0.1057	0.0261	0.3688	β
S51-25.gef	##5202.53	##5559.09	5.46	-0.1479	0.0338	N	-0.0023	-0.1626	0.0334	0.3522	N
S51-26.gef	##5164.56	##5570.05	5.44	-0.1601	0.0427	Γ	0.001	-0.1538	0.0426	0.5099	Γ
S51-27.gef	##5188.36	##5538.48	5.42	-0.1427	0.035	N	-0.0075	-0.1914	0.0302	0.3495	β
S51-28.gef	##5150.40	##5549.46	5.44	-0.1623	0.0403	Γ	0.004	-0.1361	0.0392	0.9223	β
S51-29.gef	##5174.17	##5517.90	5.47	-0.1235	0.0232	Γ	-0.0028	-0.1414	0.0223	0.3731	Γ
S51-30.gef	##5136.21	##5528.87	5.41	-0.147	0.0494	Γ	0.003	-0.1275	0.0489	0.5162	Γ
S51-31.gef	##5160.00	##5497.31	5.44	-0.1485	0.0547	N	-0.0198	-0.2771	0.0281	0.3247	N
S51-32.gef	##5122.04	##5508.28	5.43	-0.1495	0.0331	N	0.002	-0.1368	0.0328	0.7317	N
S51-33.gef	##5145.83	##5476.72	5.43	-0.1326	0.0397	β	-0.0097	-0.196	0.0322	0.909	β
S51-34.gef	##5107.85	##5487.69	5.48	-0.142	0.0361	Γ	-0.0084	-0.1969	0.03	0.4867	β
S51-35.gef	##5131.65	##5456.12	5.49	-0.1123	0.0324	β	0.0002	-0.1111	0.0324	0.7193	β
S51-36.gef	##5093.68	##5467.11	5.42	-0.1644	0.0447	β	0.006	-0.1255	0.0424	0.9896	β
S51-37.gef	##5117.47	##5435.53	5.47	-0.1168	0.0465	β	-0.0022	-0.1313	0.0462	0.6106	β
S51-38.gef	##5079.48	##5446.52	5.41	-0.1605	0.0666	β	0.0095	-0.0987	0.0626	1.2869	β
S51-39.gef	##5103.30	##5414.95	5.42	-0.0976	0.0537	N	0.0068	-0.0537	0.0512	1.1404	N
S51-40.gef	##5065.31	##5425.93	5.37	-0.1531	0.0552	β	0.0103	-0.086	0.0494	1.2635	β
CPT-ID	X [m]	Y [m]	Z [m]	μ [-]	σ [-]	dist	a_{tr} [m^{-1}]	b_{tr} [-]	σ_{tr} [-]	θ [m]	$dist_{tr}$

CPT-ID	X [m]	Y [m]	Z [m]	μ [-]	σ [-]	dist	a_{tr} [m^{-1}]	b_{tr} [-]	σ_{tr} [-]	θ [m]	dist$_{tr}$
S51-41.gef	##5089.11	##5394.37	5.35	-0.1153	0.0412	Γ	0.0048	-0.0838	0.0395	0.7557	Γ
S51-42.gef	##5051.13	##5405.32	5.32	-0.1161	0.0547	β	0.0114	-0.0419	0.0475	0.9331	β
S51-43.gef	##5074.93	##5373.77	5.29	-0.1169	0.0735	β	0.0219	0.0257	0.0518	1.1353	β
S51-44.gef	##5036.94	##5384.74	5.34	-0.1069	0.0583	β	0.0165	0.0006	0.0431	0.6721	β
S51-45.gef	##5060.74	##5353.16	5.34	-0.1026	0.0554	N	0.0115	-0.0277	0.0482	0.465	N
S51-46.gef	##5022.77	##5364.14	5.4	-0.0984	0.0479	N	0.0106	-0.0294	0.0407	0.542	N
S51-47.gef	##5046.58	##5332.59	5.45	-0.1024	0.0382	Γ	0.0083	-0.0482	0.0327	0.6483	N
S51-48.gef	##5008.60	##5343.55	5.46	-0.0851	0.0467	Γ	0.0165	0.0222	0.0256	0.2287	N
S51-49.gef	##5032.39	##5312.01	5.39	-0.0907	0.0415	Γ	0.0065	-0.0482	0.0384	0.4715	N
S51-50.gef	##4994.41	##5322.97	5.38	-0.1156	0.031	Γ	0.0026	-0.0985	0.0304	0.3712	Γ
S51-51.gef	##5018.22	##5291.42	5.47	-0.092	0.0285	Γ	-0.0024	-0.1078	0.0279	0.4393	N
S51-52.gef	##4980.23	##5302.39	5.51	-0.1116	0.0326	Γ	0.005	-0.0792	0.0304	0.3402	Γ
S51-53.gef	##5004.04	##5270.82	5.48	-0.1284	0.0356	N	-0.0065	-0.1706	0.0321	0.5109	N
S51-54.gef	##4966.06	##5281.79	5.57	-0.1118	0.0383	Γ	0.0056	-0.0756	0.0359	0.7768	N
S51-55.gef	##4989.86	##5250.23	5.5	-0.1073	0.0471	N	-0.0014	-0.1167	0.047	0.5245	N
S51-56.gef	##4951.88	##5261.19	5.36	-0.1169	0.0218	N	0.0021	-0.1029	0.0212	0.3471	N
S51-57.gef	##4975.68	##5229.65	5.41	-0.1145	0.0448	β	0.0065	-0.0721	0.042	0.79	β
S51-58.gef	##4937.69	##5240.61	5.28	-0.1096	0.0246	β	0.0023	-0.0947	0.024	0.4367	β
S51-59.gef	##4961.49	##5209.05	5.36	-0.1065	0.0411	Γ	0.0048	-0.0754	0.0395	1.2471	β
S51-60.gef	##4923.51	##5220.01	5.77	-0.1089	0.0369	N	0.0094	-0.0475	0.0293	0.3004	N
S51-61.gef	##4947.33	##5188.46	5.87	-0.1299	0.0568	β	0.0003	-0.1277	0.0568	1.1895	β
S51-62.gef	##4909.34	##5199.43	5.91	-0.1025	0.0341	Γ	0.009	-0.0441	0.0266	0.3994	Γ
S51-63.gef	##4933.15	##5167.87	5.82	-0.1574	0.0544	N	-0.0002	-0.1587	0.0544	1.0638	N
S51-64.gef	##4895.16	##5178.84	5.94	-0.1154	0.0309	Γ	0.0033	-0.0939	0.0299	0.3879	Γ
S51-65.gef	##4918.95	##5147.28	5.9	-0.1245	0.0922	Γ	-0.0148	-0.2206	0.0852	0.7399	Γ
S51-66.gef	##4880.99	##5158.24	5.96	-0.0865	0.0359	N	0.0095	-0.0249	0.028	0.4196	Γ
S51-67.gef	##4904.77	##5126.73	5.89	-0.1279	0.0562	β	-0.0013	-0.1363	0.0561	0.7729	β
S51-68.gef	##4866.81	##5137.65	5.95	-0.0781	0.0435	β	0.0009	-0.072	0.0434	0.5814	β
S51-69.gef	##4890.61	##5106.10	5.95	-0.1057	0.0308	β	-0.0014	-0.1151	0.0306	0.3139	β
S51-70.gef	##4852.63	##5117.06	5.9	-0.1216	0.0376	Γ	-0.0032	-0.1426	0.0368	0.4023	N
S51-71.gef	##4876.43	##5085.50	5.89	-0.1105	0.0428	β	-0.004	-0.1367	0.0417	0.8158	β
S51-72.gef	##4838.45	##5096.48	5.93	-0.1206	0.0393	N	-0.0071	-0.1668	0.0355	0.2669	N
S51-73.gef	##4862.24	##5064.90	5.91	-0.1266	0.0317	β	0.0008	-0.1213	0.0317	0.6579	β
S51-74.gef	##4824.27	##5075.89	5.9	-0.1227	0.0366	N	-0.0082	-0.1757	0.031	0.4355	Γ
S51-75.gef	##4848.06	##5044.32	6.02	-0.1229	0.0296	N	-0.0052	-0.157	0.0269	0.234	N
S51-76.gef	##4810.08	##5055.29	5.88	-0.1132	0.0356	N	0.0023	-0.098	0.0351	0.6578	N
S51-77.gef	##4833.89	##5023.72	5.9	-0.1355	0.0386	β	-0.0096	-0.1979	0.0312	0.7618	β
S51-78.gef	##4795.92	##5034.71	5.99	-0.1012	0.0446	Γ	0.0053	-0.0664	0.0428	0.3177	N
S51-79.gef	##4819.71	##5003.14	6.02	-0.1408	0.0378	β	-0.0083	-0.195	0.0322	0.3605	β
S51-80.gef	##4781.72	##5014.11	5.88	-0.1058	0.0425	Γ	-0.0044	-0.1346	0.0412	0.7252	Γ
S51-81.gef	##4805.54	##4982.55	5.95	-0.1367	0.0353	N	-0.0019	-0.1492	0.0351	0.3128	N
S51-82.gef	##4767.56	##4993.52	5.81	-0.1331	0.0439	N	-0.0104	-0.2004	0.0364	0.524	Γ
S51-83.gef	##4791.35	##4961.96	5.94	-0.1648	0.0611	N	-0.0127	-0.2477	0.0531	0.931	N
S51-84.gef	##4753.38	##4972.93	5.98	-0.1214	0.0465	N	-0.0085	-0.1765	0.0419	0.7007	β
S51-85.gef	##4777.18	##4941.37	5.95	-0.1375	0.0487	N	-0.0079	-0.189	0.0449	0.761	N
S51-86.gef	##4739.18	##4952.35	6.04	-0.1111	0.0413	β	-0.0097	-0.1745	0.0342	0.6676	N
S51-87.gef	##4762.99	##4920.79	5.96	-0.1444	0.0601	β	-0.0115	-0.2195	0.0534	1.1007	β
S51-88.gef	##4725.02	##4931.76	6.07	-0.1158	0.0635	β	-0.0224	-0.2612	0.0345	0.5931	β
S51-89.gef	##4748.81	##4900.19	6.12	-0.1193	0.0742	N	-0.0269	-0.2939	0.0379	0.4257	Γ
S52-01.gef	##5370.52	##5831.09	5.27	-0.1335	0.0725	β	0.0106	-0.0648	0.068	1.3522	β
S52-02.gef	##5342.03	##5841.12	5.43	-0.0632	0.0483	β	-0.001	-0.0695	0.0482	0.4141	β
S52-03.gef	##5368.34	##5857.23	5.25	-0.1133	0.0482	β	-0.0008	-0.1186	0.0481	0.6762	β
S52-04.gef	##5339.85	##5866.03	5.39	-0.0833	0.034	β	0.0045	-0.0543	0.0323	0.4518	N
S52-05.gef	##5366.17	##5880.87	5.29	-0.0657	0.0582	Γ	0.0075	-0.0167	0.0553	0.3795	N
S52-06.gef	##5337.67	##5890.95	5.32	-0.0903	0.0433	N	-0.0033	-0.1116	0.0426	0.8427	N
S52-07.gef	##5364.00	##5905.78	5.38	-0.1232	0.0409	N	-0.0061	-0.1627	0.0383	0.5983	N
S52-08.gef	##5335.51	##5915.84	5.33	-0.1335	0.0353	N	0.0028	-0.1153	0.0346	0.435	N
S52-09.gef	##5361.82	##5930.69	5.24	-0.1225	0.0597	Γ	-0.0036	-0.1457	0.0591	0.874	β
S52-10.gef	##5333.33	##5940.75	5.17	-0.1844	0.0407	N	-0.0052	-0.2182	0.0388	0.9071	N
S52-11.gef	##5359.63	##5955.59	5.13	-0.1263	0.0566	N	-0.0027	-0.1441	0.0562	0.8742	N
S52-12.gef	##5331.16	##5965.65	5.19	-0.117	0.0564	β	0.003	-0.0977	0.056	1.1858	β
CPT-ID	X [m]	Y [m]	Z [m]	μ [-]	σ [-]	dist	a_{tr} [m^{-1}]	b_{tr} [-]	σ_{tr} [-]	θ [m]	dist$_{tr}$

CPT-ID	X [m]	Y [m]	Z [m]	μ [-]	σ [-]	dist	a_{tr} [m^{-1}]	b_{tr} [-]	σ_{tr} [-]	θ [m]	dist$_{tr}$
S52-13.gef	##5357.47	##5980.50	5.16	-0.1046	0.0672	β	-0.018	-0.2217	0.0519	0.8032	β
S52-14.gef	##5328.98	##5990.55	5.18	-0.1765	0.0332	Γ	-0.0076	-0.2258	0.0279	0.8033	β
S52-15.gef	##5355.29	##6005.41	5.22	-0.1618	0.0754	β	-0.0262	-0.3327	0.0424	0.7928	β
S52-16.gef	##5326.80	##6015.45	5.19	-0.1428	0.0337	Γ	-0.0087	-0.1991	0.0267	0.8679	N
S52-17.gef	##5353.12	##6030.33	5.15	-0.1624	0.0575	β	-0.0189	-0.2855	0.0358	0.4489	β
S52-18.gef	##5324.63	##6040.39	5.12	-0.1528	0.0553	N	-0.0182	-0.2712	0.0345	0.8472	β
S52-19.gef	##5350.93	##6055.22	5.01	-0.1411	0.0698	N	-0.0252	-0.3051	0.0357	0.4904	β
S52-20.gef	##5322.46	##6065.28	5.21	-0.1288	0.0386	N	-0.0101	-0.1943	0.0303	0.8268	β
S52-21.gef	##5348.77	##6080.13	5.1	-0.1291	0.0552	N	-0.0182	-0.2476	0.0343	0.5099	β
S52-22.gef	##5320.30	##6090.18	5.09	-0.1258	0.0463	N	-0.0157	-0.2282	0.0273	0.8297	N
S52-23.gef	##5346.59	##6105.02	5.08	-0.1307	0.0384	β	-0.0121	-0.2094	0.0255	0.8529	N
S52-24.gef	##5318.12	##6115.09	4.96	-0.0905	0.0296	N	-0.0007	-0.0948	0.0295	0.503	N
S52-25.gef	##5344.37	##6129.98	5.03	-0.112	0.0324	Γ	-0.0084	-0.1665	0.0257	0.4159	N
S52-26.gef	##5315.94	##6140.00	5.11	-0.0978	0.0374	N	0.0055	-0.062	0.035	0.5582	N
S52-27.gef	##5342.24	##6154.83	5.17	-0.1098	0.0333	Γ	-0.0101	-0.1752	0.0231	0.4433	N
S52-28.gef	##5313.74	##6164.90	5.35	-0.1351	0.063	β	0.021	0.0016	0.0384	0.5653	β
S52-29.gef	##5340.06	##6179.75	5.28	-0.126	0.0527	N	0.0096	-0.0636	0.0475	0.6119	β
S52-30.gef	##5311.60	##6189.81	5.25	-0.1142	0.0435	N	0.0124	-0.0339	0.032	0.4889	β
S52-31.gef	##5337.90	##6204.65	5.23	-0.1449	0.0407	β	-0.0069	-0.19	0.0372	0.7876	β
S52-32.gef	##5309.42	##6214.70	5.25	-0.1422	0.0389	β	0.0012	-0.1343	0.0388	0.7033	β
S52-33.gef	##5335.72	##6229.55	5.34	-0.1442	0.0457	Γ	-0.0147	-0.24	0.0293	0.3057	N
S52-34.gef	##5307.24	##6239.59	5.32	-0.12	0.0269	Γ	-0.0014	-0.1292	0.0267	0.3739	Γ
S52-35.gef	##5333.55	##6254.45	5.3	-0.1375	0.0567	N	-0.0197	-0.2655	0.0321	0.3532	β
S52-36.gef	##5305.06	##6264.51	5.33	-0.1106	0.0348	Γ	-0.002	-0.1239	0.0344	0.6801	Γ
S52-37.gef	##5331.37	##6279.36	5.32	-0.1362	0.0464	β	-0.0126	-0.2181	0.0355	0.7668	β
S52-38.gef	##5302.89	##6289.42	5.14	-0.1318	0.0404	N	-0.0035	-0.1543	0.0395	0.3539	N
S52-39.gef	##5329.21	##6304.25	5.47	-0.1336	0.0486	β	-0.013	-0.2182	0.0375	0.6634	β
S52-40.gef	##5300.70	##6314.34	5.44	-0.1181	0.0413	β	-0.0034	-0.1403	0.0405	0.4651	β
S52-41.gef	##5327.03	##6329.15	5.2	-0.0812	0.0544	β	-0.0179	-0.1979	0.0339	0.5901	Γ
S52-42.gef	##5298.55	##6339.22	5.24	-0.1294	0.04	β	0.0036	-0.1061	0.0391	0.8068	β
S52-43.gef	##5324.86	##6354.05	5.28	-0.1336	0.0425	N	-0.0128	-0.2172	0.0295	0.1781	N
S52-44.gef	##5296.37	##6364.13	5.5	-0.1057	0.041	N	-0.001	-0.112	0.0409	0.7839	N
S52-45.gef	##5322.67	##6378.96	5.42	-0.1279	0.0439	Γ	-0.009	-0.1863	0.0383	0.6071	Γ
S52-46.gef	##5294.19	##6389.07	5.34	-0.1048	0.0383	Γ	0.0121	-0.0258	0.0252	0.2115	N
S52-47.gef	##5320.51	##6403.89	5.09	-0.1455	0.0372	Γ	0.0016	-0.1351	0.037	0.5287	N
S52-48.gef	##5292.00	##6413.93	5.29	-0.1062	0.0356	N	0.01	-0.0414	0.0266	0.3703	β
S52-49.gef	##5319.20	##6428.92	5.54	-0.1237	0.0421	Γ	0.0009	-0.1181	0.042	0.9283	Γ
S52-50.gef	##5291.09	##6438.23	5.74	-0.084	0.0404	N	-0.0024	-0.0996	0.04	0.5319	β
S52-51.gef	##5316.14	##6453.71	3.45	-0.1295	0.029	β	-0.0008	-0.1347	0.029	0.5123	β
CPT-ID	X [m]	Y [m]	Z [m]	μ [-]	σ [-]	dist	a_{tr} [m^{-1}]	b_{tr} [-]	σ_{tr} [-]	θ [m]	dist$_{tr}$

Statistics for tip resistance q_c								
CPT-ID	μ [MPa]	σ [MPa]	dist	a_{tr} [MPa m^{-1}]	b_{tr} [MPa]	σ_{tr} [MPa]	θ [m]	dist$_{tr}$
S51-01.gef	13.62	5.18	β	-1.645	2.928	3.3971	1.0848	β
S51-02.gef	11.11	3.29	Γ	-0.193	9.862	3.2626	0.3259	N
S51-03.gef	14.42	2.9	β	-0.743	9.592	2.3045	0.6953	β
S51-04.gef	13.45	3.87	β	0.12	14.232	3.8579	1.1327	β
S51-05.gef	14.13	3.73	N	-0.423	11.383	3.5876	0.5167	Γ
S51-06.gef	14.41	2.79	N	-0.019	14.286	2.7908	0.3138	N
S51-07.gef	12.89	4.14	N	-0.874	7.2	3.5861	0.9871	N
S51-08.gef	16.57	4.49	Γ	-0.075	16.079	4.4905	0.7964	Γ
S51-09.gef	13.91	3.84	β	-0.671	9.55	3.4915	0.531	β
S51-10.gef	15.3	5.36	β	-0.558	11.671	5.1906	0.7897	β
S51-11.gef	12.68	3.15	β	-0.907	6.783	2.2949	0.1851	β
S51-12.gef	17.9	4.8	β	0.007	17.95	4.7951	0.6932	β
S51-13.gef	14.7	3.92	N	-0.609	10.734	3.6383	0.326	Γ
S51-14.gef	12.73	3.59	β	-1.08	5.684	2.5146	0.8018	N
S51-15.gef	12.6	3.66	N	-0.316	10.545	3.587	0.3324	N
S51-16.gef	14.09	2.78	N	-0.283	12.246	2.6943	0.2304	N
S51-17.gef	15.5	3.39	N	-0.101	14.843	3.3804	0.4491	N
CPT-ID	μ [MPa]	σ [MPa]	dist	a_{tr} [MPa m^{-1}]	b_{tr} [MPa]	σ_{tr} [MPa]	θ [m]	dist$_{tr}$

CPT-ID	μ [MPa]	σ [MPa]	dist	a_{tr} [MPa m^{-1}]	b_{tr} [MPa]	σ_{tr} [MPa]	θ [m]	dist$_{tr}$
S51-18.gef	14.48	4.85	β	-0.617	10.474	4.6196	0.8644	LN
S51-19.gef	16.85	4.18	β	-0.03	16.652	4.1775	0.4867	N
S51-20.gef	11.9	2.98	N	-0.496	8.686	2.7406	0.3196	Γ
S51-21.gef	15.8	3.45	β	0.846	21.294	2.7998	0.3748	β
S51-22.gef	11.74	4.22	Γ	-1.227	3.755	3.0563	0.776	Γ
S51-23.gef	14.03	1.98	β	-0.235	12.498	1.898	0.2851	β
S51-24.gef	13.1	2.9	β	-0.779	8.033	2.239	0.3602	Γ
S51-25.gef	15.81	4.06	Γ	-0.493	12.601	3.8878	0.3844	Γ
S51-26.gef	17.36	4.6	N	-0.698	12.824	4.2938	0.5038	N
S51-27.gef	15.05	2.92	β	-0.003	15.033	2.9161	0.3427	β
S51-28.gef	17.64	4.79	β	-1.046	10.838	4.0885	0.9379	β
S51-29.gef	13.23	2.14	β	-0.43	10.431	1.8852	0.3581	N
S51-30.gef	16.14	5.25	β	-0.916	10.175	4.7784	0.5051	N
S51-31.gef	16.04	5.18	Γ	1.472	25.626	3.8277	0.3571	N
S51-32.gef	16.03	4.44	Γ	-1.038	9.27	3.6926	0.704	N
S51-33.gef	14.18	3.08	β	0.179	15.337	3.0458	0.95	β
S51-34.gef	15.09	2.93	N	0.073	15.564	2.9239	0.5142	N
S51-35.gef	12.64	3.06	β	-0.597	8.76	2.7067	0.7828	β
S51-36.gef	18.07	5.72	β	-1.301	9.615	4.8131	1.0559	β
S51-37.gef	13.26	4.06	β	-0.344	11.017	3.9803	0.6764	β
S51-38.gef	18.68	7.72	β	-1.349	9.916	7.0233	1.2969	β
S51-39.gef	11.98	4.82	Γ	-0.832	6.573	4.3989	1.0714	LN
S51-40.gef	17.26	6.21	β	-1.473	7.682	5.1251	1.2829	β
S51-41.gef	12.77	3.4	N	-0.817	7.456	2.7899	0.733	N
S51-42.gef	13.32	4.98	β	-1.273	5.027	3.9598	0.8646	Γ
S51-43.gef	14.46	7.46	β	-2.309	-0.548	5.0484	1.0896	N
S51-44.gef	12.76	5.19	β	-1.7	1.708	3.252	0.5758	Γ
S51-45.gef	12.37	4.86	β	-1.342	3.642	3.6699	0.4204	Γ
S51-46.gef	11.78	4.21	N	-1.206	3.918	3.0824	0.5822	Γ
S51-47.gef	11.89	3.48	β	-1.13	4.533	2.2277	0.5835	Γ
S51-48.gef	11.03	4.09	β	-1.611	0.539	1.4786	0.2398	Γ
S51-49.gef	10.96	3.24	β	-0.901	5.094	2.4303	0.4079	N
S51-50.gef	12.79	2.88	β	-0.754	7.856	2.2528	0.3551	β
S51-51.gef	10.91	2.28	N	-0.42	8.182	2.0539	0.4035	N
S51-52.gef	12.68	3.19	β	-0.99	6.25	2.1619	0.3036	N
S51-53.gef	13.97	3.17	Γ	-0.027	13.799	3.1661	0.5279	Γ
S51-54.gef	12.86	3.36	N	-0.898	7.04	2.5928	0.7844	N
S51-55.gef	12.51	3.66	N	-0.354	10.203	3.5614	0.5225	β
S51-56.gef	12.74	2.51	N	-0.765	7.75	1.7243	0.2981	N
S51-57.gef	12.94	4.04	β	-0.939	6.838	3.3679	0.7201	Γ
S51-58.gef	12.07	2.74	β	-0.779	6.998	2.023	0.4299	Γ
S51-59.gef	12.13	3.5	β	-0.799	6.925	2.936	1.1841	β
S51-60.gef	12.97	3.87	N	-1.308	4.46	2.3103	0.2906	Γ
S51-61.gef	15.45	5.49	β	-0.55	11.869	5.3338	1.129	β
S51-62.gef	12.44	3.5	β	-1.262	4.222	1.814	0.4047	β
S51-63.gef	18.37	6.66	N	-0.478	15.255	6.5669	1.1553	Γ
S51-64.gef	13.43	3.37	β	-0.924	7.417	2.5529	0.4244	N
S51-65.gef	15.85	6.9	β	0.524	19.259	6.7904	1.0122	β
S51-66.gef	11.3	3.57	β	-1.192	3.555	2.1715	0.3967	N
S51-67.gef	15.23	5.59	β	-0.245	13.634	5.5564	0.7855	Γ
S51-68.gef	10.67	3.03	β	-0.458	7.688	2.8321	0.5965	β
S51-69.gef	12.65	2.86	Γ	-0.508	9.344	2.5887	0.29	β
S51-70.gef	13.92	3.49	β	-0.446	11.022	3.329	0.3951	N
S51-71.gef	13.14	3.53	β	-0.285	11.284	3.4656	0.7297	β
S51-72.gef	13.81	2.94	N	-0.052	13.466	2.9391	0.2677	N
S51-73.gef	14.53	3.71	Γ	-0.737	9.738	3.2729	0.7318	Γ
S51-74.gef	13.88	2.74	N	0.157	14.902	2.7118	0.4158	N
S51-75.gef	14.14	2.54	Γ	-0.148	13.171	2.5188	0.2295	β
S51-76.gef	13.2	3.5	N	-0.829	7.811	2.8933	0.7264	Γ
S51-77.gef	15.28	3.11	β	0.311	17.304	3.023	0.773	β
S51-78.gef	12.62	3.59	N	-0.902	6.75	2.8778	0.333	N
CPT-ID	μ [MPa]	σ [MPa]	dist	a_{tr} [MPa m^{-1}]	b_{tr} [MPa]	σ_{tr} [MPa]	θ [m]	dist$_{tr}$

CPT-ID	μ [MPa]	σ [MPa]	dist	a_{tr} [MPa m^{-1}]	b_{tr} [MPa]	σ_{tr} [MPa]	θ [m]	dist$_{tr}$
S51-79.gef	15.87	3.29	N	0.13	16.717	3.2725	0.3745	N
S51-80.gef	12.7	3.32	β	-0.248	11.083	3.2651	0.7255	N
S51-81.gef	15.59	3.9	N	-0.357	13.27	3.8038	0.2983	N
S51-82.gef	15.02	3.73	N	0.443	17.902	3.578	0.5232	N
S51-83.gef	19.55	7.48	Γ	1.214	27.456	6.8988	0.9832	N
S51-84.gef	14.3	4.25	Γ	0.143	15.228	4.2382	0.7562	Γ
S51-85.gef	15.8	5.03	Γ	0.29	17.692	4.9852	0.6685	Γ
S51-86.gef	13.25	3.11	Γ	0.25	14.883	3.0517	0.7231	Γ
S51-87.gef	16.98	6.91	Γ	0.921	22.982	6.5523	1.0596	β
S51-88.gef	14.1	4.8	Γ	1.456	23.554	3.3146	0.6255	Γ
S51-89.gef	14.74	5.76	Γ	1.963	27.503	3.3954	0.5823	N
S52-01.gef	15.66	7.95	β	-1.318	7.088	7.3052	1.375	Γ
S52-02.gef	9.32	3.1	β	-0.381	6.841	2.9651	0.3854	β
S52-03.gef	12.62	4.18	β	-0.448	9.709	4.0421	0.7417	β
S52-04.gef	10.4	2.8	β	-0.758	5.474	2.142	0.4187	N
S52-05.gef	9.39	3.11	β	-0.802	4.18	2.45	0.375	N
S52-06.gef	10.76	3.11	Γ	-0.253	9.109	3.0488	0.9132	Γ
S52-07.gef	13.35	3.29	N	-0.117	12.587	3.2831	0.5715	N
S52-08.gef	14.35	4.73	Γ	-1.205	6.509	3.7671	0.5296	N
S52-09.gef	13.6	4.89	β	-0.551	10.007	4.7105	0.9012	β
S52-10.gef	19.65	5.15	β	-0.264	17.932	5.1123	0.8095	N
S52-11.gef	13.77	5.07	β	-0.241	12.2	5.0357	0.8159	β
S52-12.gef	13.1	4.96	β	-0.949	6.922	4.4209	1.2457	β
S52-13.gef	11.97	4.54	Γ	0.906	17.875	4.004	0.7716	β
S52-14.gef	18.36	3.47	β	-0.068	17.914	3.4662	0.7914	β
S52-15.gef	18.27	8.55	LN	2.554	34.902	6.0257	0.7946	β
S52-16.gef	14.66	2.69	N	0.049	14.979	2.6874	0.8638	N
S52-17.gef	17.4	5.92	Γ	1.534	27.375	4.6624	0.471	β
S52-18.gef	16	5.18	Γ	1.265	24.224	4.22	0.8125	Γ
S52-19.gef	15.15	6.24	Γ	1.885	27.406	4.3414	0.5764	Γ
S52-20.gef	13.58	2.89	Γ	0.215	14.978	2.8395	0.7179	Γ
S52-21.gef	13.72	3.96	β	1.001	20.239	3.162	0.6144	β
S52-22.gef	13.23	3.57	LN	0.861	18.838	2.9217	0.772	Γ
S52-23.gef	13.54	2.53	β	0.422	16.282	2.3195	0.7933	Γ
S52-24.gef	10.26	2.21	N	-0.447	7.356	1.944	0.4705	N
S52-25.gef	11.7	1.95	N	0.015	11.793	1.9525	0.4038	N
S52-26.gef	11.17	3.22	β	-0.85	5.666	2.5131	0.4841	Γ
S52-27.gef	11.83	1.9	Γ	0.158	12.857	1.859	0.4357	Γ
S52-28.gef	16.13	9.14	LN	-3.104	-4.017	5.4043	0.6926	β
S52-29.gef	14.02	4.92	β	-1.276	5.71	3.8732	0.7976	Γ
S52-30.gef	12.98	4.96	Γ	-1.671	2.125	2.9816	0.4695	Γ
S52-31.gef	15.32	4.01	β	-0.074	14.841	4.0091	0.7822	β
S52-32.gef	15.21	4.5	β	-0.862	9.613	4.0117	0.6991	Γ
S52-33.gef	15.35	3.17	N	0.605	19.292	2.8215	0.3265	Γ
S52-34.gef	12.8	2.47	N	-0.54	9.289	2.1136	0.3248	N
S52-35.gef	14.68	4.23	N	1.189	22.411	3.1467	0.3778	β
S52-36.gef	12.25	2.63	N	-0.454	9.299	2.3987	0.621	N
S52-37.gef	14.43	3.54	Γ	0.529	17.873	3.3142	0.7508	β
S52-38.gef	13.95	3.89	Γ	-0.33	11.8	3.8066	0.3431	Γ
S52-39.gef	14.45	3.63	β	0.517	17.807	3.414	0.5881	β
S52-40.gef	13.03	3.64	Γ	-0.449	10.107	3.4752	0.5088	β
S52-41.gef	9.96	2.61	β	0.687	14.436	2.03	0.6253	β
S52-42.gef	13.86	4.14	β	-1.045	7.064	3.319	0.7389	β
S52-43.gef	13.99	2.86	N	0.482	17.133	2.6184	0.2021	N
S52-44.gef	12.14	3.66	Γ	-0.515	8.782	3.4473	0.6849	Γ
S52-45.gef	13.98	3.28	N	0.068	14.424	3.2793	0.5432	N
S52-46.gef	12.05	4.01	β	-1.49	2.347	1.8733	0.2071	N
S52-47.gef	15.25	3.82	β	-0.747	10.393	3.3792	0.4286	N
S52-48.gef	12.02	4.04	Γ	-1.415	2.823	2.2457	0.4746	Γ
S52-49.gef	13.92	3.87	β	-0.637	9.775	3.564	0.9223	β
S52-50.gef	10.76	3.27	Γ	-0.22	9.33	3.2294	0.5402	Γ
CPT-ID	μ [MPa]	σ [MPa]	dist	a_{tr} [MPa m^{-1}]	b_{tr} [MPa]	σ_{tr} [MPa]	θ [m]	dist$_{tr}$

CPT-ID	μ [MPa]	σ [MPa]	dist	a_{tr} [MPa m^{-1}]	b_{tr} [MPa]	σ_{tr} [MPa]	θ [m]	dist$_{tr}$
S52-51.gef	10.87	2.55	β	-0.65	6.642	2.03	0.4574	β
CPT-ID	μ [MPa]	σ [MPa]	dist	a_{tr} [MPa m^{-1}]	b_{tr} [MPa]	σ_{tr} [MPa]	θ [m]	dist$_{tr}$

Appendix E

Elaboration on conditioning

E.1 Derivation of Ordinary Kriging equations

Kriging is a unbiased interpolation method, that interpolates a field at location x_0 as a linear combination of all known field locations $Z(x_\alpha)$. The krigedestimated value of the field $Z(x)$ at location x_0 is denoted as $Z^*(x_0)$, the Kriged field in general as Z^*. The kriging estimation is a weighted average of the conditioning points $Z(x_\alpha)$ by weights w_α. The unbiased estimation of the kriging requires the weights w_α to sum up to 1;

$$Z^*(x_0) = \sum_{\alpha=1}^{n} w_\alpha Z(x_\alpha), \qquad \text{with} \qquad \sum_{\alpha=1}^{n} w_\alpha = 1 \tag{E.1}$$

Next to the requirement of an unbiased estimator, kriging is the best linear estimator of the field between the conditioning points $Z(x_\alpha)$. It is the best estimator in the sense that it finds solution for a kriged field that has the lowest expected error with respect to the true field. The variance of the error $var(Z^* - Z)$ is used to quantify the error. With the help of the unbiasedness of the kriged results and equation E.1, the variance of the kriging error

$$\begin{aligned} \sigma_E^2 = var(Z^* - Z) &= E\left[(Z^* - Z)^2\right] + \left(E[Z^* - Z]\right)^2 \\ &= E\left[(Z^* - Z)^2\right] + 0 \\ &= E\left[Z^{*2}\right] - 2E\left[Z^* Z\right] + E\left[Z^2\right] \end{aligned} \tag{E.2}$$

can be rewritten into

$$\sigma_E^2 = var(Z^* - Z) = \sum_{\alpha=1}^{n}\sum_{\beta=1}^{n} \omega_\alpha \omega_\beta C(|x_\alpha - x_\beta|) - 2\sum_{\alpha=1}^{n} w_\alpha C(|x_\alpha - x_0|) + C(0). \tag{E.3}$$

Because the sum of the weights equal 1, this equation can be rewritten into:

$$\begin{aligned} \sigma_E^2 &= \sum_{\alpha=1}^{n}\sum_{\beta=1}^{n} \omega_\alpha \omega_\beta (C(|x_\alpha - x_\beta|) - \sigma^2) - 2\sum_{\alpha=1}^{n} w_\alpha (C(|x_\alpha - x_0|) - \sigma^2) + (C(0) - \sigma^2) \\ &= -\sum_{\alpha=1}^{n}\sum_{\beta=1}^{n} \omega_\alpha \omega_\beta \gamma(|x_\alpha - x_\beta|) + 2\sum_{\alpha=1}^{n} w_\alpha \gamma(|x_\alpha - x_0|) + \gamma(|x_0 - x_0|). \end{aligned} \tag{E.4}$$

To minimise this error variance, the first order partial derivatives need to be set to zero. The condition on the weights can be satisfied using the method of Lagrange. In this method an objective function $\phi(w_\alpha, \mu)$ is defined introducing the Lagrange parameter μ and containing the condition on the weights:

$$\phi(w_\alpha, \mu) = \sigma_E^2 = \sigma_E^2 - 2\mu\left(\sum_{\alpha=1}^{n} w_\alpha - 1\right). \tag{E.5}$$

The partial derivatives of this function $\phi(w_\alpha, \mu)$ with respect to all weights w_α and μ are put to 0 to find the weights . This leads to a system of equations of size $n+1$ that can be solved to find the correct weights $w_\alpha(x_\alpha, x_0) = \lambda_\alpha^{OK}$ and $\mu = \mu_{OK}$. The result is the ordinary kriging system of equation 5.16:

$$\begin{pmatrix} \gamma(x_1-x_1) & \cdots & \gamma(x_1-x_n) & 1 \\ \vdots & \ddots & \vdots & \vdots \\ \gamma(x_n-x_1) & \cdots & \gamma(x_n-x_n) & 1 \\ 1 & \cdots & 1 & 0 \end{pmatrix} \begin{pmatrix} \lambda_1^{OK} \\ \vdots \\ \lambda_n^{OK} \\ \mu^{OK} \end{pmatrix} = \begin{pmatrix} \gamma(x_1-x_0) \\ \vdots \\ \gamma(x_n-x_0) \\ 1 \end{pmatrix} \quad \text{(eq. 5.16)} \tag{E.6}$$

The weights w_α that satisfy the condition of unbiasedness and best estimation are denoted with λ_α. The correlation structure is given in the form of a variogram $\gamma(h) = \sigma^2 - C(h)$.

E.2 Estimation variance

From the OK-system (equation 5.16,E.6) it can be derived that:

$$\mu^{OK} = -\sum_{\beta=1}^{n} \lambda_\beta \gamma(|x_\alpha - x_\beta|) + \gamma(|x_\alpha - x_0|) \tag{E.7}$$

Substitution of this expression of the Lagrange parameter into equation E.3 can be reworked into the equation for the estimation variance σ_E^2. This estimation variance is the variance of the difference between fields Z anx $Z*$, which is the OK-variance as given in equation 5.17:

$$\sigma_{OK}^2 = \gamma(0) + \mu_{OK} + \sum_{\alpha=1}^{n} \lambda_\alpha \gamma(|x_\alpha - x_0|) \tag{E.8}$$

When the OK-system is written in the form

$$\Gamma\lambda = \gamma \tag{E.9}$$

and a possible nugget effect of $\gamma(0) \neq 0$ is ignored, the kriging variance is given by

$$\sigma_{OK}^2 = (\Gamma^{-1}\gamma)^T\gamma, \tag{E.10}$$

in which Γ^{-1} denotes the inverse matrix to Γ and x^T is the matrix transponent to x.
The derivation of the equations for ordinary kriging or any other kriging method goes in a similar way as demonstrated for ordinary kriging. It is possible to keep the covariance function $C(h)$ in the kriging system. Problem with this is that $C(0)$ does not drop out the equations where $\gamma(0)$ does.

E.3 Matlab calculation time

To check the computational expence of matlab operators, the following graph was produced to support table 5.1. To be able to focus on the domain of the graph with large numbers of cell, it is choosen not to produce a log-log plot, but plot a power function of the computation time t to linearise the function. Because computation time for small numbers n are less accurate than for larger numbers, no loglog-plots are used to give a line. Instead of a loglog-plot the time t is given as $t^{1/k}$ when a relation $t = n^k$ was expected. In this way the focus is on the part of the graph with larger n.

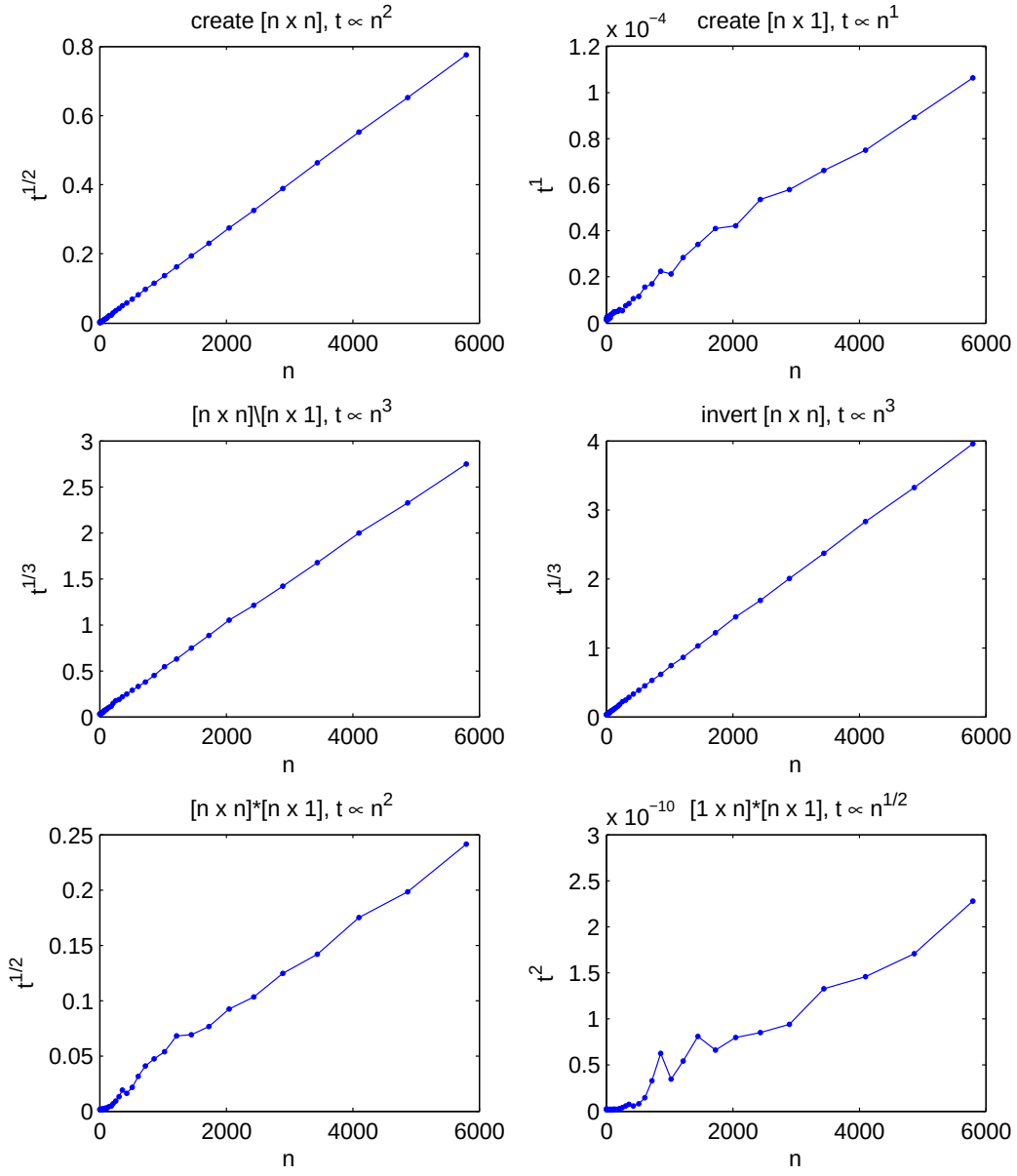

Figure E.1: Experimental calculation time for different operations in Matlab determined with matrices produced with random numbers.

E.4 Realisations of simulated fields

The realisations of simulated fields conditioned by CPT S51.18 and S51.20 taht are discussed in section 5.4.6 are given in this section. The assumed correlation structure is approximate exponential. The geometry input is:

- cell domain: 0.05*0.05m^2
- conditioning spacing: 0.40m
- θ_v: 0.63m
- ξ: 5,10,20,50
- σ: 0.038
- field domain: (-40;-10.6) (40;-2.4)
- conditioned by CPT's: $S51.18, S51.20$

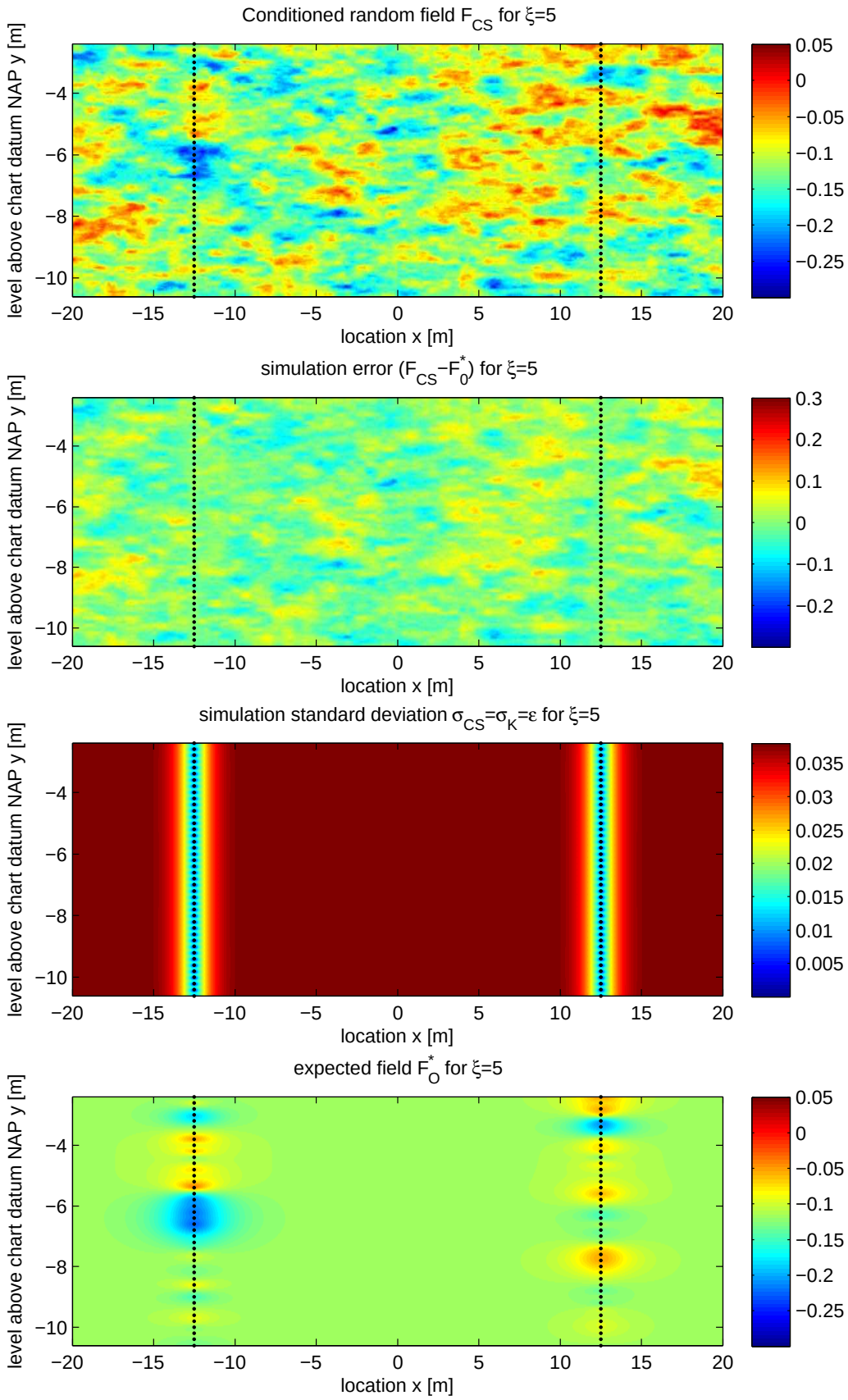

Figure E.2: Realisation of conditional simulation of a field conditioned by two stationary conditioning profiles for $\xi = 5$.

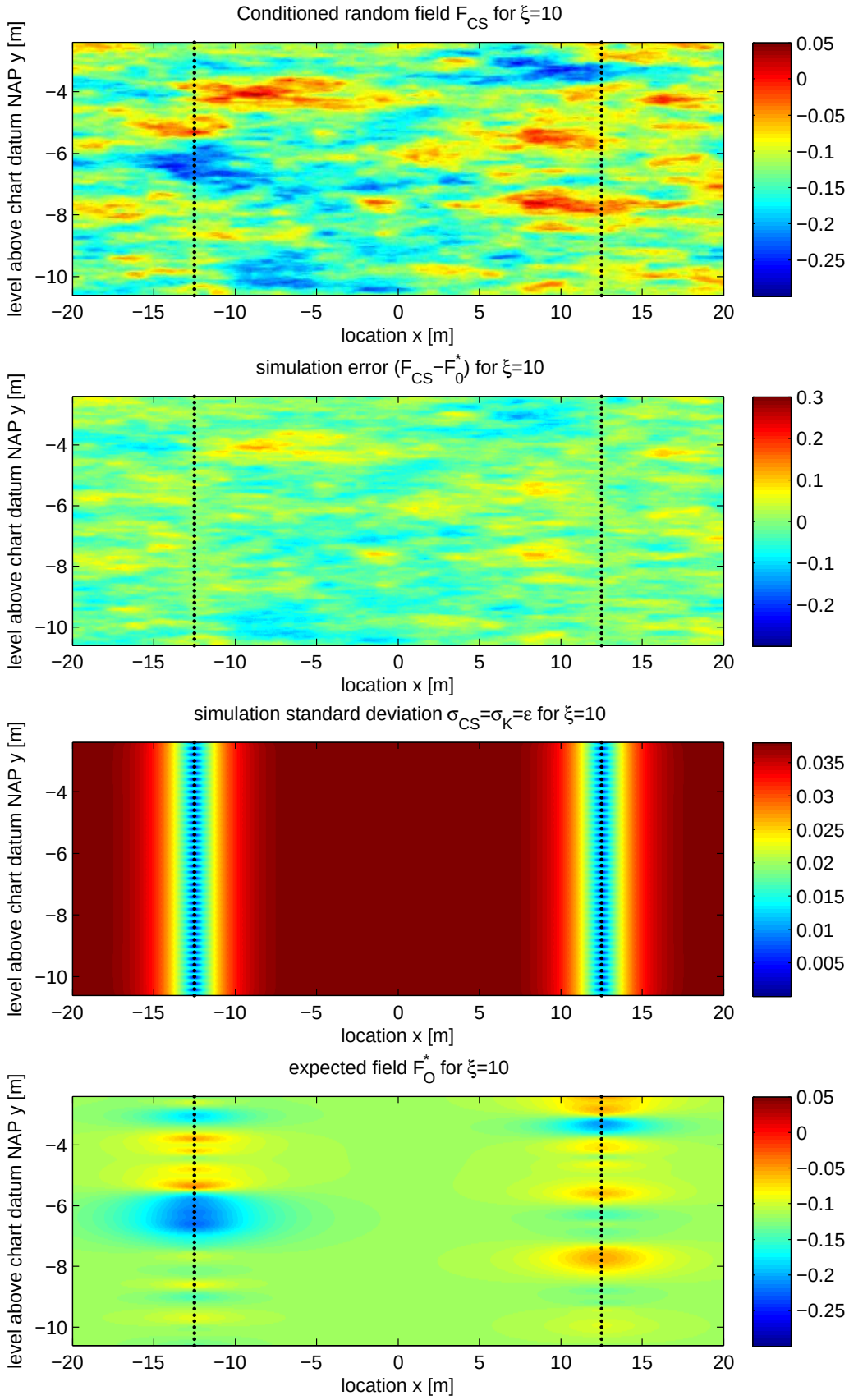

Figure E.3: Realisation of conditional simulation of a field conditioned by two stationary conditioning profiles for $\xi = 10$.

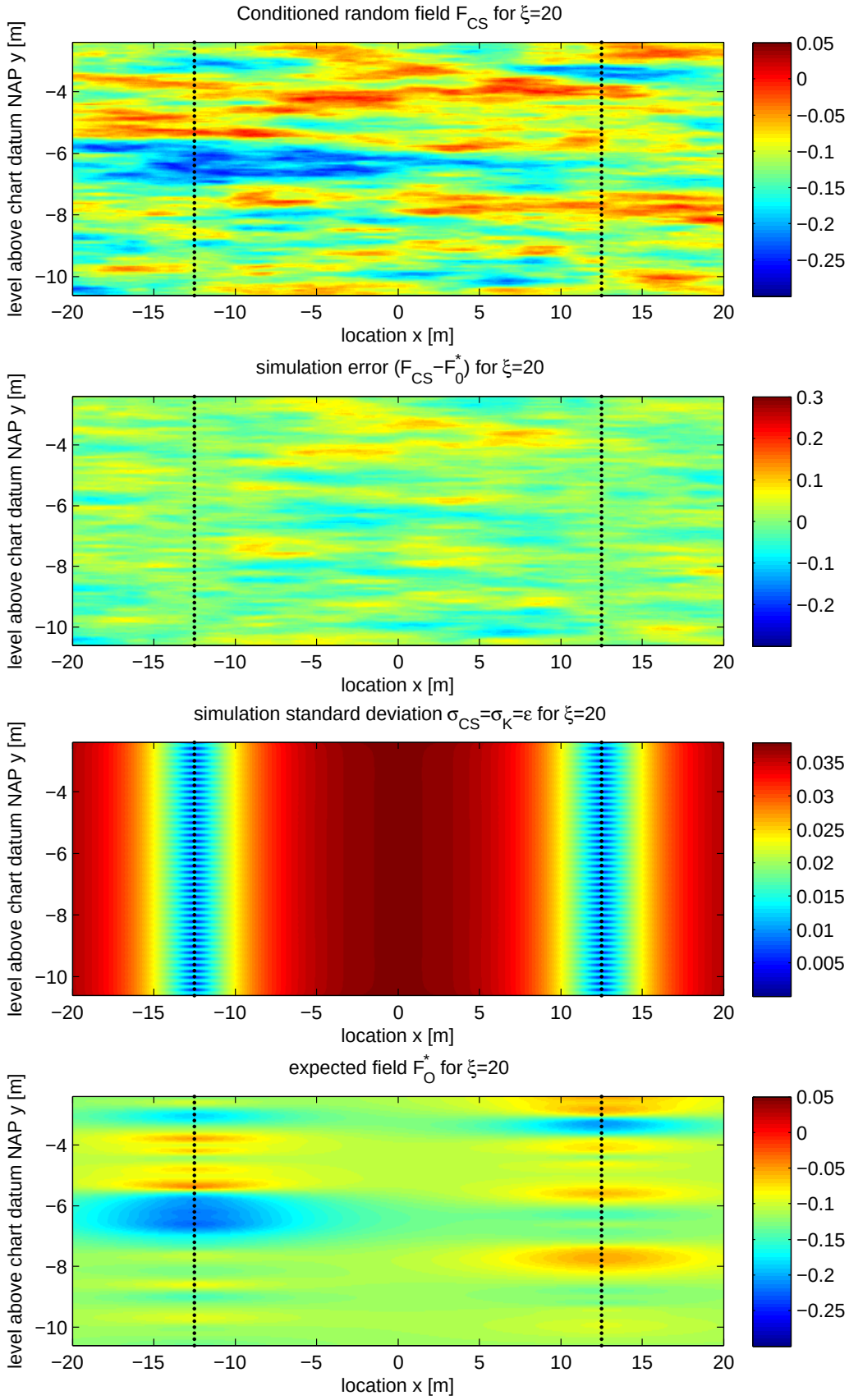

Figure E.4: Realisation of conditional simulation of a field conditioned by two stationary conditioning profiles for $\xi = 20$.

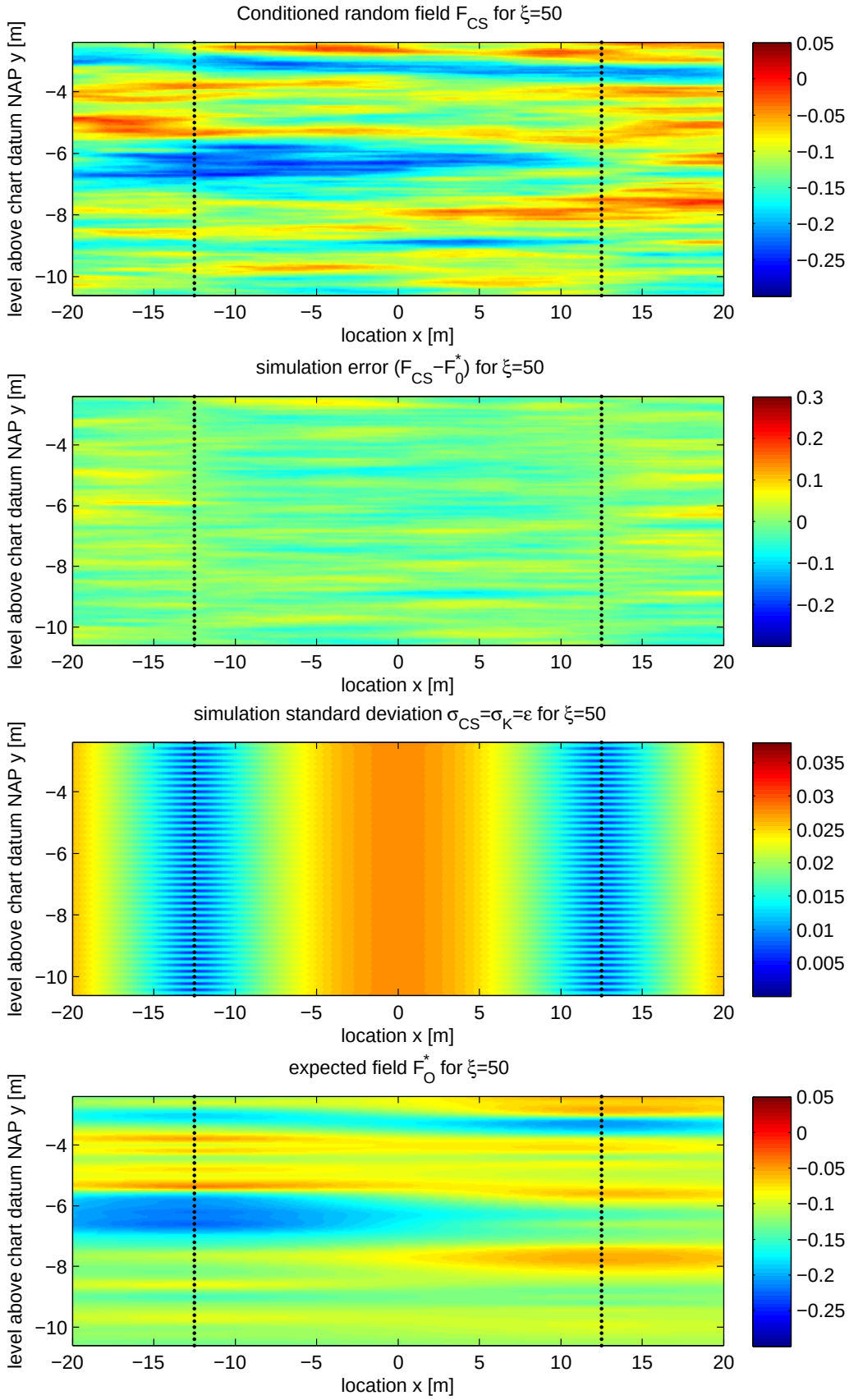

Figure E.5: Realisation of conditional simulation of a field conditioned by two stationary conditioning profiles for $\xi = 50$.

E.5 Realisations of simulated fields with depth trend

The realisations of simulated fields conditioned by CPT's $S51.01$, $S51.03$, $S51.05$ and $S51.07$ are given in this section. The assumed correlation structure is approximate exponential. The geometry input used is:

- cell domain: 0.05*0.05m^2
- conditioning spacing: 0.40m
- θ_v: 0.63m
- ξ: 5,10,20,50
- σ: 0.038
- field domain: (-40;-10.6) (40;-2.4)
- conditioned by CPT's: $S51.01, S51.03, S51.05, S51.07$

Results are given on the nexp pages:

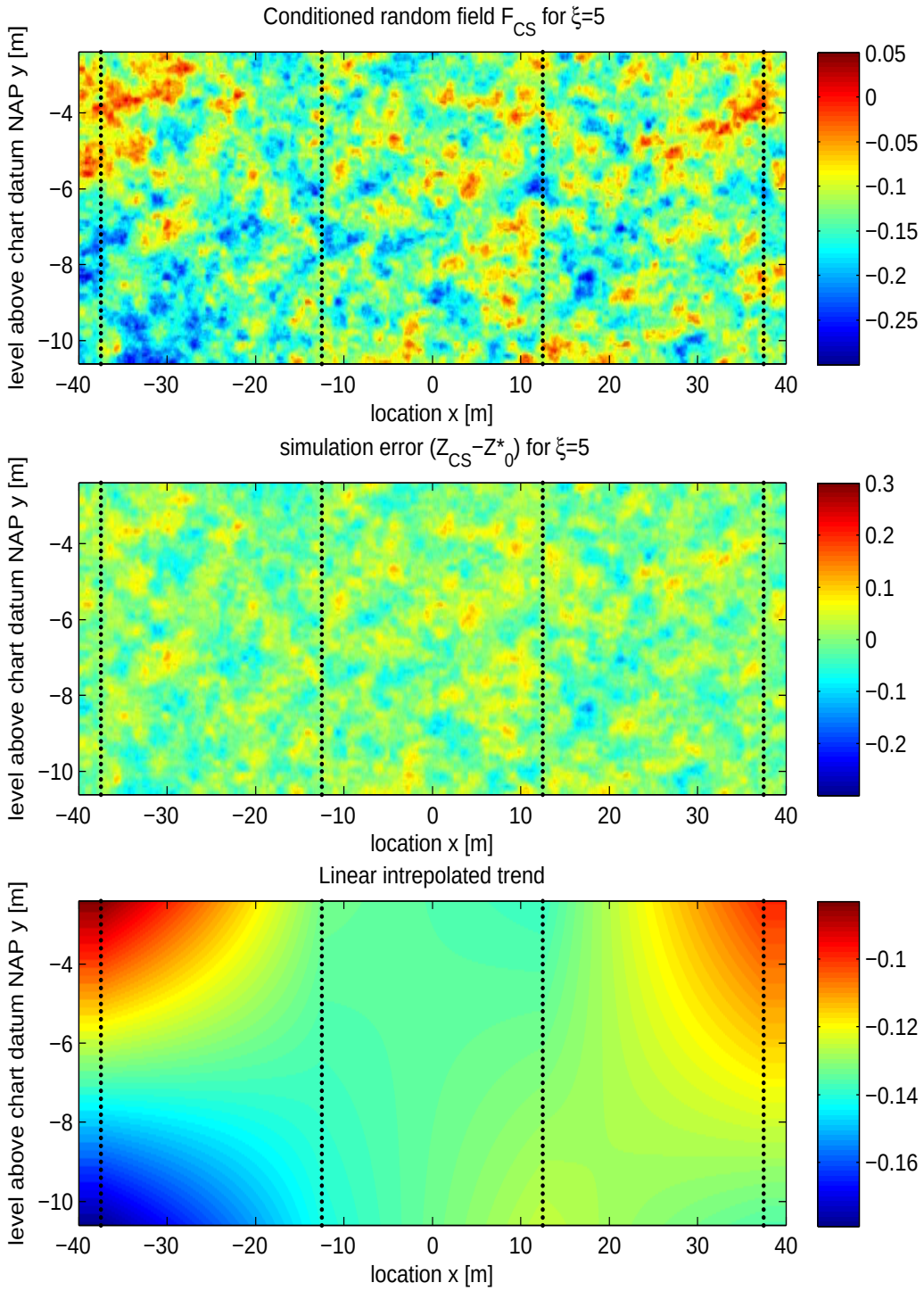

Figure E.6: A: Conditioned simulation of field F_{CS}, B: Variability in simulated field with respect to kriged estimation F_{CS}-F_{0K} C)

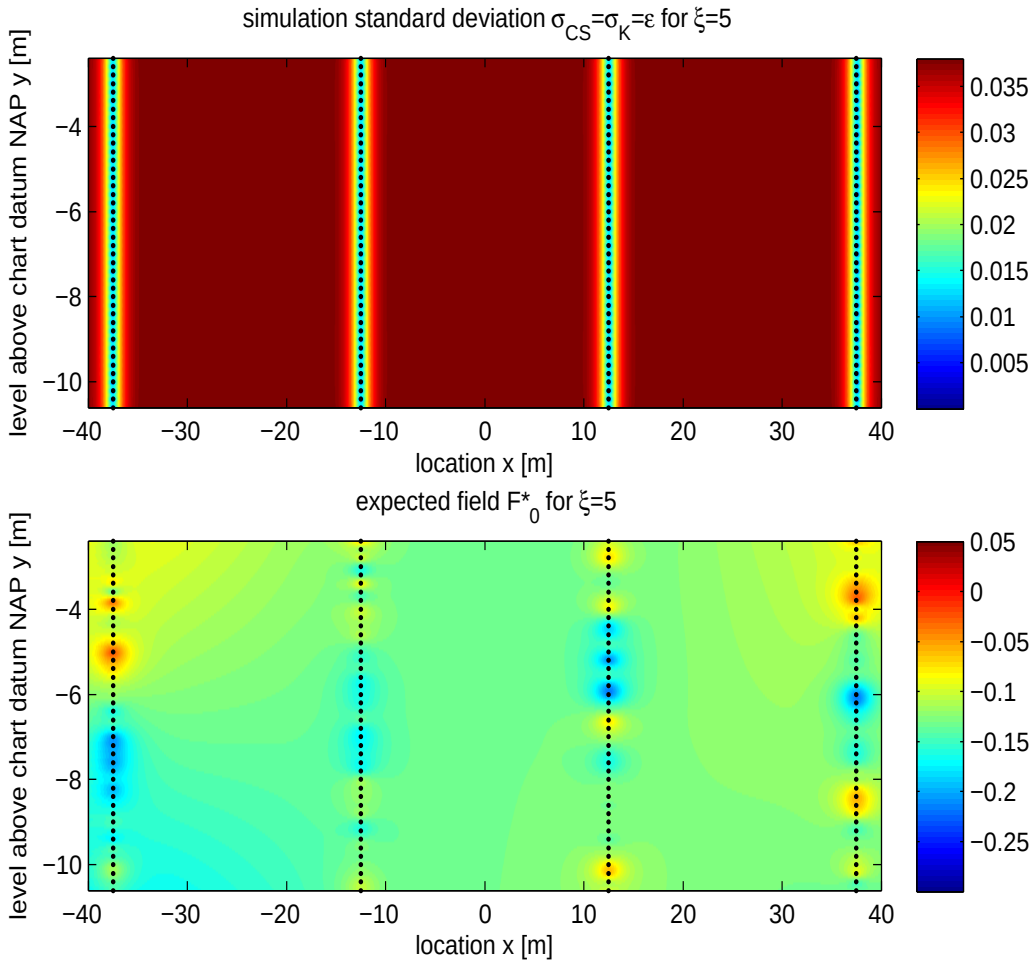
simulation standard deviation σCS=σK=ε for ξ=5
level above chart datum NAP y [m]
location x [m]
0.035
0.03
0.025
0.02
0.015
0.01
0.005
expected field F*0 for ξ=5
level above chart datum NAP y [m]
location x [m]
0.05
0
−0.05
−0.1
−0.15
−0.2
−0.25

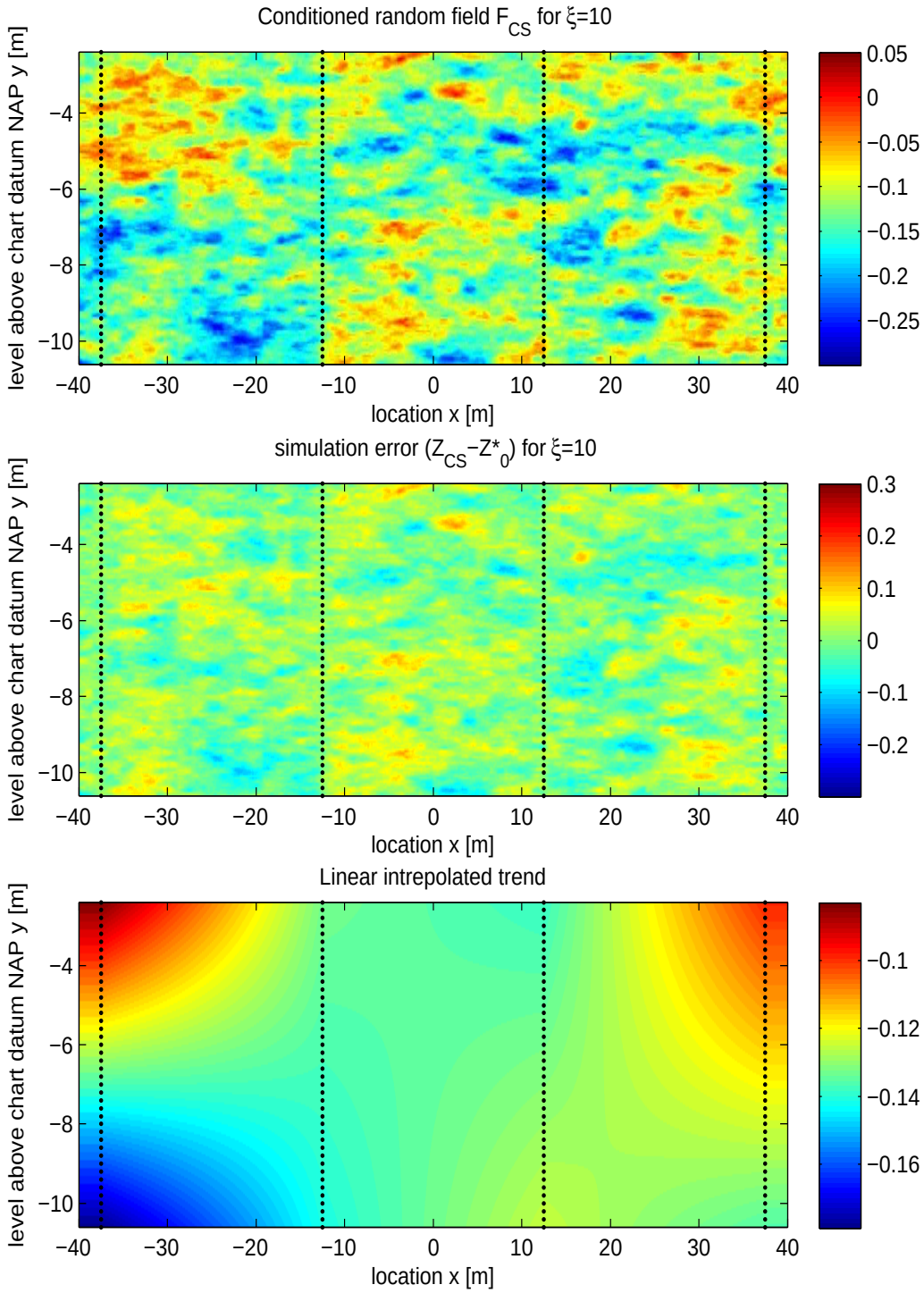
Conditioned random field F_CS for ξ=10
level above chart datum NAP y [m]
location x [m]
simulation error (Z_CS−Z*_0) for ξ=10
level above chart datum NAP y [m]
location x [m]
Linear intrepolated trend
level above chart datum NAP y [m]
location x [m]

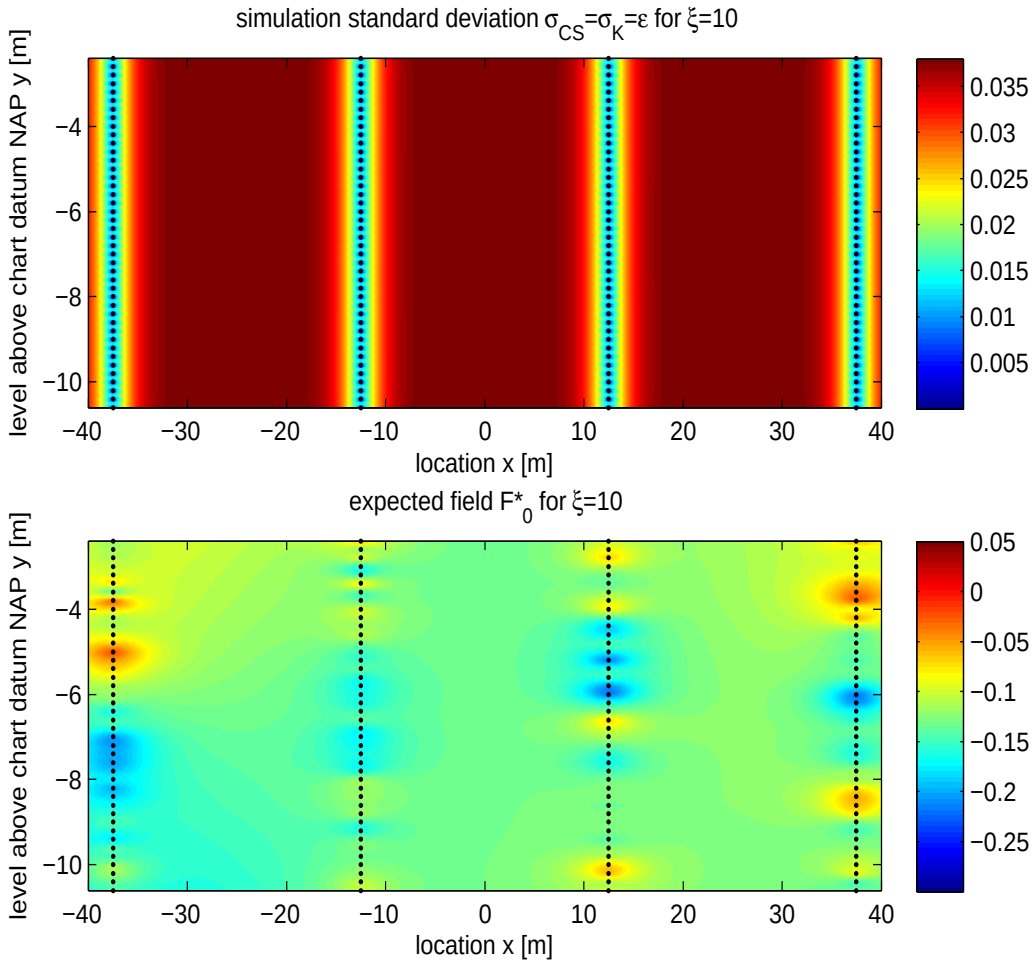
simulation standard deviation σCS=σK=ε for ξ=10
level above chart datum NAP y [m]
−4
−6
−8
−10
−40
−30
−20
−10
0
10
20
30
40
location x [m]
0.035
0.03
0.025
0.02
0.015
0.01
0.005
expected field F*0 for ξ=10
level above chart datum NAP y [m]
location x [m]
0.05
0
−0.05
−0.1
−0.15
−0.2
−0.25

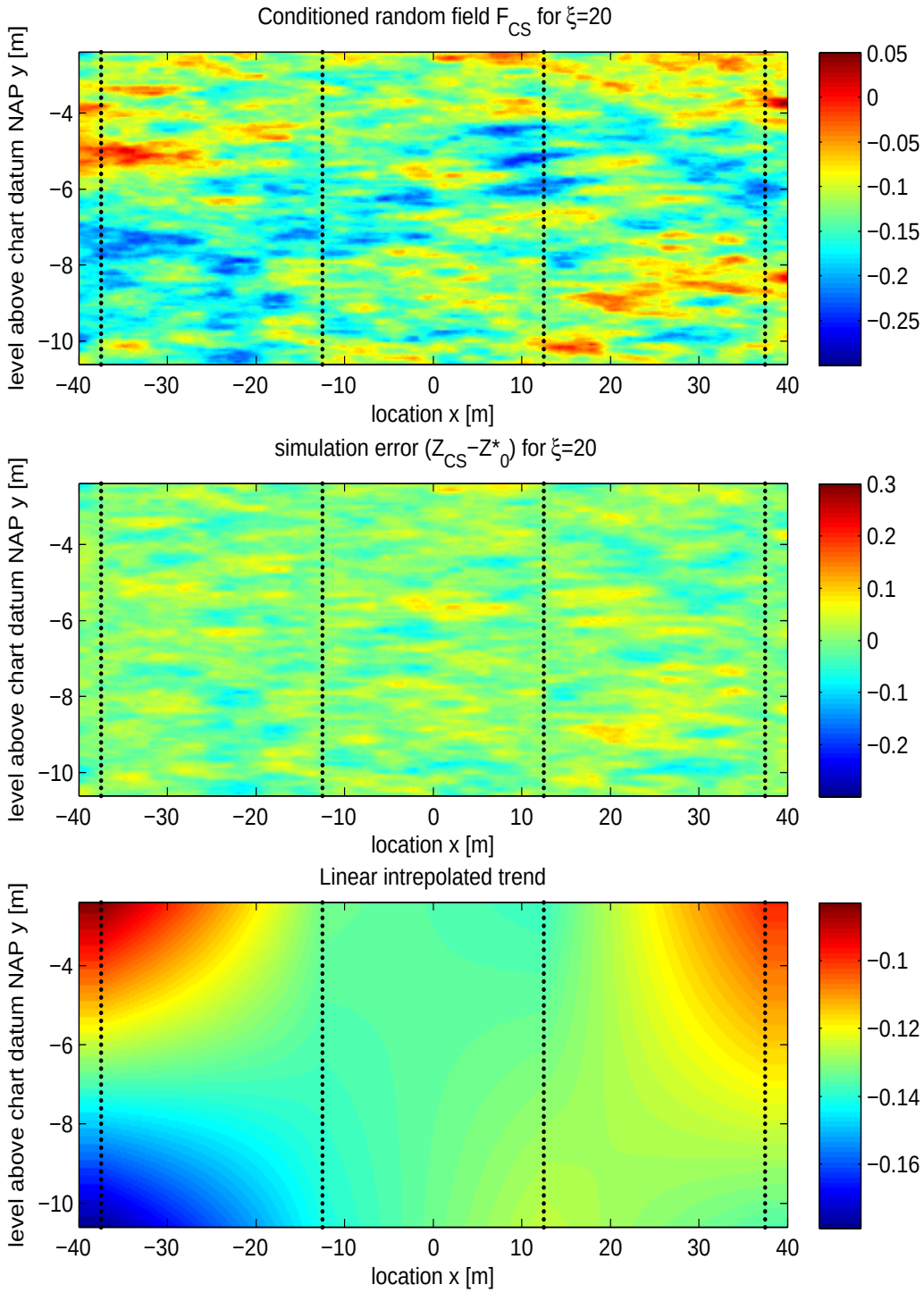
Conditioned random field F_CS for ξ=20
level above chart datum NAP y [m]
location x [m]
simulation error (Z_CS−Z*_0) for ξ=20
level above chart datum NAP y [m]
location x [m]
Linear intrepolated trend
level above chart datum NAP y [m]
location x [m]

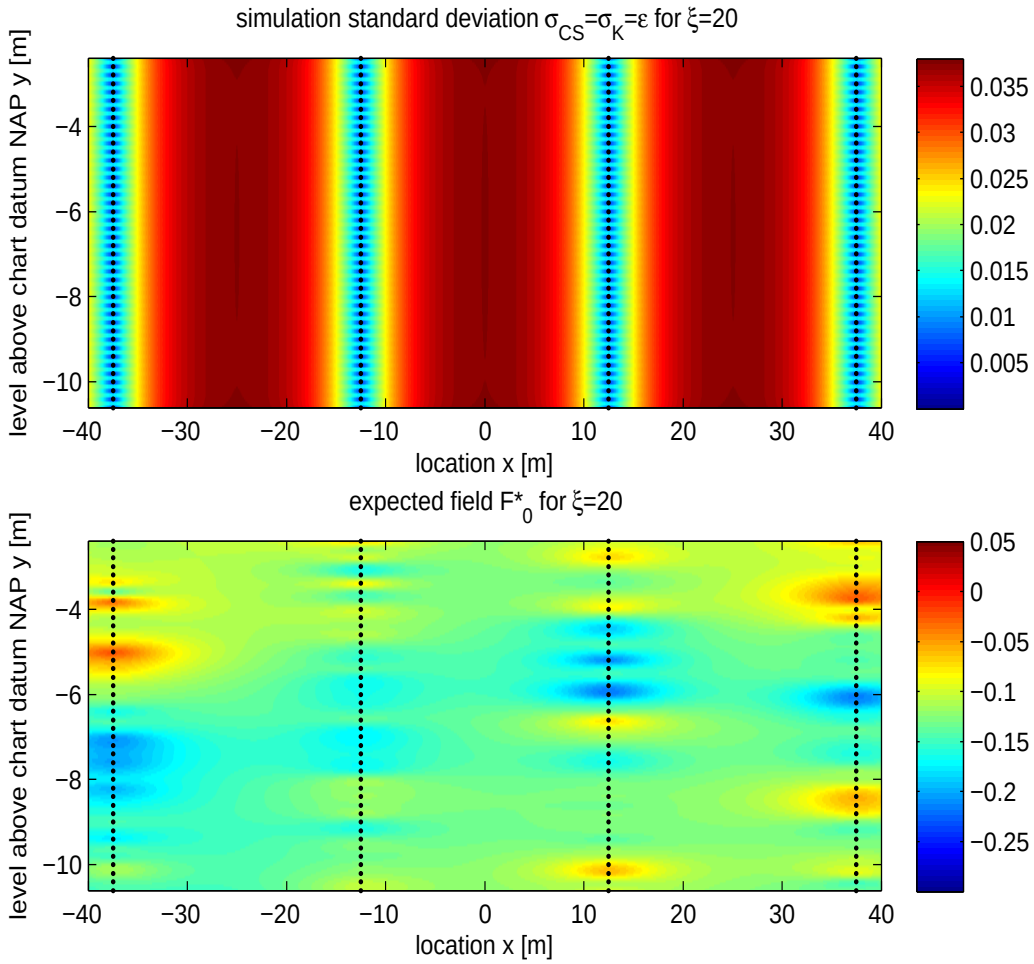
simulation standard deviation σCS=σK=ε for ξ=20
level above chart datum NAP y [m]
−4
−6
−8
−10
−40
−30
−20
−10
0
10
20
30
40
location x [m]
0.035
0.03
0.025
0.02
0.015
0.01
0.005
expected field F*0 for ξ=20
level above chart datum NAP y [m]
location x [m]
0.05
0
−0.05
−0.1
−0.15
−0.2
−0.25

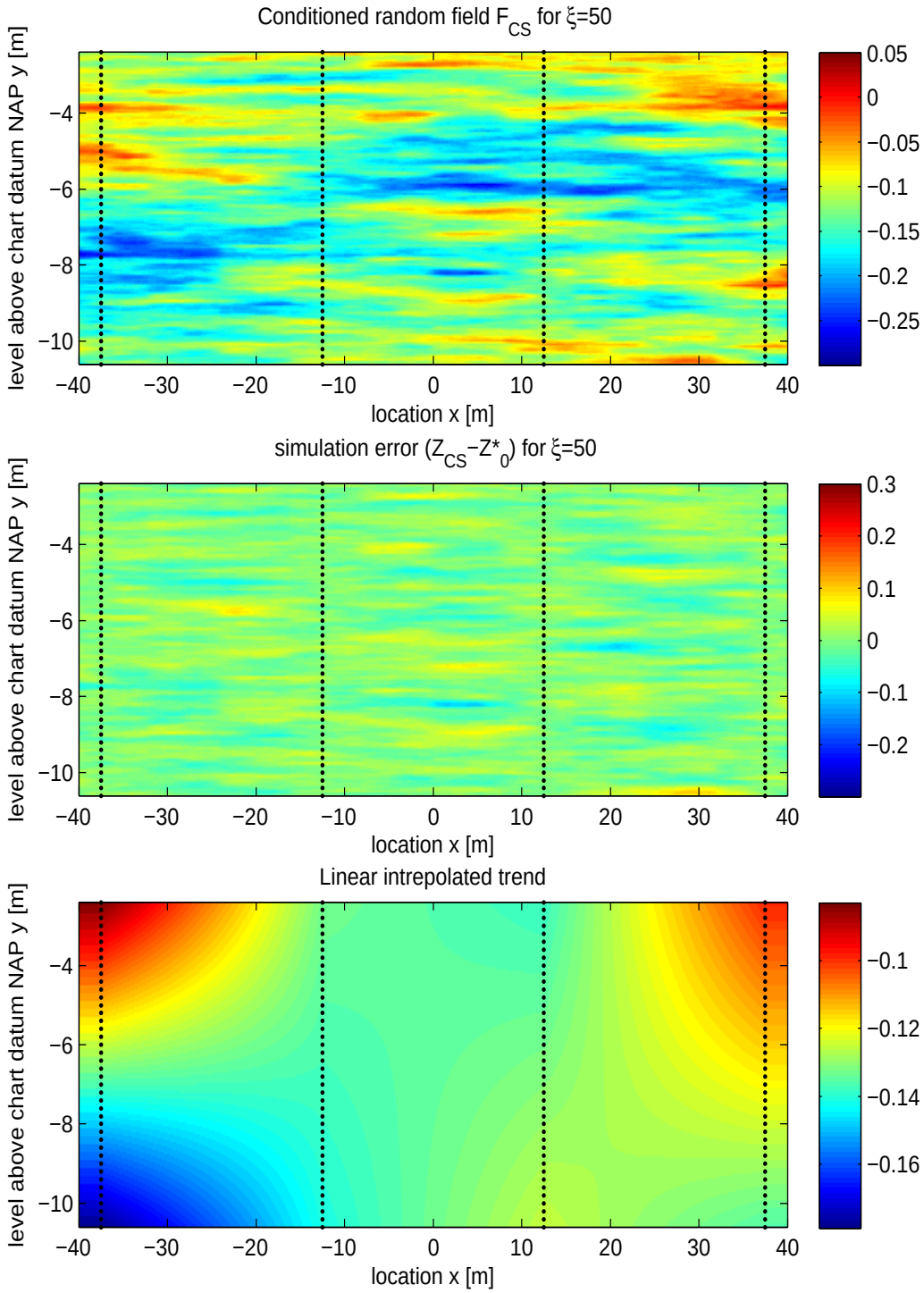
Conditioned random field F_CS for ξ=50
level above chart datum NAP y [m]
location x [m]
simulation error (Z_CS−Z*_0) for ξ=50
level above chart datum NAP y [m]
location x [m]
Linear intrepolated trend
level above chart datum NAP y [m]
location x [m]

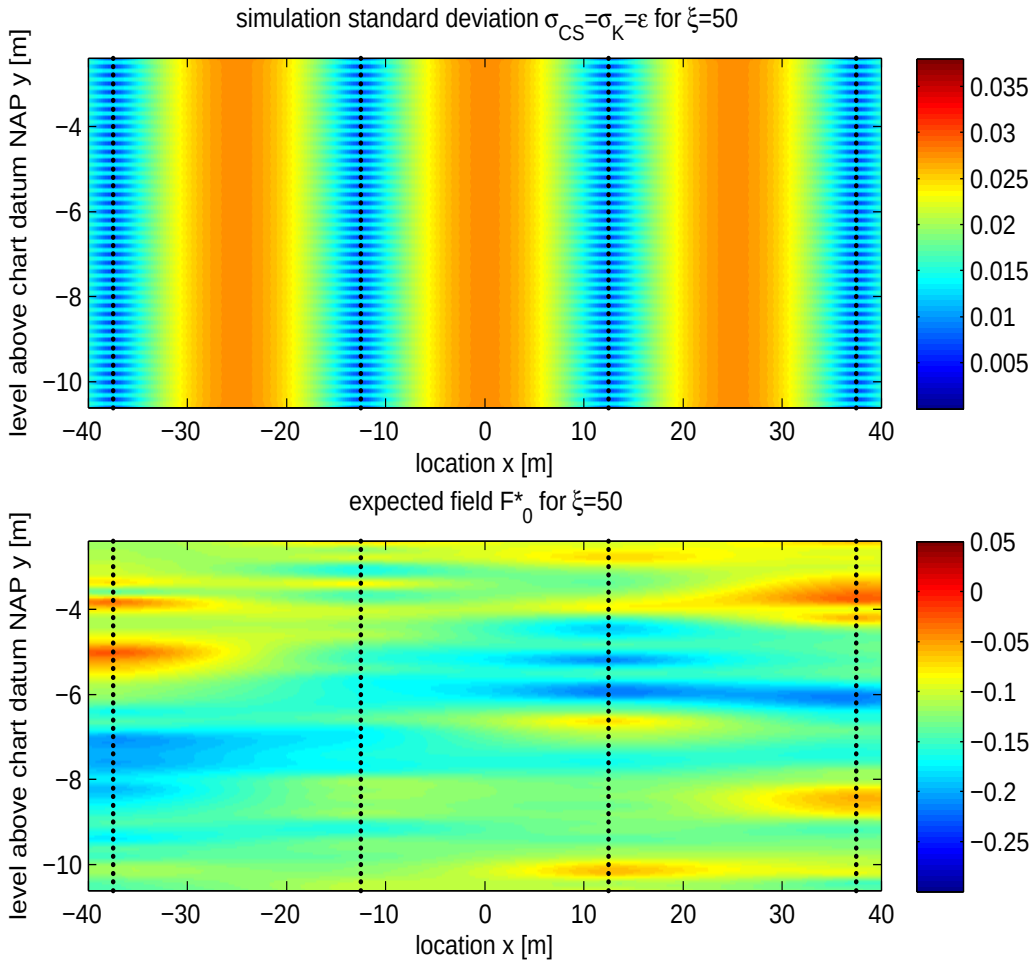

E.5.1 Dealing with variable depth trends

With the problem of adding the trend to the zero-mean conditioned simulations Z^*, the horizontal variation in the trend is subject to discussion. Because the trend in the different conditioning profiles is not necessarily the same, the trend on which the zero-mean stationary field Z^* needs to be mapped is not only depth dependent, but depends on the lateral position as well. At the exact locations of the profiles, the trend that needs to be added is the exact trend that previously was removed from the profile. What trend has to be added to the field in between the conditioning profiles is unknown and different options are possible. The different options are discussed in this section.

Reconsider the profiles in the form of $P(y) = ay + b + Z(y)$ from which the first order stationary trend removed profiles $Z(x)$ were used for the simulation of trend-removed, zero mean stationary fields $Z^*(y)$. For all profiles the values a and b that describe the trend are gathered and from the functions $a(x)$ and $b(x)$ the lateral variation in the trend can be examined. In figure E.7 the trend parameters $a(x)$ and $b(x)$ are given as a function of their lateral relative position. With this figure in mind, there are several options to deal with the trends:

- Krige the trend parameters between the profiles and map the stationary field on top of the trend field that can be constructed with the kriged parameters.
- Interpolate the trend parameters between the profiles and map the stationary field on top of the trend field that can be constructed with the interpolated parameters.
- Determine the mean trend parameters $\bar{a}$ and $\bar{b}$ over all profiles P. Use the mean trend parameters to reduce $P(y) = \bar{a}y + \bar{b} + Z(y)$ to $Z(y)$ and add the depth trend (that in this case only depends on the depth y) to the mean zero stationary field simulation $Z*(x, y)$ that was generated with the statistics of $Z^*(y)$.

Figure E.7 shows the trend parameters a and b determined from one line of CPT's. The moving average line gives a larger-scale trend in the parameters. The moving average is done for an averaging domain of 200m (9 CPT's) with equal weights.

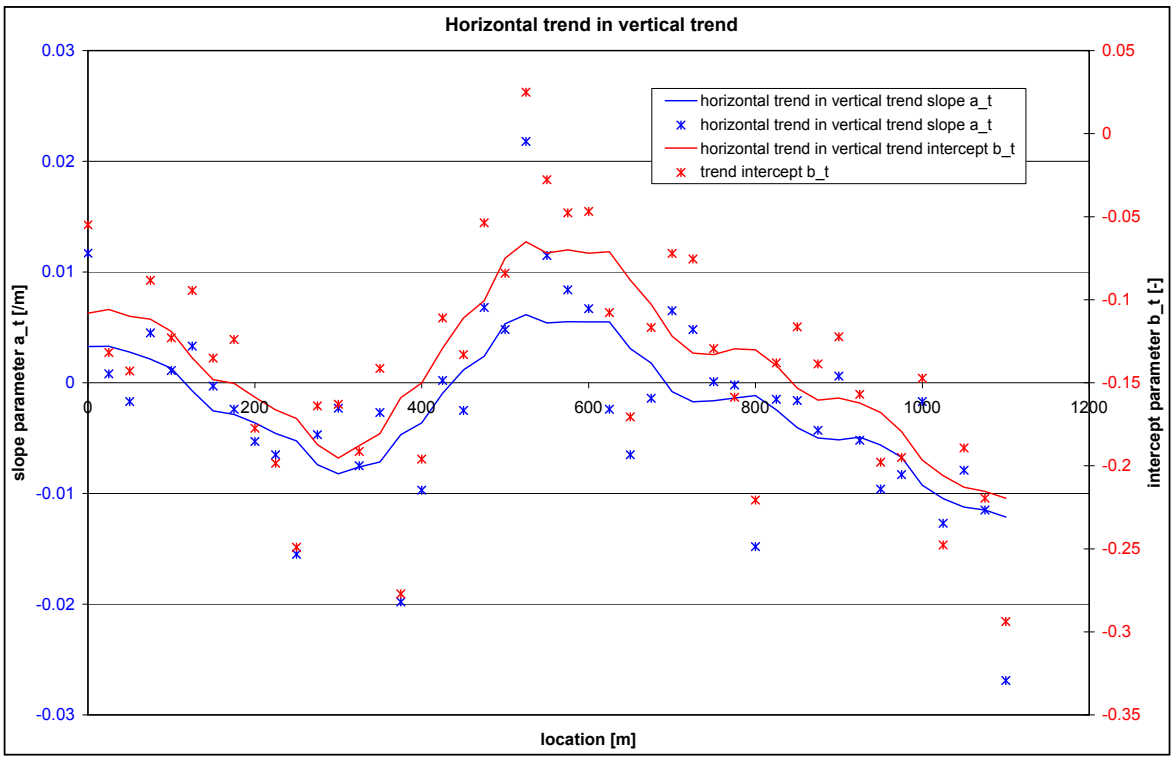

Figure E.7: Lateral variation in trend parameters $a(x)$ and $b(x)$. The lines are the 200m local average lines between the results.

The experimental correlation structure of the trend parameers can be determined. In this way the scale of fluctuation of the trend parameters a and b can be derived. The existence of a correlation structure in the trend parameters indicates that a large-scale variability exists that is not described by the correlation structure of the profiles themselves. Figure E.8 shows that the experimental correlation functions determined for parameters a and b have a scale of fluctuation in the range of 100m. Interpolation of the depoth trend parameters between the profiles therefore does reduce the variability of the sand.

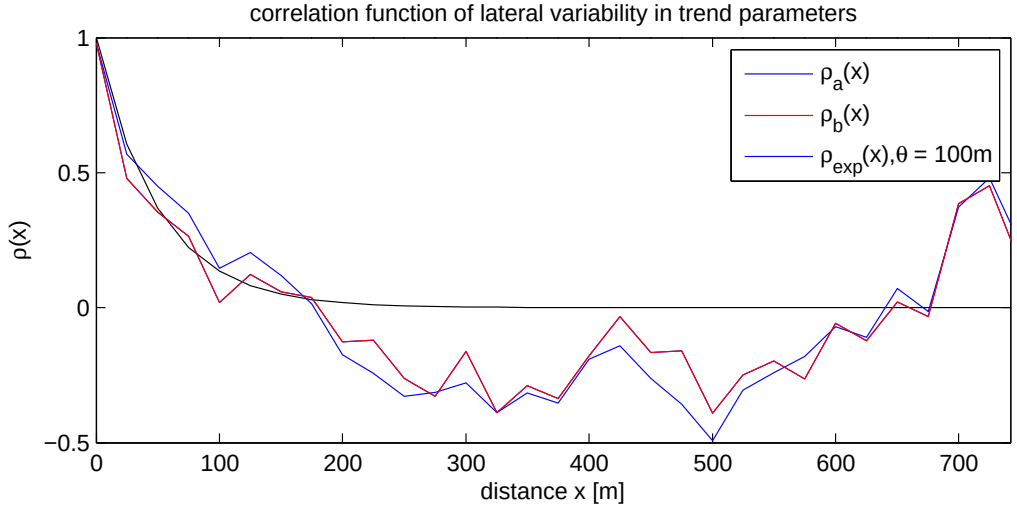

Figure E.8: Correlation function of lateral variation in trend parameters $a(x)$ and $b(x)$

A method to avoid the reduction of variability as an effect of the linear interpolation of the depth trend parameters might be avoided by choosing a constant depth trend over the full domain. In this way the variability that was left in the depth trends, now is contained by the overal trend removed profiles. The following section discusses the possibilities of removing the obverall depth trend.

E.6 Overall depth trend

Throughout this report it is assumed that the total domain that is investigated is one particular material. This means that the material properties of the sand are expected to be equal over the entire domain. The state of the material therefore is expected to be independent from position and therefore the depth trend can be expected to be equal over the full domain. In this way the variability can be seen as a cause of different depth trend in the individual profiles.
In figures E.9 the experimental covariance function has been determined from the profiles for which the individual trend has been removed and for which the overall (average) trend has been removed. The lower graph of the figure shows the theoretical covariance function that is used in the simulations in chapter 5. The theoretical correlation function has not the exact shape as the experimental correlation function. The experimental correlation function shows negative correlation for large lag h (after 1 meter).

The slightly larger result for θ_v found by the correlation function compared to the result found by the variance function is discussed in the next section.

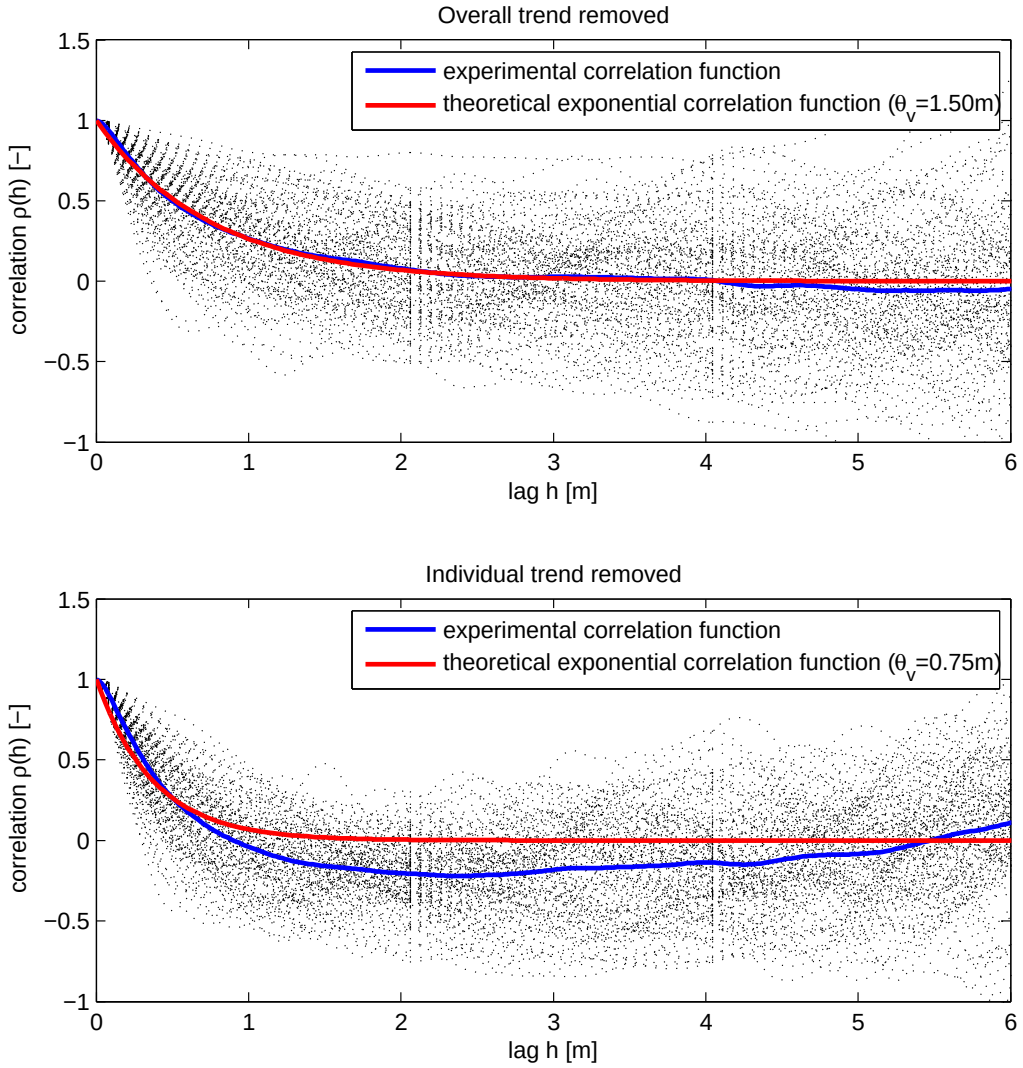

Figure E.9: experimental covariance function determined for average trend removed profiles (upper) and individual trend removed profiles (lower). The upper graph shows that the experimental covariance function matches the theoretical exponential covariance function very closely. The range of the covariance functions of the individual profiles however is larger.

The scale of fluctuation has been estimated based on the profiles of which the overall trend has been removed (figure E.9). The scale of fluctuation determined from the

E.7 Different methods to determine θ

Throughout this report several methods to determine the scale of fluctuation θ have been used. Some of them give different results and some comments can be made about them.

- When the variance function is used to determine the scale of fluctuation θ in this report, the average of all results for each profile has been taken. In this way, the θ that is derived is given bu $E[\Gamma(D)D]$. Another way to determine the most likely value for θ is first deriving the expected variance function $E[\Gamma(D)]$ in order to derive θ from this variance funcion as $E[\Gamma(D)]D$. This is more correct in the sense of variance estimation.
- Deriving the scale of fluctuation from the covariance function for individual profiles is difficult due to the large fluctuations in the covariance function compared to the variance function. The only

option therefor is to first derive the expected covariance function as the mean of all individual profile covariance functions. The best fit of a theoretical covariance function to this experimentalo covariance function gives the scale of fluctuation. The same method can be followed by using the correlation function instead of the covariance function. A slight difference between the two results can be expected, because in the case of using the correlation function, all profiles are weighted equally. In case the covariance function is used, profiles with a larger variance are weighted more and profiles with a smaller variance are weighted less in the averaging.

- The results of $E[\Gamma(D)]D$ and the covariance function are approximately equal. The result found by using the correlation function and the average over the variance function results $E[\Gamma(D)D]$ are slightly lower; in the ranges of 5% and 10% lower.

E.8 Proposed method to investigate

Combining all the comments on the conditioning that are discussed above, a possible method for the conditioning taking into account most of these

- Determine average depth trend over all profiles that are available in the domain
- Remove this depth trend from all profiles
- Transform the profiles into standard normal shape (keep the transformation procedure)
- determine the scale of fluctuation of the transformed profiles
- perform the conditional simulation of the standard normal transform of the trend-removed profiles
- transform the (standard normal) simulated fields into their original distribution (inverse transformation procedure)
- add the removed trend

This method has the advantage above the method used for the evaluation in this report that the trend is only depth-dependent and no interpolation or simulation of the trend between the different profiles is needed. The variability in the trend that is present in the methods discussed in chapter 5 is now covered by the variability from the trend itself. The difference between the trend of the individual profiles and the overall trend is covered by the conditioning points of the simulation and the larger scale of fluctuation. The original distribution of the profiles is honoured exactly due to the transformation to standard normal form before the simulation and back transformation afterwards.

E.9 Reduction of the number of conditioning points

Different methods can be figured out; attention should be paid at the averaged result that the CPT profile already is. More on this can probably be found in Lunne et al. [1997]. Another problem in the reduction of the number of points is the conditional variance that comes in play at the moment the average is taken from the CPT profile to be used as the expected value at a field location that represents the expected value in a square cell in a 2D field. I this case the conditional variance $Z(D_y|D_x = 0) \neq Z(D_y|D_x = D_y)$. These are some of the reasons that no effort has been done to introduce some sort of advanced reduction procedure.